

# Control design for micro tubular solid oxide fuel cells, demonstrating lifetime and performance efficiency

**Konstantinos Zoupalis**

Doctor of Philosophy

Aston University

November 2022

© Konstantinos Zoupalis, 2022 Konstantinos Zoupalis asserts his moral right to be identified  
as the author of this thesis

This copy of the thesis has been supplied on condition that anyone who consults it is understood to recognise that its copyright belongs to its author and that no quotation from the thesis and no information derived from it may be published without appropriate permission or acknowledgement.

## Abstract

Emerging techniques are being researched to introduce new environmentally friendly devices such as fuel cells to reshape the world into net zero carbon emissions. Currently there are different categories of fuel cells available, each category has its benefits, for this project a micro tubular solid oxide fuel cell ( $\mu$ SOFC) provided by the industrial partner Adelan Ltd. was used. The Adelan specific tubular design offers faster warm up, higher thermal flexibility and better sealing capabilities. However, Adelan Ltd wants a more robust control technique in the three core stages of the fuel cell which are start-up, warmup and shutdown. Cycling through these stages it is believed to damage the fuel cell significantly as thermal conditions inside the fuel cell core fluctuate the most.

In this research a novel electronic control unit (ECU) is designed to improve efficiency and lifetime of the  $\mu$ SOFC. Furthermore, the controller is complying to the safety concerns arisen from using a high temperature device, for the product to be commercialised. The proposed controller KJ101 is designed using a four-layer PCB to reduce electrical noises and comply with CE (or UKCA for United Kingdom). This board was able to carry over the existing Adelan control technique and make further improvement and innovation. The controller is programmed in a low-level language (AVR-C using the GCC compiler) to ensure a critical oversight of the functionality while also being able to find and eliminate critical bugs early on. This method allows to have full control to the microcontroller's functionalities and configuring them to the way that it is required for this project.

A fuel cell is currently an expensive device and highly nonlinear device therefore a mathematical model was created to understand thermal responses of a fuel cell. The firmware for the ECU was calibrated and verified using an experimental  $\mu$ SOFC unit, this board showed that the system was able to have flexible smooth and well controlled start up and shut down processes. The proposed controller was able to improve operation by stabilizing the fuel cell at a target setpoint (such as 700°C) while also offering a flexible option of setpoints when being under operation. The temperature variation was another equivalent important topic that was improved by a proposed firmware technique. Finally, this controller was to offer multi-input multi-output control, where the fuel input was adjusted to reach the required power all while the temperature remained at a specific given setpoint by the manipulation of the cooling fans.

## Acknowledgments

**I would like to personally thank my dear supervisors Dr Amir Amiri and Prof. Kate Sugden. I couldn't have asked for better supervisors guiding me to the right path but also being understanding at difficult times.**

**I would also like to thank my dear friend John Sen Gonzalez. Always willing to offer help, especially in the case of lab equipment and fuel cell refurbishing.**

## Collaborator Acknowledgements

**I would like to thank Keele University and Adelan Ltd for funding this research. This PhD became very challenging due to the global pandemic. However, both collaborators were understanding and supportive with timing and deliverables. Adelan was also kind enough to provide with their fuel in their own workshop to operate safely.**

Acronyms

AGR	Anode exhaust gas recycling
BC	Basic Controller (Adelan)
BoP	Balance of Plant
MIMO	Multi Input Multi Output
OCV	Open Circuit Voltage
OEA	Oxygen enriched air
PEN	Positive Electrolyte Negative
SOFC	Solid Oxide Fuel Cell
$\mu$ SOFC	Micro-Tubular Solid Oxide Fuel Cell

### Nomenclature

$k_{eff}^S$	Species effective mass transfer coefficient ( $\text{m s}^{-1}$ )
$D_{eff}^S$	Species effective mass diffusivity coefficient K ( $\text{m}^2 \text{s}^{-1}$ )
$D_{298}^S$	Species effective mass diffusivity coefficient at 298 K ( $\text{m}^2 \text{s}^{-1}$ )
$\dot{N}$	Mass transfer rate from sub-systems boundaries to other sub-system
$\dot{Q}$	Heat transfer rate to/from the sub-system
$C_{2+}$	Diatomic carbon
$C_{dL}$	Double layer capacitance ( $\text{A s V}^{-1} \text{m}^{-2}$ )
$C_h$	Channel height (m)
CO	Carbon monoxide
CO <sub>2</sub>	Carbon dioxide
$C_p$	Specific heat ( $\text{Jmol}^{-1} \text{K}^{-1}$ )
$d(\Delta T)/dt$	The speed of temperature difference change
$E_{act}$	Activation energy ( $\text{kJ mol}^{-1}$ )
$E_{cell}$	Cell voltage (V)
$E^{OCV}$	Open circuit voltage based on the Nernst equation (V)
F	Faraday's constant ( $96,485 \text{ Cmol}^{-1}$ )
$F_{in}$	Inlet molar flow rate ( $\text{mol s}^{-1}$ )
$F_{out}$	Outlet molar flow rate ( $\text{mol s}^{-1}$ )
H	Specific enthalpy ( $\text{J mol}^{-1}$ )
H <sub>2</sub>	Hydrogen
H <sub>2</sub> O	Water
I	Current (A)
i	Current density ( $\text{A m}^{-2}$ )
$i^*$	Pre-exponential kinetics factor ( $\text{A m}^{-2}$ )
$i_o$	Exchange current density ( $\text{A m}^{-2}$ )
$n_e$	Number of electrons

$q$	Energy source term ( $\text{J s}^{-1}$ )
$R$	Ideal gas constant ( $\text{J mol}^{-1} \text{K}^{-1}$ )
$r$	Mass source term ( $\text{mols s}^{-1}$ )
$R^{\text{ohmic}}$	Ohmic resistance term ( $\Omega \text{ m}^2$ )
$S$	Cell area ( $\text{m}^2$ )
$T$	Temperature (K)
$t$	Time (s)
$T_x(t)$	Transient local temperature along the cell length
$T_y(t)$	Transient local temperature across the PEN
$U_f$	Fuel utilisation
$V$	Volume ( $\text{m}^3$ )
$y$	Species mole fraction
$\Delta H_R$	Reaction enthalpy ( $\text{J mol}^{-1}$ )
$\Delta T_{s,s}$	Steady-state temperature differences
$FH$	Energy transfer at element inlet/outlet
$yF$	Species convective delivery

### Greek Letters

$\alpha_A^C$	Anodic charge transfer coefficient for cathode
$\alpha_A^A$	Anodic charge transfer coefficient for anode
$\alpha_C^A$	Cathodic charge transfer coefficient for anode
$\alpha_C^C$	Cathodic charge transfer coefficient for cathode
$\rho_{mol}$	Molar density ( $\text{mol m}^{-3}$ )
$\alpha$	Heat transfer coefficient ( $\text{W m}^{-2} \text{K}^{-1}$ )
$\gamma$	Reaction rate exponent
$\delta$	Catalyst thickness (m)
$\varepsilon$	Porosity
$\eta$	Overpotential (V)
$\nu$	Stoichiometric coefficient
$\rho C_p^{\text{PEN}}$	PEN thermal capacity ( $\text{J m}^{-3} \text{K}^{-1}$ )
$\sigma$	Conductivity ( $\Omega^{-1} \text{ m}^{-1}$ )

### Sub/superscripts

A	Anode
as	Air species
C	Cathode

cat	Catalyst layer
eff	Effective
eq	Equilibrium
f	Fuel
gas	Gas phase
in	Inlet
out	Outlet
$\alpha$	Air

## Contents

<b>Abstract</b> .....	<b>2</b>
<b>Acknowledgments</b> .....	<b>3</b>
<b>Collaborator Acknowledgements</b> .....	<b>3</b>
<b>Acronyms</b> .....	<b>4</b>
<b>List of figures</b> .....	<b>11</b>
<b>List of tables</b> .....	<b>14</b>
<b>1 Introduction</b> .....	<b>15</b>
1.1 Action Needed Now .....	15
1.2 Fuel Cell .....	16
1.3 Fuel Cell Applications .....	18
1.4 Electronic Development .....	20
1.5 Rationale .....	20
1.6 Thesis Structure.....	21
<b>2 Literature review on fuel cells and relevant control systems</b> .....	<b>24</b>
2.1 Fuel Cell Types .....	24
2.1.1 Proton Exchange Membrane Fuel Cells (PEMFC) .....	24
2.1.2 Alkaline Fuel Cells (AFC).....	24
2.1.3 Phosphoric Acid Fuel Cells (PAFC) .....	25
2.1.4 Molten Carbonate Fuel Cells (MCFCs) .....	25
2.1.5 Solid Oxide Fuel Cell (SOFC) .....	25
2.2 Operation of SOFC .....	26
2.3 Planar Geometrical Design .....	28
2.4 Tubular Geometrical Design .....	29
2.5 Microtubular .....	29
2.5.1 Advantages.....	30
2.5.2 Drawbacks.....	31
2.6 SOFC Performance .....	32
2.6.1 Lifetime .....	32
2.7 Fuel Cell Control .....	33
2.7.1 SOFC control and associated current challenges .....	33
2.7.2 Control methods .....	37
2.7.3 Data Exchange Discussion .....	40
<b>3 Micro-SOFC thermal dynamics</b> .....	<b>41</b>
3.1 Introduction .....	41

3.2	Test rig.....	43
3.3	Model schematic.....	44
3.4	Model assumptions.....	44
3.5	Model validation.....	47
3.6	Results and discussions.....	47
3.6.1	2D Thermal dynamics .....	47
3.6.2	Thermal behaviour along the anode channel .....	49
3.6.3	Thermal behaviour across the PEN .....	49
3.6.4	VIM simulation for base voltage impact on the thermal dynamics .....	51
3.6.5	VIM simulation for fuel humidity impact.....	54
3.6.6	VIM simulation of enriched air impact .....	<b>Error! Bookmark not defined.</b>
3.7	Chapter Summary.....	58
<b>4</b>	<b>Basic and KJ100 controllers.....</b>	<b>59</b>
4.1	Basic Controller (BC) .....	59
4.2	BC performance in real-life tests.....	63
4.3	New Controller .....	66
4.3.1	KJ100 .....	66
4.3.2	KJ100 Temperature Sensing .....	67
4.3.3	Fuel flow .....	70
4.3.4	Gas and pressure sensor.....	72
4.3.5	Power output sensor .....	74
4.4	Schematic.....	76
4.5	KJ100 Functionalities.....	79
4.6	User Interface .....	85
4.6.1	Future Plan for improvements for UMI .....	85
4.7	Battery .....	86
4.8	Future Tasks.....	90
<b>5</b>	<b>Hardware Controller Design .....</b>	<b>91</b>
5.1	Design and Development of the New Controller, KJ101.....	91
5.2	Schematic.....	96
5.3	Printed Circuit Board.....	104
5.4	Firmware for KJ101.....	106
5.4.1	Master State Machine description .....	107
5.4.2	Low level state machine description.....	108
5.4.3	Remaining low level states.....	111
5.4.4	Idle stage .....	111
5.5	KJ101 software technical description .....	112
5.5.1	PWM.....	112

5.5.2	Discrete PID .....	113
5.5.3	PID tuning.....	115
5.5.4	Data local communication and interrupts .....	118
5.6	Technical Evaluation.....	122
5.6.1	Warmup Evaluation.....	122
5.6.2	Operation Evaluation .....	123
5.6.3	Shutdown Evaluation .....	124
5.7	Transmission .....	124
5.7.1	Message Queuing Telemetry Transport.....	124
5.7.2	Data Collection Device.....	125
5.7.3	Operation of data collection device .....	126
<b>6</b>	<b>Validation and performance evaluation of KJ101 .....</b>	<b>130</b>
6.1	Introduction.....	130
6.2	Improvement #1: Smoother and well-controlled start-up process .....	130
6.3	Improvement #2: Start-up (warmup) process flexibility .....	134
6.4	Operation Stage Improvements .....	138
6.4.1	Improvement #3: Reaching setpoint with minimal variation .....	138
6.4.2	Air to fuel ratio control .....	143
6.4.3	Improvement #4: The flexibility of setpoints .....	144
6.4.4	Improvement #5: Temperature variation around the SOFC core .....	148
6.4.5	Improvement #6: Battery charging capability as a new feature .....	151
6.5	Improvement #7: KJ101 power output management.....	154
6.6	Improvement #8: Shut down improvements .....	159
<b>7</b>	<b>Conclusion and future recommendations .....</b>	<b>162</b>
7.1	Conclusion .....	162
7.2	Recommendations and the future works .....	165
<b>8</b>	<b>References .....</b>	<b>167</b>

## List of figures

Figure 1.1 Energy Contribution [5].....	16
Figure 1.2 Adelan Fuel Cell.....	18
Figure 1.3 Thesis structure .....	23
Figure 2.1 Operation of a basic SOFC (14).....	27
Figure 2.2 SOFC operation (15).....	27
Figure 2.3: Internal reforming example (14) .....	28
Figure 2.4: (left) Planar Design (right) Tubular Design (18) .....	29
Figure 2.5: (left)Early Electrolyte Supported $\mu$ SOFC (11) (right) Recent anode supported $\mu$ SOFC (21) .....	30
Figure 2.6: Damage with rate of cycling is compared; redox can be observed at low rates where thermal at high rates (24) .....	32
Figure 2.7 Standard PID Controller .....	38
Figure 2.8 First order MPC controller .....	39
Figure 3.1 Thermal test rig.....	43
Figure 3.2 SOFC tube thermocouple locations.....	43
Figure 3.3 Test rig schematic noted for physical model.....	44
Figure 3.4 Comparison of VI data captured by applying the proposed model against the practical data from real-life tests. ....	47
Figure 3.5 The temperature dynamics and cooling fan function rate. (a) temperature dynamics along the cell tube, $T_x$ , at two points captured by thermocouples #1 and #2; (b) transient local temperature difference along the cell length, $\Delta T_x(t)$ , between thermocouples #1 and #2.....	49
Figure 3.6 The transient temperature difference ( $\Delta T_y$ ) response to the 0.05 V voltage interrupt for (a) low, (b) medium and (c) high operating voltage regimes.....	52
Figure 3.7 The effect $U_f$ on steady-state temperature difference across PEN.....	53
Figure 3.8 Effect of operating voltage regime on the transient temperature difference ( $\Delta T_y$ ) response to 0.05V voltage disturbance. ....	54
Figure 3.9 Transient $\Delta T_y$ for the step changes in operating voltage (+0.05V) for operation under two different humidity levels. ....	55
Figure 3.10: Transient $\Delta T_y$ for the step changes in operating voltage (+0.05V) for operation under two different humidity levels. ....	55
Figure 3.11: Transient $\Delta T_y$ for the step (+0.05V) changes in (a) LVR (from 0.55V to 0.50V) and (b) MVR (from 0.70V to 0.65V) operating voltage and two different oxygen levels. ....	57
Figure 4.1 A short $\mu$ SOFC stack (four cells).....	63
Figure 4.2 Real test on $\mu$ SOFC thermal performance controlled by BC.....	64
Figure 4.3 BC Warmup scenario .....	65
Figure 4.4 BC Complete operation scenario.....	66
Figure 4.5 KJ100 Controller Hardware Prototype .....	67
Figure 4.6 KJ100 has an ADC that can be configured up to the clarity of 10 bits.....	68
Figure 4.7 ADC in comparison with SPI chip temperature accuracy.....	69
Figure 4.8 Recommended use of MAX31855 by the manufacturer .....	70
Figure 4.9 Solenoid LPG Fuel Valve .....	71
Figure 4.10 Circuitry designed for proportional valve .....	71
Figure 4.11 Micro Pressure Sensor fitting into the pipes .....	72
Figure 4.12 Two-way connection with KJ100 .....	74
Figure 4.13 Implementation of Power chip .....	74
Figure 4.14 KJ100 Schematic system diagram .....	76
Figure 4.15 $\mu$ SOFC four cell stack .....	76
Figure 4.16 KJ100 Electronic Component Schematic.....	78
Figure 4.17 KJ100 self-simulation test .....	83
Figure 4.18 Battery charger status .....	84
Figure 4.19 Fuel valve and air pump power output percentage (PWM) .....	84

Figure 4.20 User Machine Interface (UMI) essential parameters such as power output and temperature as shown.....	85
Figure 4.21 How a 12V battery charging profile looks like .....	86
Figure 4.22 bq2031 battery monitor chip for KJ100 pinout .....	88
Figure 4.23 Voltage Divider.....	89
Figure 4.24 Simple Questions to the user .....	90
Figure 5.1 Ferrite Beads should be closer to the noise source (89).....	93
Figure 5.2: 3D rendered image of KJ101 (top view) .....	94
Figure 5.3: 3D rendered image of KJ101 (bottom view) .....	95
Figure 5.4 Printed Board .....	95
Figure 5.5 Electrical components used to create KJ101 .....	99
Figure 5.6 KJ101 schematic root sheet 1/4 .....	100
Figure 5.7 KJ101 schematic root sheet 2/4 .....	101
Figure 5.8 KJ101 schematic root sheet 3/4 .....	102
Figure 5.9 KJ101 schematic root sheet 4/4 .....	103
Figure 5.10 KJ101 Layer Stackup .....	104
Figure 5.11 PCB Design .....	106
Figure 5.12 KJ101 High level state machine .....	107
Figure 5.13 Error checking for KJ101 .....	109
Figure 5.14 warmup state to operational state.....	110
Figure 5.15 Analytic stage description.....	111
Figure 5.16 PID tuning Incrementing proportional gain unit constant oscillation .....	116
Figure 5.17 Tuning Integral, I=0.8 .....	117
Figure 5.18 Tuning Integral, I=0.4 .....	117
Figure 5.19 Tuning Integral, I=0.2 .....	118
Figure 5.20 Tuning Integral, I=0.05 .....	118
Figure 5.21 Start-up Evaluation.....	122
Figure 5.22 Different Setpoints.....	123
Figure 5.23 Shutdown profile .....	124
Figure 5.24 MQTT Implementation in this project.....	125
Figure 5.25: Data transmission solution .....	126
Figure 5.26 Basic flow chart for the data collection device .....	128
Figure 5.27 Adelan Dashboard Proof of Concept.....	129
<i>Figure 6.1 Warmup Using the Basic Adelan .....</i>	<i>131</i>
Figure 6.2 A sudden temperature and air flow changes due to fuel being introduced into the system .....	132
Figure 6.3 KJ101 Uses Ramping Technique for a smoother warmup.....	133
Figure 6.4 Warmup temperature trajectory gently controlled, the sudden change is eliminated at feeding point due to improved incremental fuel and air input offered by KJ101. ....	133
Figure 6.5 Warmup stages for KJ101 and BC .....	134
Figure 6.6 A typical transient temperature profile during normal warmup .....	136
Figure 6.7 Contingency Mode 1 warmup using KJ101, cooling fans reduced for more heat to be generated by the electrical heater. ....	136
Figure 6.8 Contingency Mode 2 warmup using KJ101 .....	137
Figure 6.9 Contingency Mode 3 warmup using KJ101 .....	137
Figure 6.10 Adelan Fuel Cell operation stage control using BC.....	139
Figure 6.11 Adelan Fuel Cell operation stage control using KJ101.....	140
Figure 6.12 The transition from warmup to the operation stage.....	141
Figure 6.13 Sudden temperature change caused a sever crack in the CPOX area .....	141
Figure 6.14 Transition to operational stage .....	142
Figure 6.15 Transition to normal operation stage using ramping technique for air input ....	143
Figure 6.16 Both fuel and air are ramping up preserving the 10/1 ratio. ....	144
Figure 6.17 KJ101 meets different setpoints in time-effective manner while under operation .....	145

Figure 6.18 KJ101 meets different setpoints in time-effective manner while under operation .....	146
Figure 6.19 While the fuel cell is operating a command is given to KJ101 to test its reaction to a different setpoint at 690 °C .....	147
Figure 6.20 While the fuel cell is operating a command is given to KJ101 to test its reaction to a different setpoint at 680 °C .....	148
Figure 6.21 Temperature difference when using the basic controller.....	149
Figure 6.22 The temperature between the fuel cell is not the same therefore KJ101 is using software to adjust the air input to temporarily reduce temperature variation .....	149
Figure 6.23 For few minutes the air to fuel ratio is changed to increase the temperature in the T1 location. ....	150
Figure 6.24 Temperature difference changes when the air to fuel ratio is being adjusted with KJ101 .....	150
Figure 6.25 Battery charging solution for BC.....	152
Figure 6.26 Charging scenario .....	153
Figure 6.27 Battery Management System for Adelan .....	153
Figure 6.28 Power draw doesn't affect the heat increase significantly in the Adelan system .....	154
Figure 6.29 The firmware of KJ101 its stopping voltage drop below 10.5 as this is the maximum efficiency possible for the Adelan SOFC .....	155
Figure 6.30 Changing the fuel flow affecting the time required to reach the setpoint .....	156
Figure 6.31 When above 380ml/min the power is not affected .....	156
Figure 6.32 KJ101 experiment to keep a stable temperature and dynamically adjust the fuel flow according to the demand of the power .....	157
Figure 6.33 The fan is stabilising the fuel cell temperature while the power it's also being dynamically adjusted.....	158
Figure 6.34 Voltage and current changes according to the power setpoint/ demand.....	159
Figure 6.35 Immediate change in the air flow caused a sudden change in temperature endangering the fuel cell materials.....	160
Figure 6.36 Shut Down mode for KJ101.....	161

## List of tables

Table 2.1 Fuel Cell Categories .....	24
Table 3.1: The extended governing and constitutive equations for individual sub-systems..	45
Table 3.2: Model parameters .....	50
Table 4.1 Thermocouple types (82-84) .....	67
Table 4.2 Data being transferred to K100 by temperature chip .....	70
Table 4.3 SPI Configuration for the Pressure Sensor .....	73
Table 4.4 INA260 address information .....	75
<i>Table 4.5. The capabilities and limitations of KJ100</i> .....	79
Table 4.6 KJ100 Current Parameter Description .....	82
Table 5.1 KJ101 connectivity description .....	97
Table 5.2 Low power configuration options for KJ101 .....	112
Table 5.3 Initialising PWM mode for the manipulative variables .....	113
Table 5.4 PID Initialisation Software.....	113
Table 5.5 PID Structure used to organise the PID firmware .....	114
Table 5.6 Communication initialisation .....	119
Table 5.7 Timer used to calculate accurate printing intervals for KJ101 communication outputs.....	120
Table 5.8 CANBUS important messages .....	121
Table 5.9 Serial Commands to control the SIM Module.....	127
Table 6.1 Contingency mode details .....	135
Table 6.2 KJ101 power draw in different configurations .....	138
Table 6.3 Typical lead acid battery state of charge, yellow is for the contingency mode start- ups and green for normal. ....	152

## 1 Introduction

Human activities have been the primary cause of climate change since the 1800s mainly due to the combustion of fossil fuel such as coal, oil and gas [1]. The earth has experienced 1.1 °C temperature increase compared to year 1880. The consequences of this can be catastrophic as intense drought, water scarcity, severe fire, rising sea levels, flooding, melting polar ice, catastrophic storm and declining biodiversity [2]. Some of the damages have already happened, however scientists have agreed that limiting the climate to no more than 1.5 °C would help avoiding the worst climate impacts and maintain a liveable ecosystem. However, based on the current trends it is expected by the end of the century temperature global warming will reach 4.5°C [3].

### 1.1 Action Needed Now

To prevent climate changes, solutions have to be found in different areas. Currently off grid power solutions, such as construction site offices and camper vans, are generally utilising solar panels and when there is no solar energy a diesel generator is used to charge the battery [3]. To reduce NOX emissions a more environmentally friendly device such as a fuel cell can be used to efficiently charge the battery when solar power is not feasible.

Solid oxide fuel cells (SOFCs) are an essential technology for distributed power production since they have a number of advantages.

The great efficiency of SOFCs is one of its main benefits. Contrary to conventional power generating methods, which lose a lot of energy as heat, SOFCs may produce electricity from up to 60% of the energy in their fuel. They can therefore generate the same amount of electricity as other technologies while consuming a lot less fuel. This lowers greenhouse gas emissions while also contributing to fuel cost savings. [4]

Low emissions are another benefit of SOFCs. They almost never create pollutants like NOX, SOX, or particulate matter, and they emit far less CO<sub>2</sub> than conventional power production methods. They become a greener alternative for generating power off the grid as a result, especially in locations where air quality is an issue.[5]

Moreover, SOFCs offer a wide range of fuel options. They are a flexible alternative for localised power generation since they may run on a range of fuels, such as natural gas, biogas, and hydrogen. Because of its fuel versatility, SOFCs are suitable for a variety of uses, from small-scale residential systems to huge industrial installations.[6]

The possibility of decentralised power production provided by SOFCs, in addition to their technological benefits, has the potential to revolutionise the energy industry. SOFCs might decrease the need for costly transmission infrastructure and improve grid resilience by producing power where it is needed. This may open up new prospects for regional energy markets and promote decentralisation of the industry.[7]

Moreover, SOFCs may be used with intermittent renewable energy sources like solar cells and wind turbines to help smooth out their performance. This might result in a power supply that is more dependable and steadier, which is important for many applications.[8]

Lastly, SOFCs have a wide range of uses, from modest home installations to more substantial industrial ones. They can be utilised as the main source of electricity for off-grid applications as well as for backup power and combined heat and power (CHP). They are a promising technology for a variety of industries and applications due to their adaptability.[9]

In conclusion, SOFCs provide the possibility of decentralised power generation, low emissions, fuel flexibility, and high efficiency power output. These benefits make them a crucial technology for the generation of off-grid electricity and may contribute to the future transformation of the energy industry.

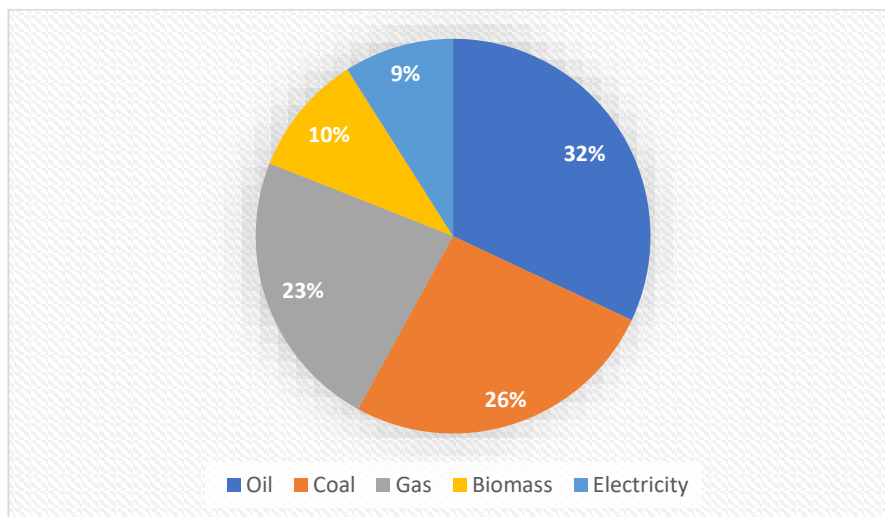


Figure 1.1 Energy Contribution [5]

## 1.2 Fuel Cell

A fuel cell is a device that converts chemical energy to electrical and thermal energies efficiently and in an environmentally friendly manner. In addition to electrical efficiency (which

can be up to 60%), high quality heat can also be a side product of a fuel cell that operates at high temperatures. This is highly useful in heat and power co-generation; and can increase their effective efficiency up to 85% [10]. Solid oxide fuel cell (SOFC) generators in the megawatt (MW) range are available from Bloom Energy. The modular Bloom Energy Server may be set up to deliver electricity in increments of 200 kW, up to a maximum capacity of several megawatts. A bigger power generating system with a MW range of output may be made using many Bloom Energy Servers.

Bloom Energy has finished several sizable projects that make use of its SOFC technology to generate electricity at MW scale. For instance, in 2019 Bloom Energy and Southern Company announced a deal to deploy 400 MW of fuel cell systems at several sites around the United States

Moreover, Bloom Energy has provided SOFC generators for small-scale systems to large-scale installations to a range of clients in the industrial, commercial, and utility sectors. The Bloom Energy Server is a flexible solution for MW-scale power generation since it may be used in a variety of applications and configurations.[11, 12].

A fuel cell has two electrodes, the anode and the cathode. In addition, every fuel cell has an electrolyte which is used to carry the charged particles from one electrode to the other, a catalyst between the electrolyte and the electrodes is used to accelerate the reactions occurring in the fuel cell. While hydrogen is the primary fuel for fuel cells, fuel flexibility is a leading feature of fuel cells. The source fuel can vary from fossil fuels to renewable ones such as methane, propane and gasoline and syngas generated from biomass [13].

A fuel cell could be also described as a battery where both rely on electrochemistry however the major difference is that a battery will eventually die once all the reactants have been consumed. Conversely, a fuel cell will not stop running whilst an external fuel has been supplied to it. It can also be thought of as a micro-factory where it simply takes the input (chemical energy) and generates electricity (electrical energy) [14].

Fuel Cells can offer several advantages:

- they can operate at higher efficiencies than combustion engines,
- they can have lower emissions than combustion engines,
- hydrogen fuel cells can emit only water therefore there is no carbon dioxide emissions and no air pollution,

- fuel cells can be quiet devices as the most usual moving part is a fan or blower for high temperature operating fuel cells.



*Figure 1.2 Adelan Fuel Cell*

### 1.3 Fuel Cell Applications

Aside from the environmental benefits, fuel cells offer a huge quality of life improvements such as less noise, less weight and an ongoing power supply. The rising need for power supply quality, density, and time performance is the primary driving factor in the portable power production market, which comprises an increasing number of innovative products (iPhones, laptops, smartwatches etc...)[11]. Furthermore, the sectors of telecommunications, computers, the Internet, and social networks have become crucial for people, emphasizing the necessity for a completely stable power source[13]. For all of these reasons, fuel cells are particularly suitable as portable power systems due to their high potential in terms of energy density, durability, simplicity of design, and low cost. A fuel cell may work as long as fuel is supplied to the device, which is readily accomplished with a small, lightweight, tank. Portable fuel cells are currently targeted at two energy sectors: the consumer electronic devices (cell phones, laptops and any other portable device requiring battery) and in the portable generators market (such as camping outdoors). Fuel Cells can also be utilised as a primary

or backup power source for telecommunications switching nodes, transmission towers, reception, and other electronic equipment that can benefit from the DC power provided by a fuel cell[13]. Another promising application for fuel cells is in the automotive industry. Currently in the UK, two fuel cell cars are available Toyota's latest model the Mirai has a range of up to 402 miles. Hyundai is also selling a fuel cell car with a range of up to 369 miles[14, 15].

For essential infrastructure, such as cell towers, where power outages can result in serious disruptions and monetary losses, solid oxide fuel cells (SOFCs) can be an efficient backup power source. In the case of a grid outage or other power disturbances, SOFCs are a dependable on-site power generating source that can provide an uninterrupted power supply.

Since the demand for wireless communication services keeps expanding, it is more crucial than ever to have dependable backup power for cell towers. The global market for mobile power solutions, which includes backup power for cell towers, is anticipated to expand rapidly over the next few years, according to a research by Research and Markets.

Because they can be rapidly and readily erected on site and may provide continuous power for several hours or even days, depending on the size of the fuel cell stack and the fuel supply, SOFCs are well-suited for backup power applications. In contrast to conventional backup power systems like diesel generators, SOFCs are emission-free, silent, and do not need routine maintenance.

In more detail Solid oxide fuel cells (SOFCs) and proton exchange membrane (PEM) fuel cells are both types of fuel cells, although their uses differ in significant ways.

High power density, rapid start-up, and effective operation at low temperatures are all characteristics of PEM fuel cells. As a result, they are frequently utilised in settings where portability and mobility are crucial, such as in vehicles like automobiles and buses as well as portable generators. PEM fuel cells can be used to generate tiny amounts of electricity in homes or businesses.

Nevertheless, SOFCs run at temperatures between 800°C and 1000°C, which is substantially higher than PEM fuel cells. They are excellent for stationary power production applications, such as in large-scale power plants, where they may produce electricity from natural gas, biogas, or other fuels due to their high electrical efficiency and efficiency. Moreover, SOFCs may be utilised in combined heat and power (CHP) systems to generate both electricity and heat for use in heating buildings and industrial operations.

In conclusion, whereas SOFCs are better suited for large-scale stationary power generation and industrial operations, PEM fuel cells are appropriate for mobile and small-scale power production applications.[15, 16]

#### 1.4 Electronics Development

In fuel cells, electronics are required to control the whole process of a fuel cell, starting from the parameter control of core chemical reactions and electrochemical reactions, up to the power delivery. A fuel cell controller can be used to increase fuel cell efficiency and lifetime, by controlling as many as possible manipulative variables of the fuel cell to achieve the best possible outputs of the device. Furthermore, with the current digitisation and the forthcoming 5G technologies, an electronic controller it is expected to offer IOT functionalities which include the ability to share information with other electronic smart devices and display analytical operation and usage data, that can be later used by experts to further enhance and make improvements to the fuel cell technology.

#### 1.5 Rationale

To enable the steady and effective functioning of SOFCs (Solid Oxide Fuel Cells), powerful electronic controllers are needed. This is due to a number of factors:

- Temperature management is essential because SOFCs operate at high temperatures, usually between 800°C and 1000°C. Any variation in temperature can result in thermal stresses that harm SOFCs. To keep the SOFC stack at a constant temperature and avoid thermal stress, a strong electrical controller is necessary.
- Control over fuel delivery: SOFCs need a steady and accurate supply of fuel, such natural gas or biogas. To maintain the ideal stoichiometric balance of fuel and oxygen for effective operation, the fuel delivery system must be carefully managed. To maintain the proper ratio and avoid fuel starvation or excess, the electronic controller monitors and modifies the fuel delivery system.
- Control of power output: SOFCs generate DC power, which needs to be controlled to provide steady and dependable power production. To monitor, regulate, and maintain a consistent voltage and current output from the SOFC stack, a strong electronic controller is needed.

In order to ensure the effective and steady functioning of SOFCs and to guard against damage or failure due to temperature changes, fuel delivery difficulties, or unstable power output, a strong electronic controller is required.

Additionally, the need for more environmentally friendly solutions is a further motivation for this PhD. Current infrastructure for energy production must be reconsidered. Adelan Ltd is a company based in Birmingham, offer fuel cells that have one of the most promising fuel cell technologies offering lightweight and noise free solution to efficiently charge batteries. In addition, Adelan fuel cells can be effortlessly combined in series to offer additional power when required. In the fuel cell research area, most projects focus on the core fuel cell technology such as the improvement of the materials or the fuel cells fabrication, other researchers are trying to eliminate resistance losses and many more. These features are really useful and very helpful to advance fuel cell technology however there is a section that tends to get neglected. Fuel cells require electronic controllers that are used to control the fuel operation and can also offer significant improvements such as smart control algorithms and strategies, which can maintain a fuel cell at specific temperature which in turn can offer significant lifetime improvements. Adelan was one of the first fuel cell companies in the UK and hence the proposed controller is being tuned using bare metal C language ensuring the controller is critically stable. Development will be validated in real time with the Adelan fuel cells. Therefore, this controller will also have to follow industrial safety measurements around electronics.

## 1.6 Thesis Structure

The **Chapter 2** is focused on the literature and research activities on fuel cells and their control. A brief overview of all fuel cell types is presented. The Adelan microtubular Solid Oxide Fuel Cell (m-SOFC), which is the case study of this thesis is specifically introduced. Additionally, the current available control strategies are presented, and their advantages and disadvantages compared in this chapter. The thermal management and dynamics knowledge is key in developing any control system. This has been identified as a research gap for mSOFC case. **Chapter 3**, therefore has been allocated to this feature of the mSOFC. In this chapter, simultaneous/complementary usage of theoretical and practical research method has been proven through a novel case study. The following section examines the thermal dynamics of SOFCs (solid oxide fuel cells) using a combination of a numerical model and an experimental test rig. This hybrid thermal evaluation tool is created to investigate and analyse the behaviour of SOFCs. The mathematical model and the practical measurement techniques allowed to achieve comprehensive thermal data set. In **Chapter 4** a basic controller (called KJ100 in this thesis) that replicates the commercial controller used by Adelan in their systems is demonstrated. This chapter aims to identify the potential for enhancements. The rationale of

chapter 4 is to keep basic capabilities of KJ100 in the enhanced version. In **Chapter 5** a new controller (called KJ101 in this thesis) has been developed based on the basic features of KJ100 while offering advanced technical capabilities. The chapter presents the design process and physical manufacturing of the KJ101 in detail. Moreover, the hardware and software functionality check to prove the functionality of the controller have also been presented in Chapter 5. **Chapter 6** aims at demonstration of KJ101 performance at system level by evaluating its function on a real-life SOFC system provided by the industry partner. Finally, the **Chapter 7** presents the project conclusion and recommendations for future research.

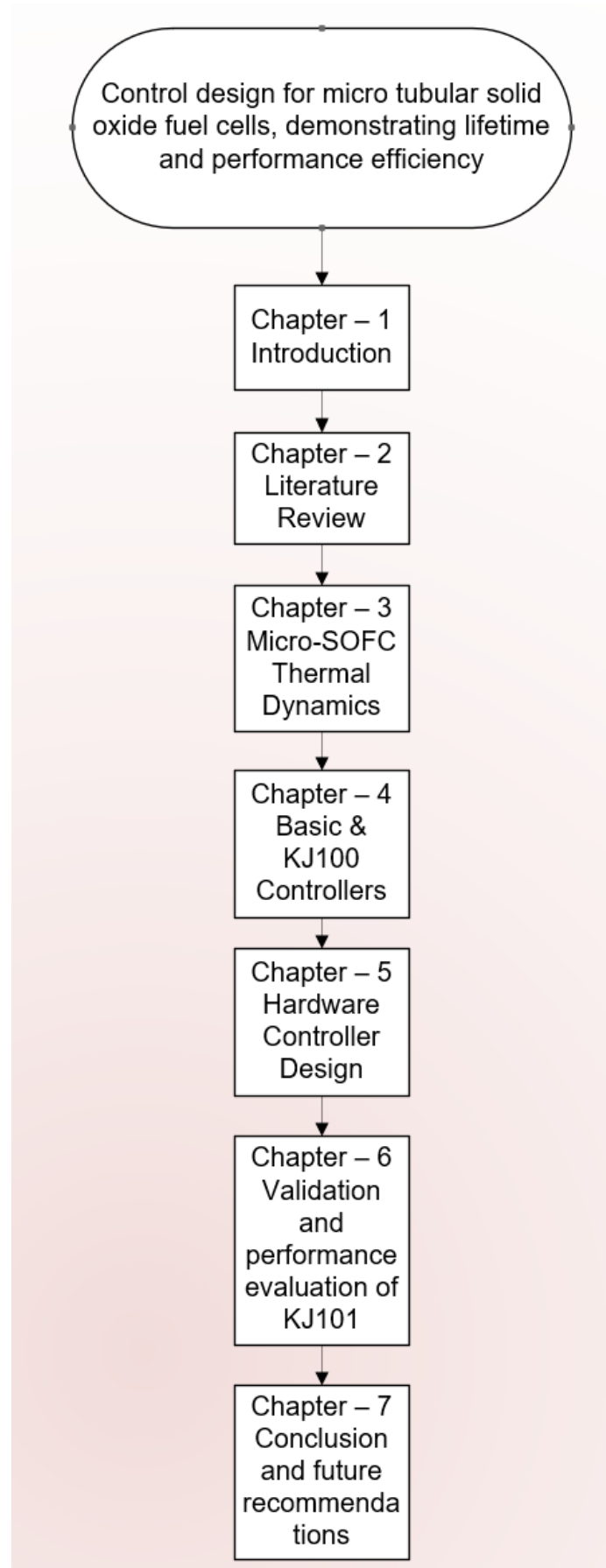


Figure 1.3 Thesis structure

## 2 Literature review on fuel cells and relevant control systems

### 2.1 Fuel Cell Types

While fuel cells are categorised primarily based on the type of electrolyte they employ, the classification can be done based on other criteria such as the operating temperature, cell geometry, etc. There are various types of fuel cells under development, each with their own capabilities, constraints, and final applications. These will be discussed in the following sections.

Table 2.1 Fuel Cell Categories

	Alkaline	Proton Exchange Membrane	Direct Methanol	Phosphoric Acid	Molten Carbonate	Solid Oxide
Acronym	AFC	PEMFC	DMFC	PAFC	MCFC	SOFC
Temperature	50-200°C	50-100°C	60-120°C	180-220°C	~650°C	500-1000°C
Efficiency	~35-60%	~40-60%	~40-60%	~40%	~50%	~45-85%
Applications	Military, Space (Apollo, Shuttle)	Portable power, Transportation, Backup power, Small distributed generation	Portable power	Distributed generation (Transportation)	Electric utility, Large distributed generation	Electric utility, Auxiliary power, Large distributed generation

#### 2.1.1 Proton Exchange Membrane Fuel Cells (PEMFC)

Proton Exchange Membrane Fuel Cells (PEMFCs) also are also known as Polymer Electrolyte Membrane Fuel Cells. PEMFCs use a thin polymer membrane electrolyte and a platinum catalyst. Their operating temperature is typically around 80°C which is a relatively low operating temperature in contrast to the other fuel cell types. Low temperature operation offers attractive features such as: a fast start; less time needed for warm-up; and, reasonable cell durability, as thermal stresses are less. Due to the low temperature and high-power density PEMFCs are currently the most commercially available fuel cells. The PEMFCs disadvantage is that it requires an expensive high-tech catalyst to separate hydrogen's electrons and protons with the addition of being very sensitive to poisoning caused by carbon monoxide (CO) in the system. Internal fuel reformation is not readily feasible due to low temperature and catalyst cost. This type of fuel cell can be used to passenger vehicles such as buses and cars [17].

#### 2.1.2 Alkaline Fuel Cells (AFC)

Alkaline Fuel Cells (AFCs) were the first fuel cells to be used in the United States space program for the generation of electrical energy and water on board spacecraft. Alkaline systems usually consist of a platinum catalyst and electrolyte of a solution of potassium hydroxide in water. AFCs can have an efficiency above 60% mainly due to improved electrochemical reactions. AFCs are not that popular due to carbon dioxide (CO<sub>2</sub>) poisoning,

even a small amount in the air can cause major issues in the existing operation of the system. AFCs have been initiated to mimic the effectiveness of PEMFCs however the same issues still occur on the AFCs and continue to cause some performance issues [17]. Most importantly, there is not much scope for reduction of costs for PAFCs, as the technology is close to maturity.

### 2.1.3 Phosphoric Acid Fuel Cells (PAFC)

Phosphoric Acid Fuel Cells (PAFCs) employ liquid phosphoric acid as an electrolyte and a platinum catalyst. The operating temperature is around 200°C [18]. PAFCs were the first fuel cells on the market. Furthermore, PAFCs have been more resistant to impurities compared with the PEMFCs. They can also achieve efficiencies of up to 85%, taking the electrical and thermal efficiencies into account when they operate as a combined heat and power system. When producing electricity only, the efficiency could be as low as the based power plants which is 33%. PAFCs are typically considered heavy and too expensive because they require much more platinum than any other type of fuel cells [17].

### 2.1.4 Molten Carbonate Fuel Cells (MCFCs)

Molten Carbonate Fuel Cells (MCFCs) consists of an electrolyte of molten carbonate. It most commonly uses a nickel catalyst. Since MCFCs operating temperature is around 650°C, which is very high it can use cheaper catalysts, compared to precious metals, can be used at the anode and cathode leading to productions/components costs reduction. The efficiency of this type of fuel cell if it's combined with a turbine can reach up to 65%, while being potentially possible to improve the efficiency up to 85% if the released heat is captured. One of the advantages is that unlike other type of fuel cells MCFCs do not require an external reformer for natural gas to hydrogen reformation. This is mainly due to the high temperature operation where internal reforming can occur decreasing the component costs. Overall the highest flaw in this system is shortened durability as high temperature operation decreases the lifetime of components and corrosion can occur [17].

### 2.1.5 Solid Oxide Fuel Cell (SOFC)

SOFCs deploy an ion conducting ceramic material (commonly Yttria-Stabilized Zirconia, YSZ) as an electrolyte, while their operating temperature ranges from 600 -1000°C. SOFC is the most effective technology for direct conversion of chemical energy contained in fuel into electric power [19]. Operating at such a high temperature creates advantages and disadvantages. The use of a variety of fuels (which contains minor impurities) such as natural gas, coal gas, LP gas, etc., becomes possible as fuel reformation reaction is feasible [20]. High temperature SOFC operation may cause challenges such as increasing the costs of materials that can sustain at elevated temperatures and also significant warm-up time needed

for operation. This results in lifetime and process control complexities that are currently the two main bottlenecks relevant to this technology development and commercialisation.

Many causes, including as chemical interactions at the electrode interfaces, thermal stresses, and mechanical strain, can lead to SOFC deterioration. Degradation testing is a crucial stage in determining the effectiveness and robustness of SOFCs. Using SOFCs for lengthy periods of time under well controlled settings and tracking their performance over time is the most typical method for assessing SOFC deterioration. For the SOFC stacks and cells to operate dependably and effectively, life and performance monitoring is essential. Current-voltage (IV) characteristics, polarisation curves, electrochemical impedance spectroscopy, and other methods may all be used to track the performance of SOFCs. These methods serve to detect probable causes of deterioration and give crucial information on the electrochemical activity of the cells. The difficulty in addressing SOFC deterioration without tearing apart the entire stack or halting the entire system is a serious problem. Certain tactics, nevertheless, can lessen the impacts of deterioration. For instance, adopting complex control techniques like load balancing and current management can assist to lessen the effect of damaged cells on the system's overall performance. Moreover, utilising sensors that can identify contaminants in the fuel stream, such oxygen or water, can aid in the adoption of preventative actions, including lowering the flow rate or using filtering systems to get rid of pollutants before they reach the stack.[21]

## 2.2 Operation of SOFC

For a basic SOFC (Figure 2.1), Anode, electrolyte, and cathode make up the fundamental layers of a SOFC. The reactant gases can travel through the anode and cathode's porous structure where they interact with the layer of the electrolyte.

Fuel goes into the anode (or fuel channel) which splits into protons ( $H^+$ ) and electrons ( $e^-$ ). When the protons move through the electrolyte layer to the cathode, the electrons flow through an external circuit, producing electrical energy (Figure 2.1). As oxygen from the air interacts with electrons at the cathode (or air channel), oxygen ions ( $O^{2-}$ ) are created. These ions go through the electrolyte to the anode, where they combine with hydrogen ions to create water.

In the end water generated and electrical energy is being generated without any hazardous emissions. With potential efficiencies of up to 85% as discussed earlier, SOFCs are very highly efficient and can run on a range of fuels, including hydrogen, biogas, and natural gas. (Figure 2.1, Figure 2.2) [22]. For efficiency, fuel cells are connected in series to produce more voltage and to calculate the open circuit voltage the Nernst equation is used.

$$E = E_0 + E_f \ln \left( \frac{P_{H_2} P_{O_2}^{0.5}}{P_{H_2O}} \right) \quad (1.1)$$

Where  $E_0$  is the voltage with the reaction free energy of cell,  $E_f = RT/2f$ ,  $R$  is the gas constant of 8.31 J/mol K,  $T$  is the SOFC operating temperature and  $P$  is the partial pressure of hydrogen, water and oxygen.

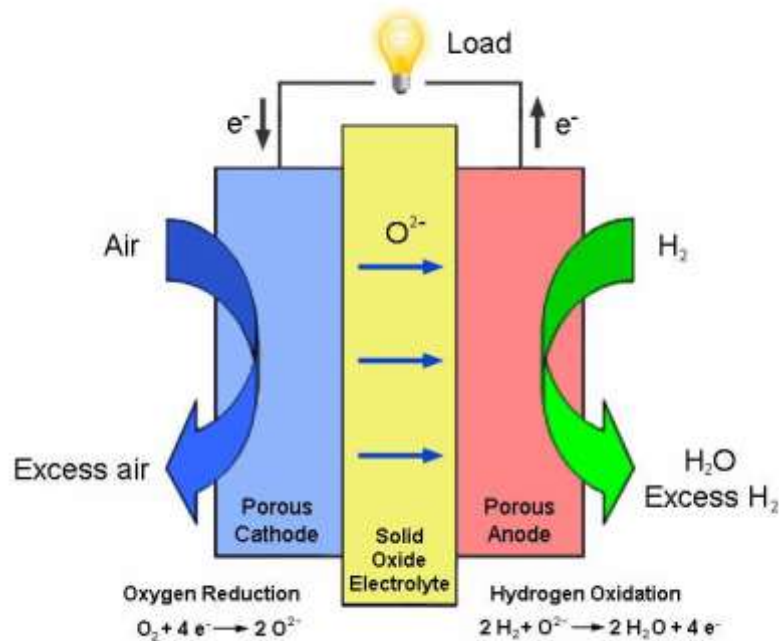


Figure 2.1 Operation of a basic SOFC [23]

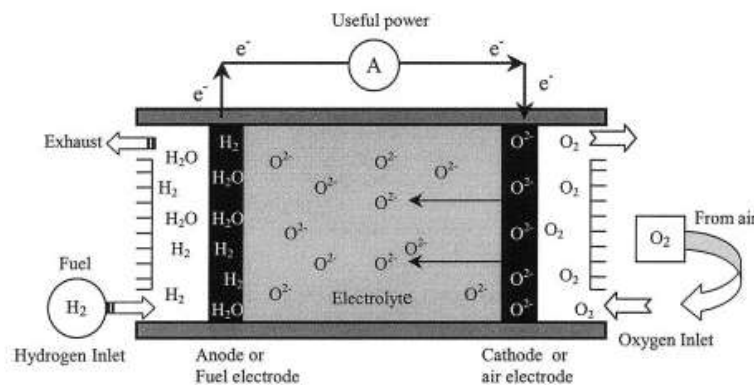


Figure 2.2 SOFC operation [24]

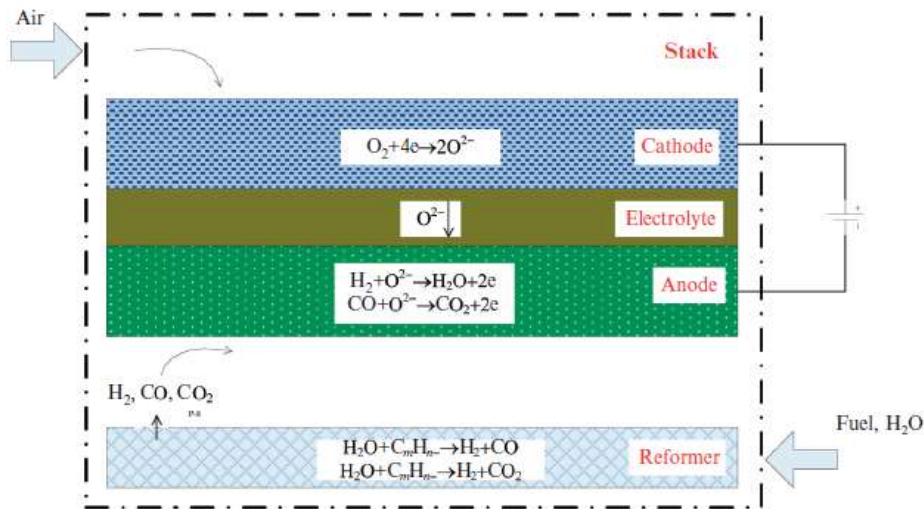


Figure 2.3: Internal reforming example [23]

### 2.3 Planar Geometrical Design

Different proposals have been made for the geometrical design of the SOFC but two remain the most common: the planar design and the tubular design [19]. The planar configuration is easy to construct as it is like a typical sandwich stacking, and it offers a relatively high-power density without too much expense [24-26]. However, there are drawbacks. A good sealing material is required for the planar design to ensure that nothing escapes from the chemical reactions.

Solid oxide fuel cell (SOFC) planar stacks cannot be constructed without interconnects, which join the individual cells in series and provide electrical connections between them. Bipolar plates and end plates, which are frequently constructed of metallic or ceramic materials, serve as interconnects in most electronic devices.

Bipolar plates are positioned in the space between the several cells; they serve as the cathode for one cell and the anode for the one next to it. In addition to providing electrical conductivity between the cells, they are made to make it easier for fuel and oxidising gases to flow. Usually employed to seal the borders of the cells, end plates are positioned at the end of the stack.

The possibility of Cr poisoning of the cathodes in SOFCs is one of the difficulties with interconnects. The majority of stainless-steel alloys, which are frequently used as connection materials because of their excellent electrical conductivity, low cost, and simplicity of production, include chromium (Cr). Nevertheless, under extreme heat and oxidising circumstances, Cr can volatilize and go to the cathode, where it can serve as a catalyst for the synthesis of molecules containing Cr, including Cr<sub>2</sub>O<sub>3</sub> and CrO<sub>3</sub>.

These substances can contribute to the cathode material's deterioration, which lowers its activity and efficiency and, in turn, lowers the SOFC stack's overall performance. The use of high-purity alloys, coatings, and surface treatments that can slow down Cr volatilization and migration are just a few of the measures that have been developed to lessen the effects of Cr poisoning.[27]

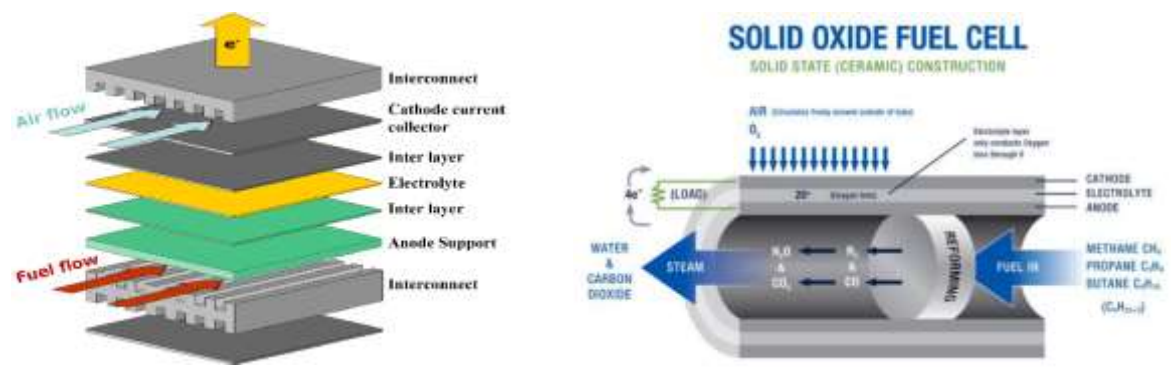


Figure 2.4: (left) Planar Design (right) Tubular Design [28]

## 2.4 Tubular Geometrical Design

The cylindrical tube that serves as the cell's core in the tubular SOFC's basic design is built of a dense ceramic electrolyte material, such as yttria-stabilized zirconia (YSZ). To form a porous layer that allows the passage of fuel and oxidising gases, the anode and cathode layers are typically applied to the outer surface of the core using a ceramic or metallic paste. The tubular SOFC functions electrochemically similarly to conventional SOFCs, with oxygen from the air or an oxygen-containing gas pumped into the cathode and hydrogen fuel injected into the anode. Water vapour and electricity are by-products of the ensuing electrochemical process. The greater surface area for fuel and oxidant gas flow, which results in better power density compared to other SOFC designs, is one of the benefits of the tubular SOFC design. The cylindrical form of the cell also enables improved thermal management, reducing the possibility of thermal stress and enhancing the longevity of the cell. The extrusion or rolling of the cylindrical form, which enables mass production at a lower cost, makes the manufacture of the tubular SOFC easier than that of other designs. [29].

## 2.5 Microtubular

Microtubular SOFCs were invented by Kevin and Michaela Kendall in 1990, where it was demonstrated that zirconia could be extruded into a small diameter tubular design [30]. These tubes were shown to be able to resist thermal shock heating from normal room temperature to 1000 degrees Celsius [30]. In addition, back then the first cells had an extruded electrolyte inside where the anodes and the cathodes were applied, through different techniques of

injection and painting. The power densities of those systems were pretty low only reaching about  $0.08 \text{ Wcm}^{-2}$ . The reason for this is because of the electrolyte ionic resistance, while its size was 200microns thick. Lately the electrolyte supported cells ceased development and new anode supported cells with very thin electrolyte started to be used to solve these problems [29].

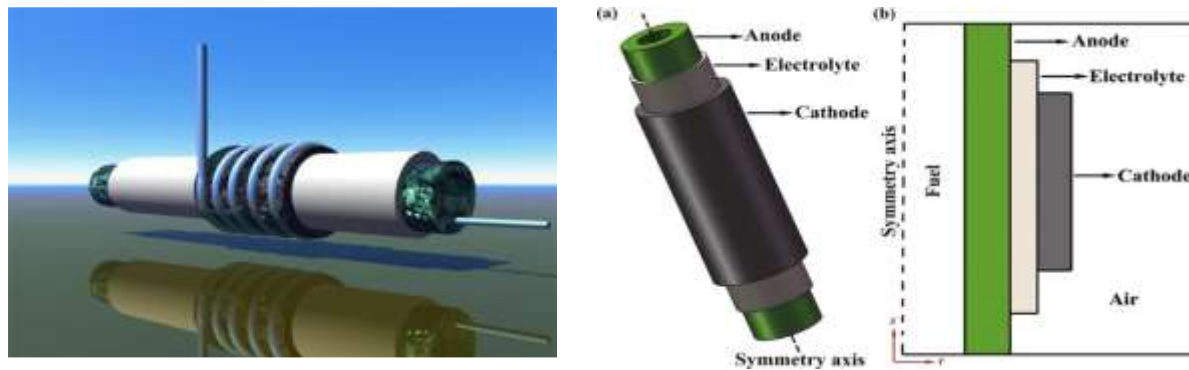


Figure 2.5: (left) Early Electrolyte Supported  $\mu$ SOFC [19] (right) Recent anode supported  $\mu$ SOFC [31]

### 2.5.1 Advantages

Even though SOFCs are not highly developed and deployed in the market they can offer 60%-65% efficiency in the electrochemical conversion in comparison with AFCs and PEMFCs [32]. Recently, interest has been shifted towards  $\mu$ SOFC due to their direct dominance in the thermal stability and their accelerated start-up capability. Micro tubular solid oxide fuel cells can offer a higher volumetric output density while increasing the greater tolerance to cycling and of course the faster start-up which it can enable the mobility of the device. A microtubular start up capability can be varied depending of the diameter of the tube, 2mm diameter tubes have been shown to reach operation temperature in 1 minute, this happens due to the geometry and the thermal shock resistance by the zirconia which is surrounded in the diameter of the tube. In addition, microtubular high power density is related with the diameter of the cell, as long as manufacturing improves and the diameter of the cell becomes smaller, less air and fuel channel space is being taken [24, 29]. Finally, it needs to be mentioned that  $\mu$ SOFCs carry all of the advantages of conventional tubular SOFCs like sealing capabilities against the planar.

A fundamental problem in the early start of  $\mu$ SOFC development was the issue that fired products could not achieve a high endurance. Therefore, polymer plastic processing was developed. Weak aggregate powders were selected which then mixed with polymer solution to be sheared at high stress to eliminate agglomerate structure. Next step would be, to extrude through a tube die the plastic mix to ensure high-quality thin wall tubes. This process would increase the bend strength from 230 MPa to 730 MPa ensuring a more uniform micro structure [29]. A traditional tubular SOFC would be too heavy to carry around and the power density

would be around 10 W/kg. Therefore, the aim for  $\mu$ SOFCs is to reach a 1000 W/kg to be compared with existing PEMFCs. For example, mobile operation would be a struggle, a drone would be unable to be operated under normal SOFC simply because the weight is of very importance and it would increase its resistance to fly, hence other approach had to be taken, and this is where  $\mu$ SOFCs can come in handy with their high power density [29, 33-35].

Lately  $\mu$ SOFCs had been considered the way to go for the Auxiliary Power Units (APUs) for trucks, due to their small factor and big power density where they could be powered by either Liquefied natural gas (LNG) or liquefied petroleum gas (LPG). For a  $\mu$ SOFC to be valid in an APU it has to at least provide 100 kW of power in the operation temperature of 700 °C. In addition, it would at least require starting below the 20<sup>th</sup> minute mark and ensuring that it can last for a continuous run of more than a thousand hours [19, 26, 29, 33].

### 2.5.2 Drawbacks

One major issue with  $\mu$ SOFCs is their lifetime and pricing, however recently techniques have been tested which can improve costs and lifetime. Micro-Tubular SOFCs are being built through at least a triple layer process requiring an anode electrolyte cathode in each layer. This means that in every step (layer) a sintering step is required therefore increasing cost. Recently research has been published using co-sintering, this technique according to Siti Munira et al., [36, 37] is fabricating them all in anode electrolyte cathode triple layer hollow fibre (TLHF) however this results in thin electrolyte which is not ideal and can cause minor conductivity issues [36, 37]. Moreover, there are also issues that planar SOFCs are not facing, a Microtubular cell cannot have a bipolar plate and the current collection techniques can be challenging and ends up in weird current collection paths. According to Kendall et al., [34] one of the first inventors of  $\mu$ SOFCs, two big issues that are considered as challenge are the thermal cycling behaviour and the redox cycling. Thermal cycling is caused by the rapid changes of temperature in a short period, this can cause micro cracking in the tubes which can drop the voltage due to increasing the system cell resistance. Redox cycling occurs when the fuel supplied has been switched off and on periodically, this will lead to micro cracks as well which will not only increase the resistance of the cell, but it was also reported that it causes delamination on the membrane of the electrolyte increasing the system's resistance even more. By cycling faster, the oxidation of the tubes can be moderated. Overall redox cycling can be observed in the system most commonly at lower temperatures. On the other hand, thermal cycling can be seen at the higher temperature range which means that both redox and thermal cycling have to operate at middle rate to tackle the degradation issues.

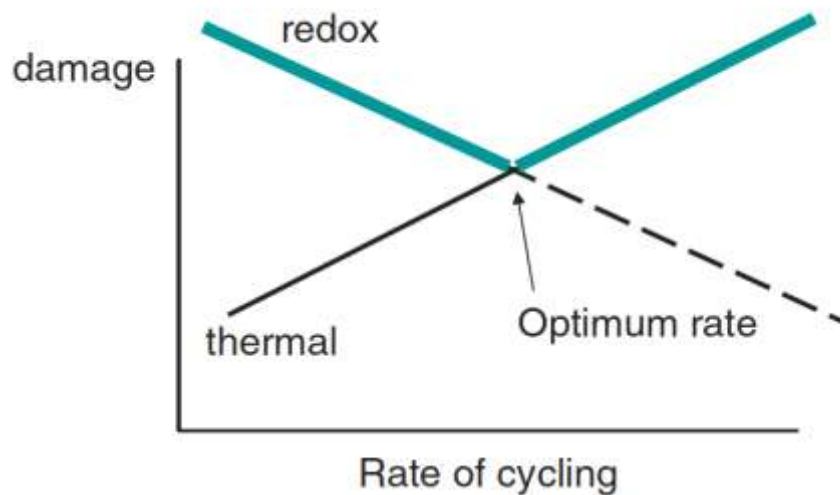


Figure 2.6: Damage with rate of cycling is compared; redox can be observed at low rates where thermal at high rates [34]

## 2.6 SOFC Performance

From this project literature review search it has been found that  $\mu$ SOFC control publications have been very constrained. Control systems are a vital part of a  $\mu$ SOFC.

### 2.6.1 Lifetime

In order to commercialise  $\mu$ SOFC's life expectancy is the key. A good product rather than being novel and innovative it also needs to prove to the general public that its life cycle is at a satisfactory state. In this case, SOFC's need to last more than 40,000 hours with one of the goals being able to maintain less than 0.2% degradation rate in the first 1,000 hours of operation [38]. A recent research from Gupta et al., [39] has stated that fuel utilization variations to sudden load changes can cause damage to the stack which in its order reduces the lifetime. This is a challenge that it is tough to balance, since the fuel is direct source to the power output of the fuel cell and when the connected load demands more power, the fuel cell must adjust to meet that request. However, for some applications where the fuel cell acts as a backup battery charger, this issue can get neglected as 12V Battery can request a specific amount of power to charge (Increasing power draw will only decrease the battery lifetime). Another aspect that affects the lifetime of a fuel cell is the thermal management, one way for a  $\mu$ SOFC to be efficient is to have a uniform thermal distribution across the cell as much as possible, temperature variation can affect power output and decrease fuel utilisation. The significant constraint to  $\mu$ SOFC lifetime originates from the degradation of its part materials, which comes about from working the  $\mu$ SOFC at raised temperatures. [40].

## 2.7 Fuel Cell Control

Controller design, including its logics and electronics plays a vital role in  $\mu$ SOFC life improvement. A well-designed controller will monitor the system effectively and efficiently while also being able to detect errors and protect the system from possible damages. In addition fuel cell controllers are expected to autonomously perform different type of tasks under various operation scenarios. As such, system reliability and viability requirements will be met.

### 2.7.1 SOFC control and associated current challenges.

A single  $\mu$ SOFC tube can provide up to 1V therefore in most cases where more voltage is required these units are being connected in series to make a fuel cell stack.

In the literature researchers have been looking at the fuel cell dynamics from both scenarios either from small scale or large scale.

In general, a fuel cell system can be operated by controlling the fuel intake to satisfy the load demand while achieving optimum performance level monitoring[41]. Amedi et al., [42] created a three-dimensional model for a single anode supported planar SOFC that was able to prove that countercurrent flow leads to a better temperature distribution among the cell density than concurrent flow pattern. The model was created by using the transport phenomena such as ionic charge transport, electric charge transport momentum transport and mass transport model. This finding claims this type of control is reachable however it does lack an actual physical electronic controller being built to show its feasibility as a generic controller has its own complexity from electronic design or firmware limitations. A trend in the literature indicates that each system requires a controller that its tuned for its specific system to achieve steadiness [43-45]. For instance, Chaisantikulwat et al., [46] showed how important is the feedback loop control (in this case PI) to maintain the voltage steady by adjusting the concentration of hydrogen that was going into the system as the designed model showed that sudden changes to load required more hydrogen to keep the Voltage stable so there was no fuel starvation that could harm the system. To ensure safety operations others have tried a multiple controller approach such as Chen et al., [47] introduced six control loops to ensure the safe and efficient operation of the anode and cathode recirculation of the SOFC-GT(Gas Turbine) hybrid system in which the anode and cathode gas feed temperature was being regulated to prevent major temperature variations and temperature gradients in the SOFC. In addition, a fuzzy fault-tolerance coupled with a Bayesian regularization neural network was successfully used by Xue et all.[48]

Researchers have also tried the Multi Input Multi Output (MIMO) approach since the fuel cell is highly dynamic and nonlinear this approach could be more suitable for control. In this SOFC-GT approach in order to monitor electricity, lumped cell temperature, voltage and gas turbine shaft velocity, Mueller and Junker [49] showed a multi-input multi output linear quadratic regulator (LQR). While the variance in fuel cell temperature is mitigated by the controller, they suggest that more advanced control research is needed, and the mean temperature shows an upward drift for large phase changes. As Jurado [50] developed a controller for power and terminal voltage using current and fuel flow as manipulated variables, using a Hammerstein model, a MIMO Model Predictive Controller (MPC) case was shown. Jurado demonstrated in this application that for MPC, the integrated time average error is 10% lower than for PI controllers. Benjamin [51] created a two-dimensional model for a tubular SOFC, which then he used to optimally design two MPC controllers one was a MIMO design and the other was SISO (Single Input Single Output) design. Even though his achievements showed stability and that MPC constraints are an asset that needs to be used for SOFC control design, this method requires a lot of computing power as in this case MATLAB and Simulink were used to develop the MPC model and run the algorithm for the controller on a desktop CPU. In cases such as  $\mu$ SOFCs this is not quite possible due to the small package and portable targets for the system, where parasitic power losses from the controller must be to the minimum.

Another way of looking the controller design is instead of asking the question how to control the Fuel Cell to ask the question what to control. Chatrattanawet et al., [52] did an investigation of an SOFC with internal methane reformer to find out the most affecting parameters and disturbances. The model he created was considering a steady state of 0.5 A/cm<sup>2</sup> and 0.72V with step changes of 10% adjusting core parameters such as fuel input, fuel utilisation and air. The results showed that the most dominant disturbances are air temperature and current density that affect cell temperature and the active restrictions that should be regulated at their setpoint were the cell temperature. Moreover, for the remaining unconstrained variable by the self-optimizing method, the fraction of unconverted methane was considered a strong Controllable Variable (CV).

Another aspect that is being overlooked is the effect that the controller is having on the SOFC's materials. Colombo et al., [53] in his study investigated the degradation and depletion of the SOFC on a system level where he developed a predictive model for ohmic and activation losses. When designing and tuning controllers to ensure proper functioning, this has to be taken into account. The breakdown of parts who have an immediate impact on the overall performance of the device is dependable on the nature and degree of the failure. Huber et al., [54] did more than 1000 hours of experiments to investigate the impact of Ni on the fuel cell

performance. Durability tests were carried out in galvanostatic conditions at 750 °C and 850 °C under fuel cell or electrolysis current, even though more degradation was found in electrolysis mode, there was still significant degradation in fuel cell, where it was also stated that the higher the temperature and the temperature changes the more likely was degradation to happen. This comes to show that a good thermal stabilization by the controller which is able to settle to a setpoint could increase the lifetime of a fuel cell. Another way for the controller to prevent degradation is to ensure faults are not happening in the system such as not compatible power load demands or sudden change to the fuel air input devices as fault in air input or in the fuel delivery could be problematic for the SOFC [55-59]

A good fuel cell performance over long periods of time, requires a robust control system, to ensure high efficiency performance and also, minimizing operations related degradation.[60]. Therefore, a good control system needs to be aware of the existing issues that have been reported and accommodate for almost all of them depending on the system dynamic possibilities. PID control objectives must regulate disturbances according to different power operations of the fuel cell. In addition, they need to improve the efficiency by stabilising the fuel cell thermal fluctuations at its best potential and finally it will need to ensure safety of all the different components of the system without malfunctioning (i.e., tubes cracking) [60]. Ahmad et al.,[61] showed how to stabilise a tubular solid oxide fuel cell by designing two PI Controllers, the first one was maintaining the output voltage by tuning the air inlet pressure, while the second one was trying to maintain a stable cell tube temperature by adjusting the air inlet temperature [61].

Adjusting the fuel cell parameters requires multiple tuning techniques as the fuel cell is so sensitive that a slow down in the parameters adjustment could cause cracks especially in  $\mu$ SOFCs. Consequently, Darjat et al.,[60] created an adaptive PID controller which had the capability of stabilising the disturbances but also changing the PID values respectively by a master controller. The resulting system secured a higher efficiency in comparison with the conventional PID controller [60].

Sakehare et al.,[62] showed the application of the fuzzy logic technique in SOFC for standalone usage and grid connection, they demonstrated how a DC-DC converter could be controlled to keep the average voltage at the desired level. This was based by generating a Pulse Width Modulation (PWM) signal compared to the required voltage and the error calculated inputs.

According to Sedghisigarchi et al., [63] Fuel Cells are designed to work at optimum temperature while small changes of the load can lead to overused or unused fuel conditions

which can cause lasting damage to the stack, the authors designed an H-infinity controller where it was varying the fuel flow rate to account for the small load changes [63].

Horalek et al., [64] showed that a Multi Linear Model Predictive Controller (MPC) could be used for a SOFC system. The controller was able to achieve stable voltage output ensuring all thermal rapid changes would not affect the fuel cell, while this was tested with different current step changes (current(I) was considered as disturbance in the control design) [64].

Common requirements for a fuel cell Electronic Controllable Unit (ECU) are to control the stack average temperature then ensuring the temperature is as stable as possible and finally making sure the output voltage is stable by manipulating the fuel ratio or any other parameter that can affect as the cooling air. A well-known issue that controls cannot fix is when there is a change in the load, the voltage of the stack will change however the controller has been designed. This is caused by the limitations of the fuel and airflow rates which is being passed to the reaction (Triple Phase Boundary) [33]. In simpler words, this is happening when different loads are connected that draw different amounts of power therefore the reaction rate inside the fuel cell will change so the controller cannot be programmed for all possible loads. However, one solution to minimise this issue could be using measurements on the output of the fuel cell to detect the voltage and the current draw of devices and adjust the control profiles of the parameters for best performance. Another possible solution is to force the fuel cell to work at maximum power draw by using a DC-DC converter then the load will draw as much power as it requires while the rest power will become heat from the converter and therefore the fuel cell will not have excess fuel since it would work at the same rate all the times.

Currently, most of the fuel cell control is based on PI and PID control. According to Huang et al. [33] future controllers will mostly use PID control. PID control works perfectly under nominal condition or when some oscillations appear to the system it gets stabilised. However, one issue is that if a big disturbance occurs the PID will stabilise it but will take long response time therefore some damage could have already happened to the fuel cell [65].

Multi-loop systems have also been used for control. Multi-loop systems act like a state machine where if one condition is met, the control would move to the other one (like conditional steps). This algorithm technique can work in the laboratory but are not efficient for the commercialised systems since the algorithms cannot adapt for every possible disturbance that a SOFC system may have. Also, going forward with the state machine loop system is not an efficient coding method since this method is considered as an open loop where the current output of the system does not contribute to the current input of the system. In addition, open loop systems are more power hungry and occupy more processing power on the chip which means it would draw more power from the fuel cell to run.

A designed algorithm for a controller is based around the fuel cell sensor's location, therefore placing sensors at the right place at the fuel cell is essential. Unfortunately, a sensor cannot be placed in all locations without consequences. For example, temperature sensors such as thermocouples will block the air flow if they go inside the system. This is important for the reaction and the cooling of the system, and yet the measurement of the temperature gradient is crucial for fuel cell efficiency and increased power output. Finally, the controller should be able to maintain the gradient temperature by using as few as possible thermocouples.

Understanding fuel cell converters plays a huge role in the fuel cell industry, a fuel cell should be protected from reverse current and load fluctuations. If it is to be used for a load the variable voltage will cause performance issues and decrease lifetime. This occurs due to the large current that a fuel cell produces and the small voltage output. Appropriate control could make use of the converter and adjust the output regarding to the load requirements. An DC/AC Inverter is in need for the conventional AC according to constructed device (ie laptop, phone charger). Furthermore, if an SOFC is used in a backup scenario where it needs to charge batteries, the controller should be flexible and fully integrated with the system so it can output different voltages and currents to charge a battery at different capacities so it can ensure battery life.

## 2.7.2 Control methods

In this chapter a search in the literature is conducted to present the available control strategies that can be followed for automating processes related to the energy section but most specifically for the fuel cells.

### 2.7.2.1 Proportional Integral Derivative Controller

The name PID comes from the fact that a PID controller continuously determines an error value,  $e(t)$ , as the variation among a desired setpoint (SP) and a measured process variable (PV), and then applies an adjustment relying on proportional, integral, and derivative terms (notated P, I, and D, respectively). Proportional integral derivative (PID) control is the most used control algorithm in the industry today [66]. PID controller reputation can be credited to the controller's adequacy in a wide scope of activity conditions, its useful straightforwardness, and the simplicity with which developers can actualize it utilising current computer innovation. PID controllers are the most adopted controllers in modern settings on account of the profitable cost/advantage proportion they can provide.

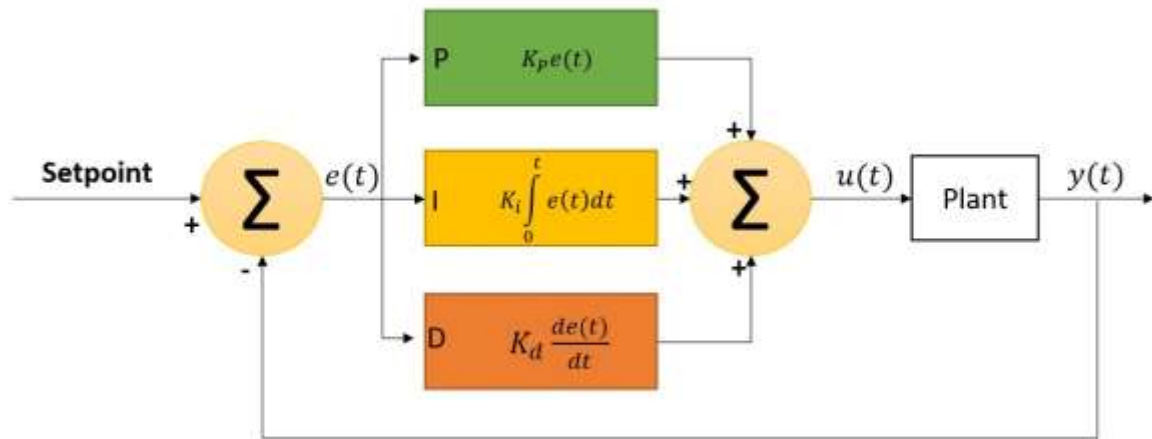


Figure 2.7 Standard PID Controller

### 2.7.2.2 Model Predictive Controller

Recently, popularity has risen in Predictive Control such as (MPC). This technique is multivariable control strategy, which is widely used in the process industry, MPC has become the method of choice for difficult multi-input, multi-output where there are significant interactions between the manipulated inputs and the controller outputs, such as in petrochemical plants around the world. The core of MPC is that the dynamic model and calculated variables are used to predict future behaviour of the system. What is also a key advantage with MPC is that it can accommodate inequality constraints on process variables. However, to deploy a MPC design a more powerful computational device is required where price is to be increased and often these devices end up being significantly larger than conventional 8-bit microcontrollers.

Even though a recent article by Short et al., [67] has demonstrated a MPC design into a microcontroller such as ARM or Arduino some core features of the MPC have been removed and the speed of which the controller will react has been significantly reduced. Finally, the development for a MPC software for an 8-bit microcontroller brings up another issue such as the MPC could take almost all the computational capacity of the microcontroller leaving no space for other functions such as transmissions and IOT implementations.

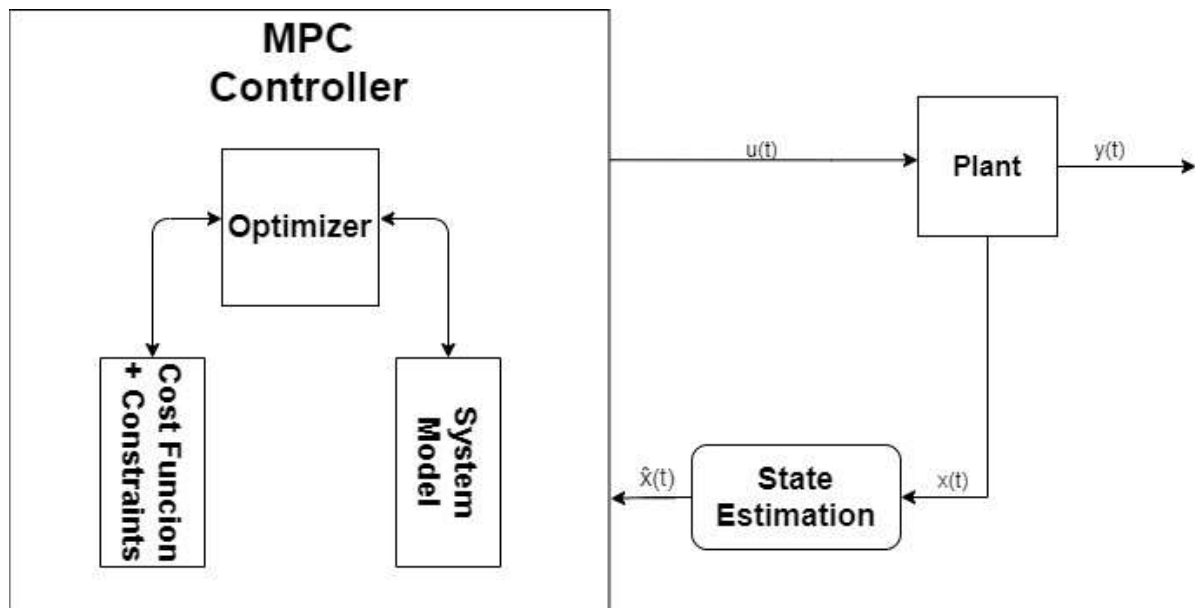


Figure 2.8 First order MPC controller

### 2.7.2.3 PFC (Predictive Function Control)

PFC (Predictive Function Control) serves as a link between PI(D) and complicated MPC. Controlling dead time and limitations might be difficult with PI(D). PFC is a basic realisable MPC that employs key variable prediction and preview. PFC may be implemented using basic software code, resulting in low licence costs. The drawback of using this control method is its tough implementation on multi-input multi-output (MIMO). In addition, this implementation it's not widely supported therefore there is a current shortage for available microcontrollers that can support this.[68]

### 2.7.2.4 Fuzzy Logic Controller

These controllers are set up to tolerate any errors and keep performance within the acceptable bounds for effective system operation. Fault Tolerant Control (FTC) systems limit the possibility of unforeseen occurrences, like as component failure, and help the intended system operate more reliably. Fuzzy logic is generally used to create the controller, which operates via fault isolation and detection before taking a corrective action through firmware.[69]

### 2.7.2.5 Choosing the right control method

From the section above it can be said that control design it's a complex process but most importantly it's a process where the choice for the right control technique has to be taken early. For Fuel Cells to accommodate the controlling technique a hardware must be created to suit its application and once that has been created changes are less likely to happen afterwards.

All control methods have their benefit and drawbacks. However, a controller is most effective when using the right resources of the hardware to select the right controlling technique. In

some applications the hardware for the system has to be compact and react fast to changes therefore in this case a PID controller would be more suitable. In the cases where a model can't be fully created and there is too much uncertainty fuzzy logic control excels as it is known as an artificial intelligence method for controllers. On the other hand a PID controller works best when a model is created which will show the right parameters for the controller to use. However this strategy can also utilise experimental data to a degree of very high accuracy utilising the Ziegler-Nichols closed-loop tuning method.

### 2.7.3 Data Exchange Discussion

In addition to the challenges relevant to above mentioned items, the data exchanges for control enhancement have not been efficient. Engineers and scientists have been working intensely to make  $\mu$ SOFC ready for the market. However, there has been a shortage of study in the literature to reflect user's feedback. In this modern era, it has been found that user analytic data is an important asset. Smart controllers that report back the data to a database can be an incredibly efficient and quicker way to improve fuel cells. Other renewable sectors have been using data exchange for data collection and remote access management.

In the wind power energy section R.S. Pukale et al.,[70] in collaboration with ENERCON showed how the data from each wind power plant was gathered and with these data it will enable them to find the power (P) and power coefficient ( $C_p$ ) for different variable according to the speed of the wind. Srbinovski et al., research highlights the ability to use an affordable wireless, battery-powered, remote data collection IoT node in contrast to a wired solution using a data logger that has minimal capacity that cannot be reached remotely. Both of the above could be used for fuel cells, possibly in stationary places to find out the optimal operation of the fuel cell by analysing the peak power draw to ensure fuel utilization is maximized while there is not a sudden change in the load. Chen et al.,[71] introduced a fault detection system that acquired thermal parameters from a local monitoring, alarm, and control system through the MODBUS protocol and stored them in a database. This technique was able to identify the problems of the diesel engine and it would be able to predict when the engine would be faulty. Fuel cell technology can also benefit from this method, for instance most of the times when a fuel cell breaks is due to one or two tubes from the entire stack break and when this occurs the rest of the tubes are more likely to short and become unusable, with this prediction it could be possible to replace the faulty tubes before they crack and cause harm to the stack. Suhadiyana et al.,[72] created and tested a controller that could be used to store and upload data from a moving mini fuel cell car, the uploaded data included information from both the car location and performance but also from the fuel cell power and performance

### 3 Micro-SOFC thermal transients

#### 3.1 Introduction

To realise SOFC widespread deployment, the lifespan - also known as longevity and lifetime - should be prolonged to assure its reliability and economy. This is currently a serious technical challenge. The SOFC longevity has been the focus of extensive research in the last decade. The lifetime expectation for marketable SOFC varies depending on its application. Japan's New Energy and Industrial Technology Development Organization is currently running a long-term longevity study of SOFCs and has a target of 10% performance loss over 10 years, i.e., 0.11%/1000 h [73]. Similarly, the US Department of Energy's Solid State Energy Conversion Alliance has a target of 0.2%/1000 h loss over 4.5 years lifetime [74]. Fundamental understanding and quantitative monitoring of SOFC degradation drivers are essential to realise these ambitious targets.

Temperature gradients, hot spots, fuel/air impurities, and mechanical stresses/failures are key contributors to the SOFC degradation, and hence its lifetime reduction. One of the major contributors to the SOFC degradation is thermal stress caused by temperature gradients and thermal transients. The temperature gradient causes different magnitudes of expansion across a component with very low-temperature regions experiencing contraction. This causes the low-temperature region to suffer compression stress by the expanding high-temperature region. The high-temperature region is exposed to tensile stress by the contracting low-temperature region. Thermal stresses are also caused by the difference between the operating temperature and the zero-stress temperature. At zero-stress temperature, there are no residual stresses. However, if the temperature is less than the zero-stress temperature, residual stresses are still present due to variations in deformation for each component caused by differences in mechanical properties. It has been found that the contributions of these factors varied depending on the location in the fuel cell [23]. The temperature gradient and the difference between the operating temperature and zero-stress temperature dominate the low-temperature region. However, in higher temperature regions the temperature gradient becomes less significant[75]. The ceramics used in the construction of SOFCs are fragile, making them susceptible to creep, rupture and cracking when put under stress. Keeping the thermal and mechanical stresses placed on the SOFC components within tolerable limits is essential to maximising lifespan. Due to the connected nature of fuel cells in a stack, a single cell failure can cause stack malfunction. The SOFC can operate with the presence of minor cracks; however, there will be an effect on the performance of the cell. The local hot spots and temperature gradient can destroy the SOFC structure physically, hence thermal management is important to mitigate thermal stress.

The capabilities for the measurement of SOFC thermal performance are currently limited to the measuring technologies and techniques. At meso-scale and macro-scale the temperature measurement, and hence the thermal gradients estimations, is technically feasible to a reasonable level. Razbani et al., [76] have experimentally measured the temperature profile over the cell surface [76, 77], for a SOFC short stack of six cells by using five thermocouples inserted inside the stack. At the micro-scale, in contrast, the experimental measurements are extremely challenging and even impossible in most cases [78]. This is because of sensor specifications and sealing issues. Alternatively, an indirect measure is used in some studies. For instance in Fardadi et al., [79] the measurable temperature of the plate has been used as an approximate temperature of the PEN (Positive Electrode- Electrolyte-Negative Electrode). Montanini et al. [78], have applied infrared thermal imaging for temperature measurement at the cathode surface. The method has been applied to a specially designed SOFC, but without measuring temperature in dynamic mode.

Numerical tools are vital for thermal behaviour studies at all scales, particularly at the micro-scale. They can provide insight that is not possible through practical tests. Most of the models used for SOFC thermal management are steady-state models [80-82]. Whilst they are extremely useful for capturing internal hotspots and non-uniformities in the steady-state operation of the SOFC, the thermal transients are not taken into account. This is a critical shortage as thermal dynamics has been proven to be a dominant mechanism in the SOFC control as is key to degradation monitoring and mitigation. The temperature dynamics play the main role in the SOFC speed in responding to various perturbations such as load variation, feed disturbance, etc. The current work aims to fill this gap by providing real-time data that can be used for time-dependent thermal stress analysis. As result, temperature-driven degradation analysis will be possible during transient processes such as startup and shutdown steps.

This chapter contributes to the field by looking at the SOFC thermal dynamics from a novel viewpoint. It provides new knowledge relevant to the effect of the operating conditions on the SOFC thermal dynamics resulting in time-dependent data. Such data and insights can promote the future controllers' design. The SOFC thermal dynamics were simulated in two directions including the fuel flow and across the PEN. While the former was experimentally possible, the latter became achievable only by applying a detailed mathematical model. The proposed model was detailed enough to capture the PEN internal variables in dynamic mode. As such the temperature was computed as a highly non-linear function of fuel cell parameters,

operation variables, and involved transport/reaction mechanisms. The spatiotemporal temperature and thermal gradients were evaluated.

### 3.2 Test rig

The test rig used for thermal assessment of tubular SOFC is shown in Figure 3.1. The set-up was provided by Adelan Ltd established in EBRI research institute.

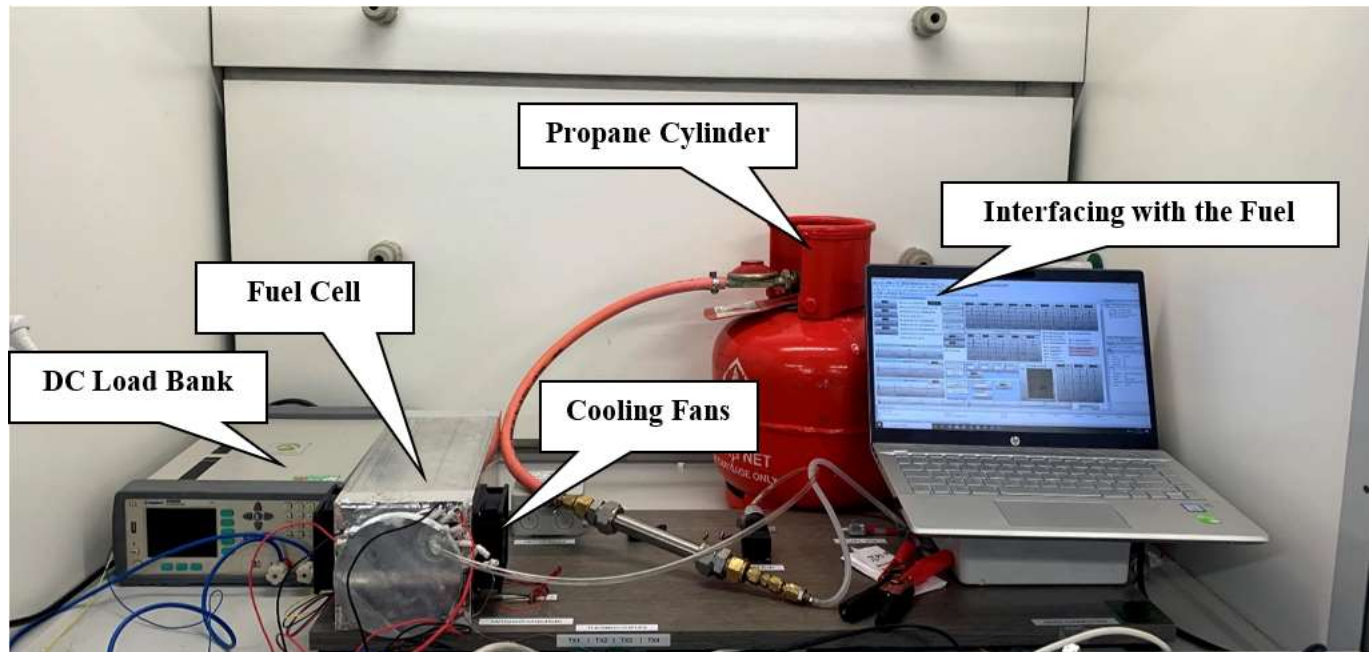


Figure 3.1 Thermal test rig

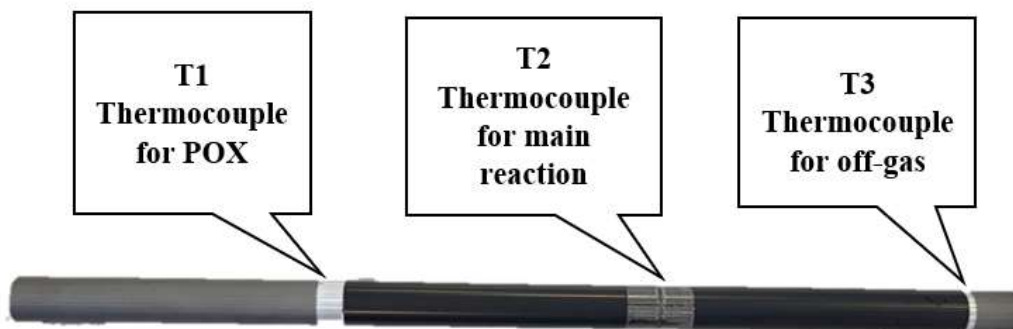


Figure 3.2 SOFC tube thermocouple locations

### 3.3 Model schematic

The model framework is presented in Figure 3.3.

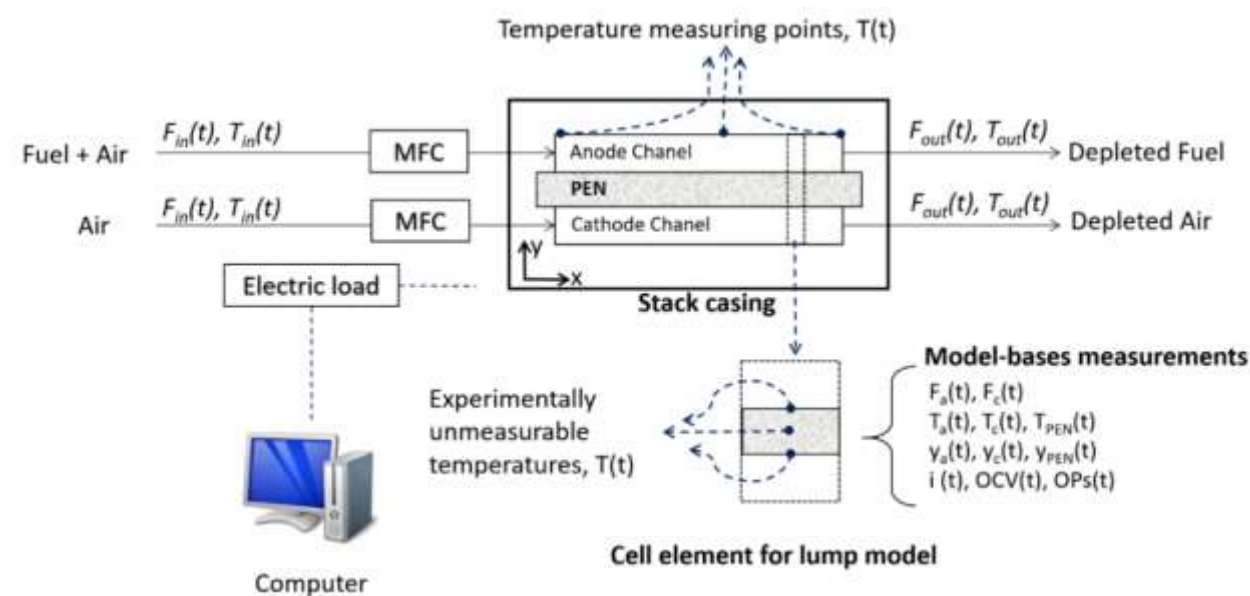


Figure 3.3 Test rig schematic noted for physical model.

### 3.4 Model assumptions

- The model is semi-2D (A material or construction that shows qualities between two and three dimensions is often referred to as semi-2D.) and dynamic. It captures variations' changes at cell inlet/outlet and across the PEN.
- The fuel consists of hydrogen and steam. Air is used as an oxygen supply and coolant. Enriched air is used for further analysis purposes.
- The solid material properties and dimensions do not change with time and operating conditions.
- No internal fuel reformation is considered.

Three sub-systems were considered the main elements of the model. The corresponding control volumes are the anode (fuel) channel, cathode (air) channel, and PEN. The mass, energy and charge balances were computed for each sub-system.

The components balances in each sub-system were written according to the Equation 3.1;

$$\rho V \frac{dy}{dt} = (yF)_{in} - (yF)_{out} - \dot{N} \quad (3.1)$$

Where  $\dot{N}$  is the mass transfer rate from sub-systems boundaries to another sub-system that occurs mainly through diffusion mechanism, and  $yF$  stands for species convective delivery, due to the gas flow, at each element inlet/outlet. Application of the generic Equation 1 for all species involved leads to a set of ordinary differential equations.

The energy balance for each sub-system was computed by using a generic form as presented in Equation 3.2.

$$\rho V C_p \frac{dT}{dt} = (FH)_{in} - (FH)_{out} + \dot{Q} \quad (3.2)$$

where  $\dot{Q}$  is the heat transfer rate to/from the sub-system and  $FH$  stands for energy transfer at element inlet/outlet due to gas flow.

The PEN energy balance was written as presented in Equation 3.3.

$$\rho V C_p \frac{dT^{PEN}}{dt} = \left( -\frac{\Delta H_R}{2F} - E_{Cell} \right) I + \left( S\alpha^a + \frac{C_p^{H_2} - C_p^{H_2O}}{2F} \right) (T^a - T^{PEN}) + \left( S\alpha^c + \frac{C_p^{O_2}}{2F} \right) (T^c - T^{PEN}) \quad (3.3)$$

The heat generated in the electrochemical reaction is transferred to the anode and cathode sides. During the transient phases, the net heat accumulation in PEN is not zero which results in a time-depended temperature.

The charge balance at anode/electrolyte and cathode/electrolyte interfaces can be presented as per Equations 3.4.

$$C_{dL}^{A/C} \frac{d\eta_{A/C}}{dt} = (i_{cell} - i^{A/C}) \quad (3.4)$$

The extended version of the balance equations and the constitutive equations for individual sub-systems are presented in *Table 3.1*.

*Table 3.1: The extended governing and constitutive equations for individual sub-systems.*

Component balances	
$\rho_{mol}^f V_{gas}^f \frac{dy^{fs}}{dt} = y_{in}^{fs} F_{in}^f - y_{in}^{fs} F_{out}^f - \rho_{mol}^f k_{eff}^{fs} S (y^{fs} - y_{cat}^{fs})$	Component balance in anode channel
$\rho_{mol}^a V_{gas}^a \frac{dy^{as}}{dt} = y_{in}^{as} F_{in}^a - y_{in}^{as} F_{out}^a - \rho_{mol}^a k_{eff}^{as} S (y^{as} - y_{cat}^{as})$	Component balance in cathode channel
$\rho_{mol}^f V_{cat}^f \frac{dy_{cat}^{fs}}{dt} = \rho_{mol}^f k_{eff}^{fs} S (y^{fs} - y_{cat}^{fs}) + r^{fs}$	Component balance for anode electrode
$\rho_{mol}^a V_{cat}^a \frac{dy_{cat}^{as}}{dt} = \rho_{mol}^a k_{eff}^{as} S (y^{as} - y_{cat}^{as}) + r^{as}$	Component balance cathode electrode
Energy balances	

$\rho_{mol}^f V_{gas}^f C_p^f \frac{dT^f}{dt} = (F_{in}^f H_{in}^f - F_{out}^f H_{out}^f) + q^f$	Energy balance: Anode channel
$\rho_{mol}^a V_{gas}^a C_p^a \frac{dT^a}{dt} = (F_{in}^a H_{in}^a - F_{out}^a H_{out}^a) + q^a$	Energy balance: Cathode channel
$\rho V^{PEN} C_p^{PEN} \frac{dT^{PEN}}{dt} = q^{PEN}$	Energy balance: PEN
<b>Charge balance</b>	
$C_{dl}^A \frac{d\eta_A}{dt} = (i_{cell} - i^A)$	Charge balance anode/electrolyte interface
$C_{dl}^C \frac{d\eta_C}{dt} = (-i_{cell} - i^C)$	Charge balance cathode/electrolyte interface
<b>Constitutive equations</b>	
$F_{out}^a = F_{in}^a - \sum \rho_{mol}^f k_{eff}^{as} S (y^{as} - y_{cat}^{as})$	Air flow rate change
$F_{out}^f = F_{in}^f - \sum \rho_{mol}^f k_{eff}^{fs} S (y^{fs} - y_{cat}^{fs})$	Fuel flow rate change
$k_{eff}^s = D^s / C_h$	Species effective mass transfer coefficient
$D^s = D_{298}^s \epsilon^{1.5} \left( \frac{T}{298} \right)^{1.5}$	Species diffusivity
$i^A = i_0^A \left[ \exp\left(\frac{\alpha_A^A F (\eta^A - \eta_{eq}^A)}{RT}\right) - \exp\left(\frac{-\alpha_C^A F (\eta^A - \eta_{eq}^A)}{RT}\right) \right]$	Anode local current density
$i^C = i_0^C \left[ \exp\left(\frac{\alpha_C^C F (\eta^C - \eta_{eq}^C)}{RT}\right) - \exp\left(\frac{-\alpha_A^C F (\eta^C - \eta_{eq}^C)}{RT}\right) \right]$	Cathode local current density
$i_0^A = i_A^* (y_{cat}^{H_2})^{\gamma_{H_2}} (y_{cat}^{H_2O})^{\gamma_{H_2O}} \exp\left(-\frac{E_{act}^A}{RT}\right)$	Anode exchange current density
$i_0^C = i_C^* (y_{cat}^{O_2})^{\gamma_{O_2}} \exp\left(-\frac{E_{act}^C}{RT}\right)$	Cathode exchange current density
$i^{cell} = (E^{OCV} - E_{cell} - \eta_{act}^A + \eta_{act}^C) / R^{Ohmic}$	Electrolyte current
$\eta_{act}^A = \eta^A - \eta_{eq}^A$	Anode activation overpotential
$\eta_{act}^C = \eta^C - \eta_{eq}^C$	Cathode activation overpotential
$R^{Ohmic} = \delta_e / \sigma_e$	Electrolyte Ohmic resistance
$\sigma_e = 3.34 \times 10^4 \exp\left(-\frac{10300}{T}\right)$	Electrolyte conductivity
$r^{H_2O} = S \frac{v^{H_2O} i^A}{n_e^A F}$	Water production rate
$r^{O_2} = S \frac{v^{O_2} i^C}{n_e^C F}$	Oxygen consumption rate
$r^{H_2} = S \frac{v^{H_2} i^A}{n_e^A F}$	Hydrogen consumption rate
$q^f = \alpha^f S (T^{PEN} - T^f)$	Fuel channel heat transfer
$q^a = \alpha^a S (T^{PEN} - T^a)$	Air channel heat transfer
$q^{PEN} = \left( -\frac{\Delta H_R}{2F} - E_{cell} \right) I + \left( S \alpha^f + \frac{C_p^{H_2} - C_p^{H_2O}}{2F} I \right) (T^f - T^{PEN}) + \left( S \alpha^a + \frac{C_p^{O_2}}{4F} I \right) (T^a - T^{PEN})$	PEN energy balance (net rate of energy accumulation)

$$U_F = 1 - \frac{y_{out}^{H_2} F_{out}^A}{y_{in}^{H_2} F_{in}^A}$$

Fuel utilisation

$$U_A = 1 - \frac{y_{out}^{O_2} F_{out}^C}{y_{in}^{O_2} F_{in}^C}$$

Air utilisation

### 3.5 Model validation

The V-I profile was used to validate the model performance (Figure 3.4). The figure illustrates that the mathematical model can capture the practical V-I data. As the V-I profile is a strong nonlinear function of temperature, it can be concluded that the model's performance in estimating the temperature is reasonable.

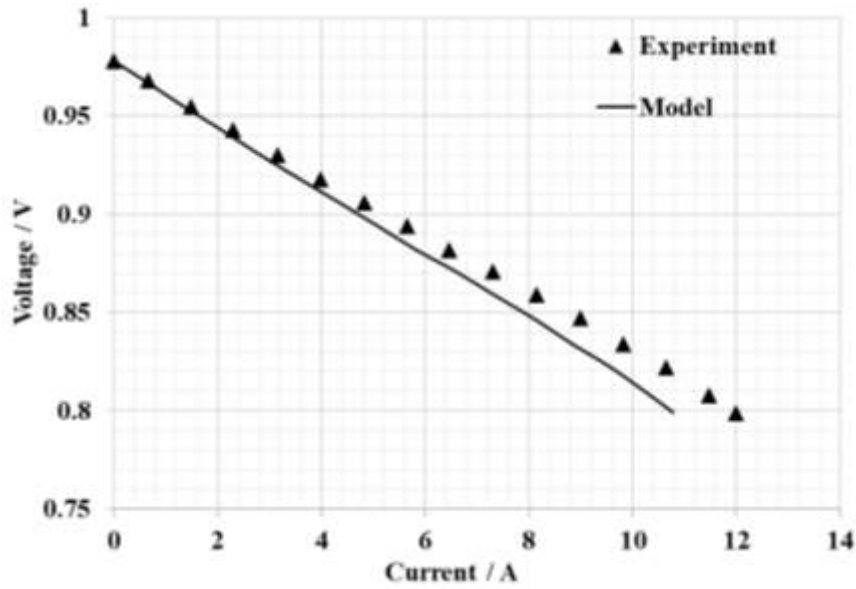


Figure 3.4 Comparison of VI data captured by applying the proposed model against the practical data from real-life tests.

### 3.6 Results and discussions

#### 3.6.1 2D Thermal dynamics

The temperature and temperature difference between two points can reach a steady-state value subject to enough time. The following terms are used in this chapter to assess the thermal behaviour of the cell.  $T_x(t)$ : transient local temperature along the cell length;  $T_y(t)$ : transient local temperature across the PEN;  $\Delta T_x(t)$ : transient local temperature difference along the cell length ( $T_{x1}(t) - T_{x2}(t)$ );  $\Delta T_y(t)$ : transient local temperature difference across the PEN ( $T_{y1}(t) - T_{y2}(t)$ );  $\Delta T_{x,ss}$ : steady-state local temperature difference along the cell length ( $\Delta T_x(t)$  at  $t >$  settling time);  $\Delta T_{y,ss}$ : steady-state local temperature difference across the PEN ( $\Delta T_y(t)$  at  $t >$  settling time). The variation of temperature difference with time is given by  $\Delta T/\Delta t = (\Delta T_{t1} - \Delta T_{t2})/(t_1 - t_2)$ , this term is crucial in the real-time evaluation of thermal stresses.

The dynamic temperature gradients formed across the SOFC dimensions are created by highly nonlinear interactions between several heat sources and sinks. The heat sources include the electrochemical reaction occurring at the three-phase boundary and the ohmic polarisation loss. As such, most of the heat is generated inside the PEN near the electrode/electrolyte interface. The internal fuel reforming, which takes place when SOFC is fed by fuels rather than pure hydrogen, can be either a heat source or sink. For instance, the partial oxidation (POX) of hydrocarbon fuels and gas-shift reaction (for carbon monoxide fuel) are extra heat sources in the PEN subsystem. In addition to heat losses to the environment and the coolant (air) to moderate the SOFC temperature at the allowed level, the endothermic internal fuel reformation process such as steam reforming of hydrocarbons (e.g., methane and propane) acts as the internal heat sinks. The temperature distribution, gradient and dynamics are ultimately dominated by the interaction of all processes.

In modelling work conducted by Ahmed & Foger [83] the internal distribution of steady-state temperature over a dimensionless axial distance was investigated. Amiri et al [84] have studied the thermal behaviour of SOFC estimating steady-state internal distributions in different layers of the cell structure including cathode, anode, electrolyte, and interconnects. The thermal transients, however, were not considered in the abovementioned studies. In this work, the data achieved from experimental tests and numerical model were used to fill this gap. The real-time mechanisms were simulated in this work to accurately capture the 2D thermal transients. The temperature transients in fuel flow direction was measured experimentally while the model-based estimation was conducted for data capturing across the PEN body. For the experimental part, the unsteady temperature was caused by startup and shutdown processes while for the model-based investigations the operating voltage change was used to induce the unsteady temperature in the system.

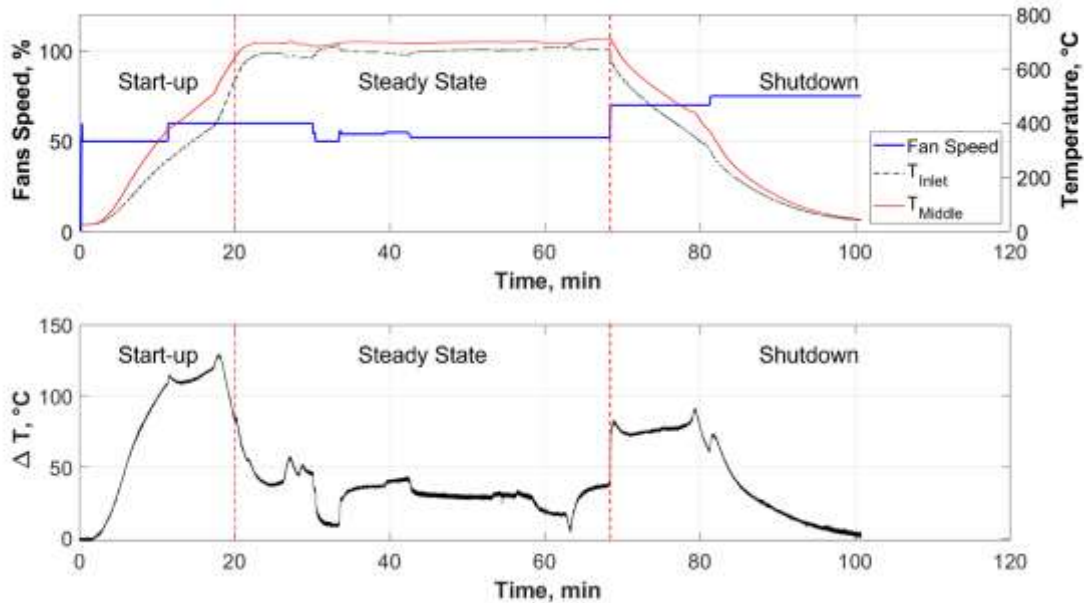


Figure 3.5 The temperature dynamics and cooling fan function rate. (a) temperature dynamics along the cell tube,  $T_x$ , at two points captured by thermocouples #1 and #2; (b) transient local temperature difference along the cell length,  $\Delta T_x(t)$ , between thermocouples #1 and #2.

### 3.6.2 Thermal behaviour along the anode channel

Cell temperatures were experimentally measured at two different points of the tube during startup, normal (stabilised), and shutdown operations. The coolant air was used to control the temperature with its flow varying with the temperature change rates. The experimentally measured real-time temperature and temperature gradient dynamics along the cell tube (fuel flow or x direction) are presented in Figure 3.5. As shown in this figure, the fan speed fluctuation was required to ensure a gentle warm-up ramp, steady-state operation and even the cooling during the shutdown step, revealing that the coolant flow must be updated in a feedback control strategy. Over the test time, a substantial temperature difference between the two measuring points was observed for all three steps (Figure 3.5a). In particular, the results reveal that while the cell experienced a temperature gradient ( $\Delta T_x(t)$ ) lower than 130 °C over most of the operation time, including startup and shutdown steps, the cell may suddenly experience a high gradient of thermal change. Therefore, fluctuations may occur in a short timeframe, they may impact the cell's performance and health in the mid- and long-term. This is because a high thermal disruption in a short time is a thermal shock that will promote cell degradation when the thermal cycle frequency is high, as in automotive applications.

### 3.6.3 Thermal behaviour across the PEN

The state transition from one steady-state operation condition to another causes significant concerns for failure. The startup and shutdown steps are two severe state transitions. In

assessing these transitional states both magnitude and speed of transition are crucial. The transient temperature and dynamics gradient in PEN were estimated using the model inputs presented in *Table 3.2*.

*Table 3.2: Model parameters*

<b>Parameter</b>	<b>Anode</b>	<b>Cathode</b>
Catalyst thickness $\delta$ , m	$2.5 \times 10^{-4}$	$3 \times 10^{-5}$
Porosity $\epsilon$	0.4	0.4
Charge transfer coefficient $\alpha_A$	2	1.4
Charge transfer coefficient $\alpha_C$	1	0.6
Activation energy $E_{act}$ , kJ mol <sup>-1</sup>	120	130
Pre-exponential kinetics factor $I^*$ , A m <sup>-2</sup>	$2.9 \times 10^8$	$7.0 \times 10^8$
Heat transfer coefficient $\alpha$ , W m <sup>-2</sup> K <sup>-1</sup>	25	25
Fluid physical properties	Calculated by Aspen Plus	
Channel height $C_h$ , m	$7.5 \times 10^{-4}$	
Cell area $S$ , m <sup>2</sup>	$5 \times 10^{-3}$	
Electrolyte thickness $\delta_e$ , m	$1 \times 10^{-5}$	
PEN thermal capacity $\rho c_p^{PEN}$ , J m <sup>-3</sup> K <sup>-1</sup>	106	
Species diffusivity at 298 K $D_{298}^s$ , m <sup>2</sup> h <sup>-1</sup>	0.22 (H <sub>2</sub> ), 0.079 (H <sub>2</sub> O), 0.04 (O <sub>2</sub> )	
Stoichiometric coefficient $\nu$	-1 (H <sub>2</sub> ), 1 (H <sub>2</sub> O), -0.5 (O <sub>2</sub> )	
Reaction rate exponent $\gamma$	1.0 (H <sub>2</sub> ), 1.0 (H <sub>2</sub> O), 0.25 (O <sub>2</sub> )	
<b>Operating conditions</b>		
Cell voltage $E_{cell}$ , V	0.80 (varying in VIM cases)	
Fuel flow rate $F_{in}^f$ , ml min <sup>-1</sup>	100	
Air flow rate $F_{in}^a$ , ml min <sup>-1</sup>	1000	
Fuel composition $y$ , mole fraction		
H <sub>2</sub>	0.97 (varying in VIM cases)	
Propane	0	
H <sub>2</sub> O	0.03 (varying in VIM cases)	
C <sub>2+</sub>	0	
CO	0	
CO <sub>2</sub>	0	
Fuel inlet temperature, K	923	
Air inlet temperature, K	923	

### 3.6.4 Variation Iteration Method (VIM) simulation for base voltage impact on the thermal dynamics

The time-dependent  $\Delta T_y$  across the PEN was considered as a crucial term for the SOFC thermal dynamics analysis. The in-depth insight relevant to  $\Delta T_y$  as a function of time was targeted. The modelling test was based on the Voltage Interrupted Measurement method for the SOFC characterisation. The simulations were conducted for 0.05V variation in the operating voltage at three different base voltages, including 0.50V, 0.65V and 0.80V. These base voltages are representative of three operating voltage regimes including low (0.50–0.60V), medium (0.65–0.75V) and high (0.80–0.90V), respectively. The voltage between the assumed regimes (e.g., 0.60–0.65V between low and medium ranges) are considered as transition values in this study. The “voltage regime” concept is introduced in this work, for the first time to the authors’ knowledge, for the SOFC performance evaluation.

The transient local temperature difference across the PEN is shown in Figure 3.6 for three voltage regimes. In the three voltage regimes, the SOFC transient thermal response for the same voltage disruption was different, revealing the importance of the voltage regime’s role in the analysis of the cell thermal dynamics and control design. As can be seen in Figure 3.6, in all voltage regimes the PEN experiences a lower  $\Delta T_{y,ss}$  at higher operating voltages. As an example, in the low voltage regime, with a base voltage of 0.50V, a steady temperature difference of about 24K was achieved while it reaches 20.9K, and 18K for operating voltages of 0.55V and 0.60V, respectively. Taking voltage regimes into account, a 0.1V variation of operating voltage may cause a max 6.3K and 4.6K variation in temperature in steady-state voltage at low and high voltage regimes, respectively. The  $\Delta T_{y,ss}$  values were repeatable for all voltage regimes showing the model preciseness. For instance, the same  $\Delta T_{y,ss}$  value was observed for  $V = 0.70V$  regardless of whether the upper or lower regime has been used to reach 0.70V.

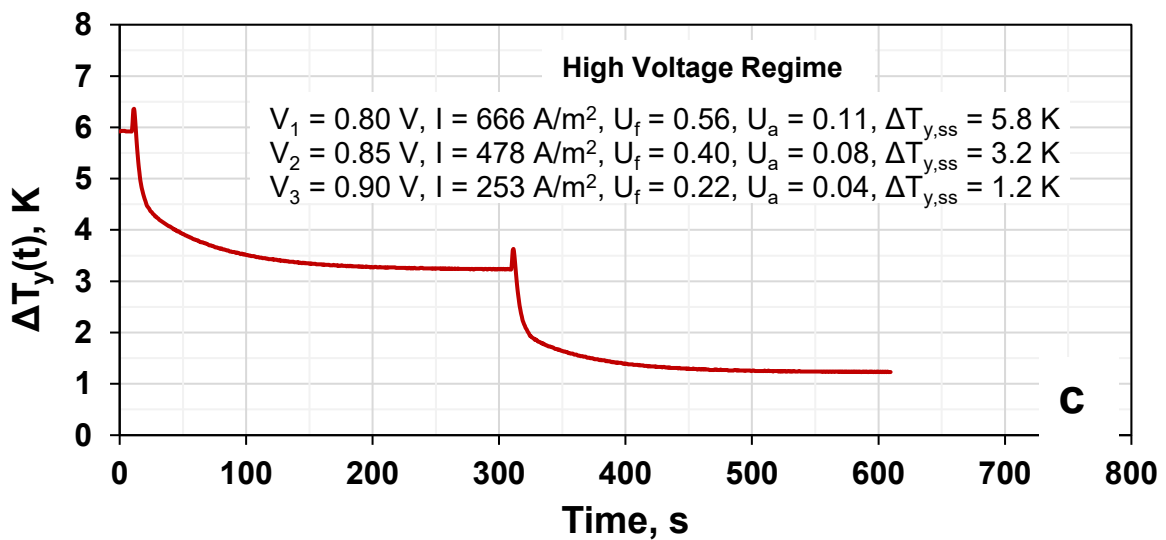
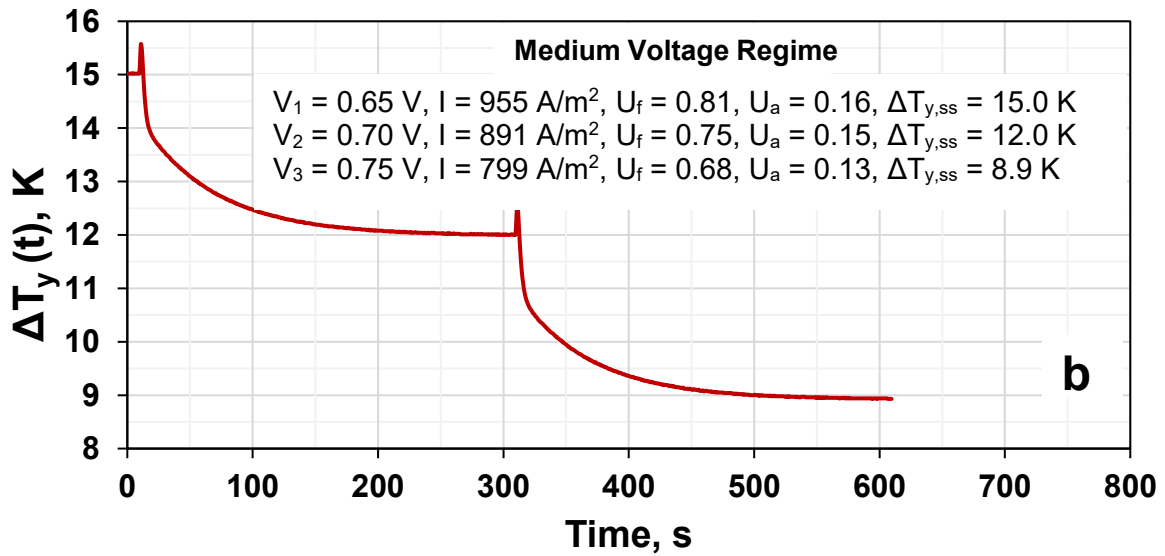
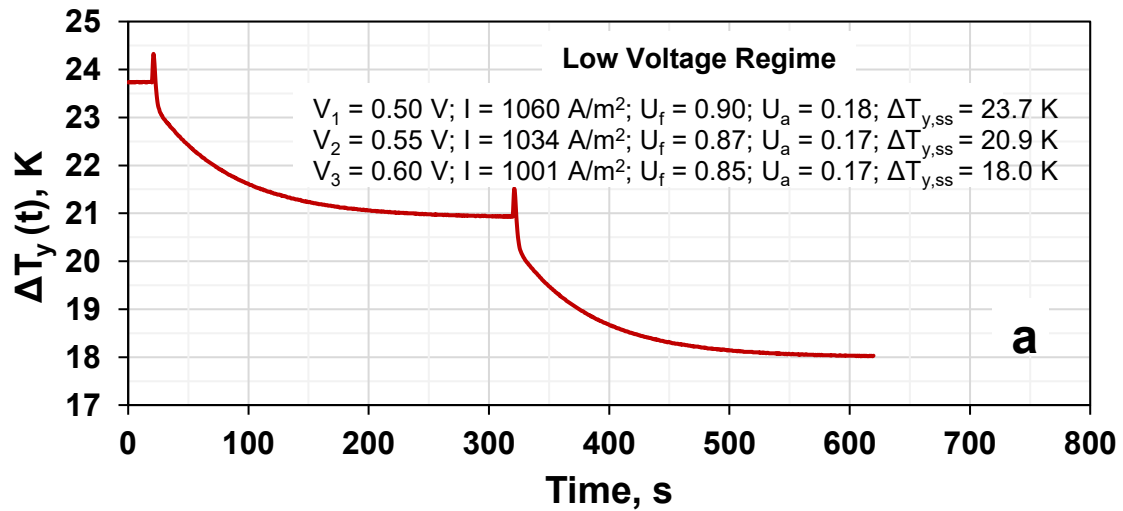


Figure 3.6 The transient temperature difference ( $\Delta T_y$ ) response to the 0.05 V voltage interrupt for (a) low, (b) medium and (c) high operating voltage regimes.

Key components in the equation for achieving high electrical efficiency in SOFC-based systems include the use of high-performance materials (electrodes, electrolyte; interconnects and accompanying contact layers and coatings) and high fuel utilisation ( $U_f$ ) along with minimisation of parasitic losses in the Balance-of-Plant (BoP) components. High  $U_f$  in the cell anode increases the risk of localised fuel depletion and fuel starvation due to concentration gradients, which can lead to oxidation of the most commonly used Ni-based anode, resulting in irreparable damage to the cell and stack. The optimum operating point is a balance between the high operating voltage and high  $U_f$ , and each comes at the expense of the other due to lowering of Nernst Voltage with increasing levels of  $U_f$  with the consequence of lower the operating voltage. This challenge is considered from a thermal viewpoint in this work. For each fuel utilisation target, the SOFC operation will fall in the corresponding voltage regime. The impact of the voltage regime on thermal behaviour is more obvious when characterisation is done through the  $\Delta T_{y,ss}$  versus  $U_f$  data. As shown in Figure 3.7 an exponential pattern is achieved for thermal gradients against  $U_f$  revealing potentially severe thermal gradients for operation at high  $U_f$  ranges (low voltage regime). The high  $U_f$ , therefore, may damage the SOFC health through a challenging thermal management in addition to the increased losses and fuel starvation concerns mentioned before.

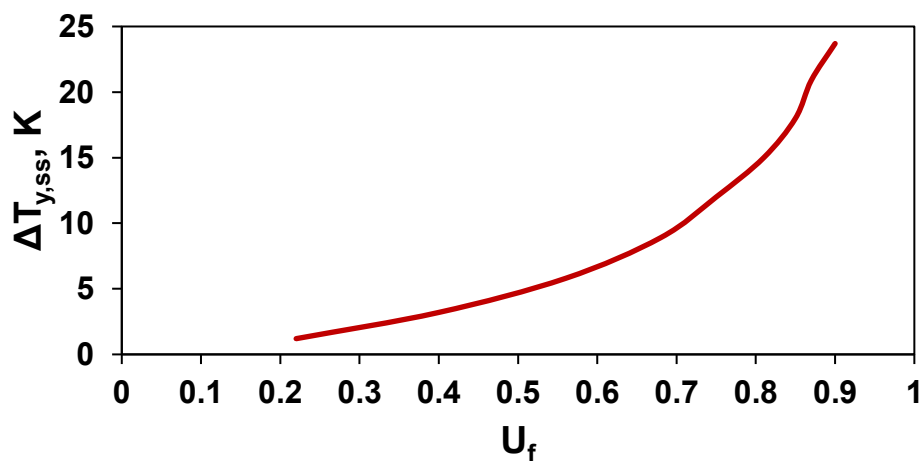


Figure 3.7 The effect  $U_f$  on steady-state temperature difference across PEN

In Figure 3.8, impact of 0.05V variation in operating voltage on  $\Delta T_y$  dynamics is shown. The undershoot and overshoot in  $\Delta T_y$  profile (as a measure of temperature difference instability across the PEN) are more considerable at low operating voltage regime compared to that at higher regime. The settling time, however, is shorter in low voltage case. Both overshoot/undershoot and settling time are crucial to be taken into account in thermal cycle analysis.

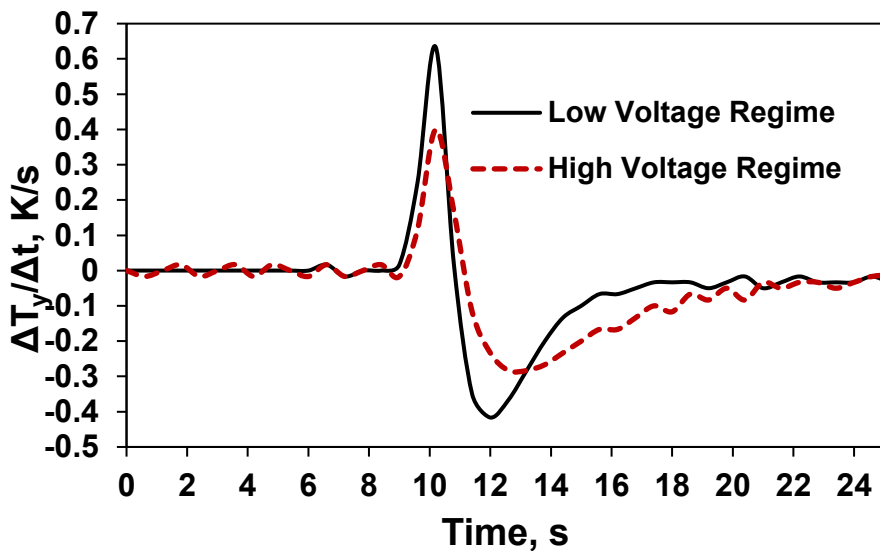


Figure 3.8 Effect of operating voltage regime on the transient temperature difference ( $\Delta T_y$ ) response to 0.05V voltage disturbance taken from figures 3.6a,b, and c.

### 3.6.5 VIM simulation for fuel humidity impact

The steam content of fuel and anode channel is key to enhancing the longevity of the proton exchange membrane fuel cell type because of its vital role in membrane health. The SOFC fuel humidity influences its state variables, internal fuel reformation, voltage losses, and ultimately the overall performance. Moreover, steam is key to mitigate soot formation on the SOFC anode prolonging catalyst and anode active life. From the steady-state performance viewpoint, the amount of steam in the fuel channel is crucial due to its dominant role in reaction rate, OCV and voltage losses. The SOFC fuel humidity may change because of various internal and external reasons causing transient responses in the SOFC. For instance, in a system with an external reformer the steam supply may change with fuel rate, to meet the steam/carbon ratio requirement, that subsequently affect the steam content of the SOFC's feed. Similarly, the equilibrium composition of the reformer product may vary with its operating condition (i.e., temperature and pressure). Moreover, the anode exhaust gas recycling (AGR) is widely used as a practical approach for the BoP water management and fuel utilisation improvement. The recycle stream contains substantial time-dependent amount of steam in transient operations. Both AGR flowrate and its composition (two interactive operating variables) dominate the steam recycled to the anode. The former case may occur when a new AGR set point is implemented, and the latter is expected when SOFC performance fluctuates due to its operating factors, such as load disturbance, leading to the anode outlet composition variation.

The role of humidity in the SOFC thermal dynamics was investigated. A stepwise perturbation in operating voltage ( $\pm 0.05V$ ) was applied and the results of the thermal dynamics were captured as shown in Figure 3.9 and Figure 3.10.

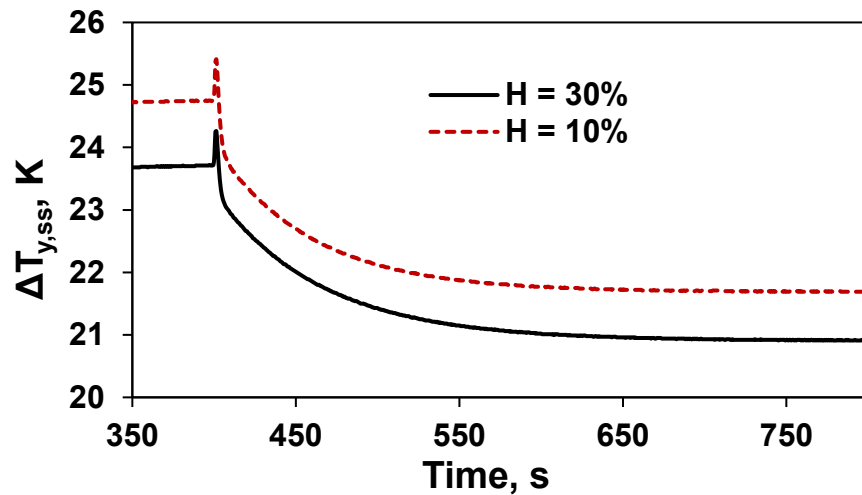


Figure 3.9 Transient  $\Delta T_y$  for the step changes in operating voltage (+0.05V) for operation under two different humidity levels.

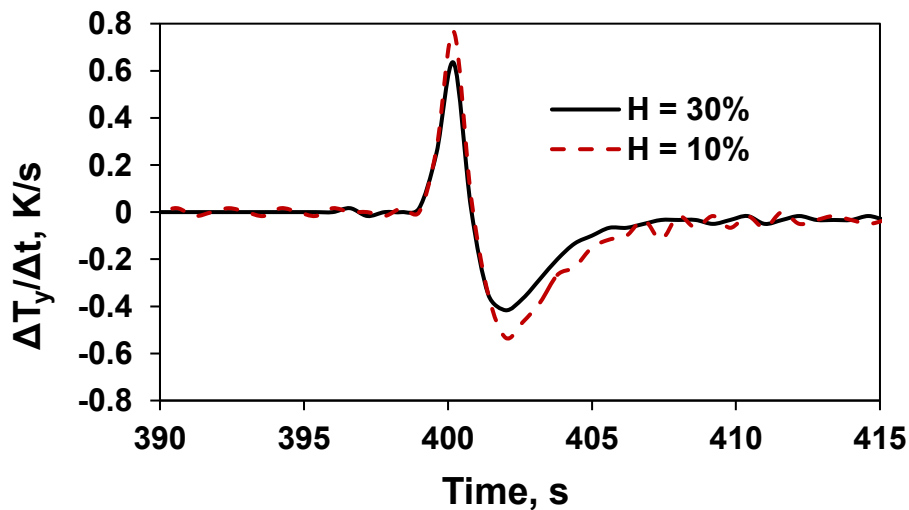


Figure 3.10: Transient  $\Delta T_y$  for the step changes in operating voltage (+0.05V) for operation under two different humidity levels.

### 3.6.6 VIM simulation of enriched air impact

Air is commonly used in the SOFC's cathode as the oxidant supply and coolant. The cathode side gas composition change is mainly due to the oxygen diffusion inside the PEN toward three-phase-boundary sites to feed the electrochemical reaction. The oxygen utilisation is normally low (ca. 10 - 20%) in the SOFC operation. In our previous works [85-87] we have quantitatively shown that the utilisation of oxygen-enriched air (OEA) can improve the SOFC's

efficiency and its thermal behaviour. The efficiency rise essentially occurs due to two reasons (i) the catalyst sites are more effectively occupied by reactants (ii) and higher partial pressure of oxygen boosts the reversible OCV. Thermal improvement can be achieved as has been observed in previous studies [85-87].

The higher partial pressure of oxygen secures the availability of sufficient oxidant throughout the cathode channel minimising the oxygen starvation risk. The utilisation of upgraded air (oxygen-enriched to an optimum level) can increase the efficiency and hence (partly) compensate the parasitic losses such as power consumed for compressing (blowing) the excess air in the system. The excess air is always required for cooling purposes [80, 88, 89]. Application of OEA and even pure oxygen in the SOFC when partial oxidation reaction is the fuel reformation path is appealing as this can minimise/avoid the formation of NO<sub>x</sub> pollutants. Furthermore, it decreases the concentration overpotential at cathode side. Note that the share of concentration polarisation is usually of minimum importance compared to the other voltage losses, i.e., activation and ohmic losses. Nevertheless, oxygen and fuel starvation are serious risks for SOFC health (by accelerating degradations), and efficiency. This supports the SOFC and electrolyser integrated systems where oxygen produced by electrolysers can be deployed in the SOFC realising mentioned potentials. Even though electrolyser's main product is hydrogen, the high-quality oxygen, as its by-product, can significantly contribute to reduction of high operating cost.

The mentioned technical and economic advantages are appealing enough to motivate further investigation of the OEA deployment in the SOFC operation. The impact of oxygen quality on the SOFC thermal dynamics has not been fully understood. In this work, the SOFC transient analysis was explored, by using thermal measures, to evaluate the cells performance operated on both natural air and upgraded air.

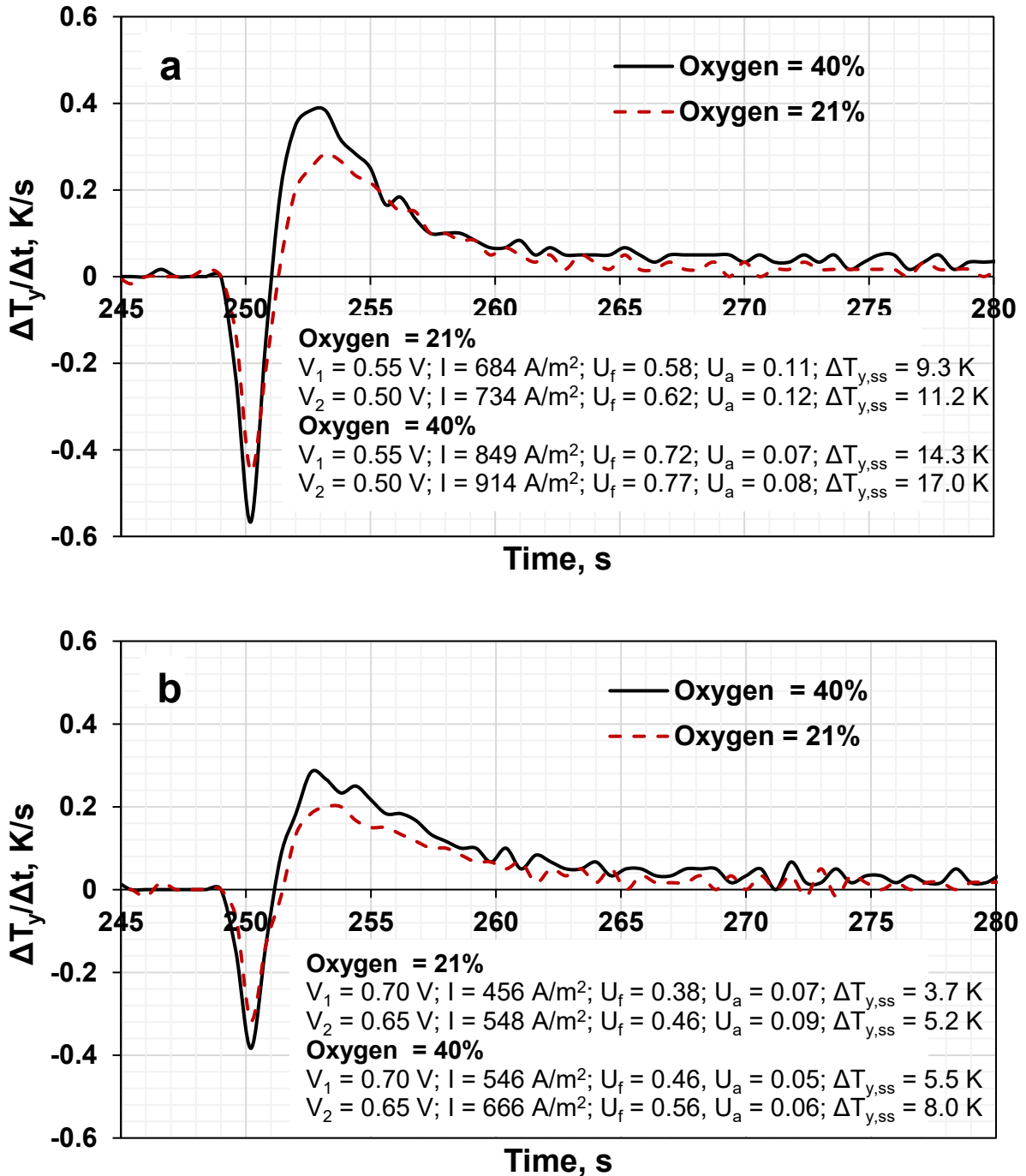


Figure 3.11: Transient  $\Delta T_y$  for the step (+0.05V) changes in (a) LVR (from 0.55V to 0.50V) and (b) MVR (from 0.70V to 0.65V) operating voltage and two different oxygen levels.

The simulation results reveal that application of the OEA in SOFC can be challenging from thermal dynamics (Figure 3.11) viewpoint. The undershoot and overshoot in  $\Delta T_y / \Delta t$  when OEA is used are greater than the case in which normal air is used.

### 3.7 Chapter Summary

The SOFC thermal management plays a key role in its electrochemical performance and longevity. Because of the measurement technical limitations, the thermal behaviour of SOFC is not fully measurable by merely deploying practical techniques. This shortage is even more outstanding when in addition to the temperature distribution the thermal dynamics capturing is of interest. In this study, both experimental and modelling approaches were used in a so-called “hybrid tool” to look into the SOFC thermal dynamics. As an outcome, one of the most crucial issues in assessing the SOFC thermal behaviour, i.e., prediction of the speed at which SOFC reaches the new steady-state condition, became feasible.

For the first time, operating voltage regime concept was proposed and used in this work for the SOFC thermal analysis. It was shown that the voltage regime identification/consideration is significantly useful to provide detailed analysis on the SOFC thermal behaviour. The impacts of the operating strategies, including deployment of OEA and the adjustment of anode side humidity on thermal dynamics were quantitatively evaluated. It was shown that both of these operation variables have effect on the SOFC thermal dynamics and must be taken into account in multi-variable-multi-objective optimisation projects. The outcome of this study is crucial for the optimum cell design in which not only the optimum efficiency is targeted but also a novel control strategy is aimed.

***This chapter has been published to Energy Conversion and Management.***

## 4 Basic and KJ100 controllers

### 4.1 Basic Controller (BC)

Adelan Ltd deploys a commercial controller referred as Basic Controller (BC) in this chapter. The controller is developed in C language environment using Microchip's MP LAB IDE 4.20. The current fuel cell system can function using this controller for basic operations. The BC is capable of controlling temperature, and properly performs the SOFC pre-commissioning including the preheating and fuel/air regulation. The BC, however, possesses several limitations that this project is designed to solve or enhance them. These limitations are mainly relevant to the BC flexibility for parameters tuning, the spectrum of manipulating variables, and the performance/action times. Table summarises the BC's functionalities and challenges that need further enhancement.

Adelan Ltd seeks innovative ideas to boost their  $\mu$ SOFC technology for widespread applications and commercialisation. Currently in the fuel cell electronics section, Adelan are seeking solutions for a smarter ECU to improve thermal stabilisation, data collection and monitoring, connectivity, safety protocols, economic solution, flexibility in software changes and fixes, increase in lifetime and performance that can be linked to the controller and finally reduce the power consumption from the ECU and its peripherals. Operating the fuel cell at a stable temperature is a solution that can be linked to improve lifetime and performance of a fuel cell. Adelan are also closer to commercialising their product, data monitoring and gathering solutions can be an important asset, analysing the device usage history possible errors can be found for future product improvements. Finally, since the fuel cell operates at a very high temperature safety measurements must be made, and a controller equipped with the right sensors could prevent user harm

Table 4.1: The BC functionalities, description, and challenges

Functionalities	Description and challenges
<p><u>Three-stage control:</u></p> <p>BC employs three main stages to achieve controllability on the fuel cell system. These stages are:</p> <p>Stage 1: Warm up stage            Stage 2: Normal operation            Stage 3: Shutdown/switch off operation</p> <p><u>Locked parameters at Stages 1 and 3:</u></p> <ul style="list-style-type: none"> <li>• Heater duty</li> <li>• Reactant air inlet flowrate</li> <li>• Coolant air inlet flowrate</li> <li>• Fuel inlet flowrate</li> </ul> <p><u>Unlocked parameter at Stage 2:</u></p> <p>Coolant air inlet flowrate</p>	<p>The main purpose of the warm-up stage is to heat up the SOFC in order to reach normal operation stage. The time that is required to perform this step is 16 minutes (Figure 4.2, Figure 4.3). Warmup profile can have sudden temperature change these phenomena can lead to cracks in the fuel cell tube. All control parameters for this stage are fixed and the controller does not receive any feedback from the fuel cell until it reaches the normal operation.</p> <p>The normal operation stage is the stage where the fuel cell is hot enough to generate power and heat. The controller starts taking feedback, to stabilise and control the temperature of this stage. The controller receives data from the temperature sensor to produce action signal for cooling fan. The cooling fans speed is the manipulating variable. The fuel cell will switch to the next operation stage once the connected battery is sufficiently charged, or the user has switched off the machine.</p> <p>In shutdown mode the controller will reduce the fuel flow and input air immediately, this process will reduce the temperature however it is not the best approach as once again there is a risk of sudden change to happen then lead to tube cracking.</p> <p>The BC controller functions properly most of times allowing the SOFC to reach targeted temperature range. Nevertheless, the pattern is not repeatable. For each operation cycle the controller behaviour may change. Consequently, there is a risk where the rate of which the temperature climbs up in the core could increase or decrease unexpectedly, hence increasing the risks for fuel cell cracks. This can be averted if an algorithm exists to</p>

	<p>monitor the rate of change of which the temperature rises. In addition, unlocking more parameters and receiving more feedback from different sources will decrease the chance of deviations from temperature which in its turn will increase lifetime expectancy however doing this will require a bit more computing power therefore a more specific electronic chip would be required.</p>
<p>PI (Proportional Integral) controller</p>	<p>The average time in the current configuration of the BC to perform the start-up is 16 minutes (Figure 4.2, Figure 4.3). The controller maintains a stable temperature for <math>\mu</math>SOFC however since it's not tuned correctly there is a higher chance for the temperature to initially overshoot or undershoot before reaching the optimal setpoint.</p>
<p>Data exchange</p>	<p>CANBUS protocol is a data transmission protocol widely applied in the automation industry. CANBUS can connect with other matching devices merely by joining two wires. This protocol is synchronous and robust, but most prominently it manages the signals from less critical to most critical therefore the most important signal alerts the user or the database first.</p> <p>BC will constantly output all information about the fuel cell operation in a systemic CANBUS connection. To collect this information another device is required that will act as a receiver, that device can be another compatible CANBUS controller, PC or commercially available receivers. BC limits this information to be accessed from only one device at a time, therefore in a possible future where Adelan will implement their system to a campervan it will be required for the fuel cell to be connected with the main control unit of the campervan to display the information in the main panel of the campervan. This solution runs the risk of leaving no access for Adelan to use the port to their own benefit. A benefit such as creating another controller that would withdraw the information from Adelan controller and</p>

	transmit it to their database to analyse system errors and performance.
Battery charging	<p>A recent focus in <math>\mu</math>SOFC development is to charge batteries so energy can be stored. The BC controls the battery charging process only based on battery voltage. In a smart/intelligent approach, the battery lifetime and safety must be considered. In more details the BC considers the battery as charged when the voltage is above a specific number and discharged when below a specific number and then immediately connects the fuel cell output to the battery to begin charging. This process will be able to function however the question is for how long as there hasn't been any algorithmic logic to manipulate the battery charging profiles. Finally, there is also no way of telling if the battery has aged.</p>
User-Machine Interface (UMI)	<p>When BC connects to a PC, a custom software called PCAN Explorer is used to inspect the current action. BC communicates with the integrated computer by using CANBUS. This UMI can display plethora of technical information such as temperature, the percentage rate of Air in and the coolant fans percentage rate.</p> <p>A problem observed with this design is that when BC's CANBUS port is used to exchange data with another controller, the UMI cannot be used since the port is occupied by another controller.</p> <p>In addition, PCAN Explorer is an expensive software that is hard for technicians to purchase and does not allow customization.</p>

## 4.2 BC performance in real-life tests

A short  $\mu$ SOFC stack of four cells (Figure 4.1) has been operated in the lab when BC was in place as controller. Temperature along the cells' tubes has been measured at two different points as depicted in Figure 4.1. Unsurprisingly, the temperatures at these two points are not the same causing temperature gradient. An ideal controller may target to minimise the axial temperature gradient as a leading objective. The temperature captured at the first point (T (inlet)) is assumed as representative of Partial Oxidation (POX) area temperature. This is an assumption, as the temperature gradient across the POX are not zero. However, the assumption is reasonable, as the thermocouple has been placed in the middle of the POX.

The casing of the stack improved allows different parts of tube externals to experience same air temperature. In other words, a well-mixed surrounding can be assumed resulting in a homogenous casing temperature.

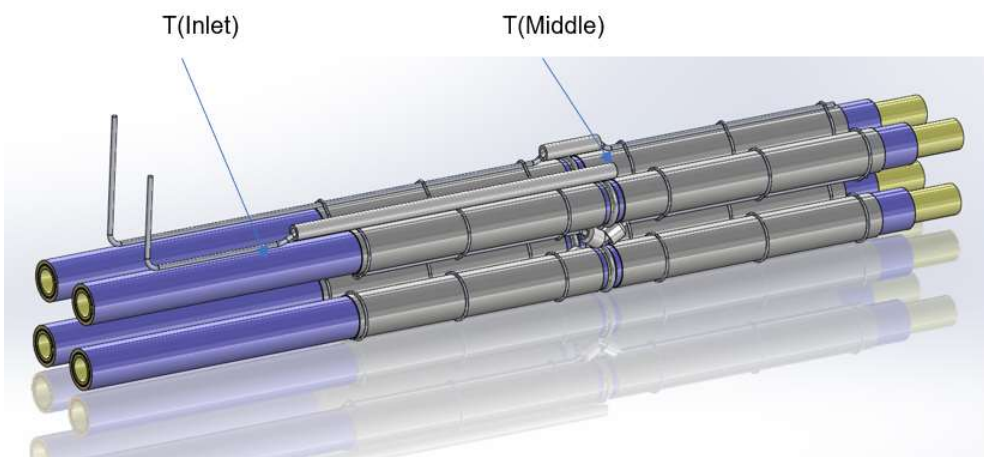


Figure 4.1 A short  $\mu$ SOFC stack (four cells)

Typical test result of BC performance in SOFC control is presented in Figure 4.2. The top profile shows temperature (at two points measured by two independent thermocouples) and fan dynamics. In this test the target temperature is set as 650 °C. The warm-up phase ended at  $t = 16$  min. about 3 min before end of this stage, the temperature was rising and suddenly dropped by 10-20 °C. At this stage parameters are locked (or open loop feedback control). The BC algorithm acts, and the temperature variation is controlled in a reasonable time, compared to the stage time length, and also the overall operation time. However, there is a damage potential, as thermal fluctuations are extremely unhealthy in SOFC thermal behaviour. High temperature up to 700°C could be a safe temperature when the ramping up is smooth. This example demonstrates the importance of a rigorous control technique and strategy for a smooth warming process. Finally, at  $t = 45$ min the shutdown stage is initiated. The

temperature is slowly dropping in this case this time BC manages to perform a nice and smooth shutdown curve.

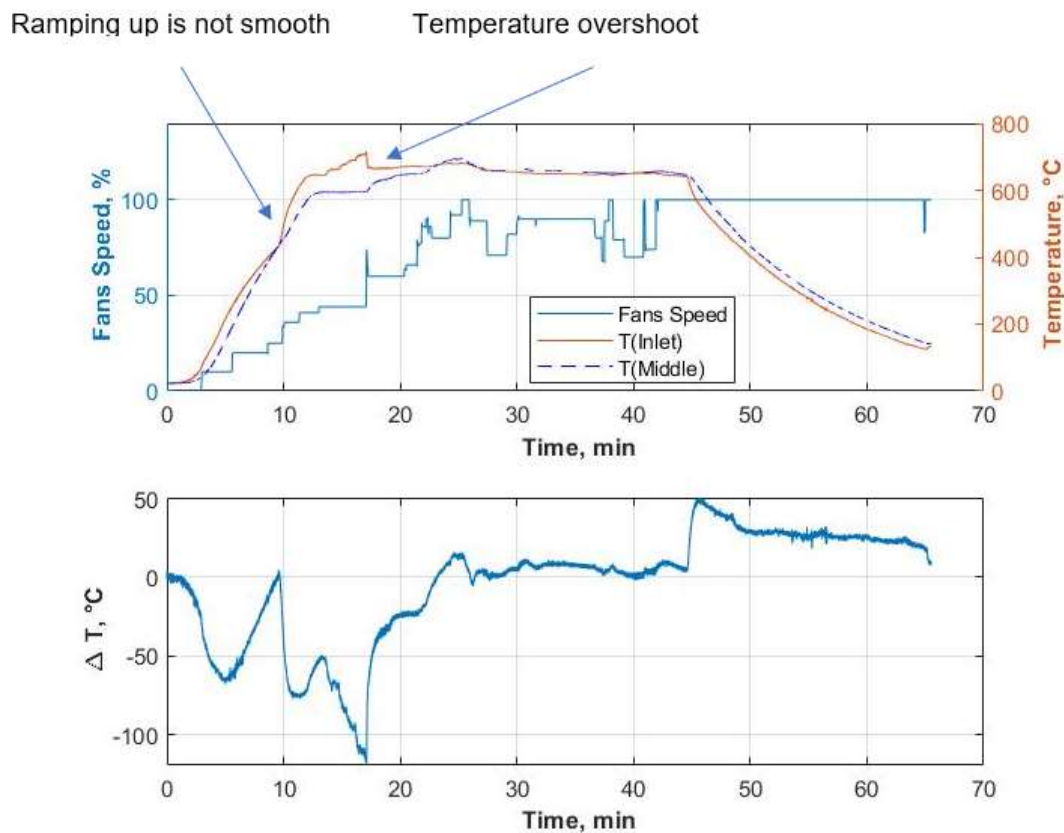


Figure 4.2 Real test on  $\mu$ SOFC thermal performance controlled by BC where  $\Delta T$  is the temperature difference between  $T_1$ (Inlet) and  $T_2$ (Middle).

Another test result of BC performance in SOFC control is presented in Figure 4.4. From first sight BC looks unpredictable raising concerns for its operation trust. For this test the target temperature is set to 700°C. Warm up phase ended at  $t=18\text{min}$ , this is the phase where the fuel cell is capable to generate power and maintain itself by producing heat through the electrochemical reaction. Simultaneously warmup stage has completed, a swift change in temperature can be instantly examined, this sudden change can be connected to the direct change of fuel. This is a challenge that's caused by poor control strategy. On top of that, BC its able to gradually increase the temperature until  $t=23\text{min}$ , then the temperature starts to decline, this demonstrates another poor control management by BC as from this example the speed of the fans has progressively increased to the point that more heat than its required is removed from the system. The controller algorithm should have adjusted the output of the fans to steadily increase in temperature. Furthermore, at  $t=26\text{min}$ , BC has started to react to the decline of temperature and the fans value has decreased and a slow increase in temperature can be seen. However, at  $t=41\text{min}$  BC once again has done the improper optimisations as the

output of the fans have increased and temperature starts decreasing again. Finally at t=45min BC has processed the value of the fans to drop even more than the previous iteration to increase temperature to 700°C. The main task of a fuel cell controller is to keep stable the temperature to the setpoint repeatedly BC fails to achieve a stable temperature as there is an overshoot of +5°C at t=57min and on another timeframe at t=60min the temperature has reached to an undershoot of -5°C. From the perspective of an engineering device, this control method can be classified as good enough since power is generated, and the fuel cell parameters are controlled in a way which is possible to sustain enough heat. Having said that, BC is not demonstrating a great controlling strategy as a temperature instability can be seen all the way through the operation phase of the fuel cell influencing the system's performance and more importantly the health of the fuel cell tubes.

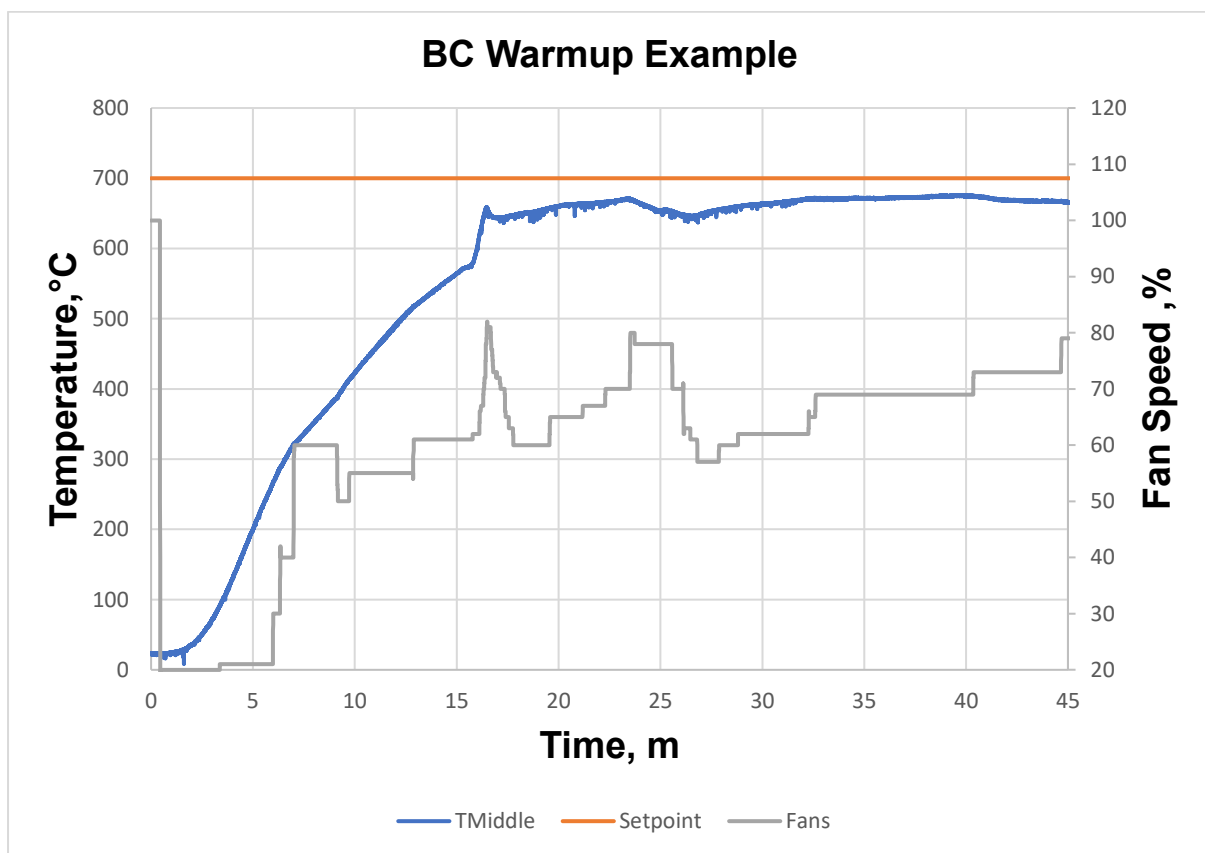


Figure 4.3 BC Warmup scenario

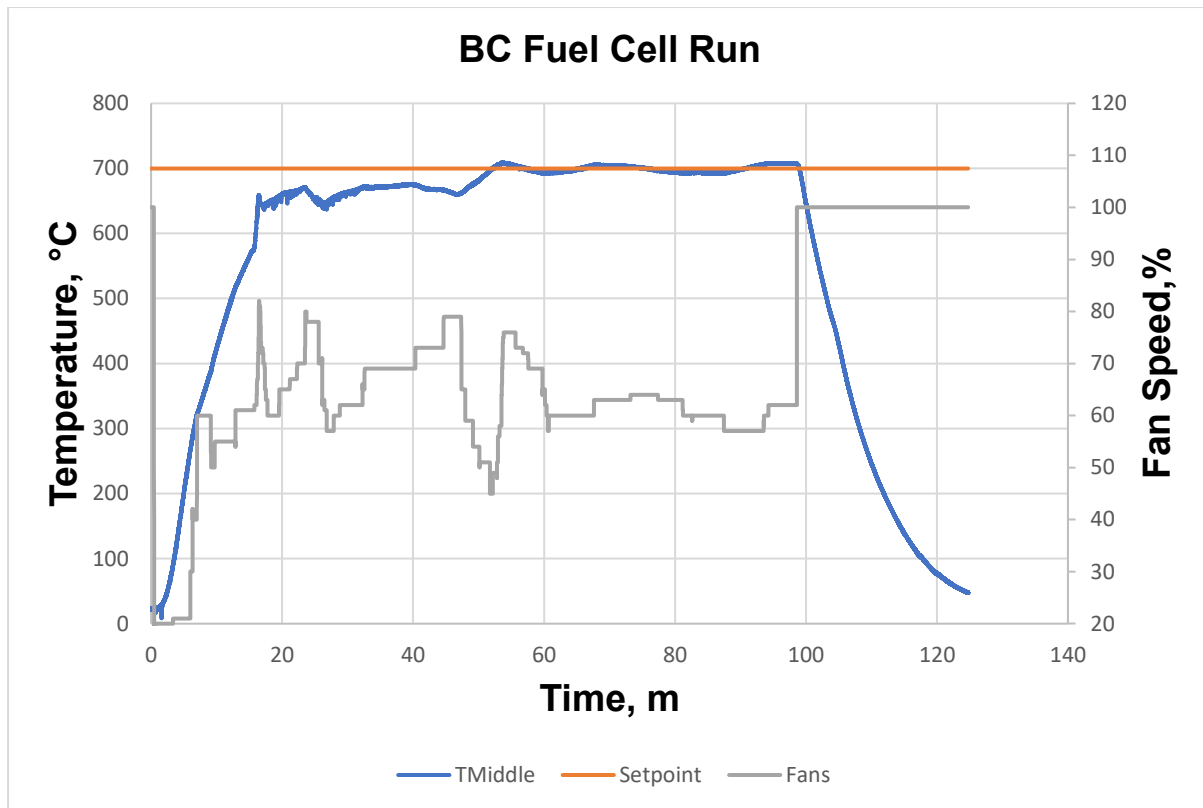


Figure 4.4 BC Complete operation scenario

### 4.3 New Controller

#### 4.3.1 KJ100

In order to improve the technical performance of the BC this project has been designed to (1) demonstrate the main capabilities and limitations of BC, and (2) improve those capabilities and address the limitations in a new controller. The new controller aims to show enhancements in both hardware and software performances. The new controller, KJ100 depicted in Figure 4.5 . It is an early prototype that was designed and prototyped at Aston University hardware with a customised program written in C language. The software was written using Atmel studio 7 (the interface where the code is written) which compiles in AVR GCC. The code that is written in C gets converted to machine language and then the CPU can read the machine language to perform the instructed tasks accordingly. The objective of the early-stage design is to conduct the proof-of-concept, initial research and testing. The purpose of this it was to show that KJ100 can control the  $\mu$ SOFC as good as BC controller. Further improvement is sought in the next sections to demonstrate the added values targeted in this research. In this view, the limitations relevant to the current prototype design to be addressed in the next chapters have also been identified in addition to its promising technical potentials. The typical hardware and software limitations are (1) an optimum design of the box internal space and wires arrangement is not met, (2) the risk of damage is considerable due

to wires, electrical chips and components movement through the enclosure, (3) The KJ100 software has still plenty of computing bugs, such as sometimes the LCD not displaying information or LEDS not indicating the right stage.



Figure 4.5 KJ100 Controller Hardware Prototype

#### 4.3.2 KJ100 Temperature Sensing

To produce the early KJ100 prototype controller various tasks had to be performed. The initial step was to find the right peripherals to use for the design toolkit. As of the nature of the fuel cell and its high temperatures a temperature sensor had to be found. Normal temperature sensors such as thermistors could not be used as the range is not high enough [90, 91]. Therefore, according to the narrow search for the right component/sensor a thermocouple would be the only fit for the project as thermocouples can have different ranges depending of their type, for this project K-Type thermocouple would be the right fit as it covers the range of the Adelan fuel cell operation temperature and there is also some more room if temperature goes over or under expectations.

Table 4.1 Thermocouple types [92-94]

Thermocouple Type	Temperature Range °C	Accuracy °C	Materials
K	-270 to 1260	+/- 2.2	Nickel-Chromium / Nickel-Alumel

J	-210 to 760	+/-2.2	Iron/Constantan
T	-270 to 370	+/- 1	Copper/Constantan
E	-270 to 870	+/- 1.7	Nickel- Chromium/Constantan
N	-270 to 392	+/- 2.2	Nicrosil/Nisil
S	-50 to 1480	+/-1.5	Platinum Rhodium- 10%/ Platinum
R	-50 to 1480	+/-1.5	Platinum Rhodium - 13%/Platinum
B	0 to 1700	+/-0.5	Platinum Rhodium- 30%/Platinum Rhodium-6%

Once the type for the sensor was chosen, the next step would be to find the correct electronic chip to be able to process all these data fast and accurately whilst being compatible with the KJ100 MCU (Microcontroller Unit). Various electronic chips that stated that could support K-Type thermocouple were tested. A noteworthy chip that could deliver was the AD8495 being manufactured by Analog Devices. According to this device datasheet [95] a high level 5mV/°C was produced to detect change from combining an ice point reference with a pre calibrated amplifier. This device was an analogue device therefore for this device to operate with KJ100 it would require the use of the ADC (Analogue to digital converter). Moving on KJ100 ADC could be configured up to 10 bits (0-1023), then using the equation below the right temperature could be found.

$$Temperature = (V_{out} - 1.25) / 0.005 V \tag{4.1}$$

$$V_{out} = ADC \text{ Reading Value} * 5.0/1023 \tag{4.2}$$

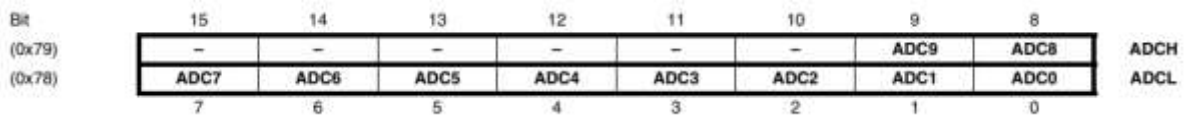


Figure 4.6 KJ100 has an ADC that can be configured up to the clarity of 10 bits

However, when the above setup was tested with various temperature scenarios it was noted that the accuracy of the readings would not be satisfactory, reaching up to +/- 10 degrees

difference than what it should be. After some troubleshooting it was found that the KJ100 ADC could not keep up with the small variations and different amplification techniques had to be taken to possibly reduce the issue. Though, this was not worth it as not only it would require extra hardware, but it would require extra repairing time just for the sensor. Consequently, the decision to move to a different electronic chip was made.

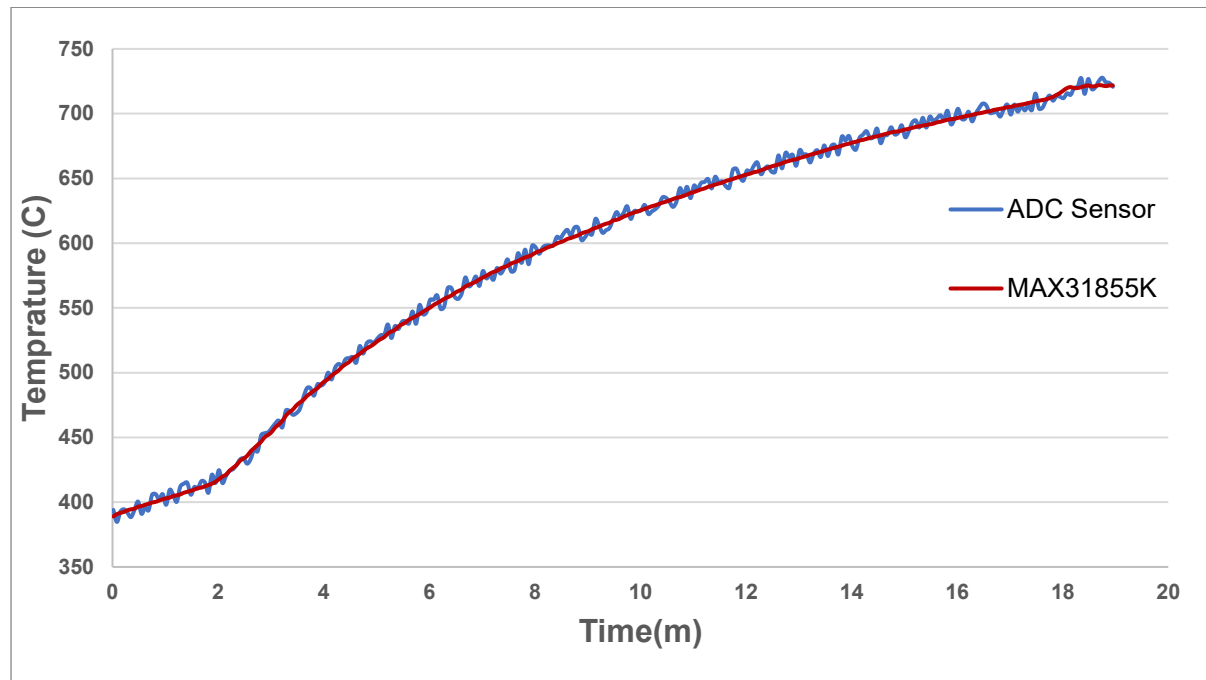


Figure 4.7 ADC in comparison with SPI chip temperature accuracy

Since the previous analogue electronic chip wasn't able to read the temperature from the thermocouple very accurately, a more suitable electronic chip was required. To make sure previous mistakes weren't going to occur a more suitable digital chip was chosen to perform the reading and the conversion on its own while simultaneously feed the data to the microcontroller through the serial peripheral interface (SPI) of KJ100. In addition, this chip offers fault detection capabilities such as when the chip has been short circuited, or a thermocouple has been disconnected. However, to use this device, SPI had to be configured on KJ100 to be able to receive the temperature readings that the MAX31855 electronic chip had computed from the thermocouples. The way this device sends data according to Table 4.2 is in 32 bits where bits 31 to 18 would carry the temperature reading of the thermocouple. Bits 15 to 4 would carry the reference junction temperature of the thermocouple, whilst bits 16,2,1 and 0 would be the device warning bits. To read this a specific software that was able to split the 32 bits and analyse them was written for KJ100.

When the whole temperature sensing was connected and arranged the main controller was able to read the temperature correctly with step changes of 0.25°C. Finally, when the thermocouple would be disconnected KJ100 would receive a temperature reading of 2047°C which is way above the max 1260°C of K-Type thermocouples and it would flag the controller to perform specific actions for this.

Table 4.2 Data being transferred to K100 by temperature chip

BIT	14-BIT THERMOCOUPLE TEMPERATURE DATA				RES	FAULT BIT	12-BIT INTERNAL TEMPERATURE DATA				RES	SCV BIT	SCG BIT	OC BIT
	D31	D30	...	D18	D17	16	D15	D14	...	D4	D3	D2	D1	D0
VALUE	SIGN	MSB 2 <sup>10</sup> (1024° C)	...	LSB 2 <sup>-2</sup> (0.25° C)	Reserved	1 = Fault	Sign	MSB 2 <sup>6</sup> (64° C)	...	LSB 2 <sup>-4</sup> (0.0625° C)	Reserved	1 = Short to VCC	1 = Short to GND	1 = Open Circuit



Figure 4.8 Recommended use of MAX31855 by the manufacturer

### 4.3.3 Fuel flow

From the literature and the sensitivity analysis we know that fuel input is an important manipulative variable to the fuel cell as it is able to directly affect the thermals and also the power output. BC controller is able to feed a specific amount of fuel to the system only, as this manipulative parameter is a fuel valve connected between the system and the LPG cylinder. This fuel valve is a 12V DC electronic device where its state is either open or close, in the intermediate warming up stages, Adelan fuel cell requires a bit less fuel flow than in the operation stage, BC is able to reduce the fuel input by switching the state of the fuel valve on and off on different timings. This technique is not providing any feedback but most importantly

it's possible that the amount of fuel that goes to the system could be not enough therefore causing a fuel starvation.



Figure 4.9 Solenoid LPG Fuel Valve

KJ100 is able to solve the fuel input control by using a controllable valve which can be adjusted by giving a PWM signal. In contrast with the BC Valve, KJ100 valve is controlled with current instead of voltage therefore a new circuitry was specifically designed for this as show in (Figure 4.9).

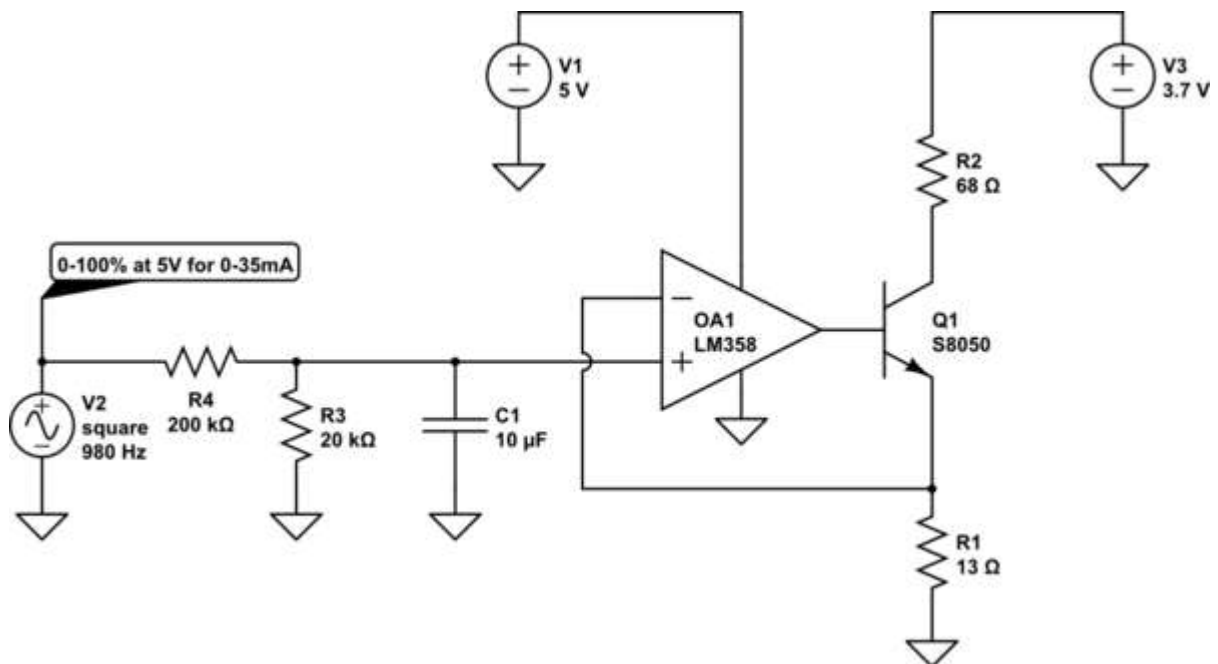


Figure 4.10 Circuitry designed specifically for the proportional valve used in this project.

Finally, once a controlling device was in place the calibration process took place where using an external mass flow fuel controller created by the reputable in the field Bronkhorst Ltd, the sensor was calibrated for the system.

#### 4.3.4 Gas and pressure sensor

In the previous sectors it was mentioned that KJ100 must reproduce all the current functionality of BC and advance to a better control. In addition to this, the new controller is also targeting to address and improve in safety concerns where possible. To do this, two safety sensors are picked up to improve operation, those are MQ6 where is a gas sensor with high sensitivity detection to LPG, Butane and propane gases and the other sensor is a pressure sensor to detect leakage across the connecting pipes between the LPG and the system. Both these sensors in this design are used to prevent leakage of propane in a different way. MQ6 sensor can be thought like a generic smoke alarm inside houses which can be calibrated to one setting, therefore this sensor will be calibrated to environmental gas leakages. On the other hand, the pressure sensor will be inside the system pipes to detect small pressure changes which could prevent bigger issues from happening before MQ6 detects them.

Two of the most possible fuel leakage scenarios could be addressed differently. For instance, if small pressure drop is found between the pipes that could mean the fuel flow has changed and some sort of small leak is happening, this type of leak possibly won't affect operation significantly therefore the controller will have time to adjust and shut down efficiently while issuing a warning command for service to the user. In the scenario however where MQ6 is triggered that means that too much propane has leaked in the environment which could indicate safety concerns therefore the fuel cell will immediately cut operation and trigger an alarm. A future update to the controller will also be able to broadcast this message to the Adelan cloud IOT.

The firmware for both these sensors was calibrated for use with KJ100. MQ6 sensor is a



*Figure 4.11 Micro Pressure Sensor fitting into the pipes*

device which connects to the analogue interface of the KJ100. A converting equation was used as it has been used in previous temperature sensors to translate the voltage output of the MQ6 to a digital value from 0-1023. The pipe pressure sensor is a very small device manufactured by Honeywell, with a product name MPRLS0015PG0000SA. Calibrating this device required again a method that was also used previously, SPI interconnection. The mater controller (in this case KJ100) must send a command to the chips address to request the data from the sensor, these commands would be the

hexadecimal numbers 0xF0, 0x00, 0x00 and 0x00. The sensor would respond and start sending the data in a 24-bit combination. Finally, an equation was used to derive the output of this sensor as shown to the following section.

Table 4.3 SPI Configuration for the Pressure Sensor

		0XF0	0X00	0X00	0X00
<b>KJ100 SENSOR FROM SENSOR KJ100</b>	<b>TO</b>	Command to specific sensor	00 HEX	00 HEX	00 HEX
	<b>TO</b>	SENSOR STATUS (Final pair of 8 bits)	DATA 24-16 (third pair of 8 bits)	DATA 15-8 (Second pair of 8 bits)	DATA 7-0 (First 8 bits)

$$Pressure = \frac{(Output - Output_{min}) * (P_{max} - P_{min})}{Output_{max} - Output_{min}} + P_{min} \quad (4.3)$$

Where,

- $Output_{max}$  = output at maximum pressure(counting)
- $Output_{min}$  = output at minimum pressure(counting)
- $P_{max}$  = maximum value of pressure range (bar, psi, kPa etc)
- $P_{min}$  = minimum value of pressure range (bar, psi, kPa etc)
- $Pressure$  = pressure in Pa
- $Output$  = total counting of digital reading of pressure sensor

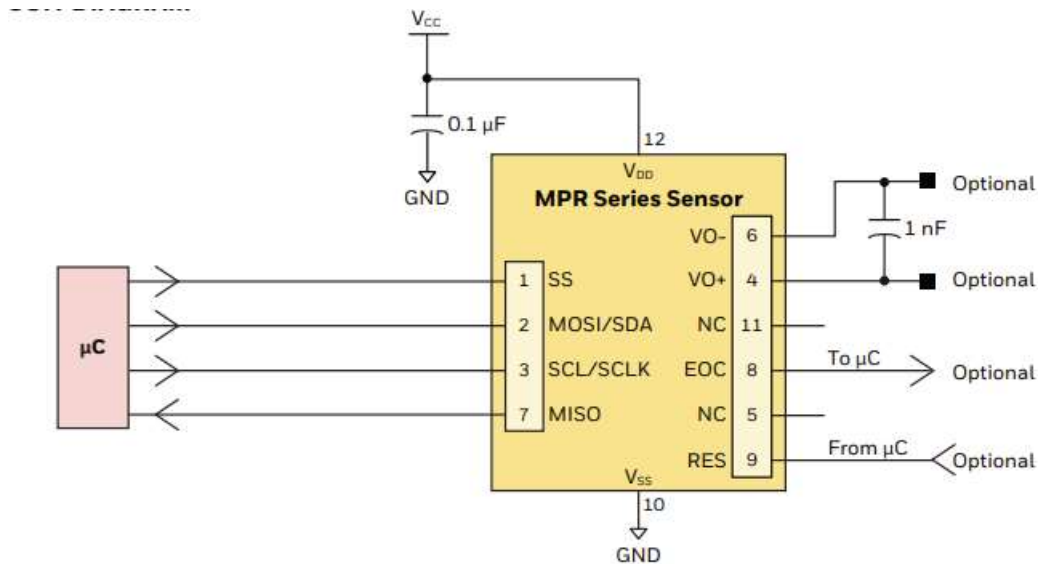


Figure 4.12 Two-way connection with KJ100

#### 4.3.5 Power output sensor

While the fuel cell is in operation mode one of the techniques to measure performance is to simply look the power output of the fuel cell at different loads over time. By looking at the history of the device power output it's a convenient way to see if the fuel cell has degraded. Current Adelan BC is not able to read the power output of the fuel cell and a secondary external machine is used to measure its power output. KJ100 is able to read the power output of the fuel cell by using an electrical chip called INA260. A planned next version KJ101 will be able to store the data and show the history of the power output of the system.

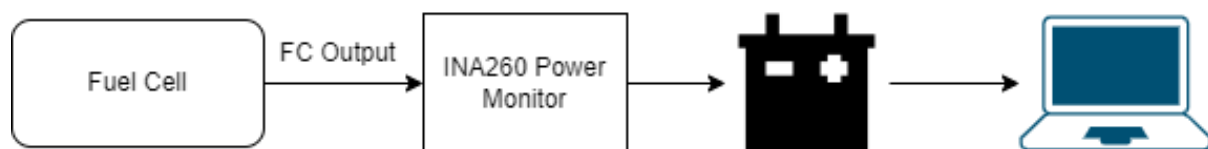


Figure 4.13 Implementation of Power chip

The INA260 is a digital output, current, power, and voltage analyser that is compatible with I2C (Inter-Integrated Circuit) and SMBus™ interface with a precise shunt resistor built-in. It enables high-precision current (up until 15A) and power readings, over-current identification (can withstand up to 100A for 10seconds) and observations at voltages in the common-mode range from 0 to 36 volts V, which is unaffected by the supply voltage. The device has a current-shunt monitor, which is bidirectional, low- or high-side that tracks the amount of current flowing through the internal current sensing resistor. KJ100 connects with the power chip using I2C this is a communication protocol that it only requires two signal wires to exchange information. Sending the commands as shown in Table 4.4 the device will send back the corresponding

instructions in 16 bit where it needs to be converted in decimal. To calculate Current and Voltage the 16 bit value must be converted to decimal value then multiplied by 1.25.

*Table 4.4 INA260 address information*

<b>Pointer Address (HEX)</b>	<b>Register Name</b>	<b>Function</b>
00h	Configuration Register	All register reset, Averaging conversion times calculator
01h	Current Register	Current flowing through the sensor
02h	Voltage Register	Voltage flowing through the sensor
03h	Power Register	Power flowing through the sensor
06h	Mask/Enable Register	Flag that can be configured when sensor reading has finished
07h	Alert Limit Register	Can be configured to alert when a certain value has reached
FEh	Manufacturer ID Register	Manufacturer identification
FFh	Die ID Register	Unique number for the specific electronic chip

#### 4.4 Schematic

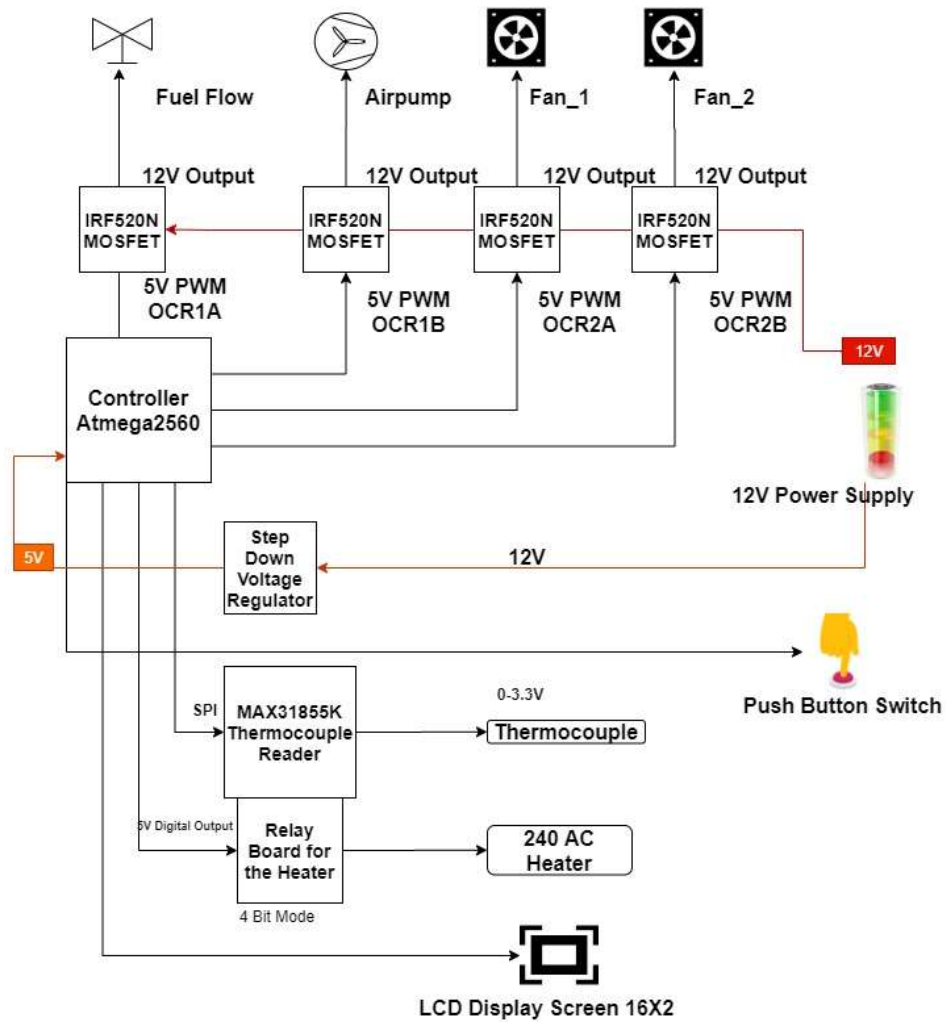


Figure 4.14 KJ100 Schematic system diagram

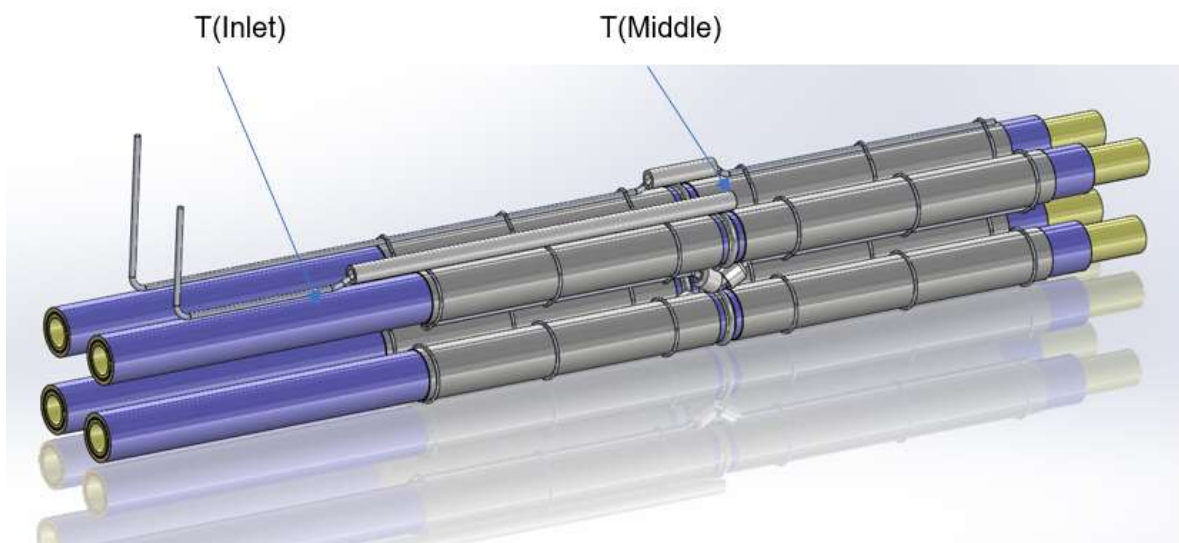


Figure 4.15  $\mu$ SOFC four cell stack

In Figure 4.16 a schematic of KJ100 hardware is shown. The controller is designed to draw power from a 12V battery as the fuel cell unit will be mainly attached to batteries from campervans which operate at 12V. In the schematic the voltage regulator (U2) is used to regulate the voltage from the source to the CPU which in its turn requires 5V. In addition, the fuel cell parameters (fuel valve, cooling fans and pump) require 12V to function, so four Metal Oxide Semiconductor Field Effect Transistors (MOSFET Q1-Q4) were used as switches. The output of the PWM (Pulse Width Modulation) from the controller is at 5V, the MOSFETS can translate this 5V pulse to 12V pulse for the parameters to switch accordingly.

The KJ100 requires noise protection therefore a standard decoupling technique with four 100 nano farad capacitors(C3-C6) and an inductor were used to reduce signal noise.

The connectors (J1,J2,J3,J9,J10,J11) are paired together by category for useability because in a scenario where a parameter needs to be inspected it will be easier to locate and get it unplugged/plugged, the peripherals connectors are codenamed J1 (Fans, Air Pump, Fuel Flow), J2 (Warming up heater), J3 (debugger connector), J9 (LCD Screen connector),J10 (Pressure Sensor Connector), J11 (Gas Sensor Connector), J12 (12V Power Supply Connector).

As previously noted, the programming language used for this build is C where it can be compiled and flashed to the KJ100 using the J3 connector in the schematic. C is a high level language where its commonly used in microcontrollers due to its ability to let the programmer have access to any type of its surrounding such as RAM (Random Access Memory),ROM (Read Only Memory) and most importantly EEPROM (electrically erasable programmable read-only memory) where some important values can be stored here, for example if a parameter would require tuning a technician could change its value by using UMI therefore the next time the controller will be operated that tuning will be saved.

The brain of this controller is an Atmega2560, this CPU is manufactured and produced by Atmel (recently bought by Microchip), Atmega2560 offers 256KB flash memory significantly more than 4KB compared to that of the BC. This means that KJ100 code storage is less limited, in addition KJ100 offers double the amount of output/input configurable pins than BC's CPU, which 16 of them are timers/counters and 16 of them are PWM capable as well, this leaves room for future changes or additions to the system whilst having the option for sleep mode which draws only 500 $\mu$ A.

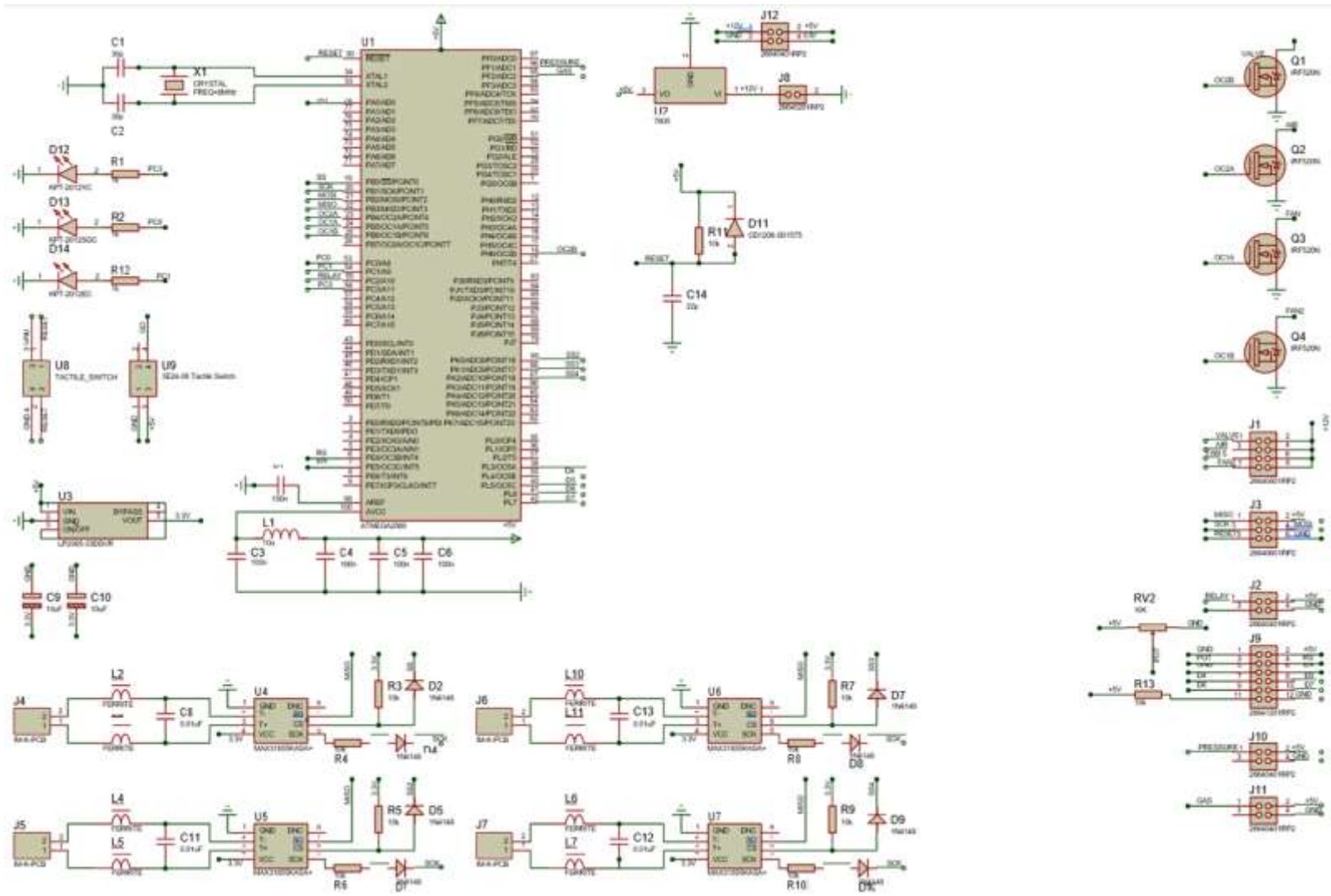


Figure 4.16 KJ100 Electronic Component Schematic

## 4.5 KJ100 Functionalities

Table 4.5. The capabilities and limitations of KJ100

Functionality of KJ100 controller	Challenges identified for improvements in KJ101 controller
<p>KJ100 bring the three main stages from BC to achieve controllability on the fuel cell system.</p> <p>These stages for simplicity are also called</p> <ol style="list-style-type: none"> <li>1. Warm up stage</li> <li>2. Normal Operation</li> <li>3. Shutdown/switch off operation</li> </ol> <p>Locked parameters at stage 1 and 3</p> <ul style="list-style-type: none"> <li>• Heater</li> <li>• Air in (to be mixed with fuel)</li> <li>• Coolant air in (used to stabilise fuel cell temperature)</li> <li>• Fuel in</li> </ul> <p>Unlocked parameters at stage 2</p> <ul style="list-style-type: none"> <li>• Coolant air in</li> </ul>	<p>At warm up stage KJ100 places the predefined values to the different parameters to reach normal operation such as BC. A future design will consider steady rate of change warming up where all parameters will be dynamically adjustable to achieve a smooth warmup until operation mode. Finally making the controller fully dynamic from start to finish.</p> <p>Normal operation in KJ100 uses the same logic as BC where the system is stabilised by adjusting the coolant air flow from the temperature sensors feedback. However, the KJ100 uses a PID technique which is widely known for its better accuracy and stability in control systems. A future version will address the current limited parameters where for example fuel can be manipulated to adjust the heat generation and the power output of the system. A strategy manipulating air and fuel in real time can increase the system thermal stabilisation and presumably achieve optimal power generation.</p> <p>Shutdown operation is being ported from BC and follows the same steps.</p>
<p>KJ100 will also enter shutdown operation if it identifies problems such as if the propane feed is not sufficient based on, line pressure.</p>	<p>Currently the identification works by placing a cheap pressure sensor in the line, though this sensor is not pre calibrated therefore a</p>

<p>It discovers extremely high temperature and ensures the thermal safety by limiting extremely high operation temperature of the <math>\mu</math>SOFC. KJ100 will also record these failed attempts and will not permit any more start-ups unless the controller is hard reset, or the fuel cell is serviced.</p>	<p>better calibrated sensor will ensure that in different environments the right value is read by the controller. The way sensors are being recorded by a digital device is through the ADC (Analogue to Digital converter), this ADC reads the value from a range from 0-1023 (10bit). Usually, reputational manufacturers give instructions on how these values have been calibrated.</p> <p>Sometimes controllers can have some internal electromagnetic interference where temperature sensors could read wrong values for less than a second. Hence, a smart algorithm is going to be in place to exclude those missteps</p>
<p>KJ100 can regulate a battery charging process of 12V Lead Acid Battery.</p> <p>The current implementation charges the battery at normal operation stage based on its Voltage, if the battery voltage drops below 12.3V the controller will initiate start up sequence and by the time the battery voltage has reached 13.4V the controller considers the battery charged. The time that it requires to charge the battery its dependant on fuel cell power output, size of battery and load of the battery.</p>	<p>12 Volt Lead Acid Batteries have been designed with a specific charging technique in mind which most battery manufacturers providers follow. Following this charging profile ensures that batteries can last longer. The first thing which is required is the size of the battery. Then from this point the maximum allowed charging current can be found where the maximum current is 30% of its battery capacity. Then different basic equations are used to calculate the cut off current which usually ranges from 3-5% of the maximum capacity of the battery (see <a href="#">Section 3.3</a>).</p> <p>What is mentioned above is a technique that KJ101 will adapt to charge the battery efficiently to reduce battery degradation.</p>

<p>The speed of data exportation using Universal Asynchronous Receiver/Transmitter is 9600 (baud rate). KJ100 also does data exportation through CANBUS using standard 2.0A 11 BIT identifier that is of interest due to its consistency for Adelan devices</p>	<p>Currently KJ100 can output CANBUS signals, however these signals are not in sync with the frequency and identification protocol that the basic control introduced. Future improvements will copy those IDs and structure them from least important to most important.</p>
<p>NA</p>	<p>Electromagnetic Interference (EMI) is the capacity of electrical gear and frameworks to work acceptably in their electromagnetic condition, by restricting the inadvertent age, engendering, and gathering of electromagnetic energy which may cause undesirable impacts, for example, electromagnetic impedance (EMI) or even physical harm in operational hardware. This is a test that electrical controller needs to pass so they can be commercialised therefore KJ101 hardware must be designed in a way to pass this test.</p>
<p>A Customised User-Machine Interface (UMI) has been designed to operate with KJ100 (Figure 4.20). The interface can display the live data of the controller such as Temperature and Power though manipulative variables are displayed in gauges such as fans speed measurement. Whilst all this are live the values are stored in the background by being written to a csv file.</p>	<p>Currently there is a challenge where KJ100 cannot receive input messages from the UMI. The problem rises from the controller itself as at this time there is an issue when the controller its set up to receive messages it stops doing all the other activities and constantly awaits, this is a problem that requires investigation. One More problem is from the UMI periphery where the UMI can realize the connection to the controller but when the value is being transmitted, the controller does not get it.</p>
<p>NA</p>	<p>Minimisation of overshoot and undershoot is shortfall in BC and KJ100. This extreme fluctuation can impact the lifetime of the fuel</p>

	cell. The overshoot is happening due to the tuning of the P-I-D terms. The controller parameters adjustment for KJ100 was based on try and error. In an improved version of KJ100 (i.e., KJ101) these terms can be calibrated by using experimental data and theoretical model to learn how the fuel cell behaves.
--	--

Table 4.6 KJ100 Current Parameter Description

PARAMETER	FORMAT
Date	DD/MM/YYYY
Time	HH:MM:SS
Stack inlet temperature	Degrees C, 1 decimal place
Stack mid-temperature	Degrees C, 1 decimal place
Battery voltage	Volts, 2 decimal places
Air fan speed	%
Air pump speed	%
Fuel Value Status	0 (off) or 10 (on) or 8(on) or 1 (on)
Pressure sensor voltage	Volts, 2 decimal places
Pressure10BitValue	10 Bit Number, 0-1023, 0 Lowest Voltage, 1023 Max Voltage
Go Button	0 (off) or 1 (on)
Heater relay status	0 (off) or 1 (on)
Battery charging status	0 (not charging) or 1 (charging)
Stack Voltage	Volts, 2 decimal places
Stack Current	Amps, 2 decimal places
Stack Power	Watts, 2 decimal places
Force Stay	1 bit, 0(False) or 1(True)

KJ100 can perform a self-test scenario. This is a useful tool that can be used to inspect the controller is performing normally before it is connected to the system. The time shown in Figure 6 is in seconds. However, this does not represent the real-time a testing system is going to take as this time is the time that the controller takes to perform the test while the temperature is increased with a step change of 10°C/s.

Clarification Notes:

- In Figure 4.17 right before the  $T=100$ , the fans speed drop to 0 that is happening because that is where the PID controller starts while the controller feedback sample rate is significantly decreased due to the time the simulation takes to run. However, in the next step change the fans speed jump to their maximum value, this again is perfectly normal and expected since from 670 the controller jumped to 680 which is a big heat gain for a second. The fans speed continue to their maximum value as the temperature continuously increases.
- Figure 4.18 shows the status of the charging controller of the battery. If its 0 the relay that connects the battery and the fuel cell is switched off while if it's a 1 the relay is switched on and the output of the fuel cell passes to the battery to start charging. For this operation to happen one criterion is for the battery to require charging while the other one is for the fuel cell to be in the right temperature to start the charge. Therefore, in this simulation-test the battery is constantly 12V and as it can be seen the relays switches to 1 only when the fuel cell is in the temperature.
- Currently the fans, air pump and fuel valve in KJ100 are measured in percentage. However, that percentage is the voltage output of the controller (PWM). In the future design, (KJ101) adding to software changes hardware changes are also going to happen while more reliable measurable devices are to be inserted to the system, these devices will be able to give real time feedback of their current action such as airflow for the fans and fuel flow for the valve.
- Warm-Up state 0-80 (s), Operation state 80-130 (s), Shutdown state 130-200 (s).

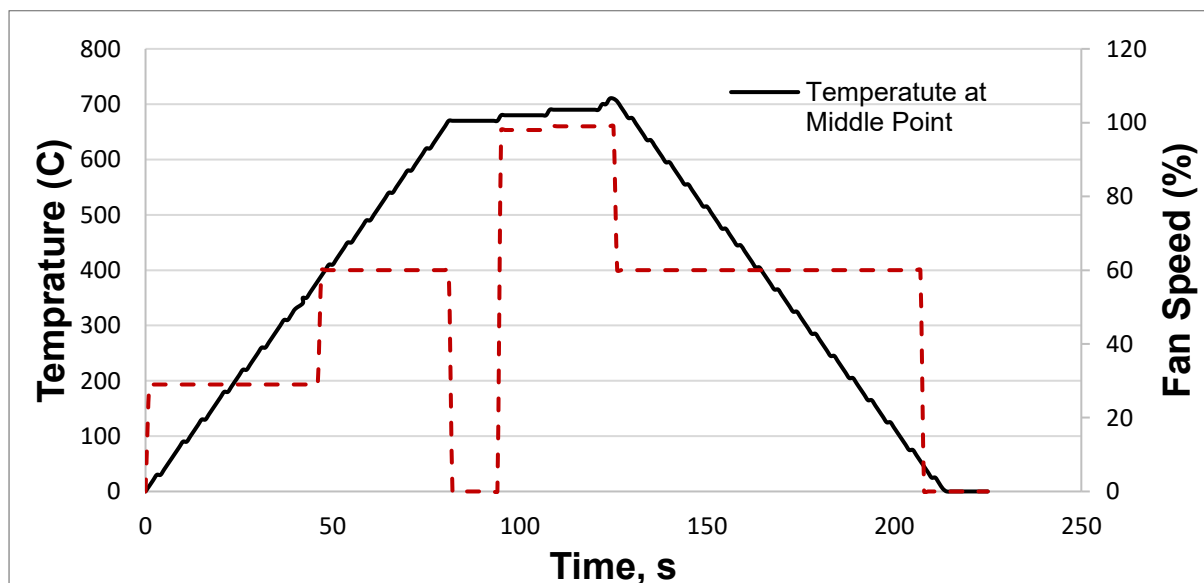


Figure 4.17 KJ100 self-simulation test

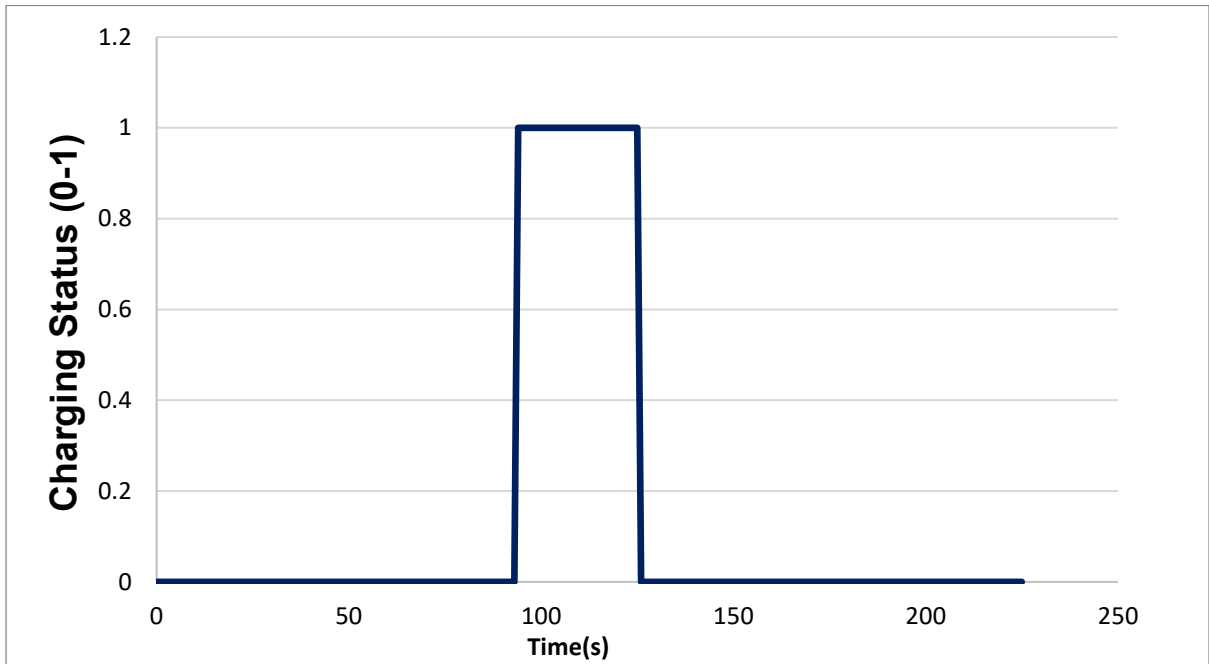


Figure 4.18 Battery charger status

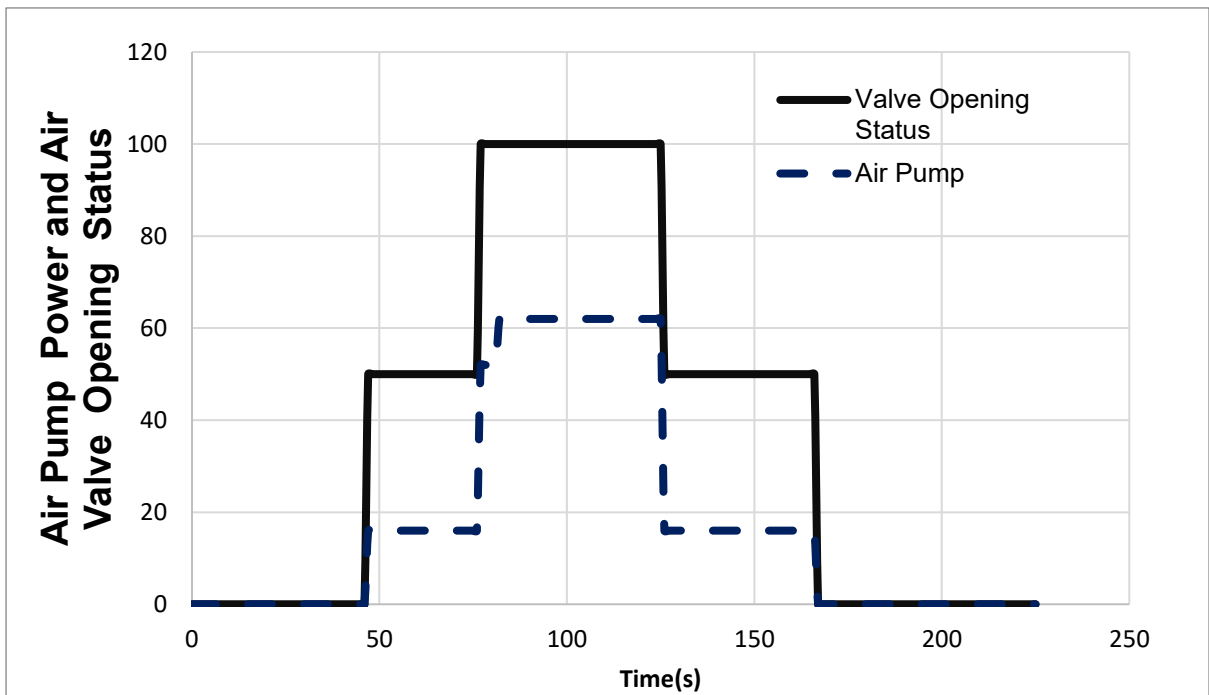


Figure 4.19 Fuel valve and air pump power output percentage (PWM)

## 4.6 User Interface

To enable the system to be easily monitored an interface was developed using Node-RED originally made by IBM. The User-Machine Interface (UMI) is shown in Figure 4.20. The data presented on UMI and those that are behind scene are saved as a CSV file on the supporting computer. These data are accessible for post-processing, post-calculations, and further presentations in a second environment such as MATLAB or Excel. The controller outputs the data in a specific serial format where it is separated by commas for example: “Variable1,100, Variable2,24” then the software separates these values by a JavaScript macro which is been written to allocate its value to a different graph.



Figure 4.20 User Machine Interface (UMI) essential parameters such as power output and temperature as shown.

### 4.6.1 Future Plan for improvements for UMI

Currently the UMI displays the output of the controller status, it graphically represents important parameters such as temperature, its able to record the fuel cell power output and display other important information such as warming up warnings. Currently Adelan dashboard can only receive outputs kj100 and display its status, with its next iteration a two-way connection will be established (full duplex) where the user will be able input data such as the current LPG size for KJ101 to estimate its current fuel status.

## 4.7 Battery

Industrial controllers that charge batteries usually go through three phases 1) constant current, 2) constant voltage and 3) trickle charge. Trickle charge is a technique for battery chargers to keep the battery charge at its max this is happening by providing to the battery the same power as its discharge rate. In this case the fuel cell being constantly on to make sure the battery is fully charged its not to be desired as the fuel cell being on, consumes the same amount of fuel in either mode. Therefore, KJ100 will be leaving the battery at 95% charge rate to ensure the fuel cell has consumed a decent amount of fuel while leaving the battery at a charge rate where it's almost full and operational. Additionally, there should be reverse current protection from the battery, there should be voltage and current sensors for the controller to check the current reading of the battery and then the controller to adjust accordingly. Also, there should be a circuitry to adjust the voltage output from the fuel cell since the fuel cell operates at its best power whereas 10.5V, yet the battery at constant current needs 10A (calculated by 10% of the battery capacity), and when at constant voltage the battery needs at minimum 14.4V while the current reaches right about 3% of the battery's maximum capacity which means it is charged. (Figure 4.21)

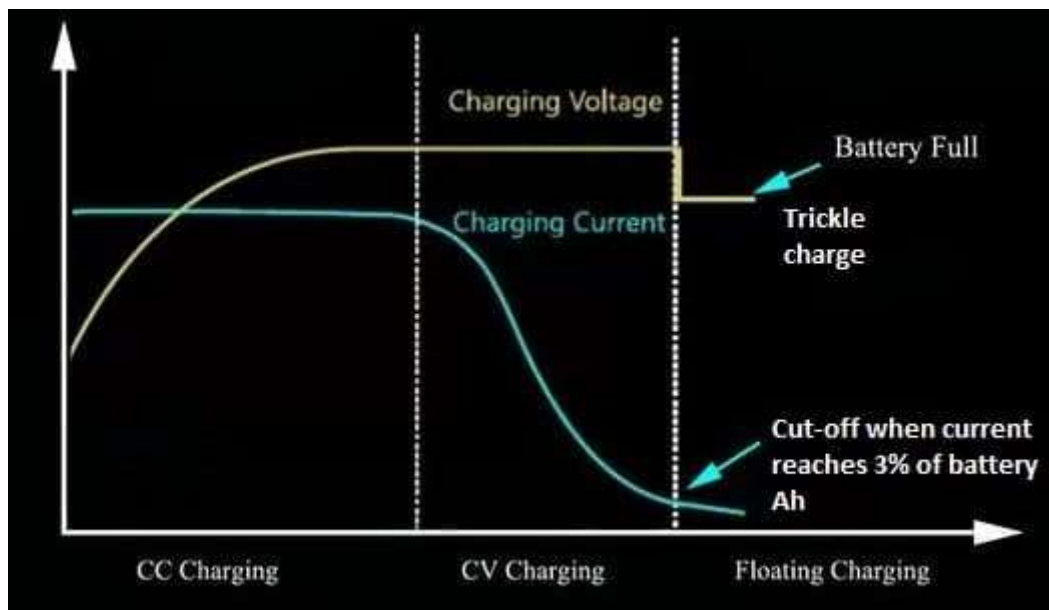


Figure 4.21 How a 12V battery charging profile looks like

The current designed system by Adelan main functionality is to keep the attached battery charged up and to ensure optimal uninterrupted operation of the connected devices. Therefore, battery management and utilisation are of a very big importance to maintain a healthy battery life. Currently BC doesn't support any battery charging maintained capability.

The battery connects directly to the DC output of the fuel cell, this connection is not efficient for both of the fuel and the battery. Currently from the sensitivity results it is known that the current Adelan fuel cell outputs the maximum power at a stable 10.5V, a direct connection to the battery would change this voltage and settle to a value that is between the 12V battery. This way the battery would charge at a very slow rate as the fuel cell will not operate at its maximum power. KJ100 can solve this by including a DC-DC converter, the fuel cell will constantly operate at 10.5V where it will feed to the converter to be transformed to the specific voltage that the battery would require at that phase to perform charging as it will be discussed to the next section.

To perform this task KJ100 must be equipped with the right hardware initially. This hardware needs to read the current level of the battery, then able to output the right amount of Current and Voltage during the battery charging phase. KJ100 analogue inputs can receive up to 5.5V therefore a custom voltage divider was created, the output of the battery will feed to the input of the voltage divider where the corresponding value will be mapped to the output of the voltage divider from a range of 0-5V (Figure 4.23) and with the right analogue to digital manipulations KJ100 will be able to read the battery voltage.

BQ2031(Figure 4.22) is an electronic chip manufactured by Texas Instruments where its main purpose is intended to improve the charging of lead-acid batteries. The bq2031 can regulate constant-voltage, constant-current, or pulsed-current charging thanks to a variable pulse-width modulation regulator [96]. In addition, with the of the switch-mode design power dissipation is kept to a minimum for high charge current applications like the case of the fuel cell which outputs up to 10A. This chip will begin charging immediately as the connection is done or the battery has been swapped therefore a relay is between the battery and the controller (fuel cell can charge the battery only in operation mode).

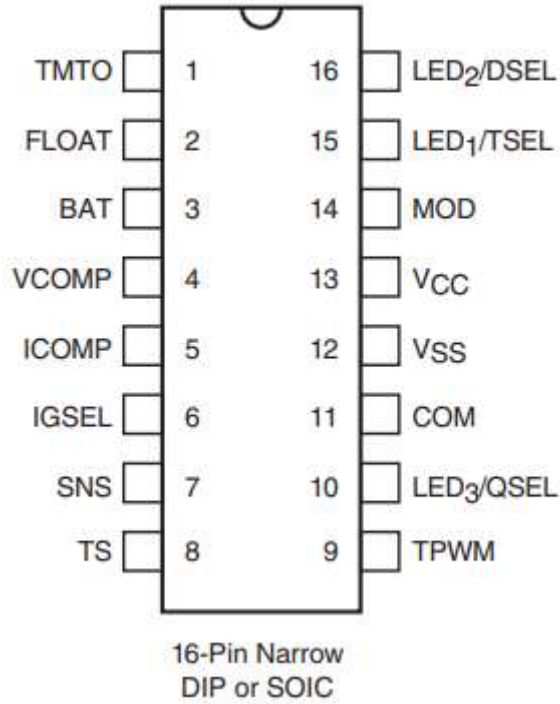


Figure 4.22 bq2031 battery monitor chip for KJ100 pinout

The battery voltage divider that was used earlier to read the voltage of the battery was also used to connect a scaled battery pack voltage to the BAT pin of the electronic chip which then would provide an appropriate value of float voltage to the FLOAT pin. Typically, the resistance values are provided by the battery manufacturers specifications notes. However, to avert the possibility of the divider draining the battery while the battery is disconnected the RB values have to be calculated to the minimum possible value which is between 150kΩ and 1MΩ.

$$\frac{RB1}{RB2} = \frac{(N * V_{FLT})}{2.2V} - 1 \quad (4.4)$$

$$\frac{RB1}{RB2} + \frac{RB1}{RB3} = \frac{(N * V_{BLK})}{2.2V} - 1 \quad (4.5)$$

$$I_{MAX} = \frac{0.250V}{R_{SNS}} \quad (4.6)$$

Where:

- $N$  = Number of cells
- $V_{FLT}$  = Desired float voltage
- $V_{BLK}$  = Desired bulk charging voltage
- $I_{MAX}$  = Desired maximum charge current

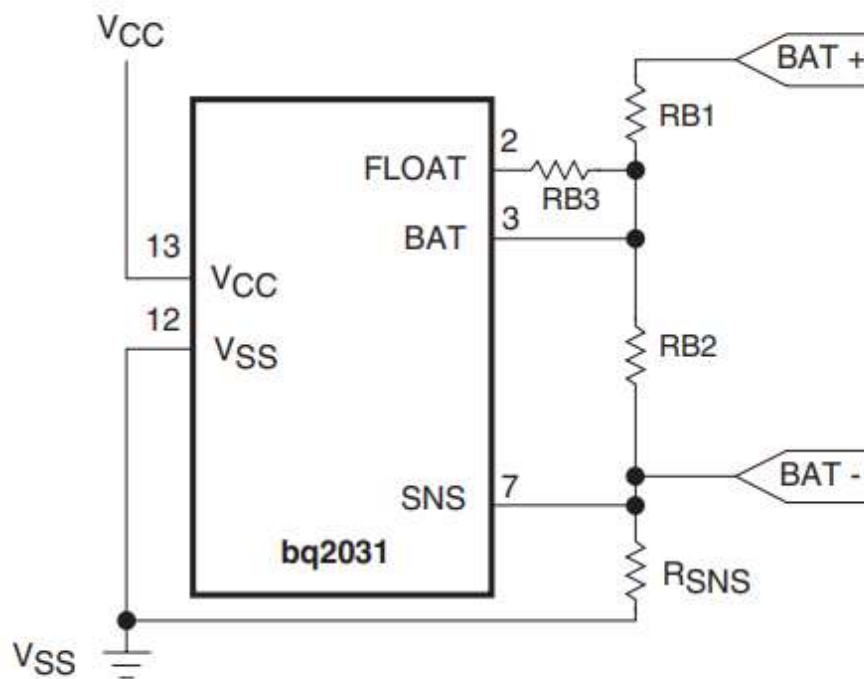


Figure 4.23 Voltage Divider

For safety purposes KJ100 if it detects the battery is lower than the threshold the system will try trickle-current charging for a period then if the battery voltage doesn't rise to the allowed range, the timer will run out and perform fuel cell shutdown. This technique in contrast with BC will prevent the case of charging damaged or polarity reversed batteries. Finally at all times KJ100 will monitor the battery temperature and will stop charging and flag a user warning if battery temperature rises above normal.

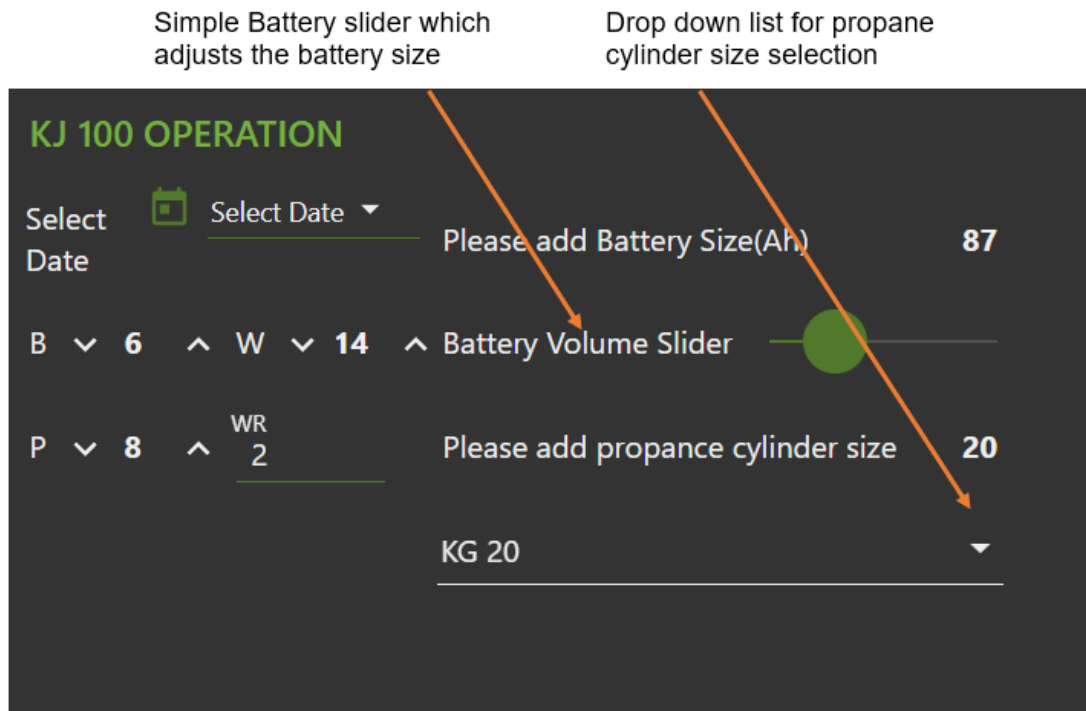


Figure 4.24 Simple Questions to the user

#### 4.8 Future Tasks

Whilst the KJ100 was demonstrated to be able to control the fuel cell there were a number of issues that needed to be resolved:

- There must be a battery charging circuitry for safety such as a reverse current protection or a fuse within the proposed controller.
- All the different hardware components that have been tested need to be combined in a unified design. For example, the board should have pins to connect to the devices immediately without anything external to be required.
- The board should comply with Electromagnetic Combability (EMC) rules.

Once these issues have been resolved in the hardware side of things then the workload will be mainly shifted to software improvements. Priority on software improvement will take the battery charging technique whereas it has been mentioned earlier the software will need to account for the whole cyclic behaviour of the battery such as voltage control and current control. Next software addition will be to have a rate of change behavioural prediction of the temperature, since it has been proven that the sudden increase or decrease in temperature can do severe damage to the fuel cell, the suggested algorithm will be able to adjust the operational parameters in such a way where it will balance out as much as possible of those rapidly increasing/decreasing temperature changes.

## 5 Hardware Controller Design

### 5.1 Design and Development of the New Controller, KJ101

In the previous chapter the limitations and the shortages of the current Adelan controller BC were shown. It was found that BC was not opting in for maximum efficiency and performance, in addition some critical features were missing such as battery charging circuits. KJ100 was proposed, KJ100 was engineered in house in EBRI labs to empower initial steps such as writing and compiling the software. KJ100 was able to perform the same tasks as BC. Furthermore, KJ100 was enhanced with more features, such as being able to change the fuel flow accurately and being able to detect faults and deal with them to ensure safety from various sources. However, KJ100 was created as a prototype unit, and it had its own limitations.

Few of the limitations of Adelan KJ100 that had to be addressed:

1. **Electromagnetic combability** was not considered, since this project is in partnership with an industrial company, the company would not be able to sell this as its required by law to pass EMC
2. **The hardware approach for KJ100 was modular**, even though this approach will accelerate the making of the prototype it has one major flow. Each module was purchased from a different supplier and each supplier had designed their module as it would fit in their design, therefore this would introduce uncertainty to KJ100
3. **Hardware was packed**, to connect each module with the main Micro Controller Unit (MCU) multiple wires had to be used. Each module had little to no secure connection therefore wires could possibly be pulled out while in operation
4. **Operation under hot temperature**, since all the cables and the modules would reside inside the enclosure, the temperature without cooling will increase, which can affect the longevity of the MCU and at very rare occasion cause a sudden shutdown
5. **Heavy duty devices**, once again the prototype was modular, and each purchased module was designed from various providers to test the functionality of each chip. Which would result in more power draw by not using efficient circuitry
6. **Impossible for mass manufacturing**, to scale this every single module would have to be printed individually and the rest of the components mounted to a location this would introduce unnecessary costs and time.
7. **Noise in the system**, component placement plays a significant role in electronics especially when it has to do with sensitive signals, in this case KJ100 was experience some noise interference therefore in some cases the thermocouples would report the wrong value while in warming up the fuel cell.

Therefore a solution to this problem is designing a custom Printed Circuit Board(PCB) which would be designed specifically for Adelan fuel cells where it would save space, reduce cost, be EMC designed and repeatable for production ensuring quality. In the following section a discussion is made about the designing process of the PCB and the next version of KJ100.

The electronic circuit can be designed with multiple component positions and track routes. Nevertheless, every PCB is designed accordingly to each application criticality and requirements and as Bradley et al., has shown following design guidelines can lead to a reduction of 22dB [97].

Various chip and silicon manufacturers recommendations that can be done to reduce noise are:

- An individual ground plane. Signal traces ideally should be routed as close as possible to the ground plane to further reduce crosstalk between other traces from other components[98].
- In a four-layer design, ground and power plane should have their own individual layer
- If ferrite beads are used, they should be closer to the noise source( Figure 5.1)
- To place the bypass capacitors as close as possible to the corresponding component with different values usually ranging from 0.001 $\mu$ F to 1 $\mu$ F
- Series termination should be used to decrease the signal reflections related with other digital signals. Usually, a 50 to 100 $\Omega$  resistor for output pins and a 35 to 50 $\Omega$  for an input pin
- Power plane offset it is recommended, this offset should block signal traces to come close to the board edge by 1.27cm where an exposed grounded fence should be presented to allow for electrostatic discharge
- If a part of the plane needs to be broken down it would be better to be done with a row of holes than a long slot[99]
- A PCB design can be improved by categorising the various zones, for example it would be better to have the digital signals away from the analogue ones, as digital signals generate high frequency digital noise and it could interfere with analogue operations. In the same manner a high current zone can be also created to separate the board[100].
- If there are two adjacent signal layers in the circuit board structure, routing should be performed horizontally on one layer and vertically on the other. This reduces the risk of coupling (crosstalk) between the two layers of conductive tracks.

- 45-degree angle trace turns are more preferred than 90-degree turns which can increase radiation
- If there is space available power and ground traces should be wider than the rest of the design
- All unused I/O pins should be connected to power or ground or firmware configured as outputs to eliminate switching noise from the main MCU[101]

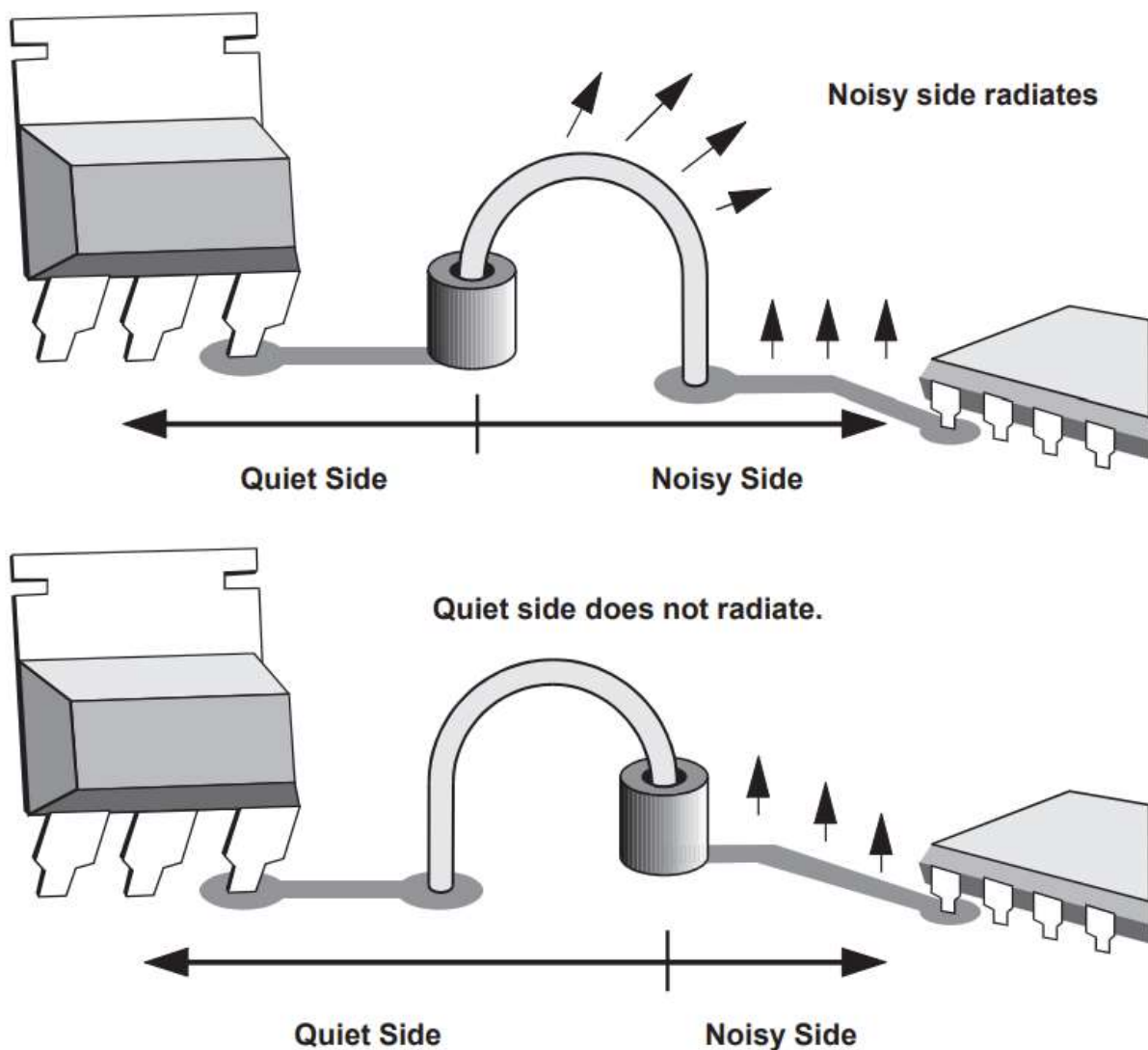
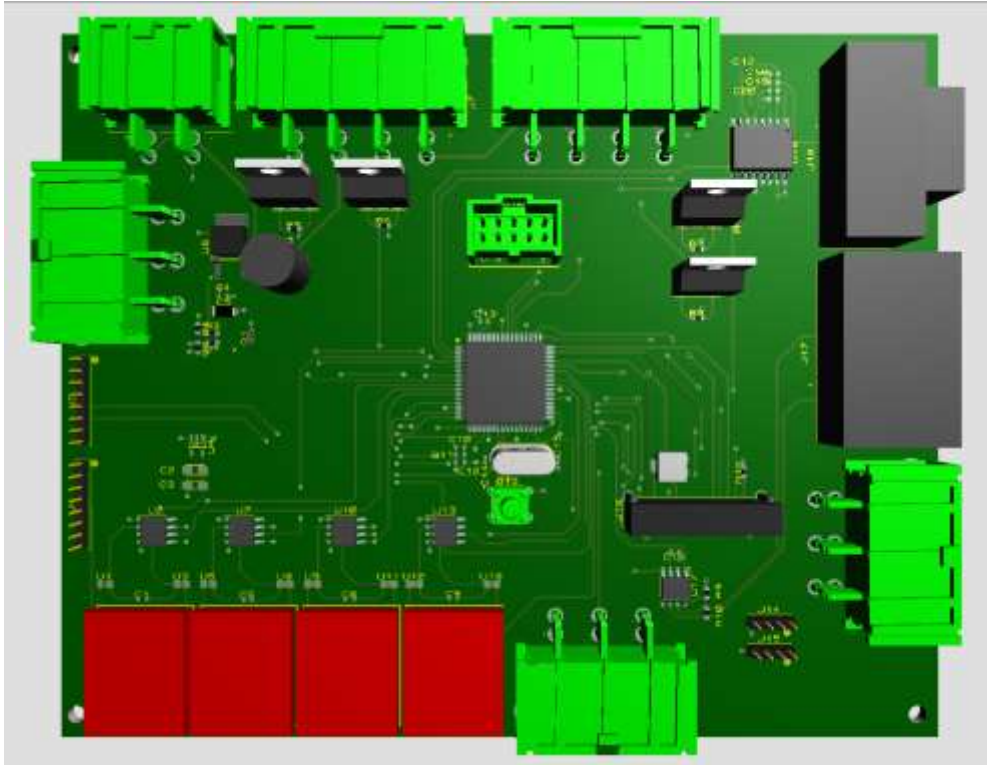


Figure 5.1 Ferrite Beads should be closer to the noise source [99]

Below two images are generated by Proteus PCB designing software tool. The images are 3D rendered by the software after the PCB was routed. KJ101 is designed to enhance the capabilities of KJ100.

The KJ101 main CPU is an AT90CAN128, this microchip has 64 Pins of which 90% of them are utilized for the control strategy and the fuel cell required peripherals. The most important feature of AT90CAN128 in comparison with ATMEGA2560 is the CANBUS channel included within the chip whilst offering the capability of configuring the CANBUS channels throughout the chip registers, increasing code efficiency and decrease unexpected communication errors.



*Figure 5.2: 3D rendered image of KJ101 (top view)*

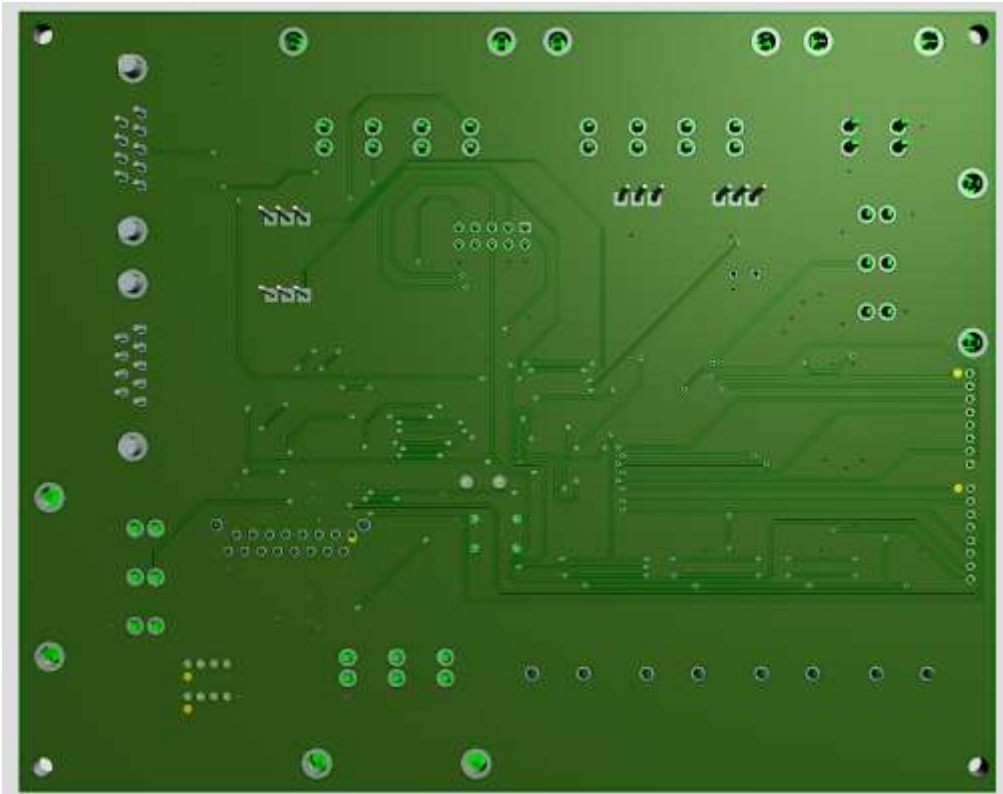


Figure 5.3: 3D rendered image of KJ101 (bottom view)



Figure 5.4 Printed Board

## 5.2 Schematic

KJ101 schematic has also seen some changes as it has been split into four sheets for ease of access and readability. One of the things in the first root sheet is the power delivery connector which can connect to a 12V leisure battery where the voltage is stepped down to 5V for the CPU to operate and then reduced furthermore to 3.3V by another voltage regulator to operate the thermocouple chips.

The second root sheet is displaying the four thermocouple chips (MAX31855) that are able to detect the thermocouple temperature changes in the mV range, this translation is then being fed to the main CPU through the SPI channel (MISO, CLOCK, SS).

The third schematic is for the CANBUS and RS232 connections, for both of them a transceiver chip is being used. The transceiver for the RS232 connection can translate the 0-5V signal of the microchip to the 0-24V range for personal computers compatibility which is useful debugging information from the firmware. This means that it also reduces costs in cable purchases as there is no need for expensive FTDI (Future Technology Devices International Limited) cables as the translator is included inside the controller design and a normal rs232 cable will be able to display all the debugging information. The CANBUS transceiver is included in the design as it is a standard chip being used universally from different companies to ensure compatibility with all other existing CANBUS devices. It is worth noting that these two connectors (in the current design) RS232 and CANBUS with the right firmware can be used to convert an RS232 signal to CANBUS or vice versa.

One of the main requirements for KJ101 is to be able to operate with a 12V input as it would have to be powered by a 12V campervan battery, therefore that voltage is directly designed to pass to the controller and then the controller directs this to the fuel cell hardware manipulated parameters. In addition, for this to be compatible, power amplification is required for the 12V devices such as air fans. The PWM signal gets amplified from 5V of the CPU to 12V by the IRF520N MOSFETS. Finally, in most fuel cells out there, the power output of the fuel cell directly connects to the load (in this case battery) however KJ101 will be in the middle and this will happen by having a 12V battery relay where it will switch ON only when the controller has detected that it is safe to connect, this cannot be neglected as if the battery draws power from the fuel cell at a point where the fuel cell is not in operation mode (for SOFS not being hot enough) it can directly destroy the fuel cell or even cause a short circuit at few cases.

Table 5.1 KJ101 connectivity description

Pin Number	Pin Declaration	Description
9	Chip Select 5	Signal that selects Pressure Sensor over SPI
10	Chip Select 1	Signal that selects thermocouple 1 over SPI
11	SCK	Synchronized clock over all SPI connections
12	MOSI (Master Out Slave In)	When with chip select a chip has been selected this output the data
13	MISO (Master in Slave Out)	When external chips have been prioritized by Chip select the AT90CAN is able to read the data
14	OC2A (Output Compare Register 2A)	This is register when it overflows 0-255 it triggers an interrupt in the system. This interrupt is being counted and calculated in the code using the 8MHz oscilloscope to time out the samples the PID is taking.
15	OC1A	Timing frequency interrupt for when an RS232 is sent (currently set to 4 Seconds)
16	OC1B	Timing frequency interrupt for when a CAN message is sent (currently set to 1 Second)
17	OC1C	The output compare register is set as FAST PWM. The code inside KJ101 is written to accommodate for this mode. While a macro exists inside the code to adjust the percentage manually or dynamically from the PID feedback loop.
27	RXD1	Receiver from serial rs232 connection
28	TXD1	Transmitter from serial rs232 connection (used to display controller status information)
30	TXCAN	Transmitter from CANBUS connection (used to display controller status to a CANBUS supported device)
31	RXCAN	Receiver from CANBUS connection (used to receive CAN signals to manually interfere with the controller)

35	PC0	L.E.D.
36	PC1	L.E.D.
37	PC2	240V electrical heater relay
38	PC3	L.E.D.
39	PC4	Battery relay acting as switch to connect the battery with the fuel cell when it is required
40	Chip Select 3	Signal that selects thermocouple 3 over SPI
41	Chip Select 4	Signal that selects thermocouple 4 over SPI
44,45,47,48,49,50	LCD Enable, Reset, Data Pin 1,2,3,4	4X24 Conventional small LCD Display
46	Chip Select 2	Signal that selects thermocouple 2 over SPI
51	PA0	Input switch
54,55,56,57	JTAG Pins TDI, TDO, TMS and TCK	Pins that are utilized by an external debugger to upload the user written firmware.
61	ADC0(Analogue to digital converter 0)	Analogue propane sensor

Category	Quantity	References	Value	Stock Code
Capacitors	14	C1,C4,C6,C8-C13,C16-C20	0.1 uF	C0603C104K5RAC-TU
Capacitors	2	C2-C3	10µF	TAJS106K006RNJ
Capacitors	1	C5	47 uF	T55A476M6R3C0070
Capacitors	1	C7	220 uF	UHE1E221MPD1TD
Capacitors	2	C14-C15	20 pF	C0402C200J4GACTU
Resistors	3	R1-R2,R12	220 Ohms	CPF0603B220RE1
Resistors	3	R3-R4,R11	330 Ohms	CPF0603B330RE1
Resistors	5	R5-R9	10 kOhms	RC0603FR-0710KL
Resistors	1	R10	120 Ohms	CPF0603B120RE1
Integrated Circuit	8	U1,U3,U5,U8-U9,U11-U12,U16	60 Ohms 100 Mhz	BMB2A0060LN2
Integrated Circuit	4	U2,U7,U10,U13	K-Type	MAX31855KASA+
Integrated Circuit	1	U4	5V IN, 3.3V OUT	LP2981-33DBVR
Integrated Circuit	1	U6	12VIN,5V OUT	LM1117DT-5.0
Integrated Circuit	1	U14	8-bit Microcontrollers - M	AT90CAN128-16AU
Integrated Circuit	1	U15	Tactile Switch	1-1825910-8
Integrated Circuit	1	U17	CAN Transceiver	MCP2551T-I_SN
Integrated Circuit	1	U18	RS232 Transceiver	MAX232CWE+
Transistors	4	Q1-Q4	100V N Type Mosfet	IRF520N
Diodes	1	D1	20 mA 2V	150060SS55040
Miscellaneous	1	J1	Molex 2 Pin	43160-3102
Miscellaneous	3	J2,J13,J18	Molex 3 Pin	43160-3103
Miscellaneous	2	J3-J4	25630801RP2	NorComp 25630801RP2
Miscellaneous	4	J5-J6,J8-J9	K-Type socket	IM-K-PCB
Miscellaneous	2	J7,J11	Molex 4 Pin	43160-3104
Miscellaneous	1	J10	Molex 10 Pin	90130-1110
Miscellaneous	1	J12	90325-3016	Digikey 90325-3016-ND
Miscellaneous	2	J14-J15	25630401RP2	NorComp 25630401RP2
Miscellaneous	1	J16	9 DSUB Female	182-009-213R531
Miscellaneous	1	J17	9 DSUB Male	182-009-113R531
Miscellaneous	1	RV1	10K	Digikey 3214G-103EDKR-ND
Miscellaneous	1	X1	8 MHz CRYSTAL	RES038

Figure 5.5 Electrical components used to create KJ101



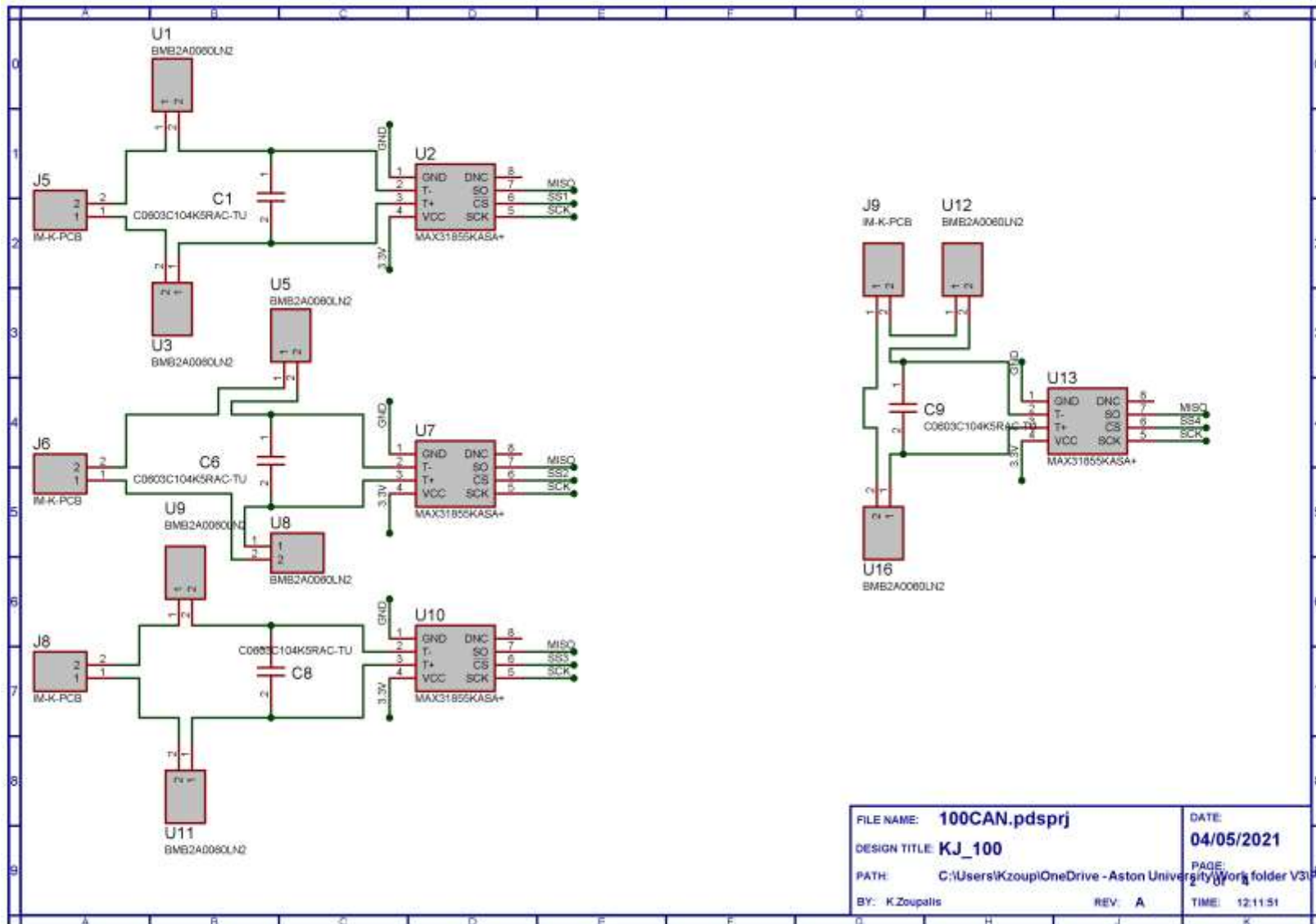


Figure 5.7 KJ101 schematic root sheet 2/4

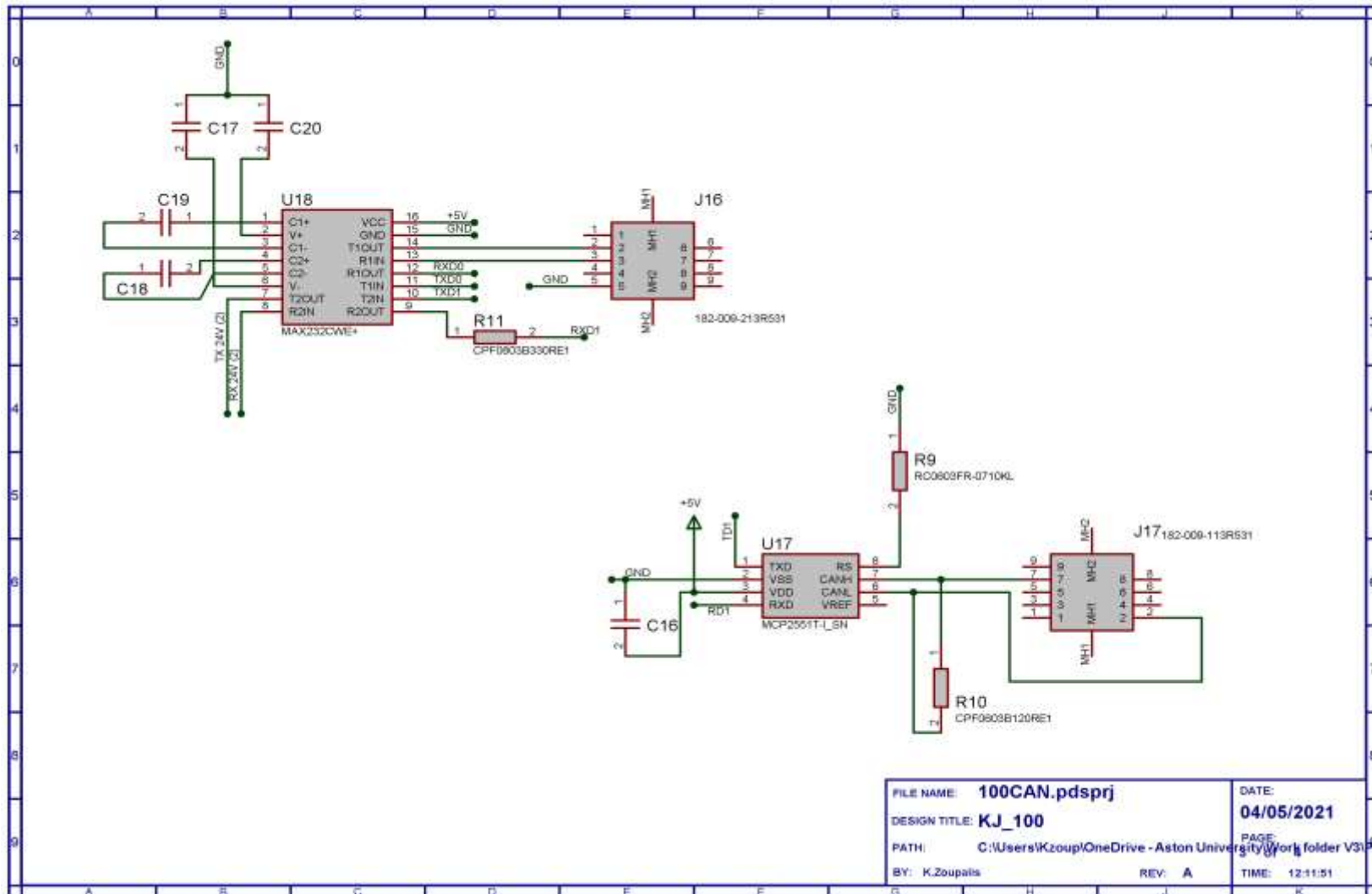


Figure 5.8KJ101 schematic root sheet 3/4

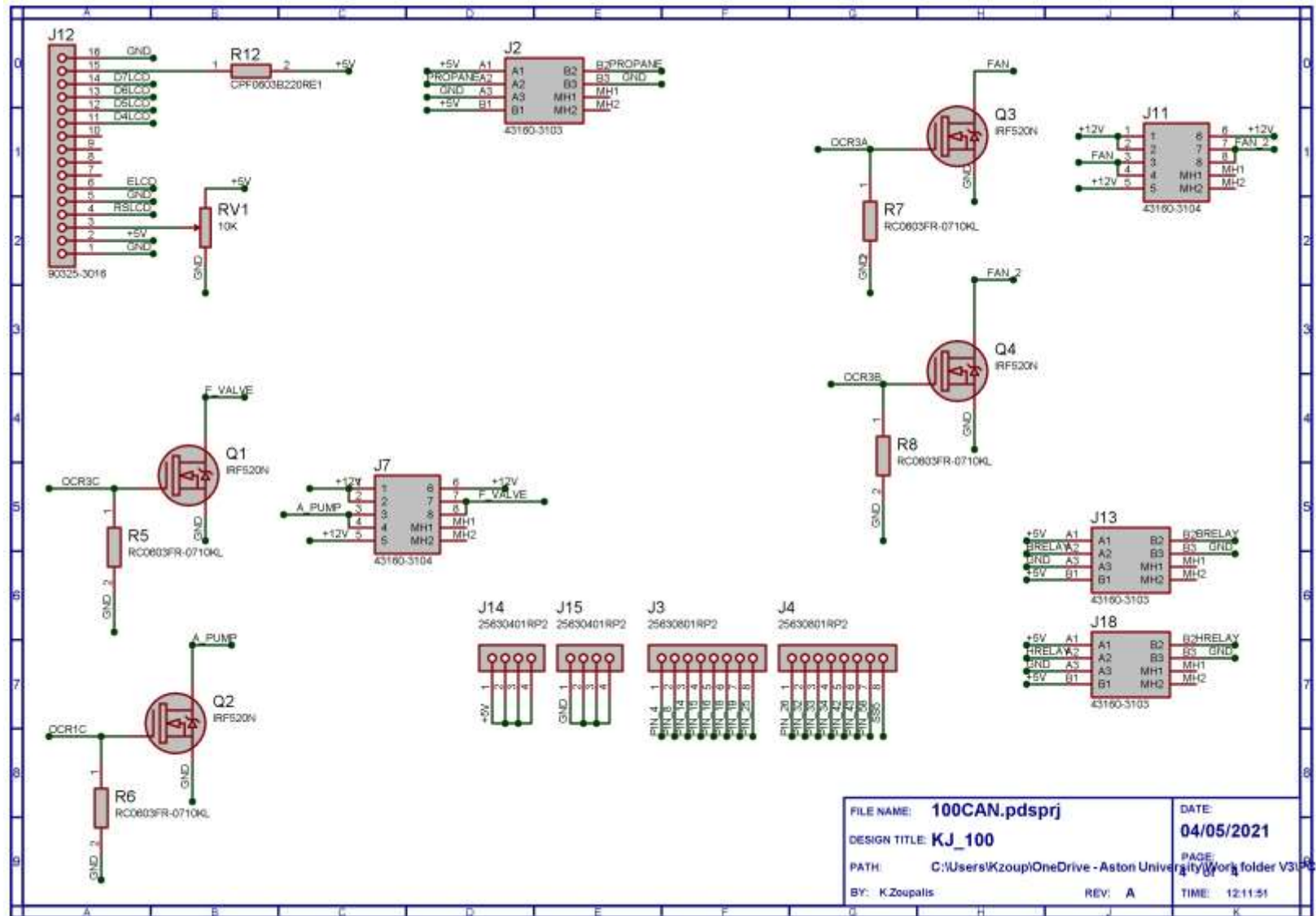


Figure 5.9 KJ101 schematic root sheet 4/4

### 5.3 Printed Circuit Board

To create the schematic the following decisions were made:

To use a four-layer design where:

- The first layer will be for delicate signal (such as thermocouples data)
- Layer 2 will be used as a ground plane,
- Layer 3 will be the power plane(5V)
- Layer 4 will be used for heavy duty once more for signals (12V devices data bus).

This design approach is fairly common, and it is recommended by different PCB manufacturers to reduce noise emissions and susceptibility. What makes manufacturing efficient and able to do multi layers are the holes that are drilled inside a PCB, there are 3 type of holes that usually can be found in a PCB these are called vias, (Figure 5.10). A through-hole and mechanical hole.

A via hole is used for the connection between the layers by adjusting its length, vias are holes filled with copper between the layer and depending on its length it is used to conduct electricity from one layer to the other, these through holes they decrease the amount of tracks required to connect the components within the PCB, for example since KJ101 has ground and power planes all components that require ground and power connections can just simply connect through a via as shown in Figure 5.10. but also reduce noise emission if used properly such as in this case where the ground plane is straight after the signals layer.

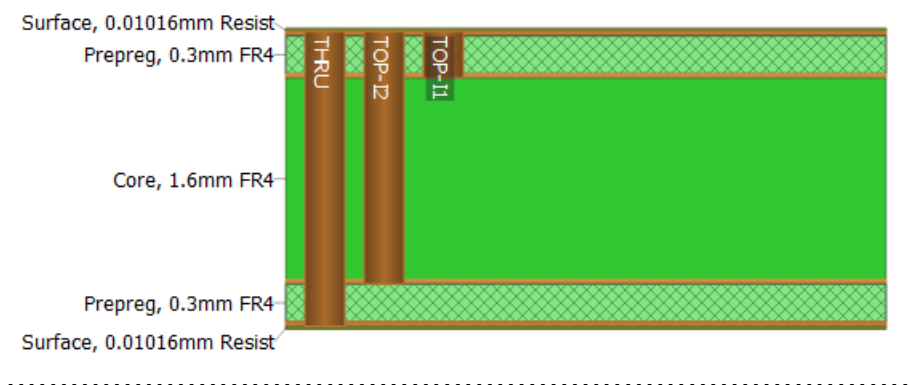


Figure 5.10 KJ101 Layer Stackup

Once the KJ101 layer establishment was decided the routing process was undertaken. All the components that have been chosen for this project are expected to be placed accordingly to a location in the board. The location of the components is important in terms of user interaction. For example, it would be unwise to connect external connectors in the middle of

the board as not only it would be harder for the user to connect the device, but it would also make the routing process harder in the design phase. However, it is worth mentioning, distance from some components can increase or decrease noise emission.

Close to the CPU different value capacitors (C10, C11, C12) have been placed as close as possible from 5V to ground, this is done to prevent voltage switching. Voltage switching happens because in the real-world wires and tracks can act even at a small amount as inductors or resistors which can drop the voltage momentarily, therefore placing bypassing capacitors ensures this voltage switching happens to a minimum where it does not affect the CPU.

Then next component would be the placement of the crystal oscillator labelled as X1 and according to Texas Instruments recommendations crystal oscillators are recommended to be as close as possible to the chip input and outputs as this keeps the susceptibility of the loops on the PCB low to noise. In the same manner as decoupling capacitors C10-C15 have been placed as close to the chip to reduce noise oscillations.

The core chip (AT90CAN128) labelled as U14 in the design (Figure 5.11) was the first component that was placed, since is the brains of the project it goes without saying that almost all components will one way or the other have a connection to it therefore it would help with reducing the number of routes required and also shorten the distance.

Moving on a space was allocated in the left side of the PCB where J1 and U6 is located, this space was chosen as the “heavy duty”, in this place components that could generate more noise than other components were isolated together, this was done willingly as those components could generate high noise to each other without affecting process. Heavy duty could generate higher noise due to the voltage regulator stepping down the input voltage 12V to 5V, however 12V batteries are not really 12V as they range from 10.5V (discharged) to 14.7V (charged) that is why the big capacitor labelled as C7 was used to smooth out the voltage inputs and even if strange power oscillation happens that won't affect the process.

Small voltage variations in the mV range won't affect the main chip where it is rated at 2.8-5.5V. Having said that, this could easily affect thermocouple measurements, thus their placement is on the other corner of the PCB with strong filters before voltage is passed to them, another voltage regulator is used U4 where it converts the 5V output from U6 to 3.3V. U2, U7, U10 and U13 are the chips accountable to sense the micro voltage changes and then

feed the information to the main chip through SPI communication protocol, the step change being sensed by the chips is  $41.276\mu\text{V}/^\circ\text{C}$ .

Furthermore, this design has some connectors left for possible future usage without necessarily going back to the design process, these are the connectors J3 and J4. In addition, there is +5V and GROUND in ports J14 and J15 respectively. For instance, if it's decided to use a humidity sensor, the control output of the sensor would connect to one of the left ports of J3 and J4 while the sensor could be powered by 5V from J14 and Grounded by J15. Finally Figure 5.11 shows the PCB final design after manufacturing checks have been done, without going to many details the red colour tracks are in the top layer while the blue coloured is in bottom layer, while a connection between these layers could be done by the via holes that were mentioned earlier.

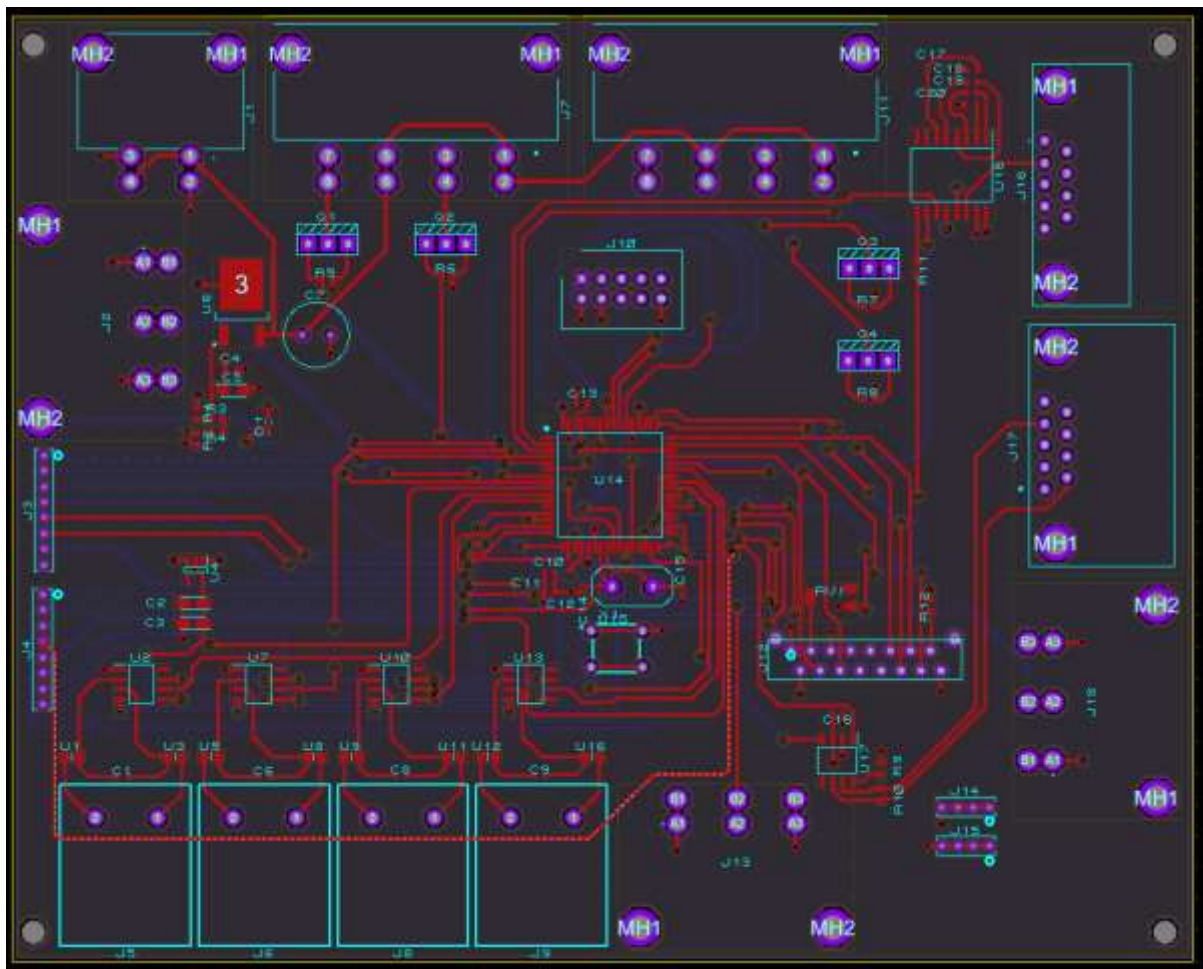


Figure 5.11 PCB Design

#### 5.4 Firmware for KJ101

KJ101 will follow the same philosophy as KJ100 the firmware written is in C using the IDE (Integrated Development Environment) Atmel Studio. While the code was in development stages, a full communication was established with Adelan experts to meet the safety

standards of the fuel cell operation early on. To make sure safety was the top priority the KJ101 code was structured as a state machine. The most important state will be executed first and if that condition is passed then the next less important state will follow. This design hierarchy ensures that the controller stays locked between the stages and there will be no possibility of it being lost.

#### 5.4.1 Master State Machine description

Initiating the controller, an if statement is verifying if the controller is idle or in operation, this is determined by the press of a button or by a signal given remotely by a master controller. When entering the state IDLE the controller goes to sleep mode to preserve power, this mode will be achieved only if the criteria of the fuel being safe is passed. On the other hand, when the controller switches to the 'start controller' state the parameter variables are loaded, then while safety state 'should controller be in shutdown' is true, the system starts heating up until it reaches a temperature setpoint and at that point operation mode takes place. It's at this stage where the fuel cell is able to generate sufficient power to operate and charge a battery. Therefore, the thermal dynamics could easily change and its where the controller with its algorithm will adjust the parameter values to ensure it keeps the temperature stable at a specific setpoint.

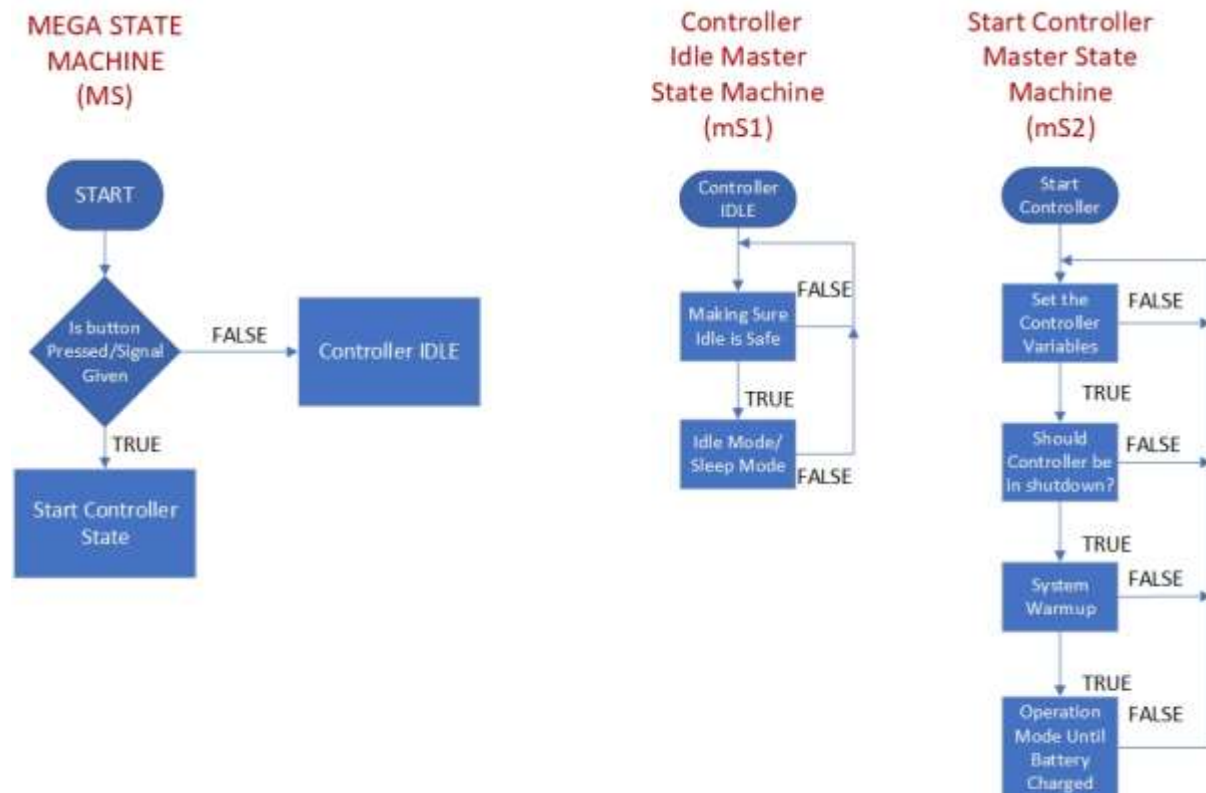


Figure 5.12 KJ101 High level state machine

## 5.4.2 Low level state machine description

In the previous section the key logic of the controller has been summarised where it emphasised the hierarchy of the state machine. A mega master state includes a master state and inside that master state there are more states which are executed. In the following section each state machine will be described to indicate the analysis of this design ensuring safety first but then also creating the most efficient and simple to follow algorithm.

### 5.4.2.1 Should controller be in shutdown

A fuel cell system is a delicate device where different unnatural incidents can significantly reduce its lifetime. Disturbances such as fuel/air starvation and big temperature spikes are of the most importance. This is why “should controller be in shutdown” state was created. The state criteria are checked every second and if any of the flags is being raised the system will go to each respective shutdown stage. Following Figure 5.13, the state will initially check for the temperature and if there is any leakage in the system such as propane leak. The pathway of the shutdown process is dependant off the current temperature the error is found, when the temperature is below 380 °C system will enter to normal shutdown stage 2 state.

Finally, this case has shown that a state designed like this would benefit more in the simplicity and longevity of the system. In the case where a new mechanism detection would be added to the fuel cell, the algorithm would be easier to adapt as the programmer/engineer would have to place his new detection algorithm inside the should controller be in shutdown state and then the core logic of the fuel cell controller won't change but there will be a new fault

detection state including the previous ones.

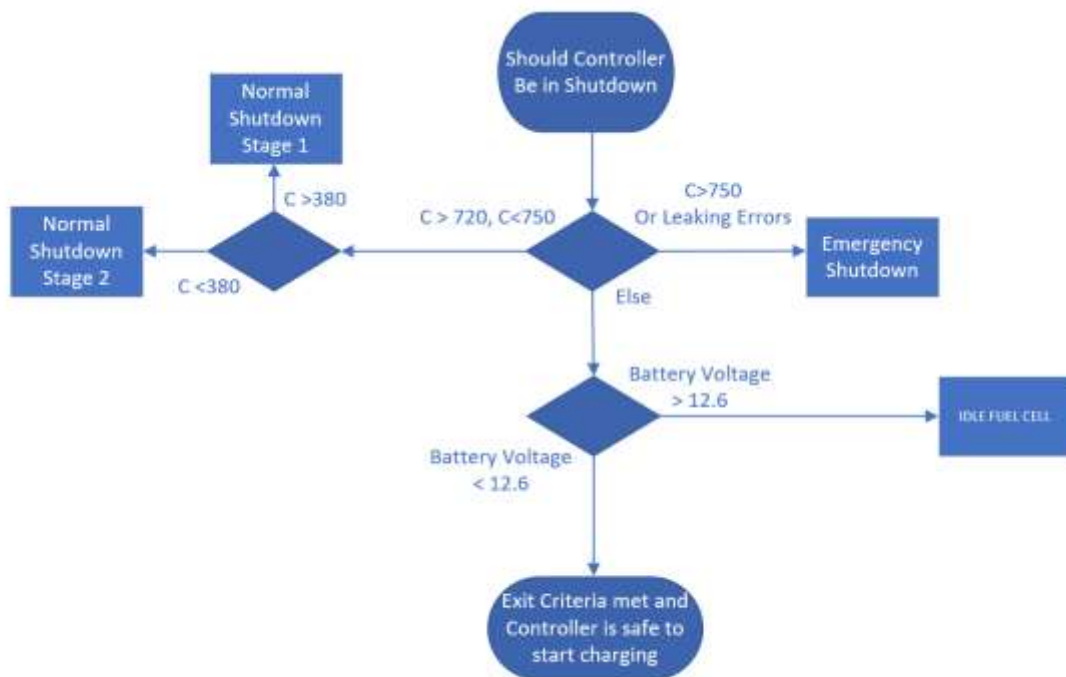


Figure 5.13 Error checking for KJ101

#### 5.4.2.2 System Warmup

Turning now to the system warmup stage, this state initiates when all fault detection mechanisms have passed. First and foremost, four thermocouples are used to detect the fuel cell temperature, thermocouple 1 (TC1 or most times referred in the literature as  $T_{inlet}$ ) is used to read the temperature near the partial oxidation of the  $\mu$ SOFC. Thermocouple 2 (TC2) is used for the main control purposes during the stabilisation stage. The remaining thermocouples are used for reference and are currently not affecting the system operation. As explained earlier, during system warmup the controller will check if TC1 is below  $380^{\circ}\text{C}$  to perform stage 1. Furthermore, the next step is a bit more complicated as the entry condition is for TC1 to be higher than  $380^{\circ}\text{C}$ , this is important as a little amount of fuel mixed with air flows in the  $\mu$ SOFC, meaning partial oxidation is about to begin thus the temperature will rise a bit quicker. However, while this stage is running the exit condition shifts to TC2 as this is the thermocouple located in the middle of the fuel cell reaction and when the system reaches the specified temperature the system warmup flag is set meaning the system is ready to start generating power and enter the operational stage irrelevant of the TC1 temperature.

### 5.4.2.3 Operation Mode

Last machine state is the “operation mode until battery is charged”, this phase is the critical act of the controller as this initiates SOFC’s power generation. In more details, the controller sets of a boundary for the cooling fans, currently at 40% this limit has originated from multiple sensitivity analysis tests from the core system where it has proven that it won’t break the system, since some amount of air is essential to flow around the heat exchanger of the system to prevent sudden overheat by the chemical reaction heat generation. Moving on, the fans parameter can scale automatically by the controller dynamically from 40-100% according to the temperature setpoint. As mentioned in the previous section, the operation mode commences at 620 °C and as it can be seen by the graph in Figure 5.14 once the temperature rises, TC1 is closing the gap to TC2 more rapidly. This is because that this at state the fuel cell is less vulnerable to thermal shocks from 400 °C and above as the ceramics used to build the  $\mu$ SOFC have passed the critical warm up stage that could damage the ceramic bond. One thing that needs to be mentioned is that since the specific controller is designed for  $\mu$ SOFC to charge a battery, start-up is of importance and the fastest safest possible time is to be chosen for the fuel cell to reach charging state, as the fuel cell is wasting external energy till reaching 620 °C, this is also one of the benefits of making a custom controller for a specific system.

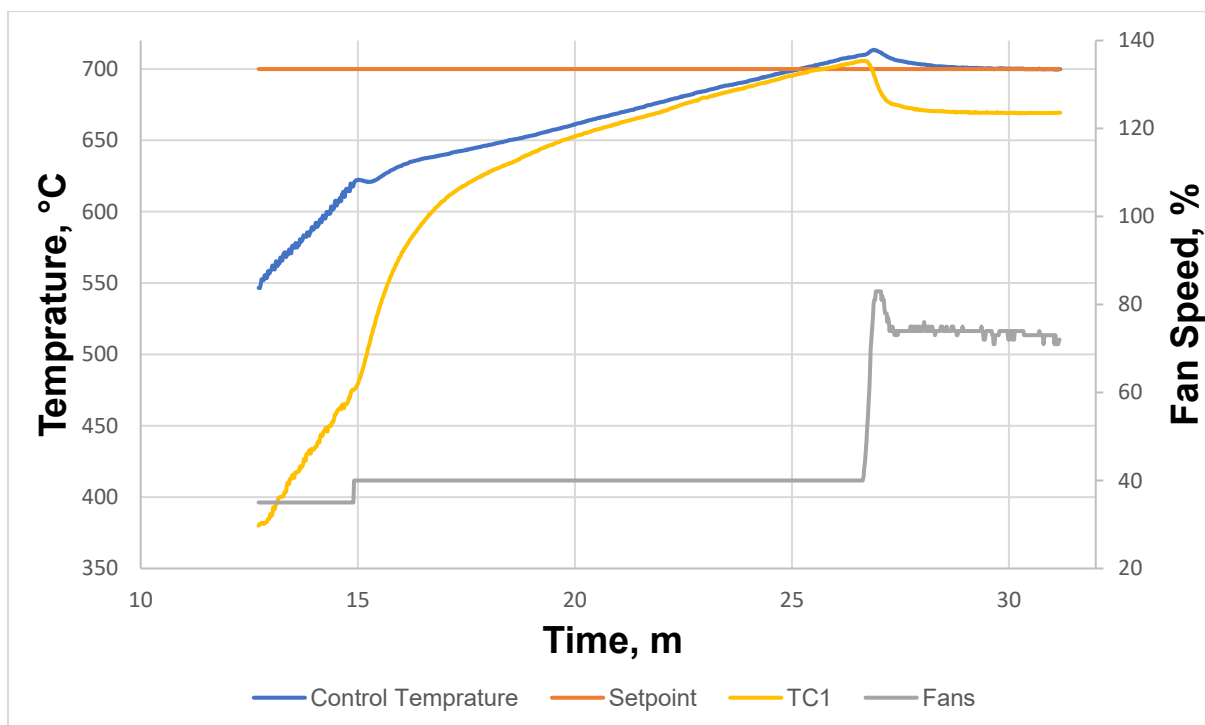


Figure 5.14 warmup state to operational state

### 5.4.3 Remaining low level states

The following section is having all the states that are within other states, these states are usually the states that are for to operate the parameters. The decision for which state is to be operated is being made by the master states. For example, in Figure 5.15 stage 1 and stage 2 are two different states where are called out during the warmup stage master state. Stage 1 is the initial start-up where it turns on the external heater to help with the rising of the temperature. While in stage 2 is when the fuel cell starts to become active (generating a small amount of open voltage) this means a small amount of fuel must flow to ensure there is no fuel starvation. This fuel going into the systems ends up increasing the rate of change of the temperature rising.

Another state to look at is the error stage, this stage can be triggered by any other master or main state in the system and once that has happened everything will end up to that state. This state is being entered if the ForceStay flag has been set to 1 which means the controller has found an error that is preventing the operation of the fuel cell to prevent damage to the system.



Figure 5.15 Analytic stage description

### 5.4.4 Idle stage

Idle state should not be neglected, as at this stage the fuel cell has already finished charging the battery and has fully performed the cooldown process. Therefore, at this stage the only think that is drawing power expect the load is KJ101, therefore losses have to be minimised. Currently KJ101 draws 12V and 0.9A which is around 10.8W this is almost 10% of the current fuel designed power output, for that reason a solution must be found to reduce power draw particularly when the fuel cell is not operating, as some power is required to execute the warmup of the fuel cell. To reduce power the MCU of KJ101 will become very handy as this chip is able to enter different sleep modes according to the configuration. For this case Idle sleep mode will be used as I/O functionality is needed to check the voltage of the battery.

Where if the voltage drops, an interrupt pin change will be triggered to wake the controller. Finally, KJ101 after the configurations its able to draw 1mA

Table 5.2 Low power configuration options for KJ101

Sleep Mode	CPU CLOCK	FLASH CLOCK	I/O CLOCK	ADC CLOCK	MAIN CLOCK SOURCE ENABLE	TIMER ENABLED	INT7: 0	I2C	EEPROM	ADC	OTHER IO
IDLE			X	X	X	X	X	X	X	X	X
ADC Noise Reduction				X	X	X	X	X	X	X	
Power Down							X	X			
Power Save						X	X	X	X		
Standby					X		X	X			

## 5.5 KJ101 software technical description

KJ101 is written in c language using the Atmel/Microchip studio 7 included complier. In this section some of the features that have been significant in the software development are going to be mentioned.

### 5.5.1 PWM

Parameters such as the fans are being used by the controller dynamically to stabilise the temperature at a given setpoint. However, for this to be achieved some calculations had to be made to ensure software combability with the hardware. The specific fans used in the system are typical 25KHz PWM fans, therefore the signal given to that fan must be as close as possible to that frequency. If this is mismatched there is going to be an issue with the commands as the range of the fans could be different. To solve this a deep dive into the AT90CAN128 timers had to be made, a register called Output Compare Register was tuned for this. KJ101 has a 16MHz crystal oscillator which is way too big for the specific PWM parameter, usually the hardware prescaler could be used to slow down the frequency however in this case non would give the required frequency output as the prescaler can provide a division of 1,8,64 and 128. Therefore, instead of swapping out the crystal oscillator which would slow the other operations of the controller a different approach had to be made. Two registers were used where one would act as the top and the other as the bottom meaning one register will count down from 320 to 0 and the other would count up from 0 to 320 and when they would meet that is going to trigger an event to send the signal, therefore in more detail this equation is being derived.

$$\text{Parameter Frequency} = \frac{\text{Crystal Oscillator}}{\text{Prescaler Value} \times \text{Defined Counter} \times \text{Number of Registers}} \quad (5.1)$$

Therefore, to get 25KHz  $\frac{16000000}{1 \times 320 \times 2} = 25000$

Table 5.3 Initialising PWM mode for the manipulative variables

Register	Mode	Description
TCCR3A	COM3A1=1 COM3B1=1 WGM30=1 WGM31=1	Setting up the first 8 bit register of the PWM to phase correct mode
TCCR3B	CS30=1	Prescaler set to 1
ICR	=320	Number to calculate PWM frequency

### 5.5.2 Discrete PID

From control theories it is fairly known that the calculation of PID occurs from the summation of the gains of the proportional term, the integral term, and the derivative term. However, this theory has to be implemented in a machine language to be effective. Therefore, a brief overview is going to be discussed below about the implementation of each term inside KJ101 software using C computing language.

To begin with, a function is designed that initialises the PID controller and the core variables are being built. Those variables are set to zero to avoid any memory leakage or the machine to randomly overwrite the address Table 5.4. To make things less complicated in the library a structure named "PID\_Data" has been produced, that structure will carry the information that will manipulate the PID controller accordingly. Some of these variables are last processed value, the error addition, the P, I and D constants.

Table 5.4 PID Initialisation Software

Parameter as written in the firmware	Initialisation value
pid->sumError	0
pid->lastProcessValue	0
pid->P_Factor	p_factor
pid->I_Factor	i_factor
pid->D_Factor	d_factor
pid->maxError	MAX_INT/(pid->P_Factor+1)
pid->maxSumError	MAX_I_TERM/(pid->I_Factor+1)

Table 5.5 PID Structure used to organise the PID firmware

Variable Type	Variable as written in the firmware	Variable Description
double	LastProcessValue	Last process value, used to find derivative of process value.
double	sumError	Summation of errors, used for integrator calculations
double	P_factor	The Proportional tuning constant, multiplied with SCALING_FACTOR
double	I_Factor	The Integral tuning constant, multiplied with SCALING_FACTOR
double	D_Factor	The Derivative tuning constant, multiplied with SCALING_FACTOR
double	maxError	Maximum allowed error, avoid overflow
double	maxSumError	Maximum allowed added error, avoid overflow

Now with the previous mentioned functions being established this brings the opportunity to focus on the creation of the PID controller core equations. Hence, a new function named “PID\_Controller” is created, this function is executed every time the controller is within the operation mode state, this function executes roughly every 314ms to make sure that the controller will react immediately on feedback changes.

As it can be seen in Table 5.5 Proportional gain is calculated by the P term given constant multiplied by the error, where the error is simply the setpoint minus the current temperature reading.

$$Error = Setpoint - Current Temperature \quad (5.2)$$

$$P = P * Error \quad (5.3)$$

To calculate the integral all errors are being summarized and temporarily stored. That temporary value is being checked if it's over the limits to avoid integral runaway which is

essentially the machine being lost (memory leakage) or overflown. Once the check has passed the I term is finalised which is I multiplied with the summation of the errors.

$$\text{Summed Errors} = \text{Summed Errors} + \text{Error} \quad (5.4)$$

$$I = I * \text{Summed Errors} \quad (5.5)$$

The last term, the derivative (or sometimes referred predictive term) is calculated by the multiplication of D term with the subtraction of the last value minus the current.

$$D = D * (\text{Last Temperature Reading} - \text{Current Reading}) \quad (5.6)$$

Finally, the PID controller is adding the three terms which will correspond to the current output of the fans. However, one last check is there to make sure the output is a positive value. All the PID calculations have been made in 16 bits (65,536) to ensure more accuracy to the calculation then its shifted again to 8 bits (256) to be placed to the fans (0-100%).

### 5.5.3 PID tuning

Since the PID software for KJ101 has been compiled, the parameters tuning is required. The PID tuning in this system was done by analysing experimental data from Adelan including new current ones. In addition, Adelan was able to provide a dummy unit which was able to emulate the thermal reactions as the core one. To start the tuning, the P constant term was set to a

value where the unit will achieve a constant thermal stabilisation unit constant oscillation was occurring.

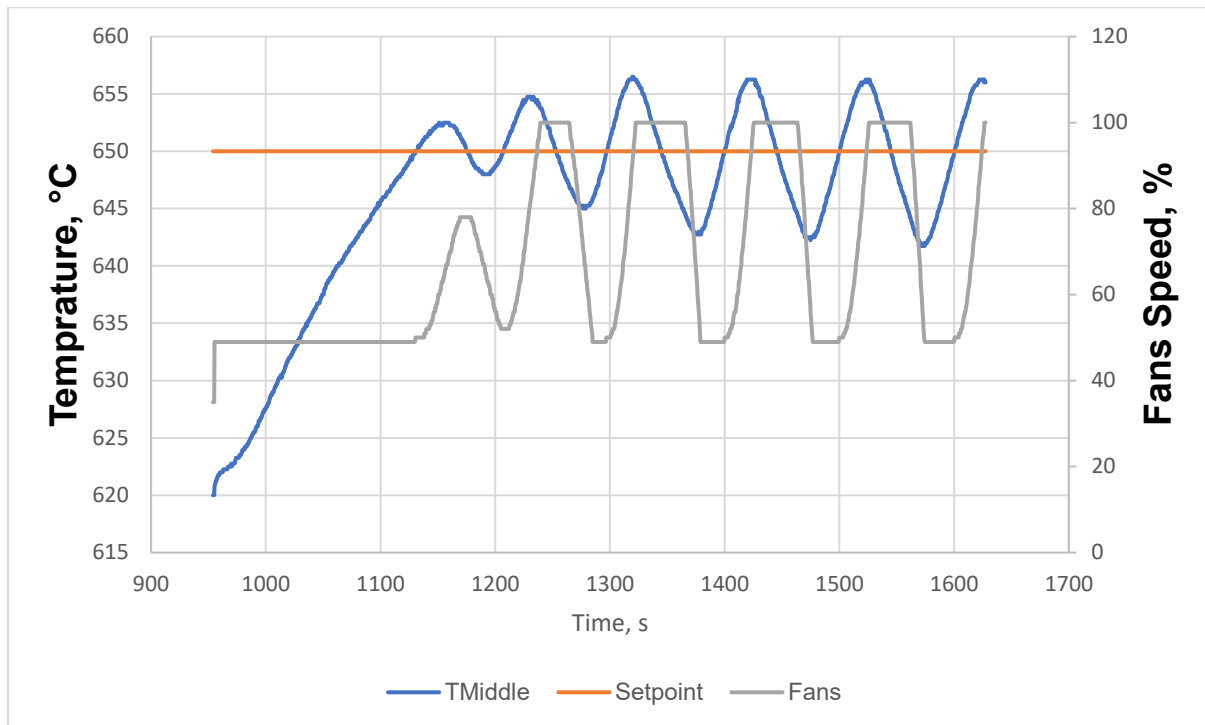


Figure 5.16 PID tuning Incrementing proportional gain unit constant oscillation

The following phase would be I term tuning. According to Adelan past results it would be more suitable for the I term to start with a very low value as the systems variable changes gradually. Decreasing the I term indicates that the system overshooting is dropping considerably from being more than 10 °C overshoot to almost +2 °C. To the following graphs the I term initially was set to 0.8(Figure 5.17), at that stage thermal stabilisation could be achieved however some initial overshoot and undershoot scenarios could be observed. Thus, for the next experiment the Integral was dropped by half, and it immediately shows less oscillation however the same +17°C overshoot (Figure 5.18). Furthermore, the integral term was dropped by another half this time at 0.2 and the oscillation almost ceased however still an overshoot can be observed (Figure 5.19). Finally, the system did not see any oscillation or overshooting when the integral term was set to 0.05, the temperature gradually increased from 620°C to

700°C and it steadily stabilised at 700°C (Figure 5.20).

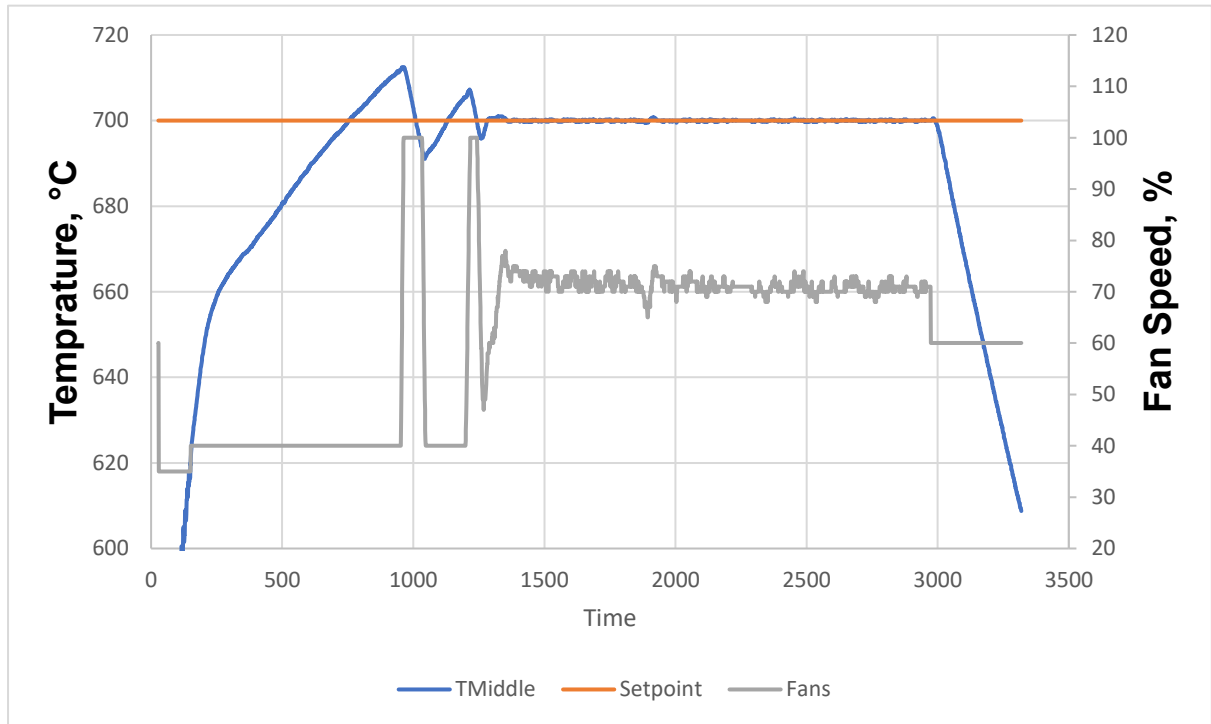


Figure 5.17 Tuning Integral,  $I=0.8$

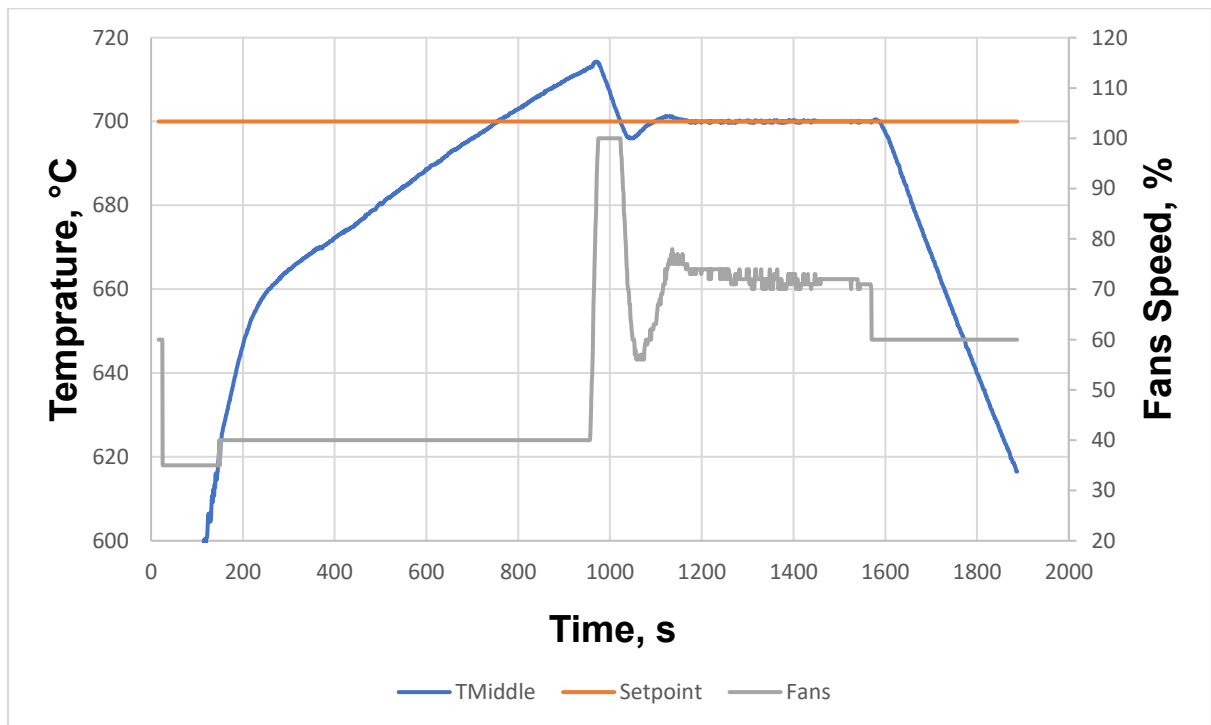


Figure 5.18 Tuning Integral,  $I=0.4$

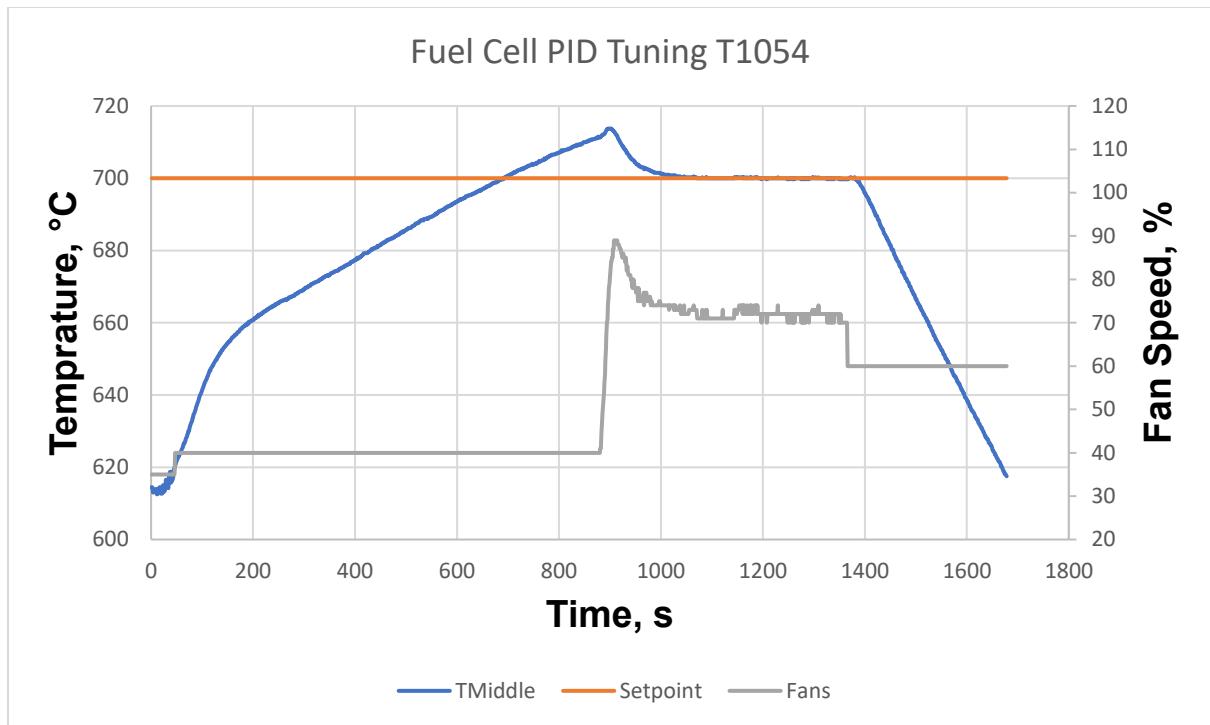


Figure 5.19 Tuning Integral,  $I=0.2$

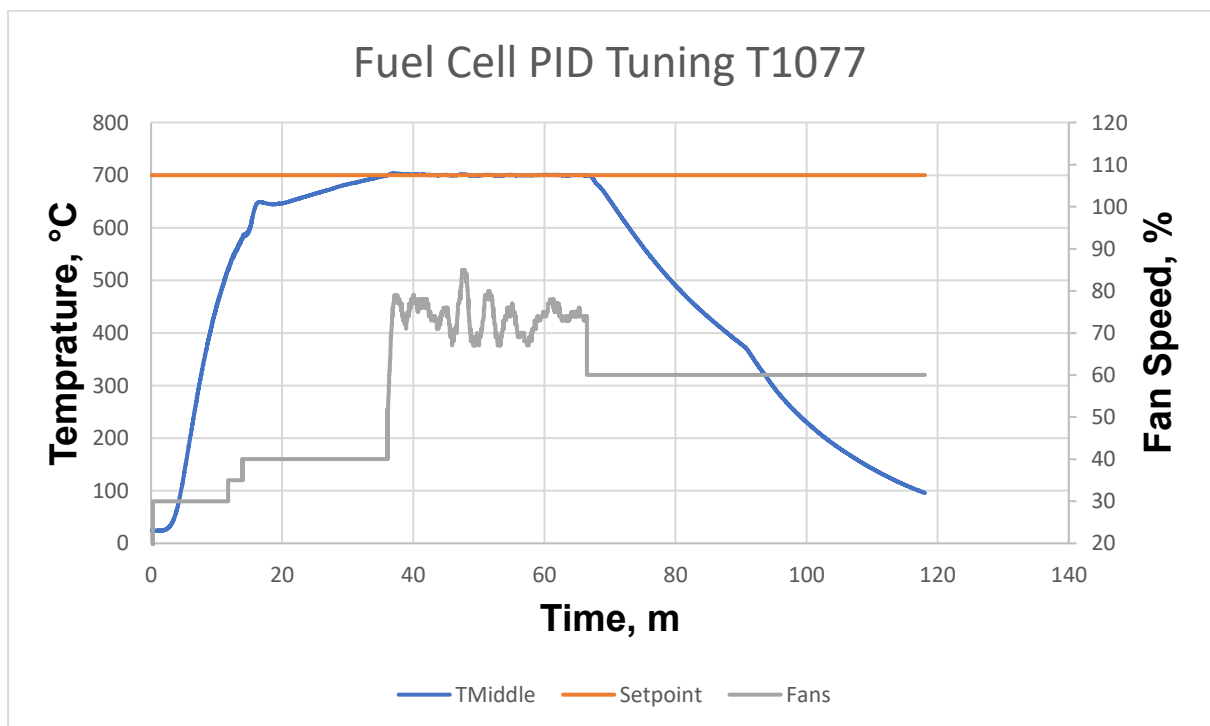


Figure 5.20 Tuning Integral,  $I=0.05$

#### 5.5.4 Data local communication and interrupts

For the previous experiments to be feasible a debugging protocol had to be engineered. For KJ101 two communication protocols were developed. UART communication and CANBUS. In this project it was selected to use UART for communication with the PC and CANBUS for

IOT connections with other devices. To set up UART (also referred as RS232) a configuration of the KJ101 CPU was required. To enable the UART port, register UCSR0 had to be configured (Table 5.6) by enabling the bit to transmit (TXEN) and receive (RXEN). Moving on, the communication with the computer is critical information and the timing accuracy is of the essence. However, a solution to this would be to enable AT90CAN128 (KJ101CPU) global interrupts and timers, with the right calculations a 1 second reporting could be achieved (Table 5.7). This was achieved by setting the prescaler of the timer to 1024, while the frequency of the CPU is set at 16MHz which means the timer will increment 15,625 times per second. Therefore, to find which number to use in the code, this following equation can be used, where adjusting the time required the equivalent number will be generated to use in the code.

$$\text{Printing delay value} = 15625 * \text{TimeRequired}(s)$$

Table 5.6 Communication initialisation

Register	Mode	Description
USART_BAUDRATE	=19200	Changing the number of this parameter affects the baud rate the controller communicates with the PC
UBBR_VALUE	$(((F\_CPU/(USART\_BAUDRATE*16UL)))-1)$	Macro calculating the right value for the machine to input the user given baud rate
UBRR0H	$(\text{UInt8\_t})(UBBR\_VALUE \gg 8)$	KJ101 CPU uses two 8-bit registers to store the baud rate input (which both combine to a 16 bit). Therefore UBBR_VALUE which stores the number for the respecting baud rate is shifted 8 times to the right as UBRR0H is storing the most significant bits
UBRR0L	$(\text{UInt8\_t})(UBBR\_VALUE)$	The remaining 8 least significant bits are stored. UBRR0H AND UBRR0L combined

		will make up the number of UBBR_VALUE
--	--	---------------------------------------

Table 5.7 Timer used to calculate accurate printing intervals for KJ101 communication outputs

Register	Mode	Description
DDRB	PB5=1	Make PORTB 5 an output
TCCR1B	WGM12=1 C12=1 C10=1	Setting up the 16 bit timer
PrintingDelay	=15625	1 Second to reach CTC (Capture Compare) Therefore, the interrupt gets generated every 1 second
TIMSK1	OCIE1A=1	Enabling the interrupt flag. The timer is being incremented in the background while the software is executing other instructions. When the printing delay reaches 15625 this interrupt event is triggered then the software returns to its previous execution immediately

As mentioned above CANBUS is another method of communication with other local devices and in the following table the ID's that are being send out by KJ101 are labelled. Note KJ101 is configured as a standard CANBUS 2.0a meaning one ID can have up to eight packages and each package can sent an integer from 0 to 256.

Table 5.8 CANBUS important messages

<b>ID</b>	<b>Name</b>	<b>Description</b>
<b>256</b>	MPC_RUN	This ID has 1 package on it. If it changes from 0 to 1 for a second (like a push button) it switches the ON/OFF state of the device
<b>1</b>	Power	This ID consists of four packages. Package 1 and 2 consist of the fuel cell voltage and current output. Package 3 and 4 hold the information for battery voltage and current draw. Since CANBUS can have only integers a 12.6 would be transmitted as 126 and the receiving device will convert to decimal.
<b>2</b>	Temperature	ID consists of eight packages. It reports the temperature since the temperature varies from -50 to 2047 more than one package will be required therefore each thermocouple will be using two packages. The receiving device will be able to convert this by using bit shifting.
<b>3</b>	Operate_State	1 Package which will consist of the state of the operation
<b>4</b>	Delivery	6 packages in use. Package 0 and 1 will show the the fuel flow. Package 2 and 3 will hold the air flow data. 3 and 4 will display the air input that's gets mixed with fuel data.
<b>5</b>	Relays	Package 0 will indicate the status of the heater relay while package 1 will indicate the status of the battery relay.
<b>6</b>	RTC	All packages are in use to transfer the local time of the device

## 5.6 Technical Evaluation

To evaluate KJ101 performance one of Adelan's fuel cell system thermal unit was used. This system was capable of operating almost the same way as an actual Adelan fuel cell system but with the major difference that it was unable to produce power. This thermal unit was able to provide details relevant to POX and its thermodynamics with a reasonably low cost. It was refurbished faster when became necessary.

### 5.6.1 Warmup Evaluation

To evaluate the warmup stage, KJ101 should be able to smoothly increase the system's temperature. To this end, KJ101 should be able to follow the same instructions as it was described in the state machine. Hence, at the start while the operation began fans switched to 30% and with its turn electrical heater was switched on for the warming up process to begin. This process took place for roughly 13 minutes and at that stage TC1(Thermocouple 1) reached 380°C, which means it's time for the next warmup stage to begin. As it can be seen in Figure 5.21 fuel valve started pulsing (calibrated to 38ml/min), air pump switched on (calibrated at 380ml/min) and finally fans speed increase by an additional 10%. Moving on, at  $t = 15$  min, the battery status indicator switched to 1, at this stage the fuel cell temperature has reached at 620°C. The system is ready to perform the normal operation and generate power.

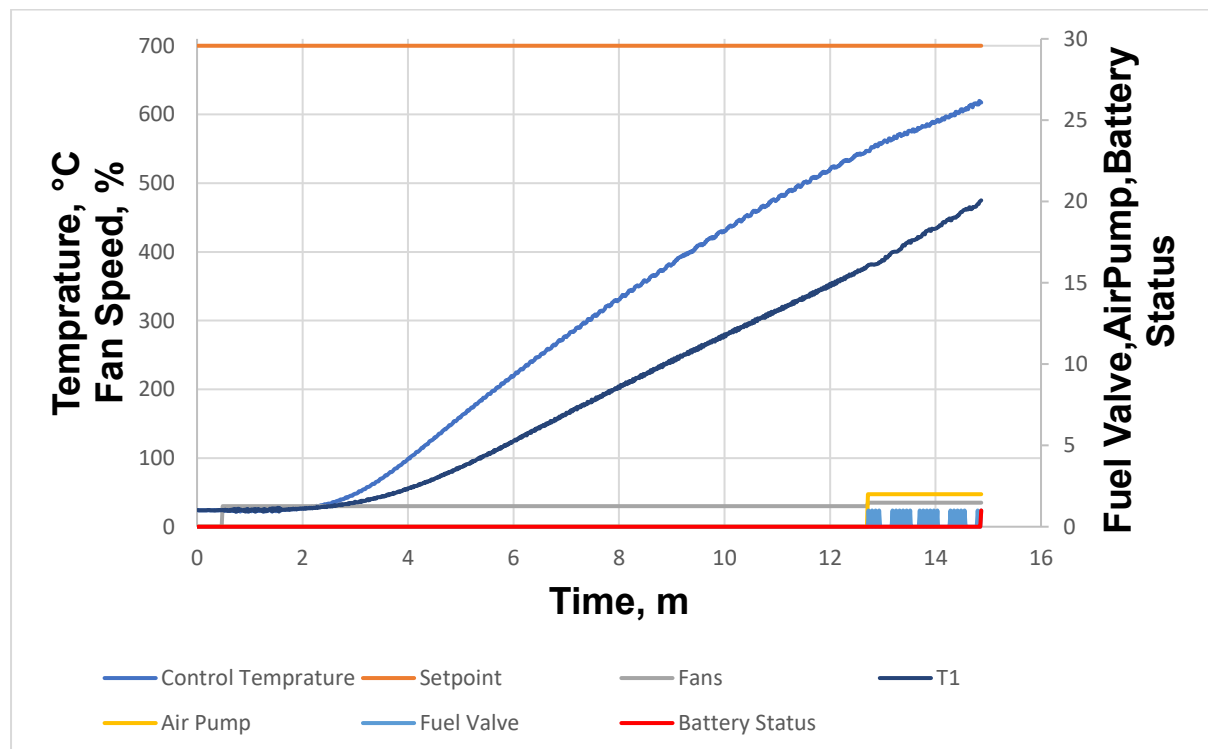


Figure 5.21 Start-up Evaluation

### 5.6.2 Operation Evaluation

In one of the experiments, the control unit setpoint could be adjusted in real time by commands using the RS232 communication wired to the PC. The commands to different setpoints are given downwards by 10 °C in each step change. The gain is currently 1850 while the integral term is at 0.20 and according to previous experiments, a slight overshoot is to be expected while the controller is warming, until the initial setpoint which is 700 °C. KJ101 is able to stabilise at all setpoints with minimalistic disturbances. It can be observed that according to these tests there is a settling time for the controller to achieve the objective, that time is approximately 3 minutes. In the graph the fans are showing a jump to 100% (full power) at some points, the reason for this is the command, which is given for a new setpoint, while the system at that stage thinks it is at “overshooting temperature” meaning it will do everything possible to drop the temperature as soon as possible. However, when the fan is blowing at 100% there is an excessive amount of air flowing through the system and once the temperature approaches the setpoint the excess air inside the system will drop it a bit lower and that is why 3 minutes are required to reach setpoint.

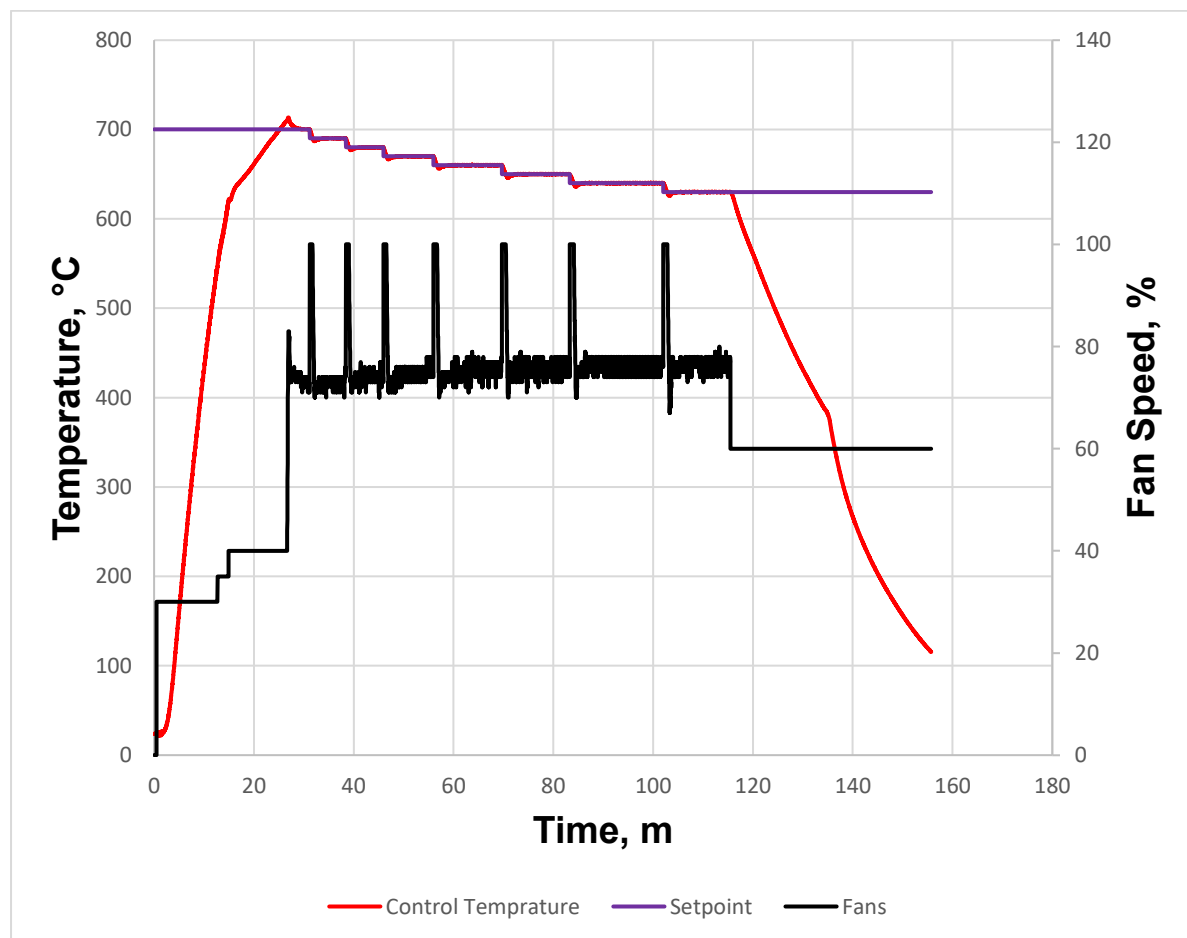


Figure 5.22 Different Setpoints

### 5.6.3 Shutdown Evaluation

In another experiment, to test the shutdown is performing as in the simulations. The shutdown command was given, as it can be inspected the parameters are adjusted for shutdown, battery connection has been switched off, fuel flow has been decreased and the air pump slowly decaying (Figure 5.23). In the next stage all parameters have switched off by the controller when below 380°C. Fans are constantly running to drop the temperature steadily

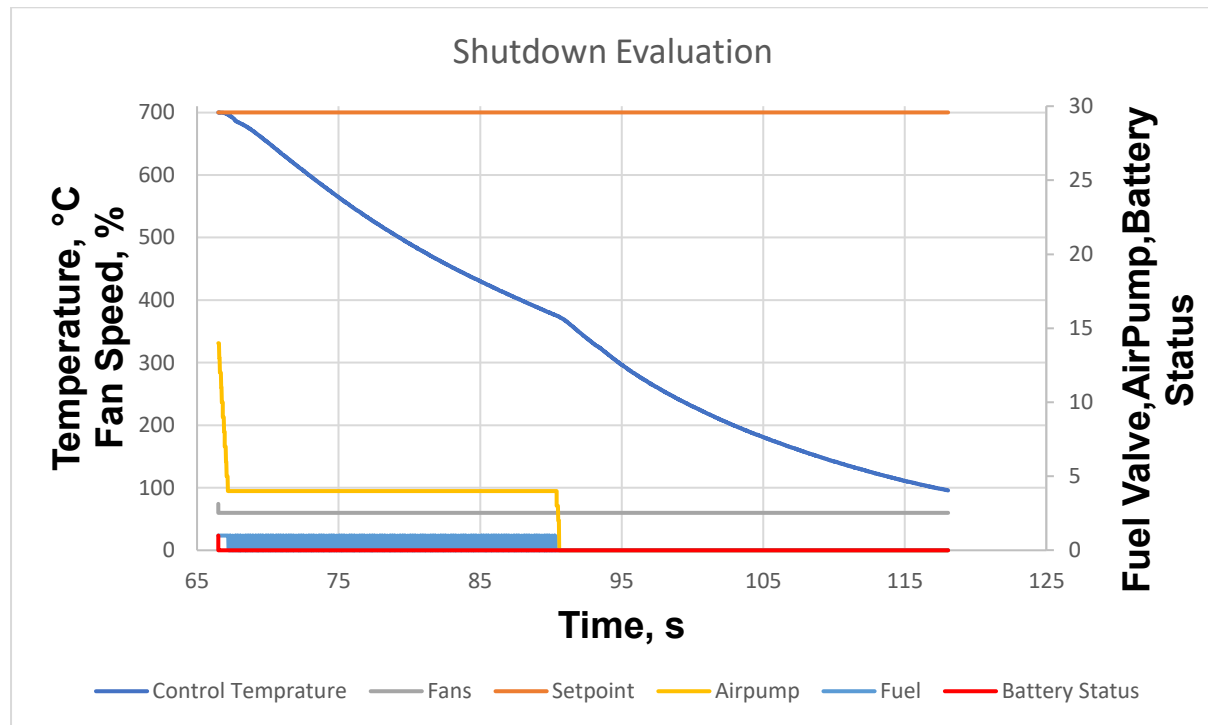


Figure 5.23 Shutdown profile

## 5.7 Transmission

In the previous design, a user interface was designed for KJ100, this machine was able to demonstrate valuable statistics to the user. However, this was done locally through serial communication which requires a direct physical connection to a device. With the design of KJ101 few inputs and outputs were purposely left unconnected to enable a new communication technology to the Adelan SOFC.

### 5.7.1 Message Queuing Telemetry Transport

MQTT is a technology which could benefit SOFC's tremendously. A common communications protocol for the Internet of Things is MQTT. It is intended to link remote devices with a compact code footprint and low network traffic by acting as a very lightweight publish/subscribe message transport[102]. MQTT it's not used in fuel cell industry but its currently used in a variety of industries such as automotive, logistics, manufacturing, smart home, consumer products and transportation.

### Where MQTT can be:

- Lightweight and efficient, therefore since it requires fewer heavy resources it can be utilised by a small microcontroller as in this project.
- Bi-directional, with MQTT a device can communicate to the broker and request data (subscribe) or send data (publish) at the same time.
- Scaled, currently there is no limit of devices that can be connected to the data management layer or broker.
- Reliable Message Delivery, data are sent with the three quality of services (QoS) which can be defined by the device where 0 is the less effective while 2 being the most effective for message delivery but the slowest.
- Great for unreliable networks, when the connection is lost by the device especially in the case of mobile network, MQTT has a fast reconnect feature which persists until connected with the broker.
- Secure, standard encryption methods can be used such as TLS and OAuth

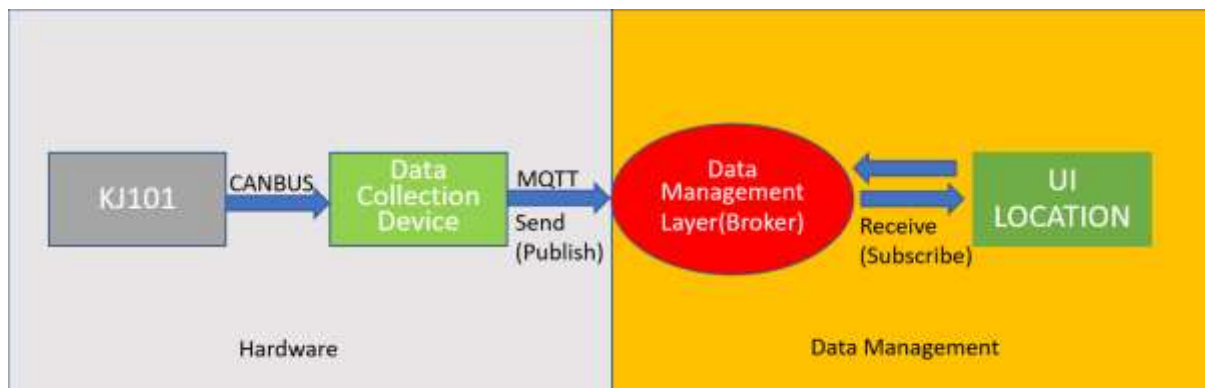


Figure 5.24 MQTT Implementation in this project

#### 5.7.1.1 Connectivity

The data collection device to be useful it requires internet connectivity and to do that there are two options. First option is going to be through Wi-Fi which comes on board with ESP32, and the second option is going to be through mobile network utilising sim800L. Wi-Fi firmware for the esp32 is provided by the manufacturer and the functions have to be briefly adjusted. There is a function where it holds information such as SSID (the name of the Wi-Fi) and its password. Once those have been changed the device will be able to connect to the internet. However, for mobile network connectivity sim800l was utilised and to communicate with

#### 5.7.2 Data Collection Device.

Currently KJ101 is the responsible device for the monitoring and operation of the  $\mu$ SOFC, in the same time the controller is outputting operation data in real-time through the CANBUS local port. This port opens the possibility for the data to be extracted to the cloud. However,

KJ101 doesn't support internet connection, and this was a design choice to leave the IOT capabilities optional to the user. Therefore, another board could be designed where it can retrieve the data locally in CANBUS and then transmit the data to the cloud through Wi-Fi or mobile network. Due to the pandemic covid 19 and big delays of manufacturing the idea of generating an altogether PCB was impossible for the time frame of this PhD therefore the solution was made with aftermarket development boards which could prove the concept of the transmission. So, to develop this solution a ESP32, an SPI CANBUS MCP2515 and SIM800L was purchased. The ESP32 was the main microcontroller with in build Wi-Fi functionality, MCP2515 is a microchip that can be configured through SPI with the ESP32 to read CANBUS from KJ101 and finally SIM800L was a module which can connect to the mobile network through a SIM card if there is no Wi-Fi available.

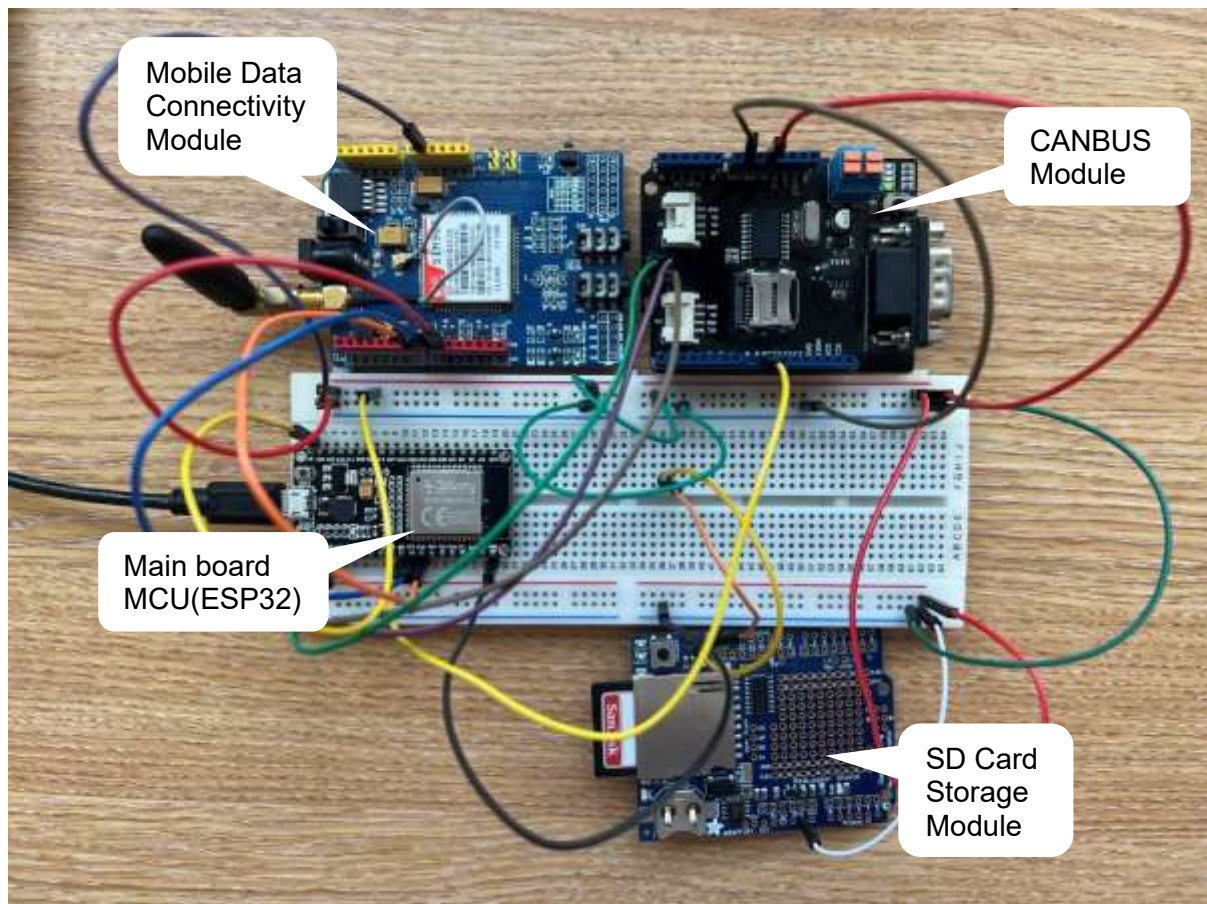


Figure 5.25: Data transmission solution

### 5.7.3 Operation of data collection device

For ESP32 to communicate with SIM800L a custom firmware was made. The connection was made through UART/RS232. According to the manufacturers datasheet SIM800L can read strings and perform corresponding actions (Table 5.9 Serial Commands to control the SIM Module). Once a typical sim card is inserted the data device will send a command to SIM800L

with the APN network settings for the module to establish a connection with the network provider. Once this has been verified the data collection board will convert incoming CANBUS data from kj101 to a string and then send that to the module while module will transfer to the cloud using MQTT protocol. It's worth mentioning that once Wi-Fi signal is found the SIM800L will go to sleep to save power by sending the command AT Sleep.

*Table 5.9 Serial Commands to control the SIM Module*

String sent from main device	Functionality
AT	Sending this command is to check if the connection between the main board and the GSM module has been established
AT+CSQ	Signal Quality in 5 bits, value range is from 0-31, 31 is the best
AT+CCID	Instructing the module to read the sim data and report back. It's also a way to check if the SIM is plugged
AT+CREG	Checking if has registered with the network provider
ATI	Reports back module version and name

The data collection device is being structured to perform one task only and that's to transmit valuable fuel cell data to the cloud so Adelan can analyse and learn about the fuel cell usage. In more detail, the device starts by checking if there is CANBUS connection, then it will scan the area for any known Wi-Fi connection if non it's found for one minute it will then switch to backup mobile network. While internet connection is established all incoming CANBUS data will be converted and packaged to a specific JSON object to be send to the broker with an individual topic (each device will have unique assigned topic). In case the device losses access to the broker it will store the data for 30 minutes trying to reconnect to the broker. An SD card reader will be utilised to store locally the data if internet connection fails.

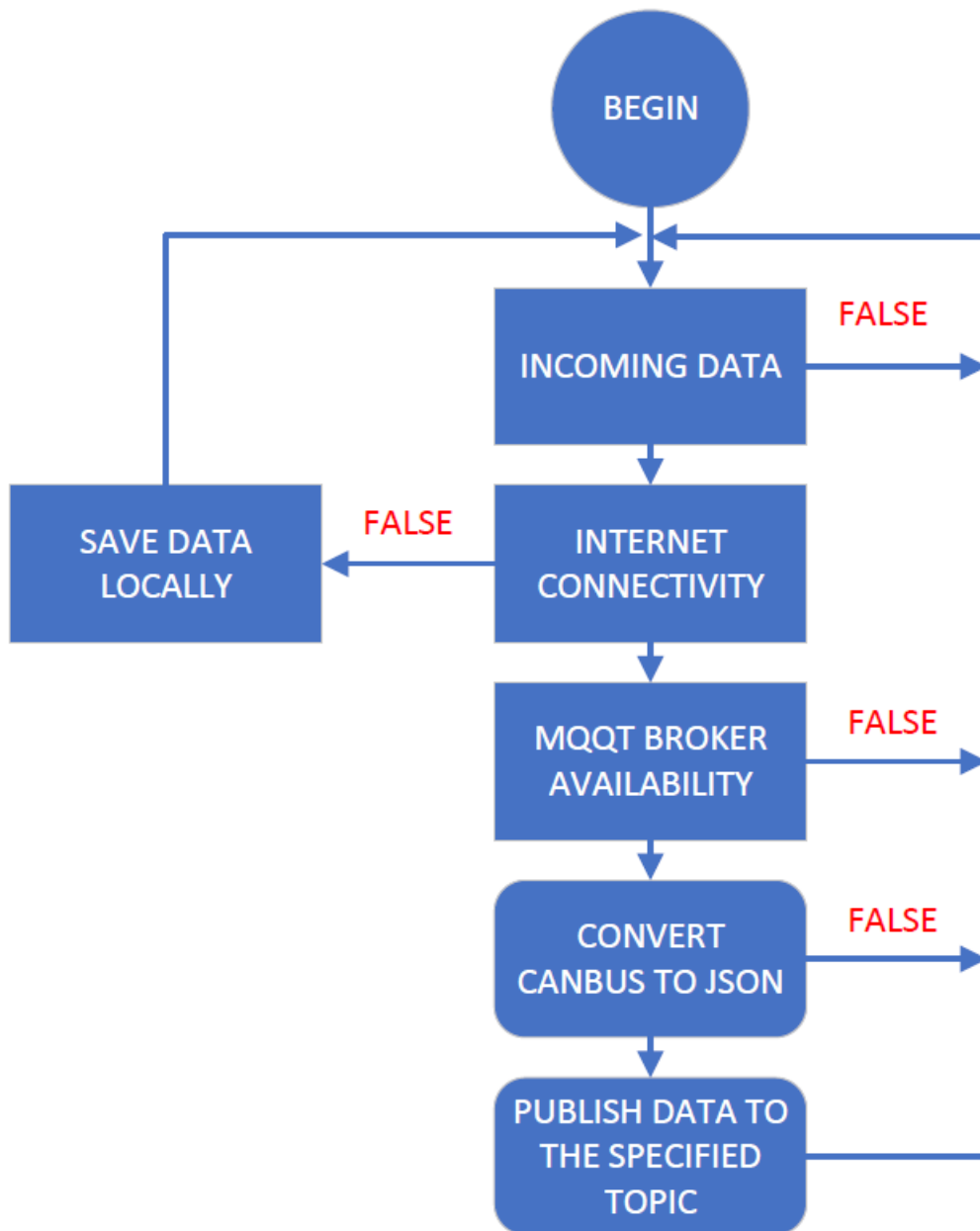


Figure 5.26 Basic flow chart for the data collection device

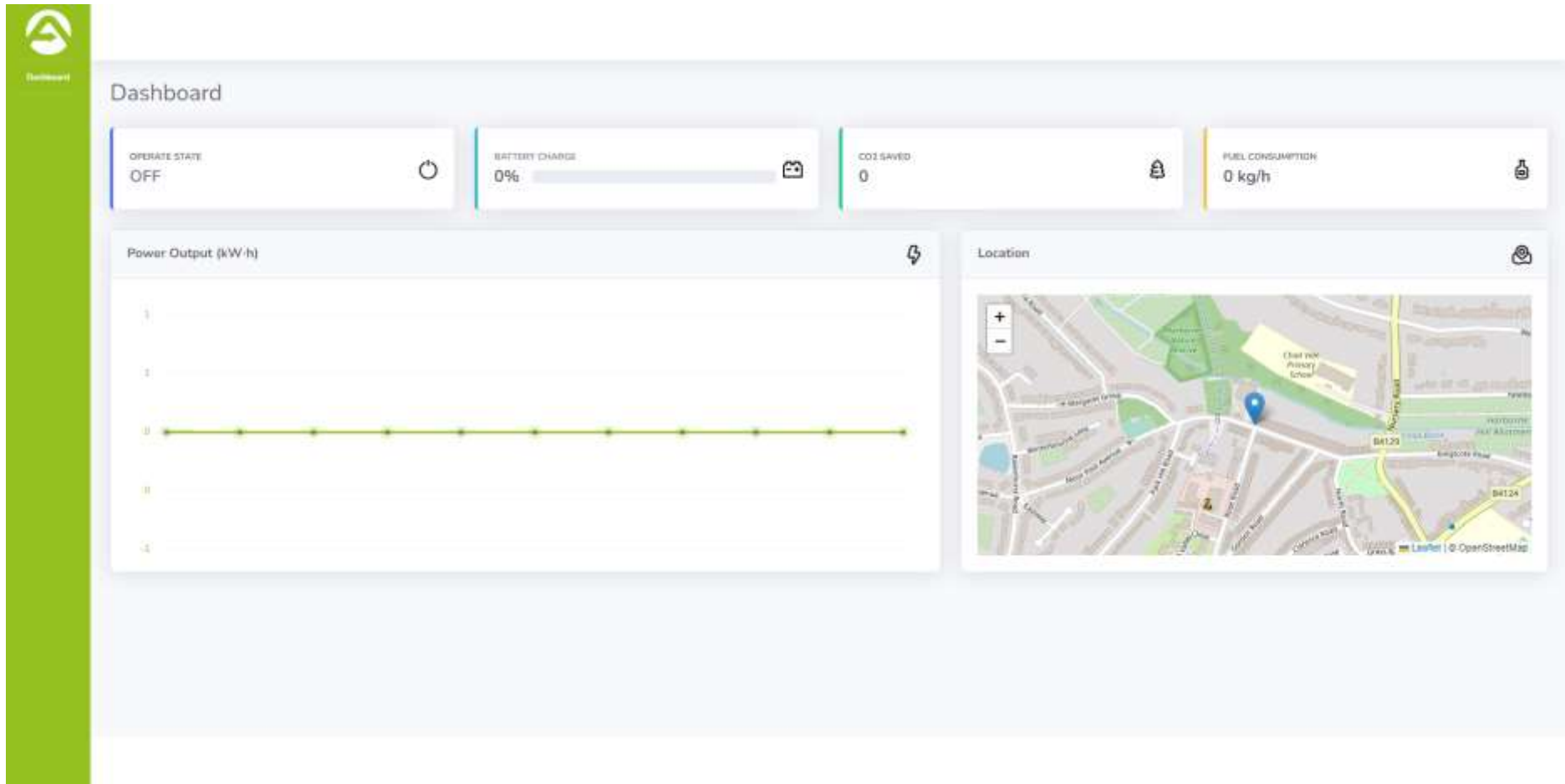


Figure 5.27 Adelan Dashboard Proof of Concept

## 6 Validation and performance evaluation of KJ101

### 6.1 Introduction

This chapter presents and explains several improvements that the new controller developed in this project offer over existing controllers. To achieve this various techniques and algorithmic patterns have been used to improve the operation of the micro tubular fuel cell system from Adelan Ltd above and beyond the commercial controller and KJ100. The three fuel cell stages (warmup/operation/shutdown) have been controlled and manipulated to increase the SOFC efficiency and longevity where possible.

KJ101 aims to utilise all of the available connected sources of the plant to deliver consistent and controlled warmup profile cycles and then reach a thermally stabilised operation by using fuel flowrate and cooling fan speed as main manipulating inputs. The power increase alongside the thermal stability were of interest in this study. In addition, KJ101 is designed to monitor the battery charge, defining when it is ready to initiate and shut down. The shutdown procedure has been designed to remove the heat out of the system homogenously across the fuel cell channels, improving the longevity and sustainability by minimising the negative impacts of the local temperature gradient. Another feature of the proposed controller is a reasonably quick shutdown, where a physical switch is present to initiate the faster removal of heat for specific scenarios that will be discussed in Section 6.5.

The improvements achieved in KJ101 are described for each stage of the SOFC operation in the sections below.

### 6.2 Improvement #1: Smoother and well-controlled start-up process

As described in the previous chapter, KJ101 was designed to control the fuel cell parameters and improve its functionality where possible. Multiple tests were carried out to find optimal ways to reduce start-up time and temperature variations. The KJ101 control algorithm has also been adjusted to smooth out the sudden temperature changes that typically result from variation of fuel and air input. These additional features are targeted to increase the lifetime of the cell.

The Adelan  $\mu$ SOFC uses an electric heater to start warming up until reaching operation mode. This heater requires power to operate, and this power is drawn from the battery however in the start-up mode there is no way for the fuel cell to generate power until it reaches 620°C. To tune the algorithm for KJ101 the electric heater was repeatedly tested for the time it required

to complete the start-up phase. KJ101 has an important task, to maintain enough charge in the battery for the fuel cell to be able to always operate as a viable top up battery charger.

In the following experiment the same Adelan system has been tested with two different start-up scenarios. The first scenario employed KJ101 but with the same algorithmic logic that has been deployed by BC (where BC was the commercial controller). The fuel cell takes on average 15 minutes to warmup, however in the transition periods as can be seen in *Figure 6.1* there is a sudden temperature variation occurring at fuelling,  $t = 12.6\text{s}$  that is not desirable in practical applications. This is graphically presented in more details in *Figure 6.2* such a sudden change may cause local and overall, thermally induced stresses shortening the fuel cell system lifespan in the long run.

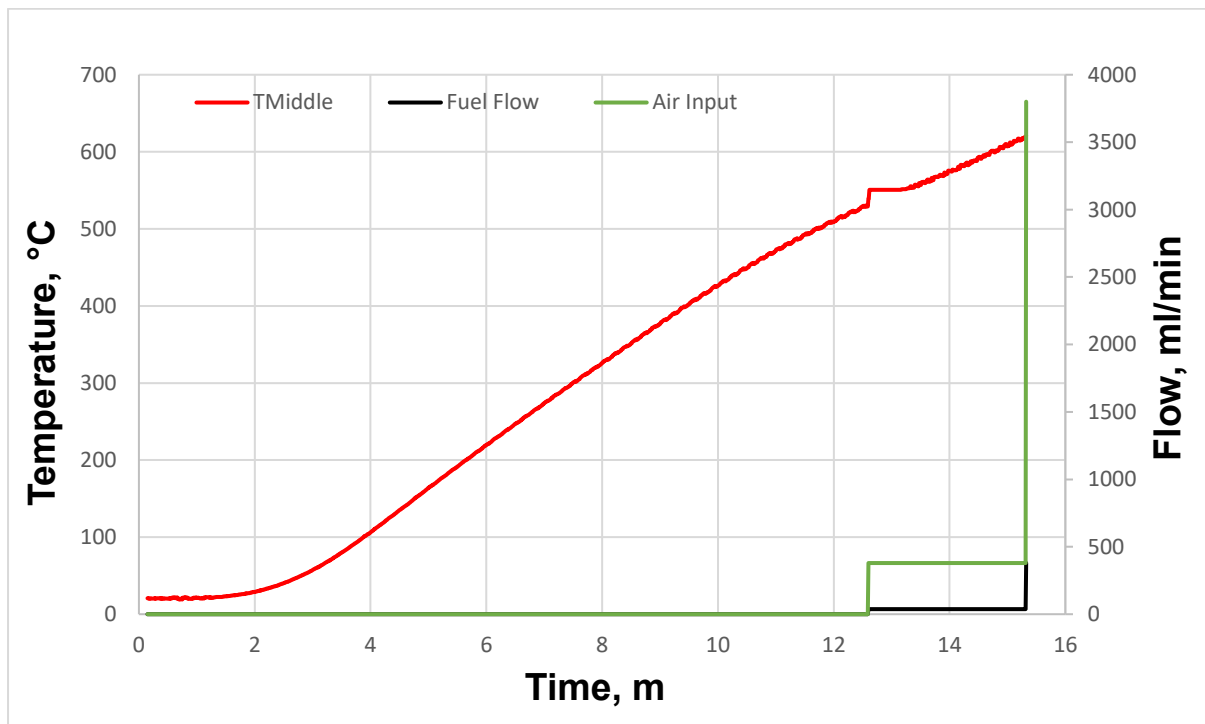


*Figure 6.1 Warmup Using the Basic Adelan*

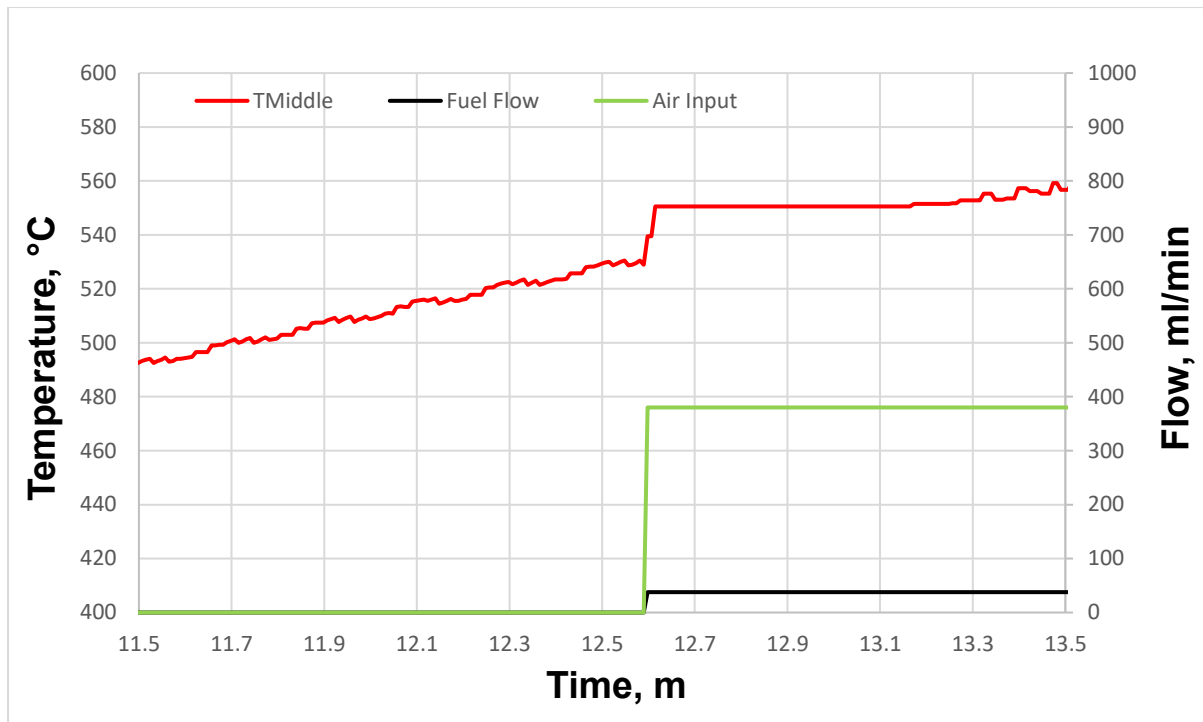


Figure 6.2 A sudden temperature and air flow changes due to fuel being introduced into the system

The SOFC its designed to self-sustain itself at higher temperatures through the heat release by the chemical reaction to generate power. In general terms the more fuel results in more heat. In this instance, the temperature suddenly changes that can be linked to the sudden fuel flow increase. Therefore, in the next experiment the algorithm in the warmup state will be modified, at the time when the system temperature will reach 380 C near the POX area, the fuel and air input will increase by 2.52 ml/min and 25.2 ml/min respectively until the required amount has been reached in the required stage 38 ml/min of LPG and 380ml/min of air. Then once again the same pattern will occur at  $T = 580$  C. In general terms this ramping philosophy will follow KJ101 everywhere, when a change is required, it will happen with a ramping technique.

In the next test, the KJ101 algorithm has been improved to amend the fuel and air input flowrates in an incremental pattern as can be seen in Figure 6.3. This modification, results in a smoother transition, in contrast to the previous test, because of the fuel exothermic chemical reaction occurring in a slower rate therefore releasing heat in a gentle pattern allowing the system to adjust smoothly.

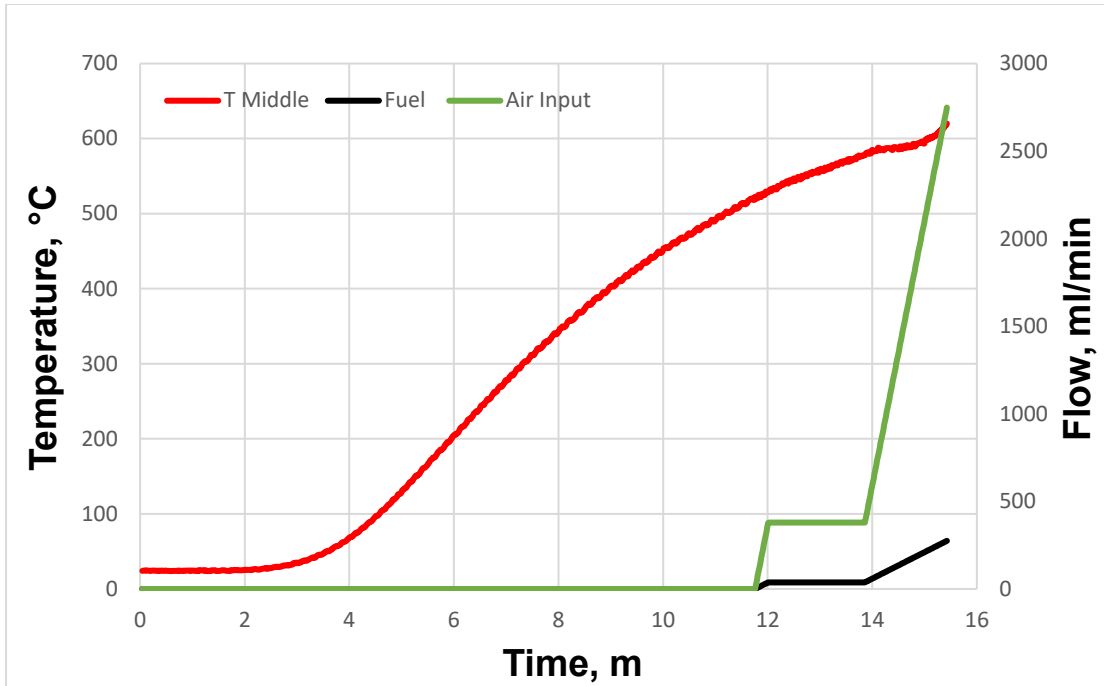


Figure 6.3 KJ101 Uses Ramping Technique for a smoother warmup

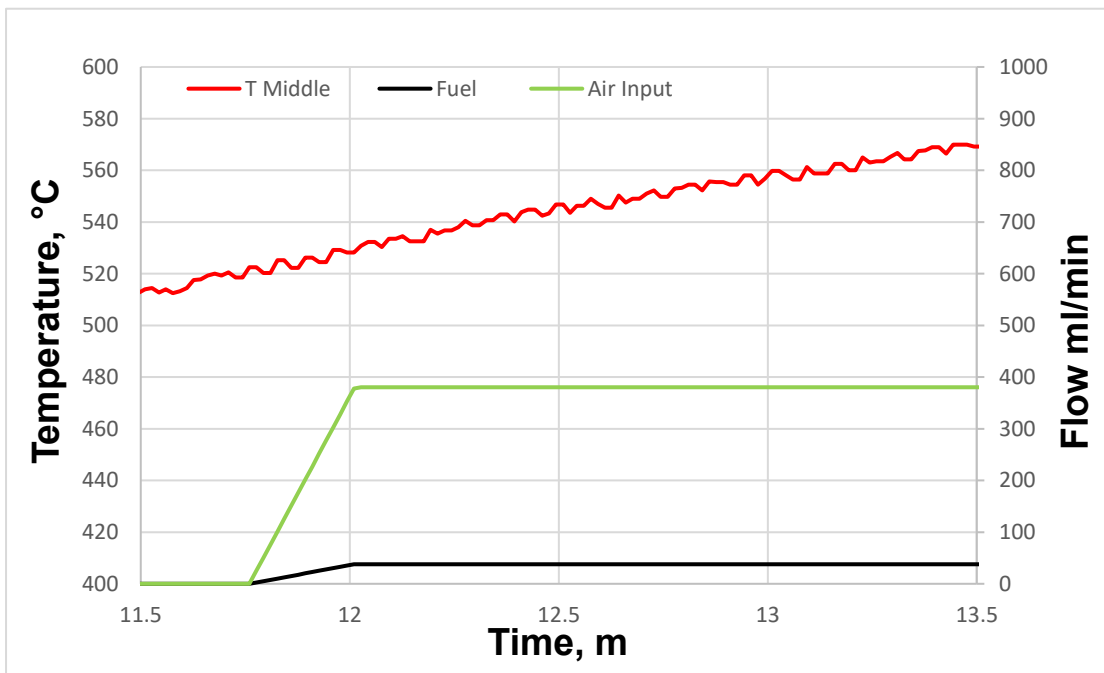


Figure 6.4 Warmup temperature trajectory gently controlled, the sudden change is eliminated at feeding point due to improved incremental fuel and air input offered by KJ101.

In Figure 6.5, the performance of KJ101 and BC in ramping the SOFC temperature are shown. As it can be seen in this figure, the warmup stage can be completed in shorter time and with no fluctuation when KJ101 is applied.

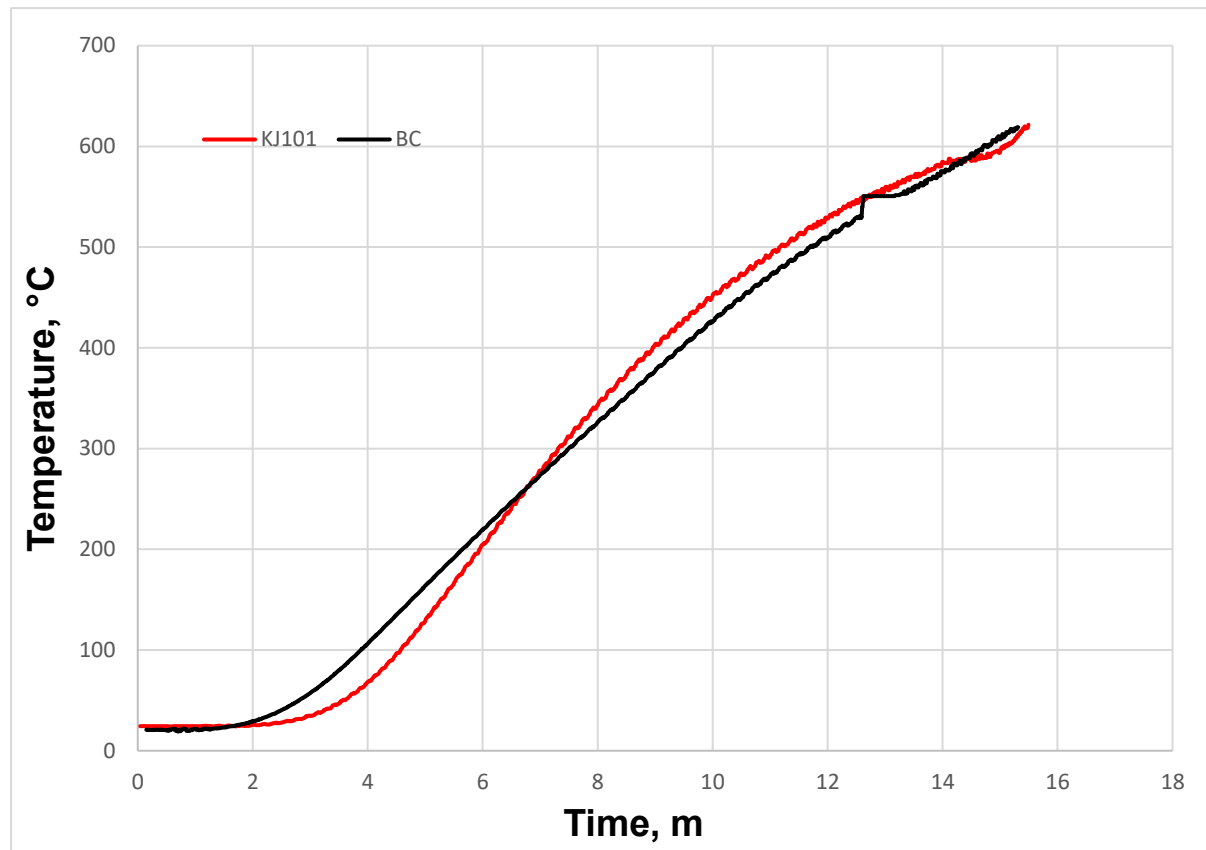


Figure 6.5 Warmup stages for KJ101 and BC

### 6.3 Improvement #2: Start-up (warmup) process flexibility

As mentioned above, the default start-up operation for the system takes roughly 15 minutes with an average rate of change of  $0.6^{\circ}\text{C}$  per second. However, in some cases there might be a need for the fuel cell to complete the start-up phase at a faster rate. For example, a scenario when for some unforeseen reason the drain on the battery is larger than expected and will outpace the charging rate. In this case, KJ101 has three contingency modes. Each contingency has been tested to finish the starting up by an equivalent time depending on the remaining battery charge. The right contingency mode is selected according to the level remaining of the battery. For example, if the battery is at 30% its contingency mode 3, for 35% its contingency 2 and for 40% its contingency 1.

Table 6.1 Contingency mode details

	<b>Contingency 1</b>	<b>Contingency 2</b>	<b>Contingency 3</b>	<b>Normal Start-up</b>
<b>Warmup Stage 1</b> <b>T= Room Temperature</b>	Fans 20% Heater ON Air in OFF Fuel in OFF	Fans 15% Heater ON Air in OFF Fuel in OFF	Fans Off Heater ON Air In OFF Fuel In OFF	Fans 30% Heater ON Air in OFF Fuel in OFF
<b>Warmup Stage 2</b> <b>T=380</b>	Fans 25% Heater ON Air in 400ml/min Fuel in 40ml/min	Fans 20% Heater ON Air in 450ml/min Fuel in 45ml/min	Fans 10% Heater ON Air in 726ml/min Fuel in 76ml/min	Fans 35% Heater ON Air in 380ml/min Fuel in 38ml/min
<b>Pre-Operation Stage</b> <b>T= 580</b>	Fans 30% Heater ON Air in 3800ml/min Fuel in 380ml/min	Fans 25% Heater ON Air in 4000ml/min Fuel in 400ml/min	Fans=15% Heater pulsed Air in 450ml/min Fuel in 4500ml/min	Fans=40% Heater ON Air in 3800ml/min Fuel in 3800ml/min

From multiple tests in room temperature these modes have been calibrated to perform the same actions, mode 1, 2 and 3 take 12.2, 10.4 and 7.5 minutes, respectively. According to the Adelan experts these modes might shorten the lifespan of the fuel cell but not that significantly since the rate of change has been maintained unanimously across the warmup. These modes are to be used as last resort for emergency power, the controller will update the plants LCD screen to inform the user if he would like to proceed with the contingency mode. KJ101 is the only controller that can detect the battery level and proceed to the right contingency mode as seen in the next figures.

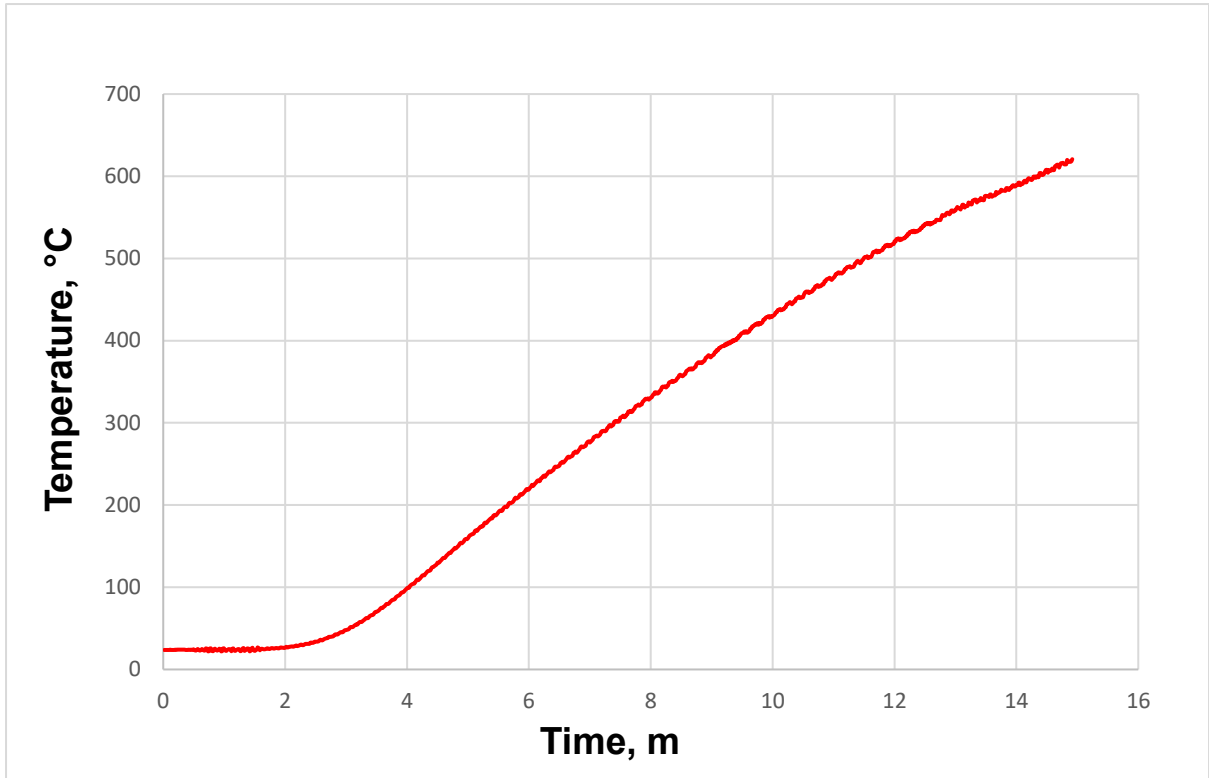


Figure 6.6 A typical transient temperature profile during normal warmup

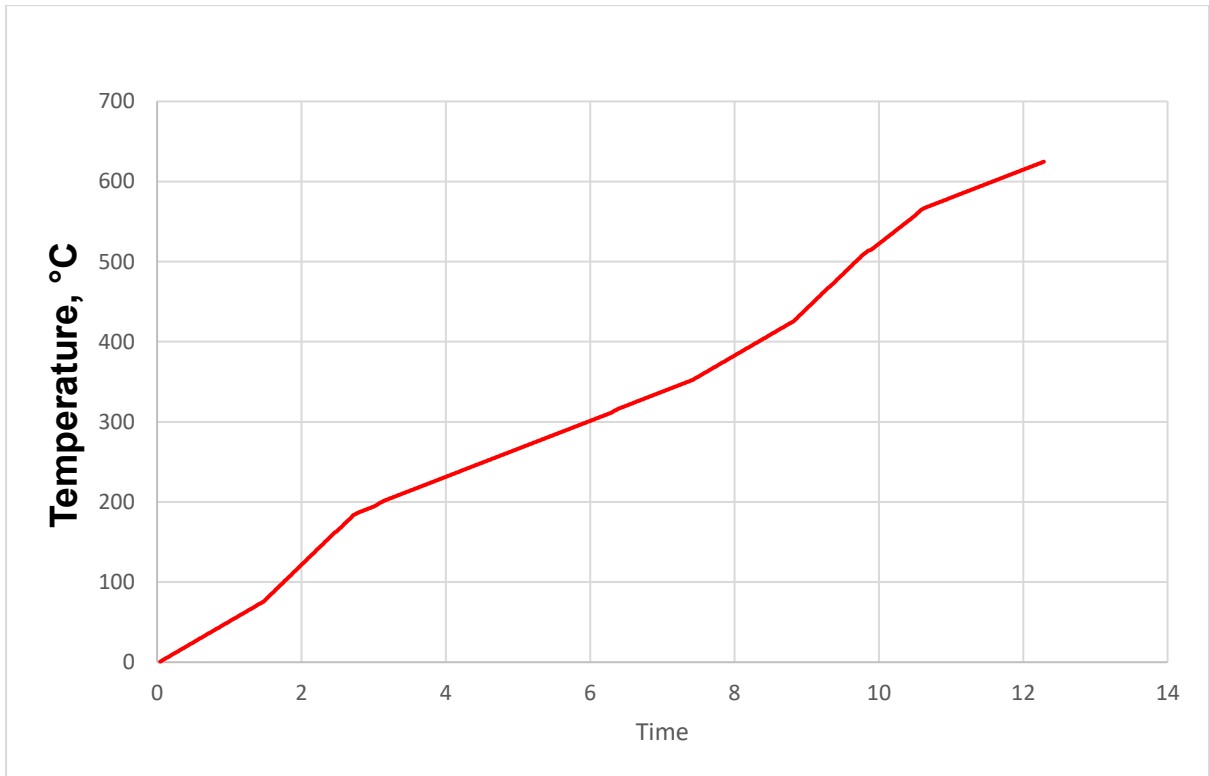


Figure 6.7 Contingency Mode 1 warmup using KJ101, cooling fans reduced for more heat to be generated by the electrical heater.

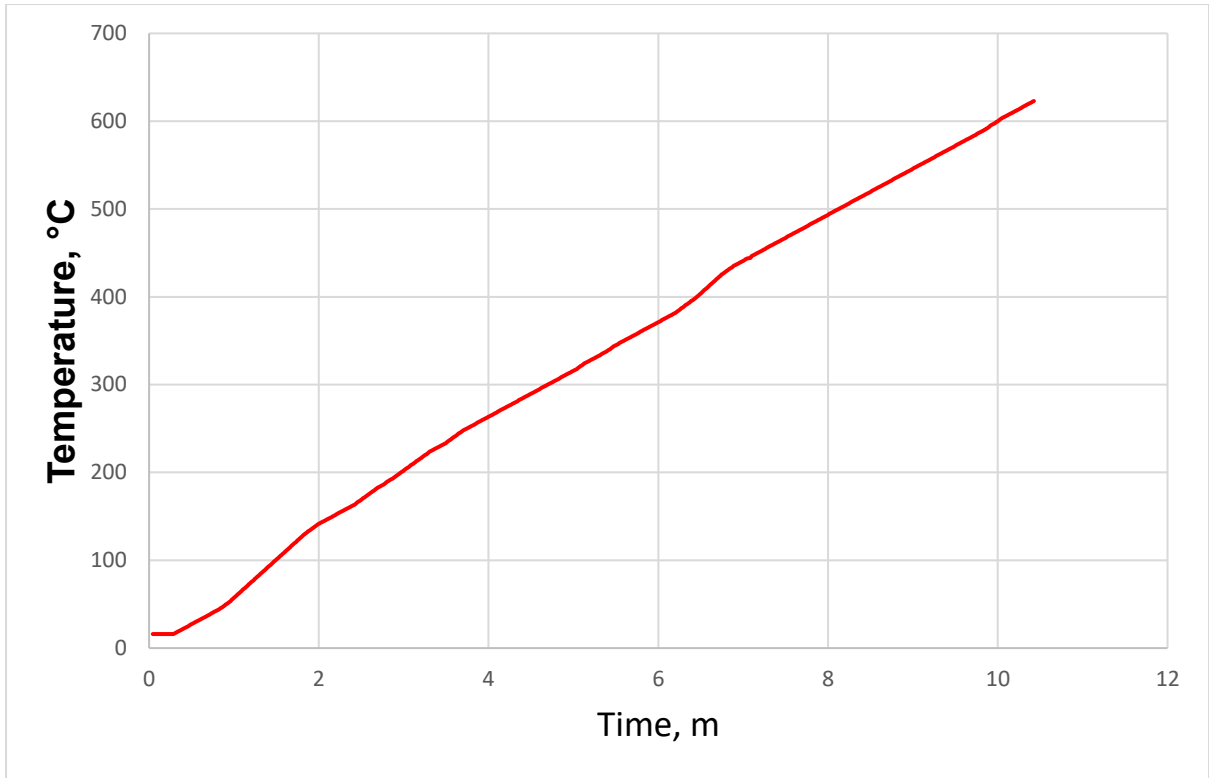


Figure 6.8 Contingency Mode 2 warmup using KJ101

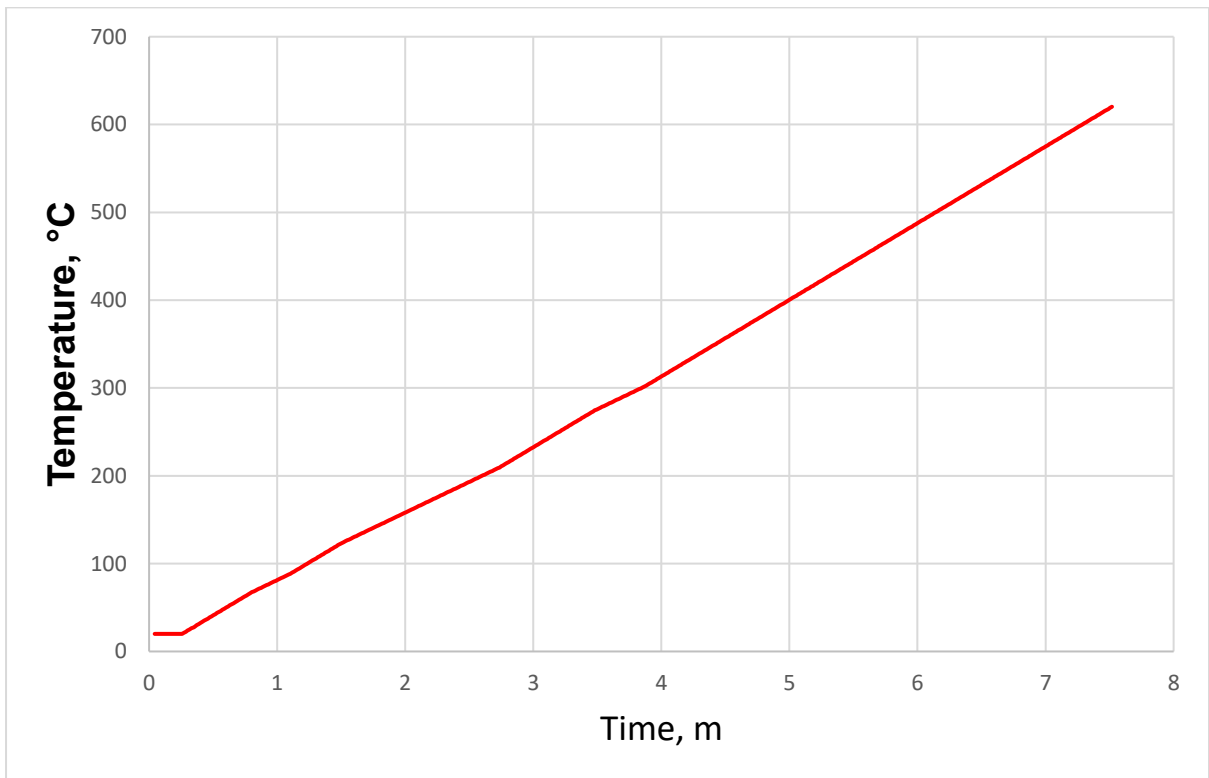


Figure 6.9 Contingency Mode 3 warmup using KJ101

Table 6.2 KJ101 power draw in different configurations

Mode	Warmup Stage 1 (0 to $\approx$ 500) Power draw from KJ101 (W)	Warmup Stage 2 (500 to 620) Power draw from KJ101(W)	Warmup Completion (minutes)
Normal Warmup	7	10	15
Contingency Mode 1	6.5	9.5	12
Contingency Mode 2	6.1	9.3	10.4
Contingency mode 3	6	8.9	7.5

The KJ101 can run the warmup process through various temperature trajectory depending on the process demand such as battery charge level. As a whole unit the controller can use contingency modes to reach to operation stage even when battery is low. Battery can be lower than optimal for various reasons, such as bad usage from the user. Having this contingency mode, the Fuel Cell system can be used in a situation where the battery is lower than optimal. Fuel Cell efficiency and longevity must be reassessed for each scenario. However, this capability will mostly be used in emergency situations to restore the battery.

## 6.4 Operation Stage Improvements

### 6.4.1 Improvement #3: Reaching setpoint with minimal variation

In this section the controller is tested for its performance in the normal operation phase that may lead to the lifetime increase. One of the options to improve the lifetime of the fuel cell is to smoothly stabilise the temperature with as few of sudden temperature variations as possible. Increasing the power in SOFCs requires increase the fuel flow which subsequently results in temperature increase due to the exothermic nature of the overall reaction. The released heat and temperature increase must be regulated by a proper control mechanism that acts timely and effectively. A series of tests were carried out to optimise the control parameters for this target.

The aim for this experiment was to examine if KJ101 can stabilise the system temperature during the normal operation stage. Its performance, then, has been compared with the current Adelan controller. The KJ01 in this lab test used a normal start up. Both controllers (KJ101 and BC) were instructed to act dynamically from 620°C to reach the set point = 700°C.

The BC met the operation stage setpoint in 30 minutes with an average rate of temperature change of 2.6°C per minute (Figure 6.10). In the KJ101 case temperature steadily rose to the setpoint with an average rate of change of 11.4°C per minute, until eventually the temperature rose above the setpoint for 3 minutes and the fans had no fluctuation (Figure 6.11). While BC was increasing the temperature, a sudden drop happened at  $t = 45$  min, which delays the

reach for setpoint. This sudden change can cause a crack in the tube. BC wasn't fast enough to react to the change and reduce the speed of the cooling fans. On the contrary, KJ101 reaches setpoint in almost linear fashion but passes the setpoint for 3 minutes to evaluate and adjust the speed accordingly to reach setpoint. For the remaining time KJ101 it stabilises to the setpoint for the remaining time under operation stage, BC temperature varies for a significant time and then settles at 695°C five degrees lower than the setpoint. In this instance the controller should have lowered the fan speed a bit more to allow more heat and reach setpoint but as seen in Figure 6.10 the fan is basically staying steady for an extended period. The observations showed that the KJ101 performs better as its more stable, reliable and its controlling technique reacts as its expected in comparison with the uncertainty of BC.

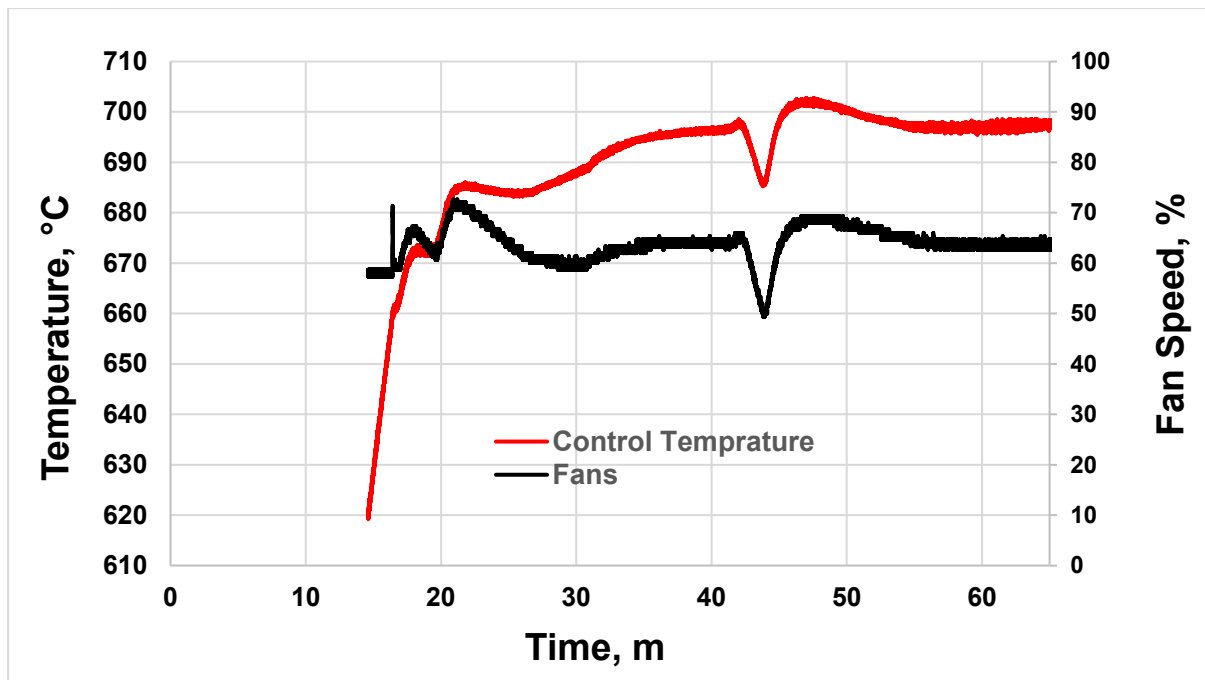


Figure 6.10 Adelan Fuel Cell operation stage control using BC.

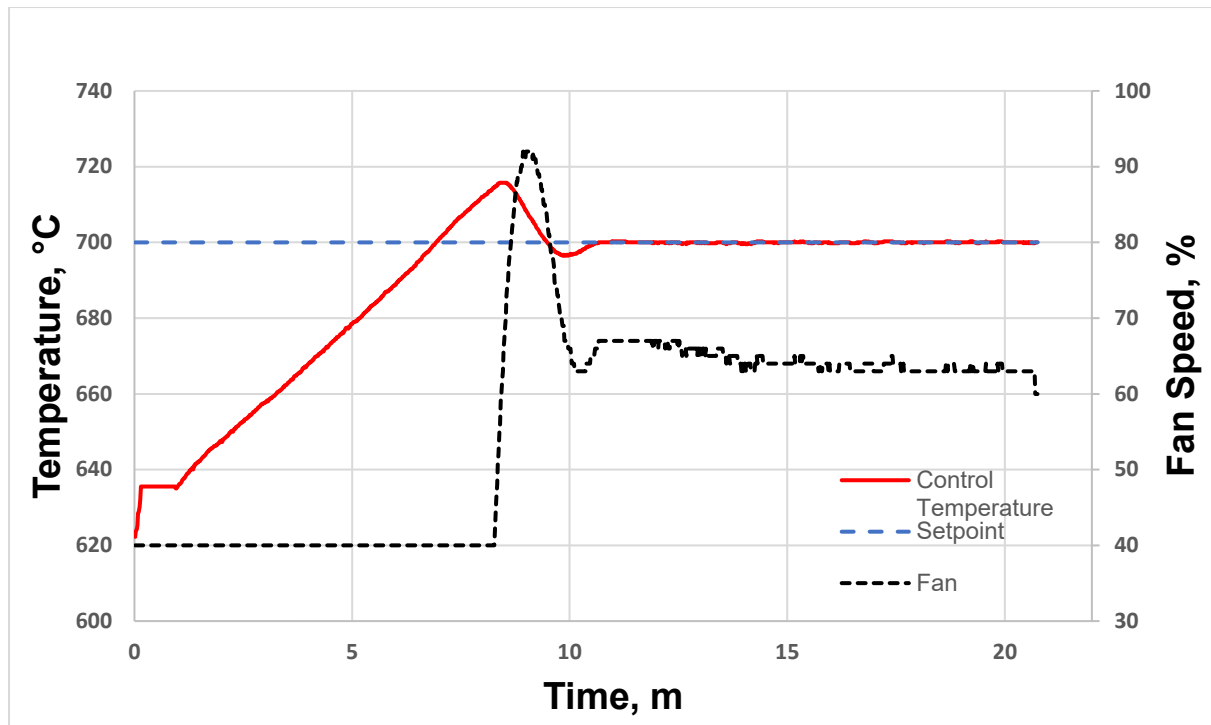


Figure 6.11 Adelan Fuel Cell operation stage control using KJ101.

The fuel cell was exposed to the same conditions for 4 more times. After several of hours of operation it was found that the fuel cell system dropped performance and required refurbishing as a fuel cell tube in the system was cracked. The tube was cracked at the front end where POX is located Figure 6.13 The proposed controller was able to demonstrate better results from the basic controller however they were still not adequate. This experiment was replicated multiple times yielding the same results then it was concluded that this is an indication that a sudden change of temperature was the main reason behind this problem.

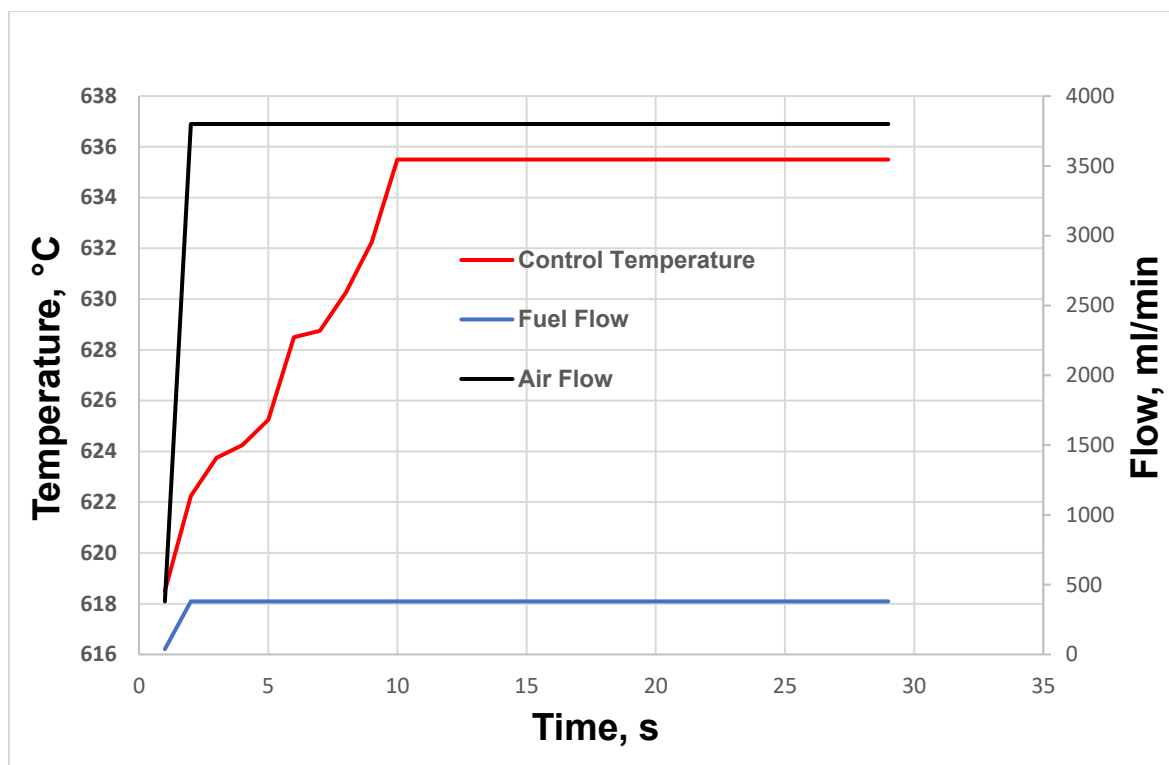


Figure 6.12 The transition from warmup to the operation stage



Figure 6.13 Sudden temperature change caused a sever crack in the CPOX area

In this investigation the fuel cell was set to stabilise at 700 °C. The fuel is mixed with air, the fuel input is 380ml/min and the air input 3800ml/min meaning a ratio of 1/10. As can be seen in Figure 6.14 the specific fuel cell required 13.1 minutes to reach 700 °C for the first time, after that the calibration process followed which required 3.3 minutes for stabilisation. Once

calibration concluded the fans capacity varied from 69% to 73%. In the same experiment, the air pump device has slowly increased the mixture of air by 50ml/m per second to avoid thermal flake in the POX location. It is worth mentioning that the fuel flow rate is not adjusted smoothly yet, therefore this could be the reason a small, but sudden, change in temperature can be still seen in the beginning of this stage. From this experiment results, the KJ101 can maintain the system temperature by quickly calibrating to the setpoint while being able to respond at very fast rates when step changes are about to happen. For the first time, an experimental  $\mu$ SOFC stabilisation is achieved to a minimal of  $0.50^{\circ}\text{C}$  after calibration. A ramping up technique is introduced to reduce thermal shocks.

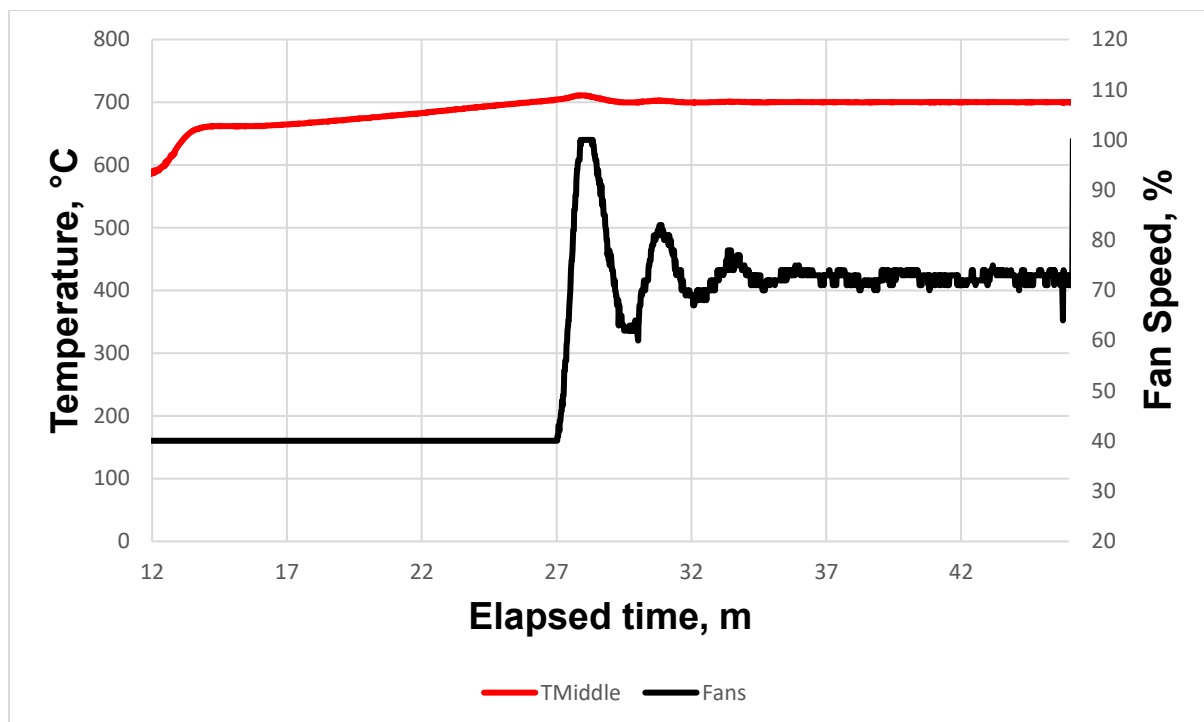


Figure 6.14 Transition to operational stage

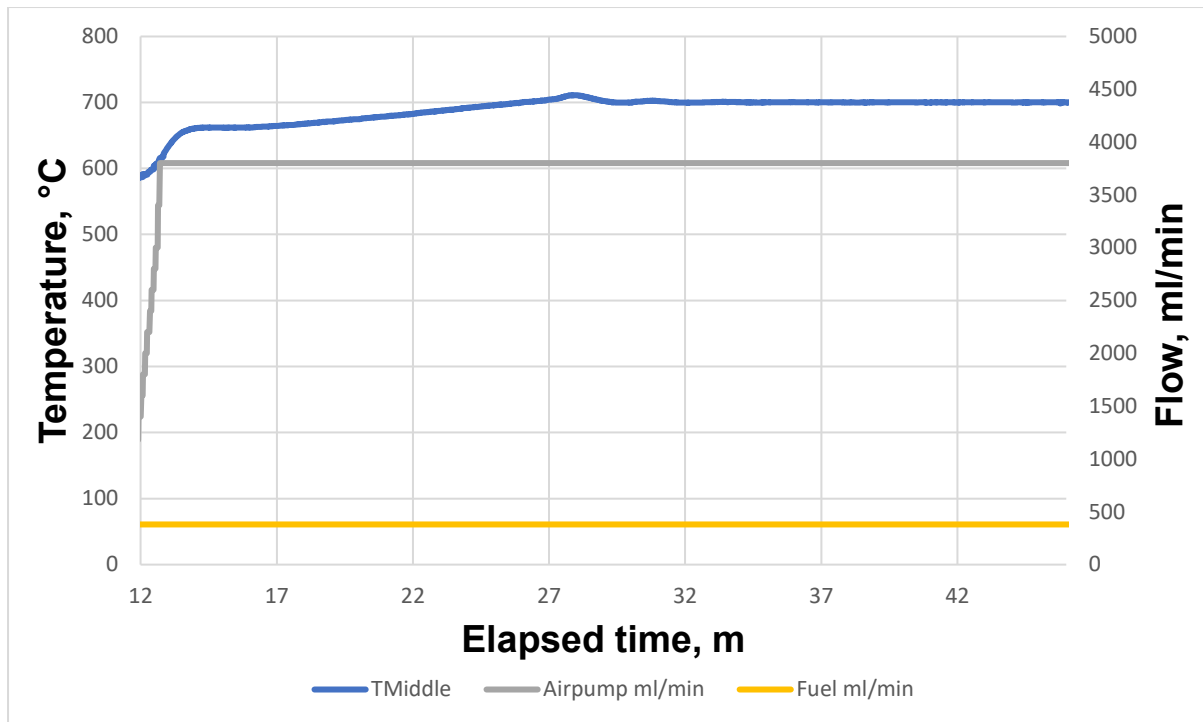


Figure 6.15 Transition to normal operation stage using ramping technique for air input

#### 6.4.2 Air to fuel ratio control

Previous test showed that slowly increasing the air flow when entering operation stage of the  $\mu$ SOFC significantly improved the temperature. A test was conducted to test the KJ101 capability Air to Fuel ratio control (Figure 6.16). The fuel flow will slowly increase at the same time as air to keep the 1:10 ratio. The remaining parameters were kept constant. At first sight from the graph shows a difference in the beginning of the stage, where temperature is increasing steadily without sudden changes. Another variation can be inspected with respect to time, operation stage is reached within 14 minutes. This side result can be linked to the fuel input, this  $\mu$ SOFC design generates additional heat from the chemical reaction, whereas in this test the fuel flow was ramped up slowly which it's unavoidably slowing down the rate of the chemical reaction. In some cases, this extra minute to reach to the optimum temperature setpoint would reduce performance in terms of power output for that time. However, the gains are outweighing the performance loss for a minute as with this technique the lifetime of a  $\mu$ SOFC can be improved significantly.

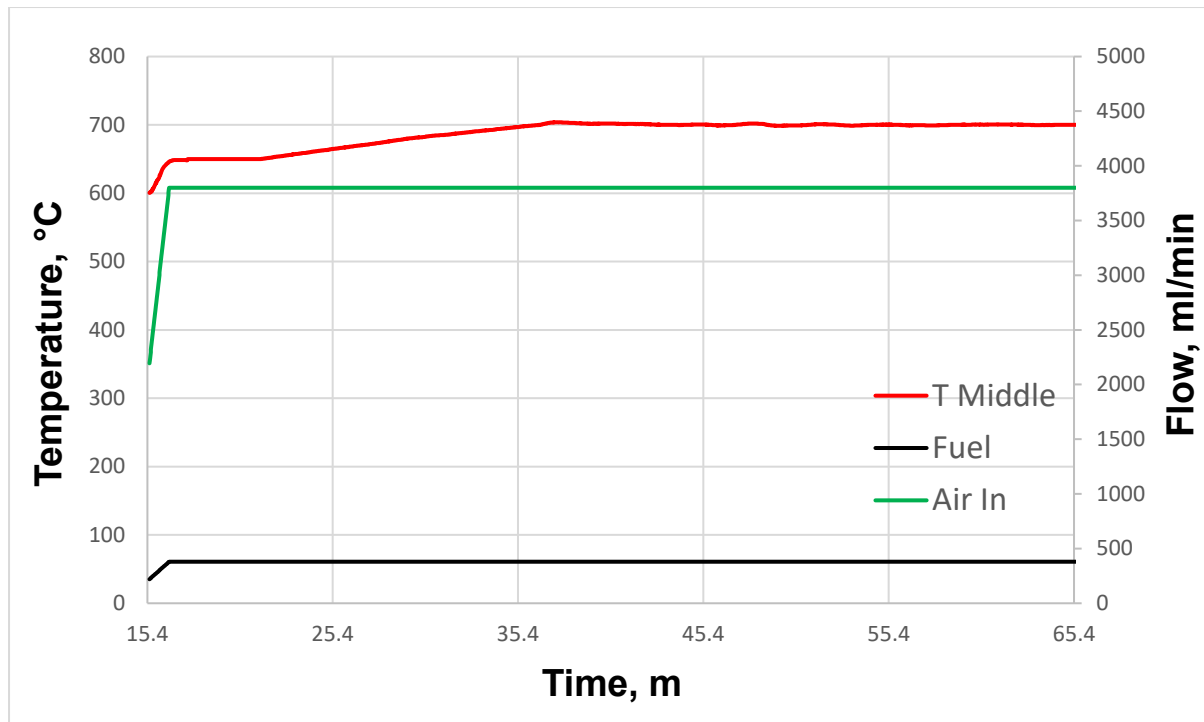


Figure 6.16 Both fuel and air are ramping up preserving the 10/1 ratio.

#### 6.4.3 Improvement #4: The flexibility of setpoints

In the previous section the temperature stabilisation improvement techniques from KJ101 were demonstrated. In this section the controller was set to change target setpoints while under operation. The setpoints were changed by a command using the console (connection between the KJ101 and the PC using RS232) of the KJ101, the setpoint could be altered by any value between 620 °C and 710 °C. This is to show and verify the flexibility of the controller. Experimental results use the same  $\mu$ SOFC system from Adelan.

In the first experimental test in this section, as shown in Figure 6.17 and Figure 6.18, the objective is to check the reaction of the controller at different temperature conditions. The warmup operation has gone smoothly and rapidly using the default warming setup profile. Initially the temperature overshoots by few degrees Celsius, this is to be expected as there is a calibration period. KJ101 is for the first time able to fully control the system and is able to stabilise at all given setpoints ranging from 700°C to 630°C with very minimal changes.

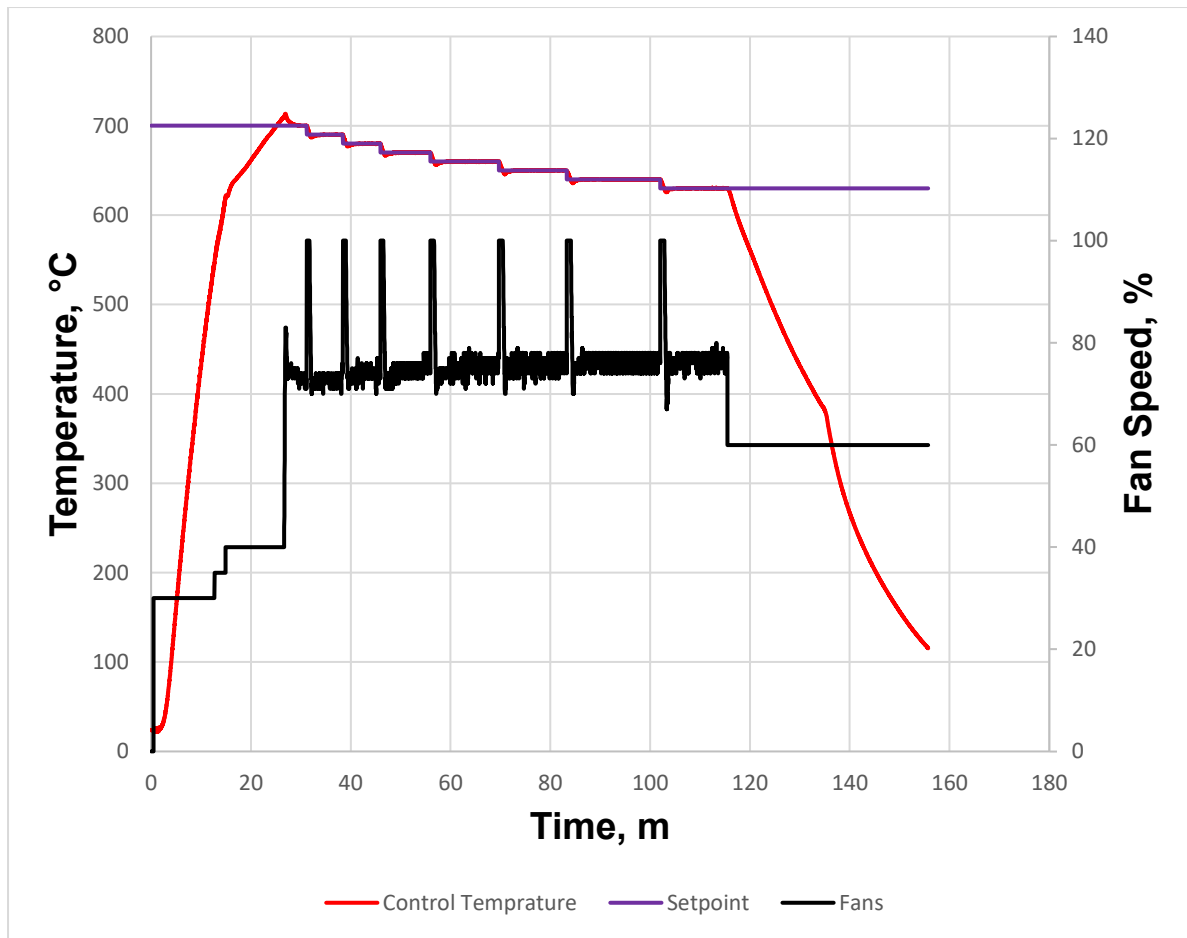


Figure 6.17 KJ101 meets different setpoints in time-effective manner while under operation

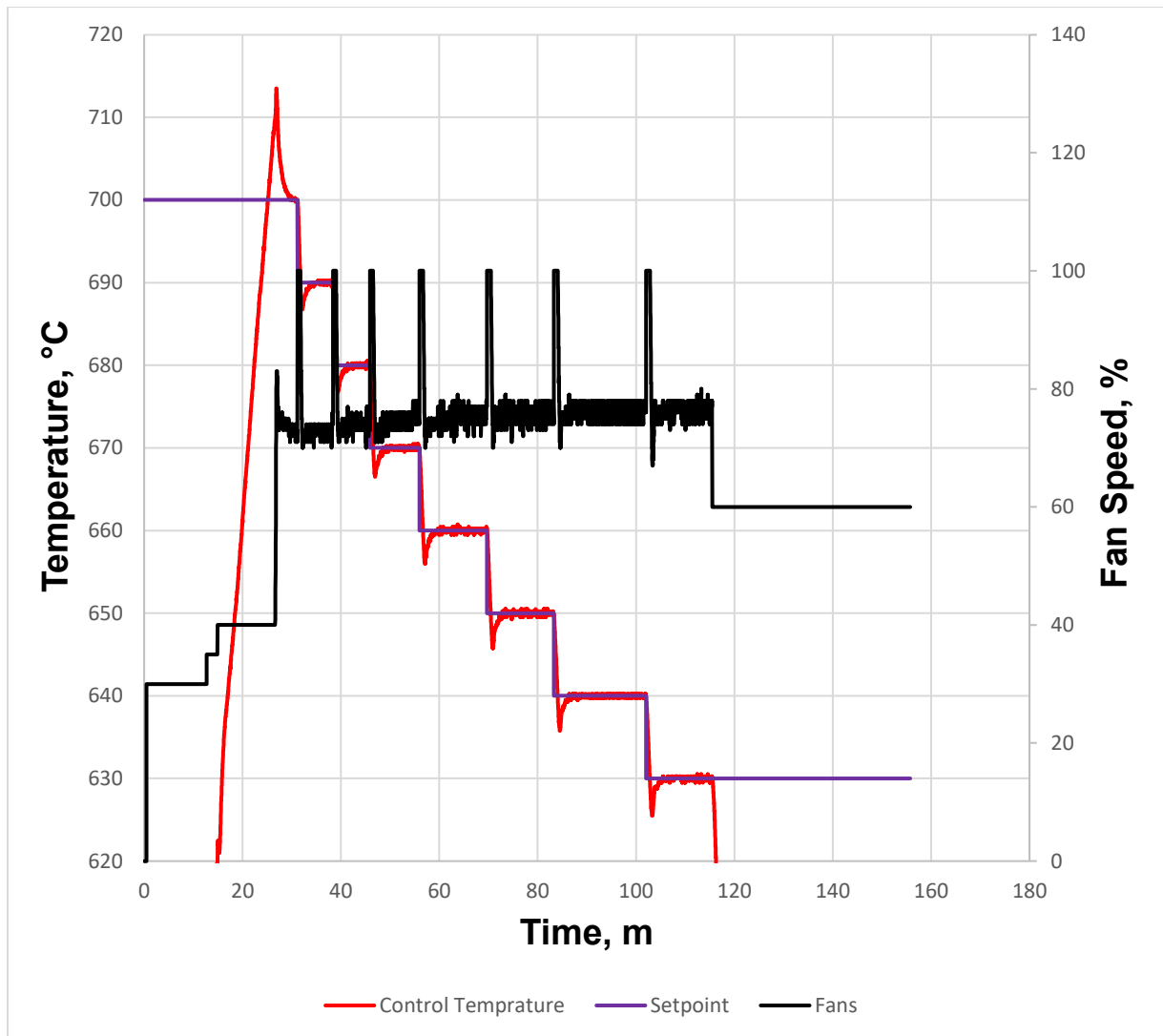


Figure 6.18 KJ101 meets different setpoints in time-effective manner while under operation

The first setpoint was set to 700°C. The system is seeing a slight overshoot in the beginning of the process this an expected result as the controller is trying to learn and calculate the behaviour of the fuel cell. For several minutes the fuel cell was allowed to settle at 700°C. The command for the next setpoint was then entered for the cell temperature to drop to 690°C. The controller can be seen to immediate react to the changes, for this phase change the controller is now acting as if there is a 10°C overshoot, therefore the first response to this change is for the fan speed to rise to exhaust the heat until it reaches 690°C. The system reached the set temperature at a rate of 0.05°C per second, where it slightly missed the new setpoint by 3°C and undershoots for 3 minutes. At this point the controller is calibrated to be super gentle and targeting stabilisation to an impressive result of +/- 0.5°C, however as in this case this can have a small drawback, when the system deviates from the setpoint drastic changes are happening, such as full-blown fans for an extensive period. This interaction can be fixed however as can be seen in this Figure 6.19. Though, this could complicate things

even further for the reason that if the controller was to overshoot without any command given, it would not increase cooling immediately, which could end up shortening the fuel cell lifetime. One thing that needs to be reiterated is that this controller is there to increase lifetime and performance efficiency of the fuel cell by stabilising the temperature as much as possible and in this case 3 minutes of overshoot impacts the power output for a very short of time to ensure lifetime. For the following setpoint step changes an exact same pattern can be seen Figure 6.20 which is thanks to the controller algorithmic strategy. This is the first time an Adelan  $\mu$ SOFC has been able to change setpoints at the same time during operation. This result proves that the controller its able to stabilise at any setpoint and consequently opens a new way of utilising the temperature control of a fuel cell for various applications.

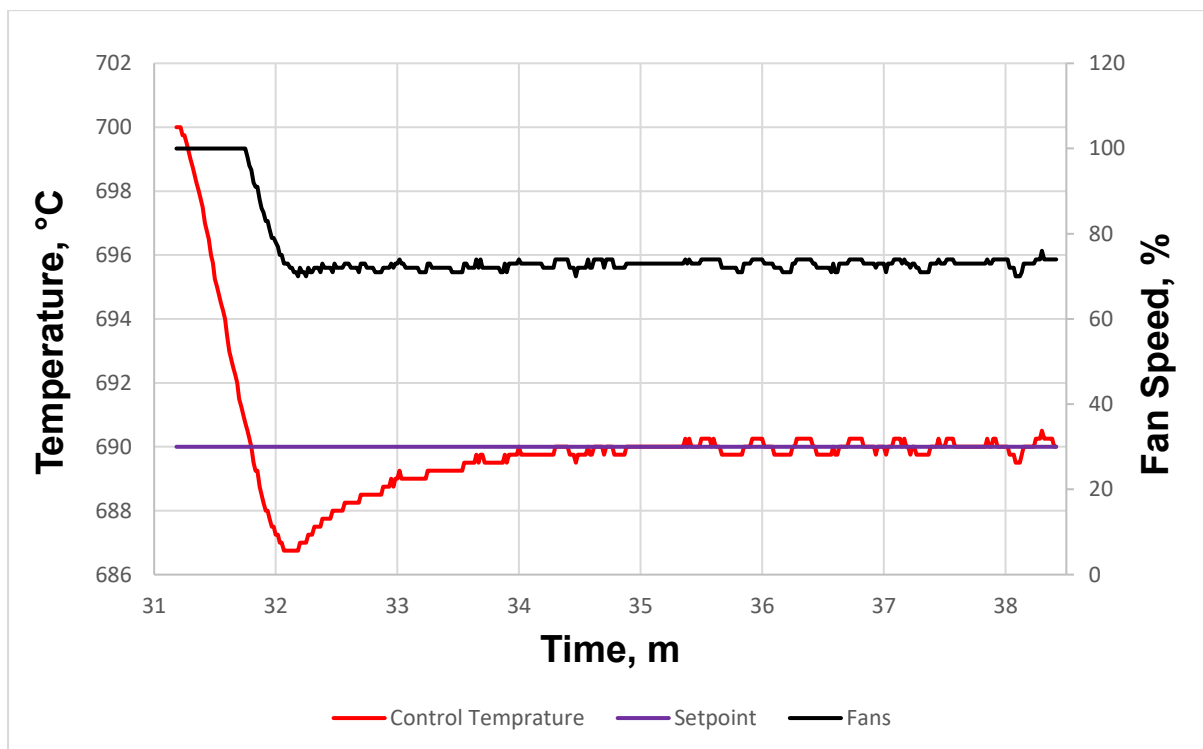


Figure 6.19 While the fuel cell is operating a command is given to KJ101 to test its reaction to a different setpoint at 690 °C

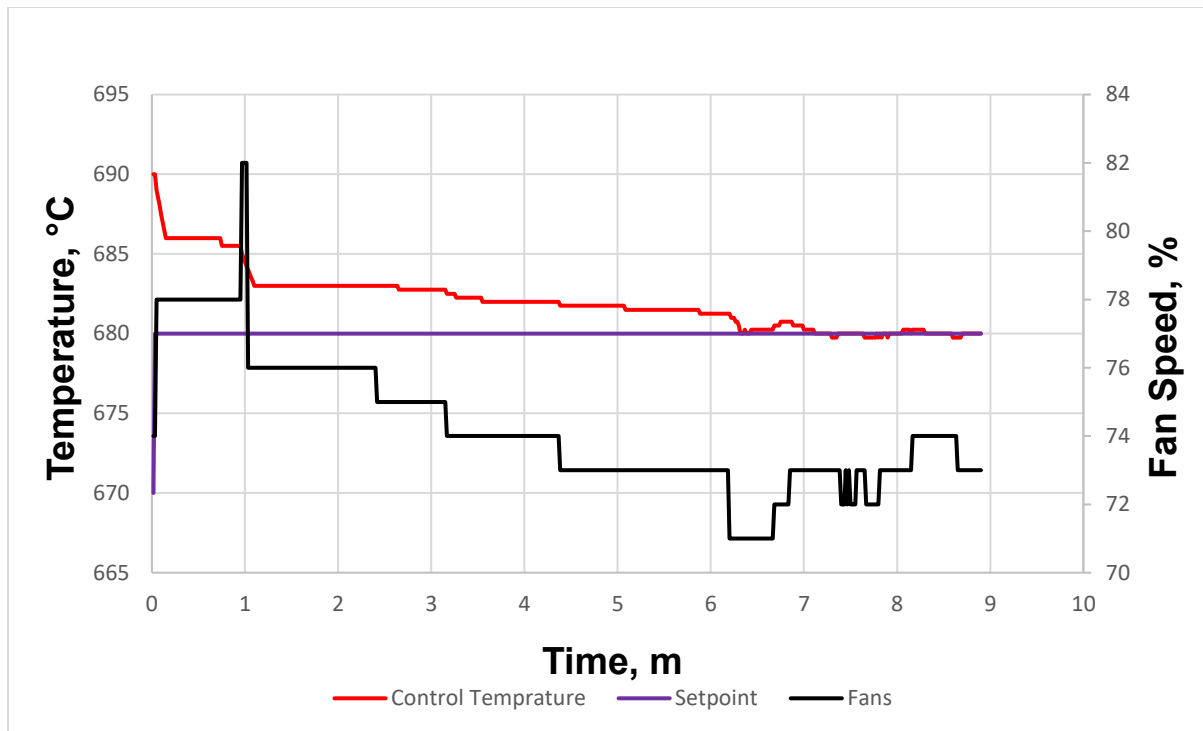


Figure 6.20 While the fuel cell is operating a command is given to KJ101 to test its reaction to a different setpoint at 680 °C

Having the option to have different setpoints while under operation is a very powerful tool. From the literature it is known the higher the temperature of the  $\mu$ SOFC the more power to be generated. However, while the fuel cell is under operation, the load might require less power. In this instance the controller could slowly adjust to a lower setpoint to consume less fuel while also consuming less electric power for the fan speed. If the load changes again the controller will be able to put the system back to the maximum setpoint.

#### 6.4.4 Improvement #5: Temperature variation around the SOFC core

The sensitivity analysis in Chapter 3 revealed that the air to fuel ratio change may result in sharp rise in the temperature near the location of the inlet thermocouple. The practical data from the Adelan fuel showed that the temperature difference between the inlet and the middle points can be typically between 30 °C to 40 °C in the operation stage.

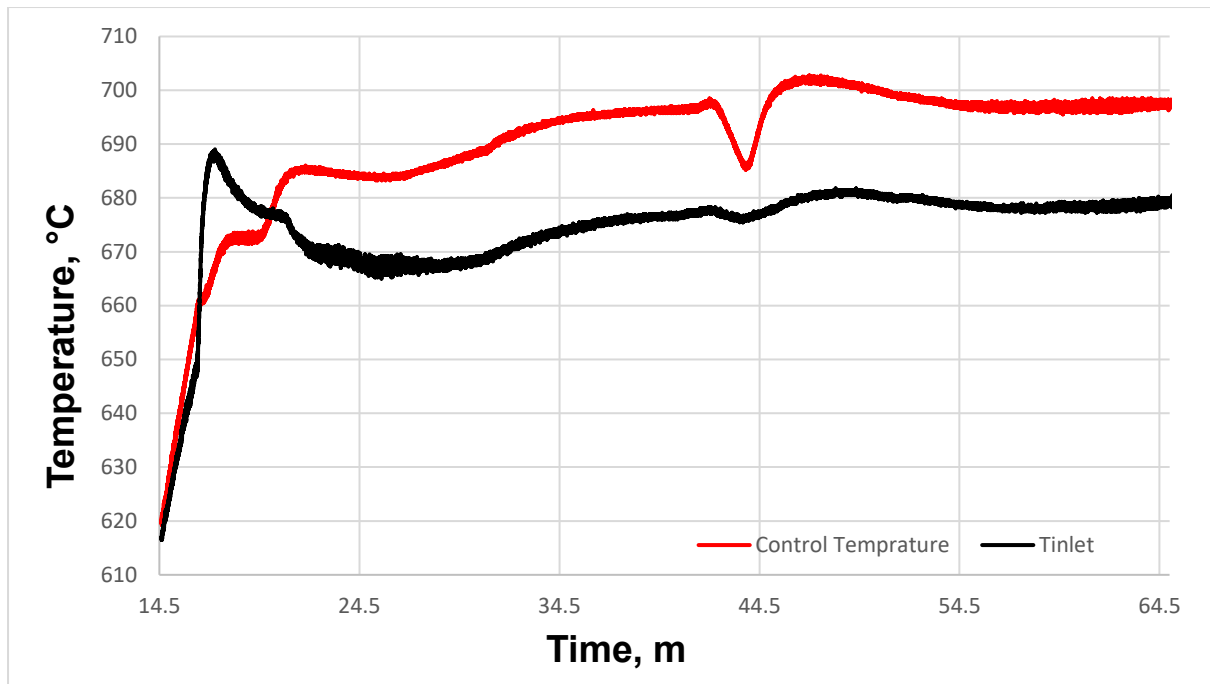


Figure 6.21 Temperature difference when using the basic controller

In the following experiment Figure 6.22 to Figure 6.24 KJ101 will use a new control strategy for the air flow utilising ramping technique to evaluate whether the change of air to fuel is something to be considered for adjustment for a short period in hope to bring inlet temperature closer to the main middle temperature.

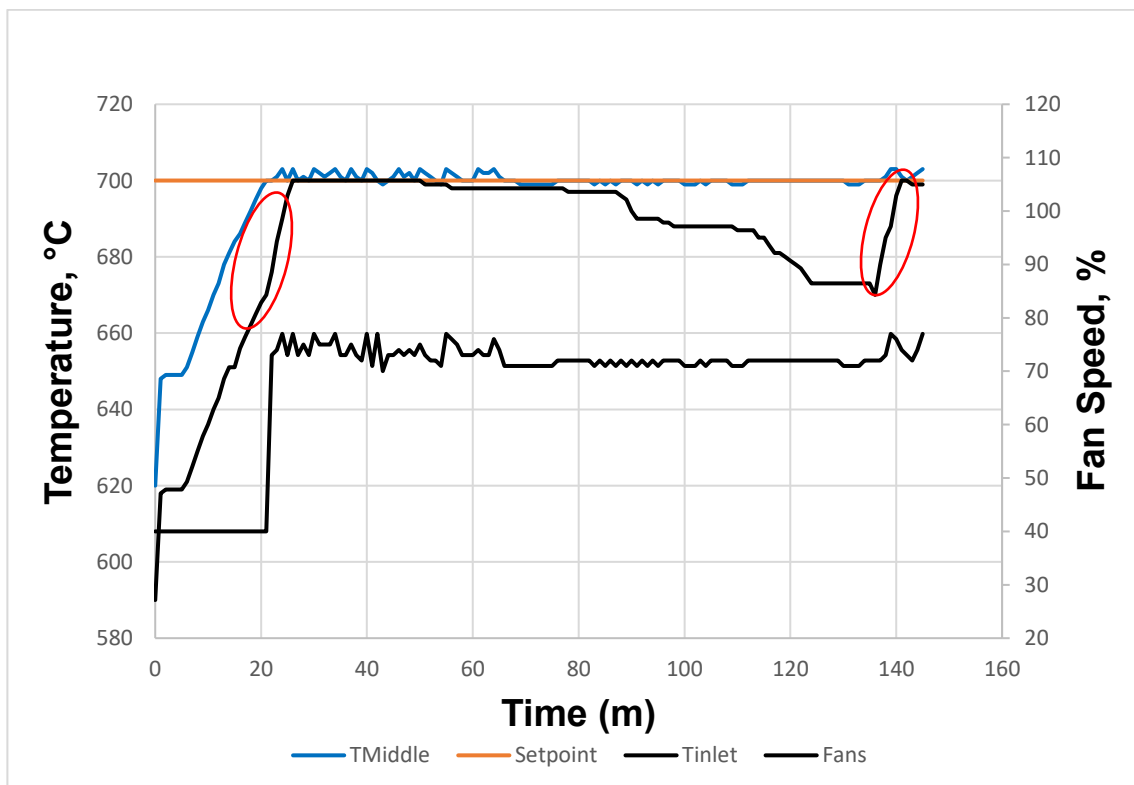


Figure 6.22 The temperature between the fuel cell is not the same therefore KJ101 is using software to adjust the air input to temporarily reduce temperature variation

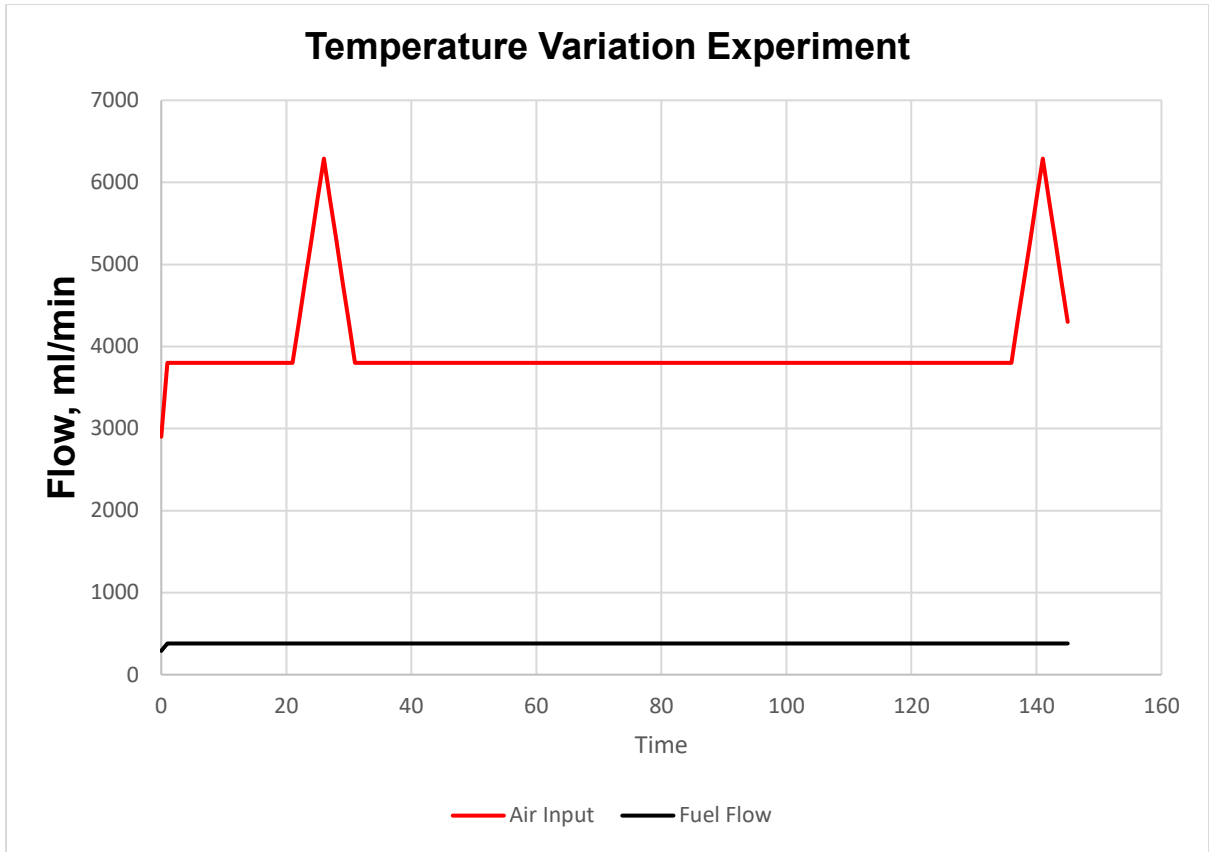


Figure 6.23 For few minutes the air to fuel ratio is changed to increase the temperature in the T1 location.

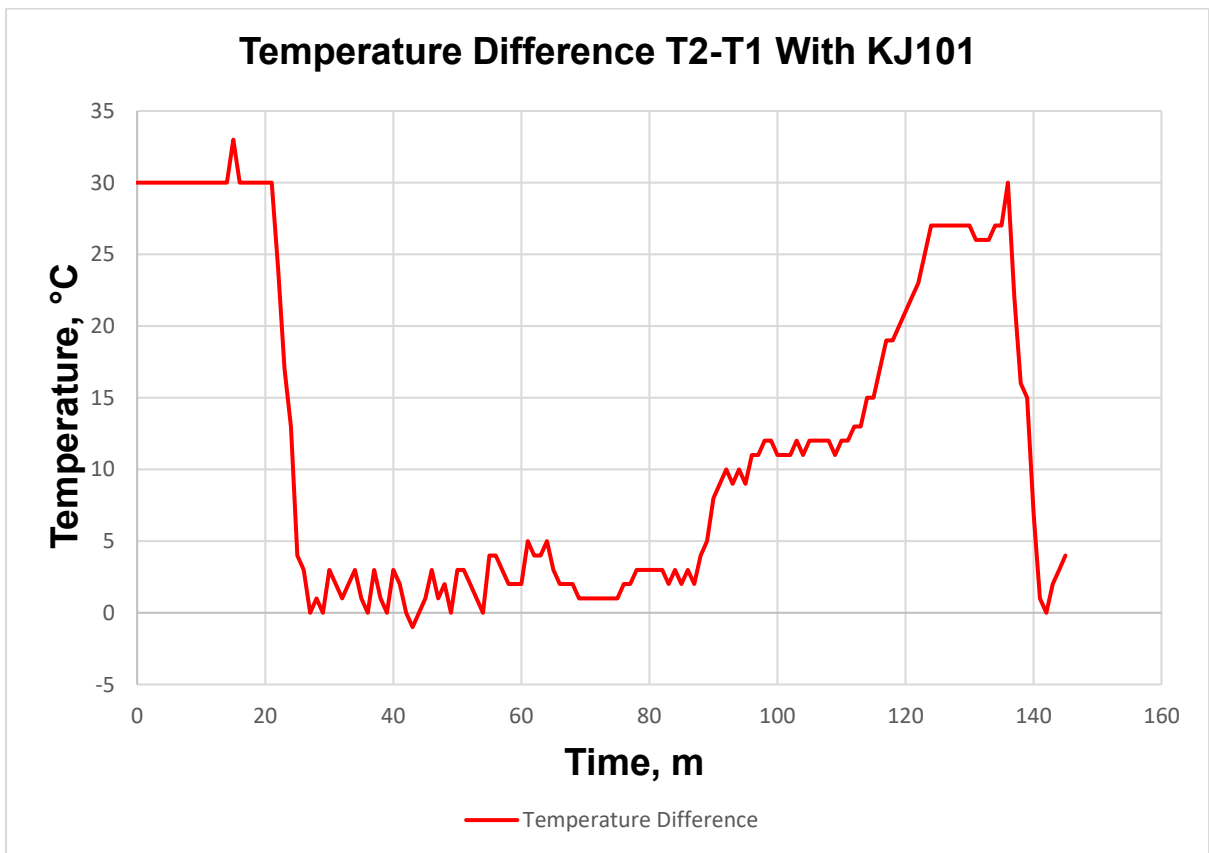


Figure 6.24 Temperature difference changes when the air to fuel ratio is being adjusted with KJ101

From the testing it can be noticed that when KJ101 detects the temperature difference is too large a slow ramp up begins in the air flow to increase the temperature in the inlet of the fuel cell. In this case the inlet temperature rises significantly and by the time it reaches at 700°C (Same as Middle) the airflow starts ramping down back to its initial state to continue preserving the fuel to air ratio. The temperature in the middle location hasn't been shifted at all, and the other parameters as fan speed has remained in the optimum range as from previous experiments.

After 45 minutes as it was expected, the temperature starts to drop which in the end settles to a minus 30 °C from the middle hotspot. The airflow will once again start to increase the air flow to match the temperature. After repeats of this experiment the cycle has two phases, the ramping of the airflow and then natural drop of the airflow to its original fuel to air state until the difference between Inlet and Middle is to 30°C. The controller requires 5 minutes to alter the 30°C while the system naturally takes 2 hours to drop from 700°C to 670°C for  $T_{inlet}$ .

A closed feedback loop control could be implemented, the air flow could be the manipulative parameter while the output would be T1 setpoint to 700°C. However, this change would make the fuel to air ratio impossible to be 1 to 10 as the controller would prioritise for T1 to be 700°C. Therefore, KJ101 currently uses the best possible solution of trying to satisfy both conditions to ensure this fuel cell gets better performance and lifetime. It goes without saying that not preserving the ratio even for a short period of 10 minutes could reduce life of the fuel cell, however having different temperature across the fuel cell could affect both performance and lifetime therefore this control strategy to have the least impact to the fuel cell was chosen. This is an issue that can be improved by an ECU, but it could never be eliminated, it could benefit more if for a future design a different mechanical solution was present, to spread the heat evenly by relocating the fan to enable different pathway for the cooling air.

#### 6.4.5 Improvement #6: Battery charging capability as a new feature

For the Adelan  $\mu$ SOFC the main usage of the specific model allocated for this project is to act as a top-up battery charger. Therefore, for KJ101 to be a viable option as an industrial controller it is required to perform a battery management function. Current basic controller doesn't have any power management technique neither its equipped with the right hardware to account for it. The BC its utilising a 12V switching relay that will enable the connection between the fuel cell and the battery. When this is happening the fuel cell current flows through the battery and charging begins. BC it's not equipped with a DC-to-DC converter, in this case the voltage of the fuel cell will stabilise at the same level as the current level of the battery. This architectural design doesn't allow the fuel to work at its maximum potential which is 10.5V

and 10A. At this rate the fuel cell it's not generating its maximum rated power which means the battery will take long time to recharge, which is not very desirable as customers would prefer their batteries to charge as soon as possible.

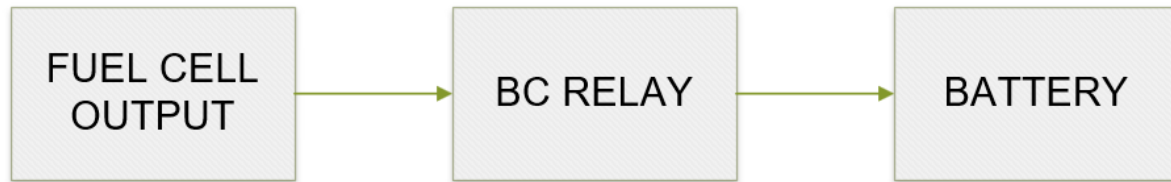


Figure 6.25 Battery charging solution for BC

In the following experiment the battery has been consumed to a level where the Adelan  $\mu$ SOFC should start the charge. This test its using 3800 ml/min of air mixed with 380 ml/min of propane where it is set to stabilise at 700°C. In this experiment, the KJ101 should be able to charge the lead acid battery. First things the relay connected to the battery from the fuel cell switches at 620°C. The fuel cell is generating power which is connected to an external DC-DC converter then KJ101 battery management is kicking in Figure 6.26 The fuel cell power output is changing accordingly to the demands of the DC-DC converter where these demands are changing due to the battery management system of KJ101. For the battery to reach 98% it required 8.4 hours. This result was very valuable as for the first time an experimental controller was used to monitor the battery charge where at the same the Adelan  $\mu$ SOFC temperature was monitored to ensure the best performance.

Table 6.3 Typical lead acid battery state of charge, yellow is for the contingency mode start-ups and green for normal.

Voltage	State of Charge (%)
12.6	100
12.5	90
12.42	80
12.32	70
12.20	60
12.06	50
11.9	40
11.75	30
11.58	20
11.31	10
10.5	0

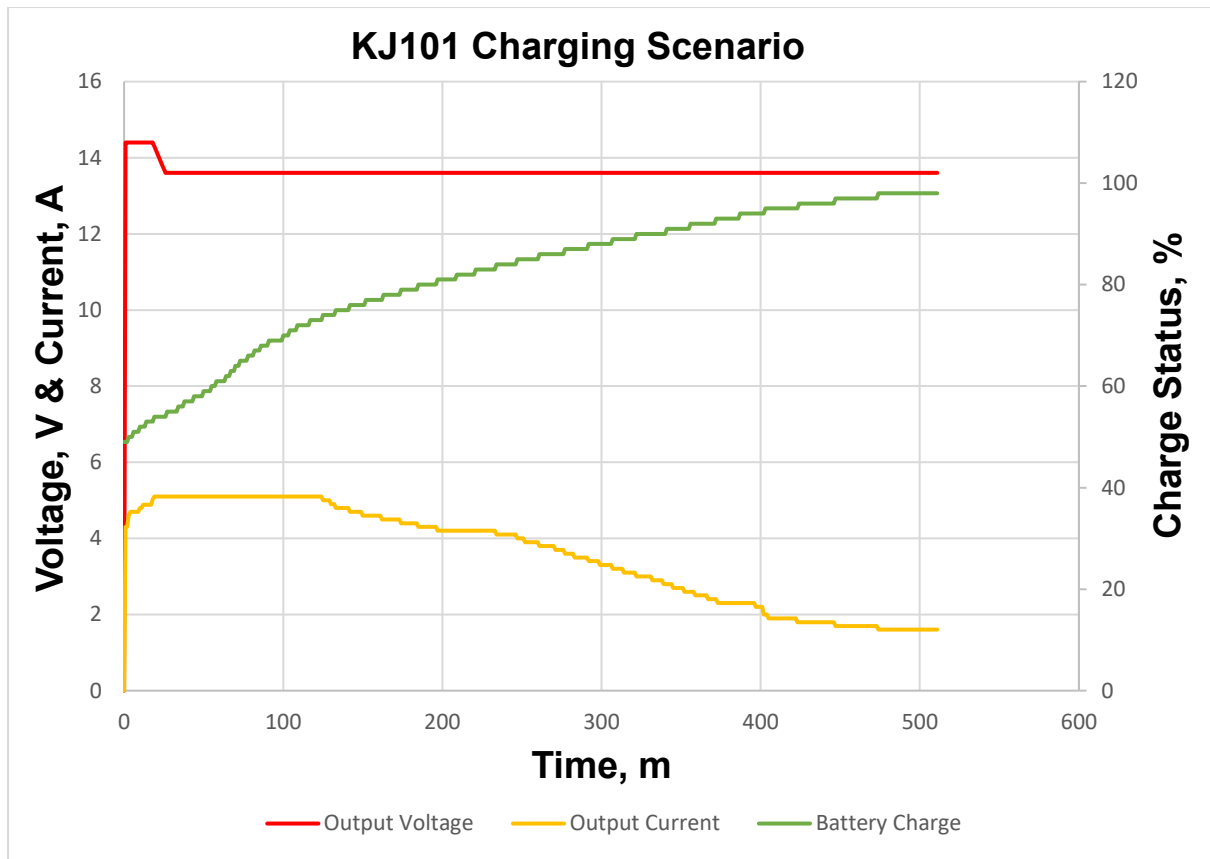


Figure 6.26 Charging scenario

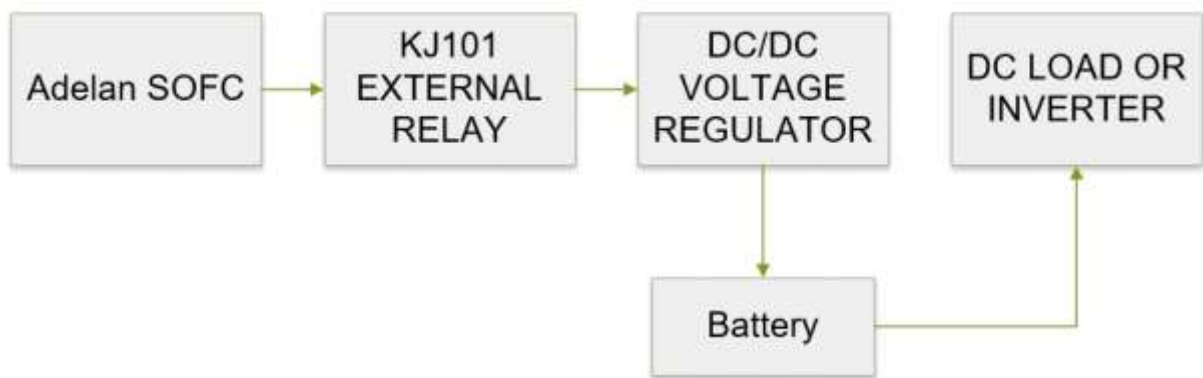


Figure 6.27 Battery Management System for Adelan

## 6.5 Improvement #7: KJ101 power output management

In this section the fuel cell is evaluated by checking its power output. As it has been discussed, the Adelan fuel cell is designed to act as a top up battery charger, in this way KJ101 has been designed with that in mind. Initially experiments were conducted to check the output of the fuel cell on different setpoints.

Figure 6.28 shows a scenario where the output of the fuel cell is at open circuit voltage then the current draw was adjusted. From 16V of open circuit the current was slowly incremented, to inspect if more power draw would offer any significant heat increase. In addition, KJ101 is adjusting the voltage when below 10.5V to not extremely stress the fuel cell.

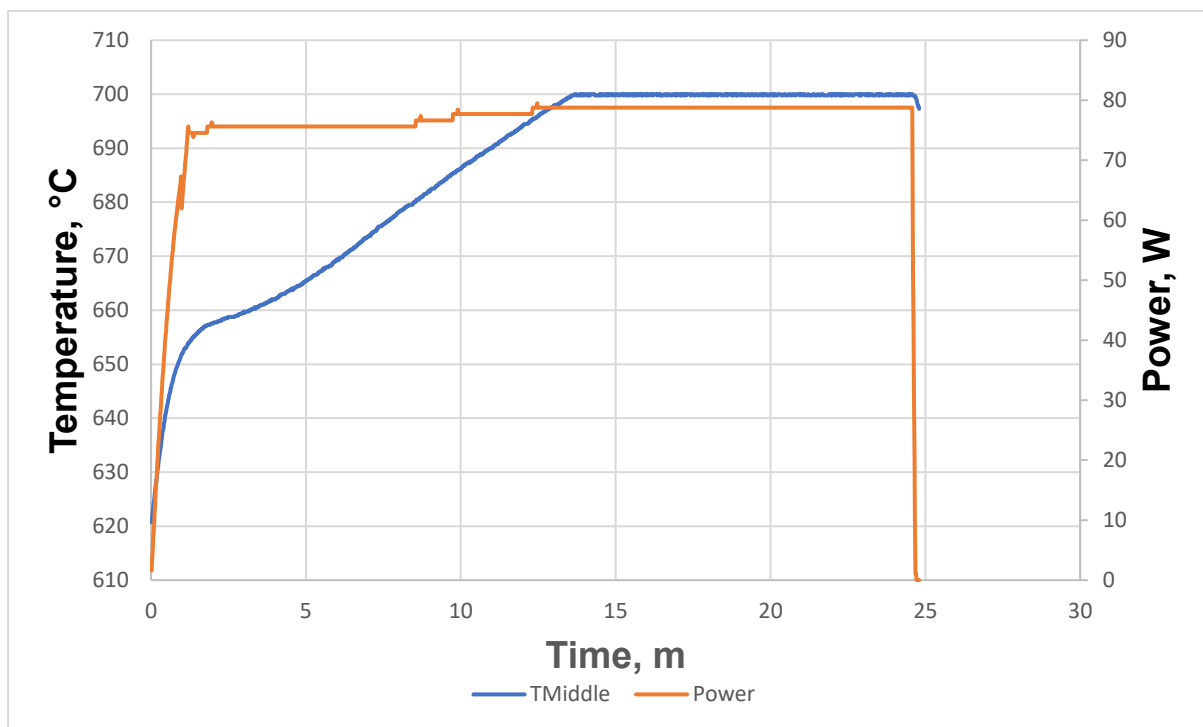


Figure 6.28 Power draw doesn't affect the heat increase significantly in the Adelan system

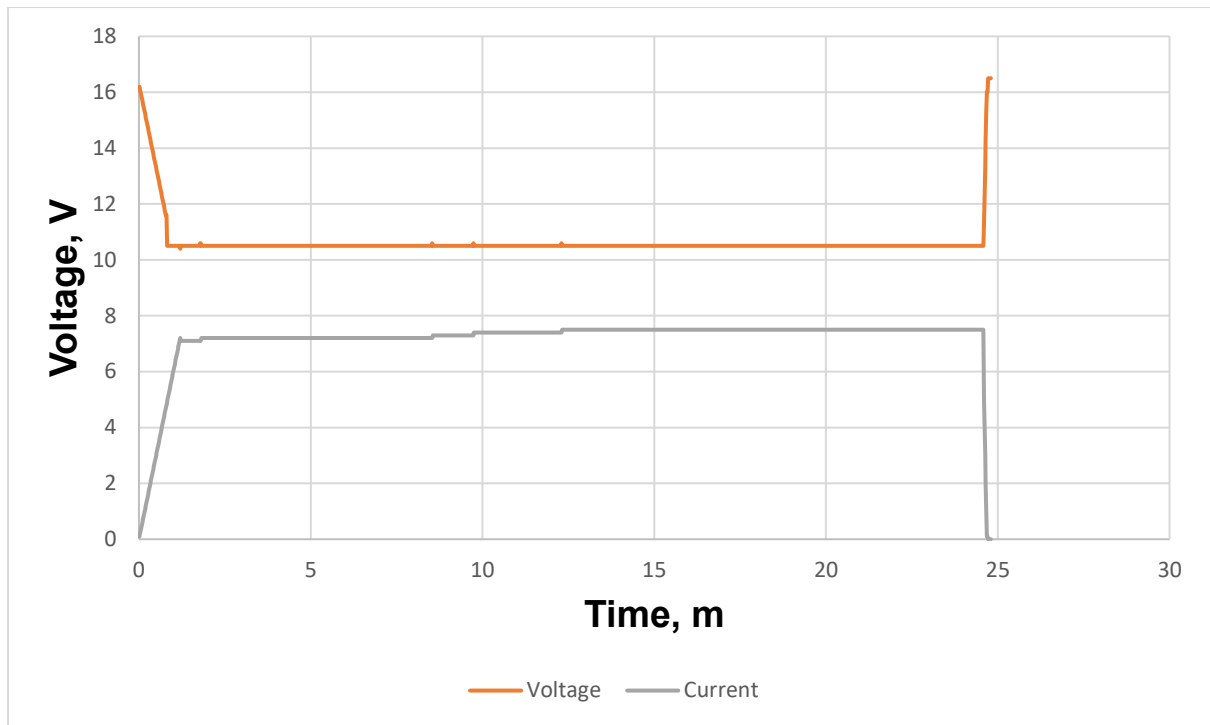


Figure 6.29 The firmware of KJ101 its stopping voltage drop below 10.5 as this is the maximum efficiency possible for the Adelan SOFC

In Figure 6.29 , it is apparent that more heat resulted in more power, however the power draw at 620°C did not decrease the time required for setpoint as it was the same as with OCV.

Another test was then performed to check the change of fuel, and how that would affect the power output, but also the heat release inside the system core. These graphs indicate that fuel increase generates more heat and more power. Any fuel increase above 380ml/min doesn't increase the power output as its shown.

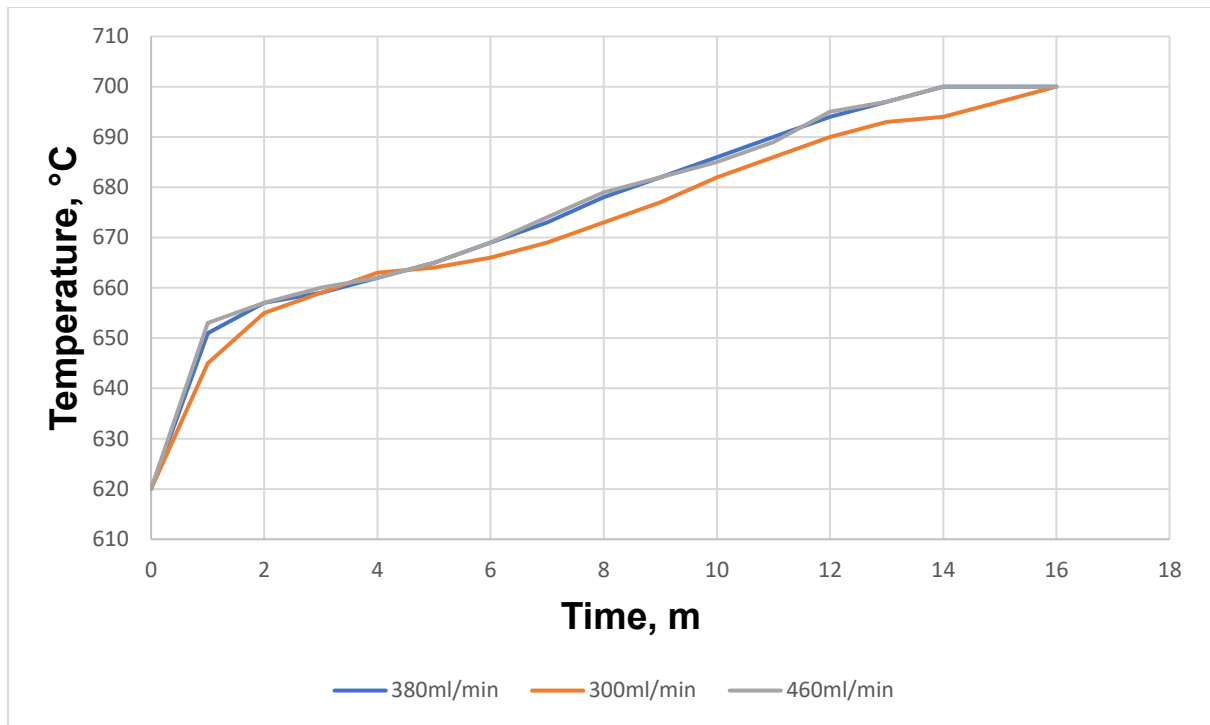


Figure 6.30 Changing the fuel flow affecting the time required to reach the setpoint

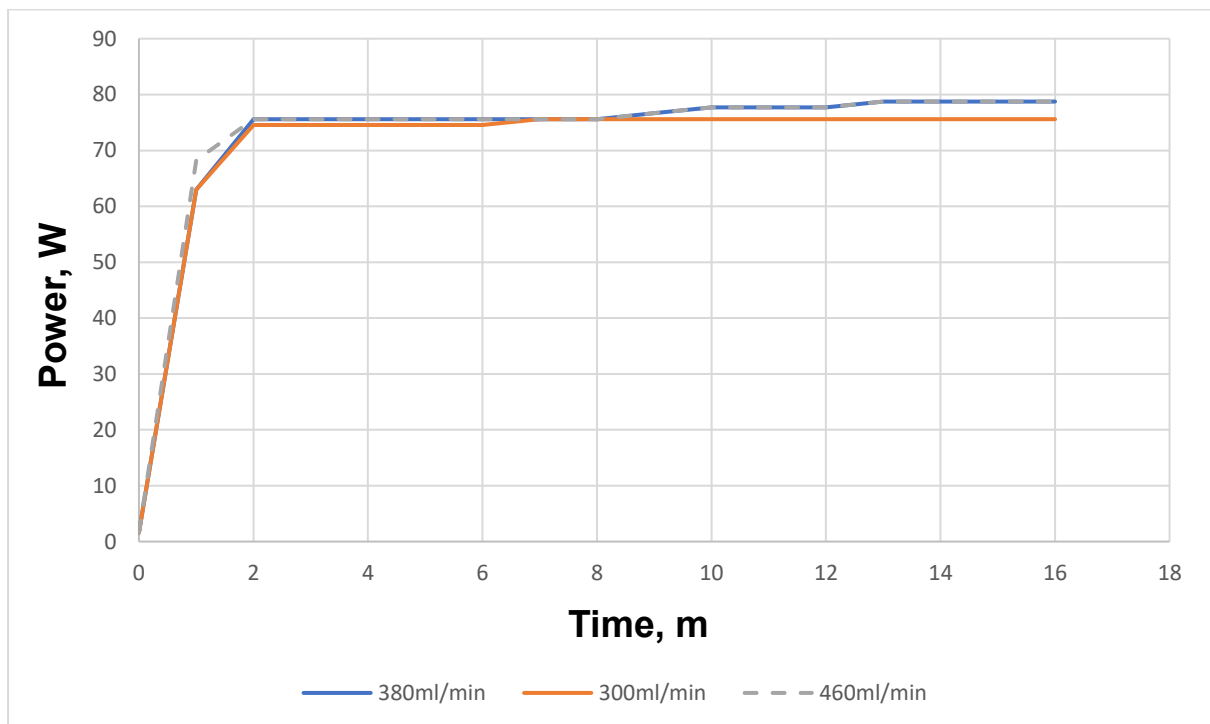


Figure 6.31 When above 380ml/min the power is not affected

A feedback loop was tested for KJ101, fuel flow was the manipulative variable while power output was the target. It's important that when the fuel cell enters the operation stage that the power output is incremented slowly, KJ101 increases current by 0.1A per second as a sudden load change is one of the most important factors that damages cells. This means that KJ101

has two loops one for the target temperature setpoint and one for the target power output. In the Figure 6.32 both loops engage at 620°C, and the power output target was set for 25W, 50W and 75W in all cases the controller was able to reach the target power requirement. This double loop design is a technique that could benefit SOFC's to increase efficiency when the power requirement changes from one load to another to reduce fuel consumption. This is a feature from KJ101 that can be used to in addition to the temperature control, this technique ensures that the fuel cell will draw the amount of fuel required instead of having a stable option. The following graph results are from the same experiment checking the changes that the fuel variation did to the system in all parameters.

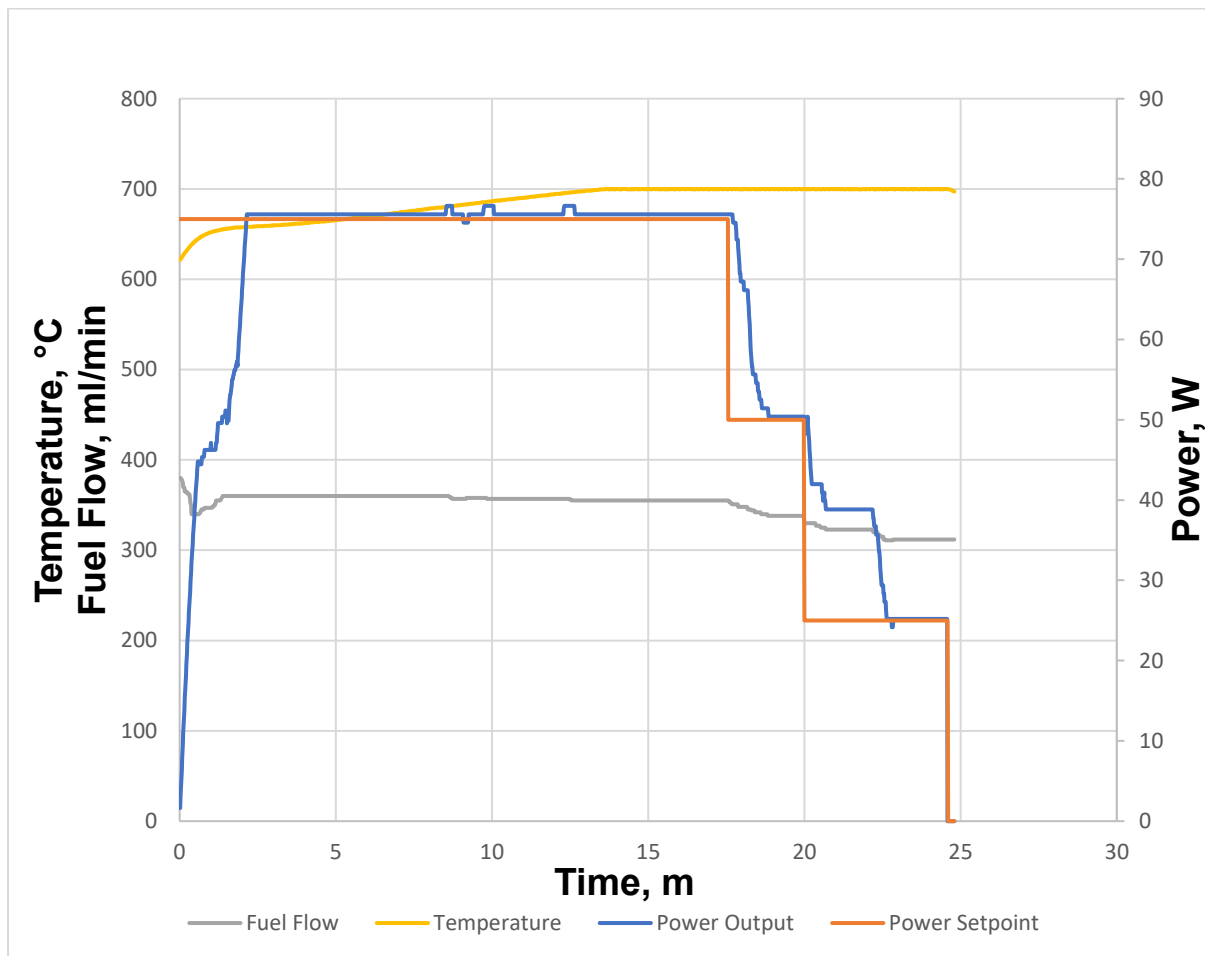


Figure 6.32 KJ101 experiment to keep a stable temperature and dynamically adjust the fuel flow according to the demand of the power

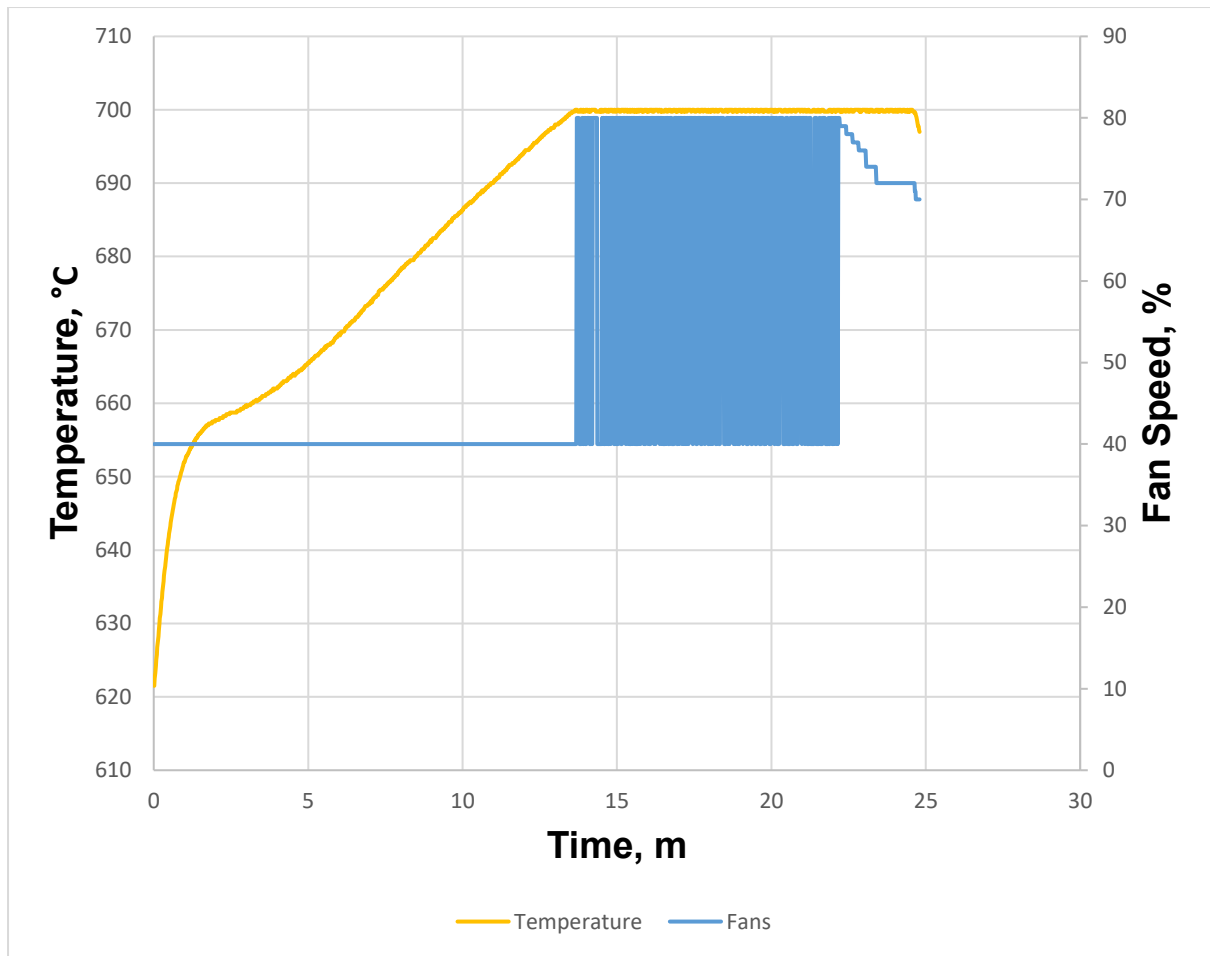


Figure 6.33 The fan is stabilising the fuel cell temperature while the power it's also being dynamically adjusted

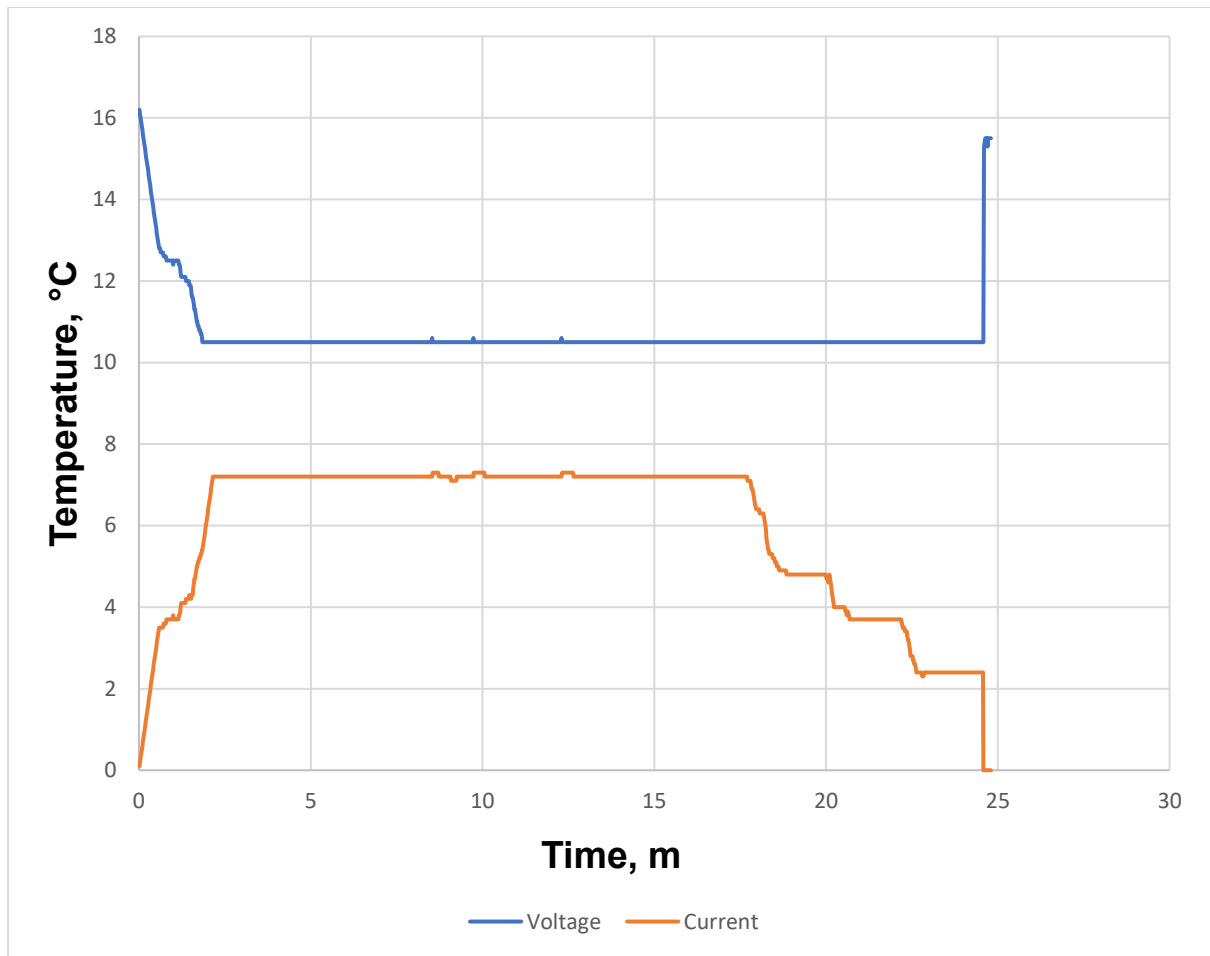


Figure 6.34 Voltage and current changes according to the power setpoint/ demand

## 6.6 Improvement #8: Shut down improvements

This part discusses the changes and improvements that KJ101 offers when the fuel is shutting down after a successful charging cycle or it has been requested by the user.

The current controller being deployed by Adelan is about to finish its operation Figure 6.35, the physical shutdown button is pressed. From first sight the temperature immediately rises significantly up to 750°C which is very dangerous for the fuel cell as the designed materials for this fuel cell are not chosen to be able to withstand more than 730°C. One of the reasons that may cause this sudden temperature change can be attributed the high air input when shutdown stage has started as in this stage the air and fuel flow drop immediately not allowing enough time for the system to adjust. In addition, more air is going through the system as the fan speed goes immediately to 100%.

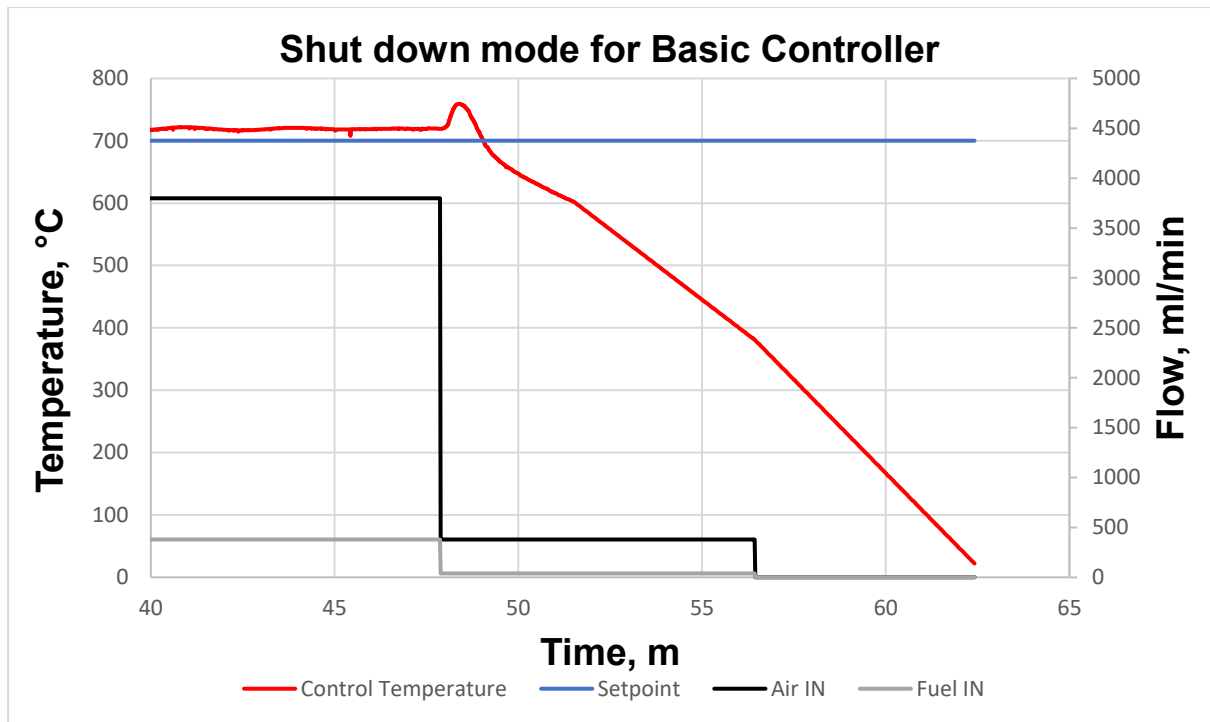


Figure 6.35 Immediate change in the air flow caused a sudden change in temperature endangering the fuel cell materials

In the next experiment KJ101 will use the smoothing technique that has been previously tested for start-up. In this test it is expected for the sudden temperature change to be eliminated. Moreover, the fan speed will be dropped to allow more time for the system to settle. When KJ101 starts in Figure 6.36 shutdown phase, initially the parameters to fuel and air will slowly ramp down to eliminate sudden temperature variations in the same manner as in the warmup stage. Fuel and Air are slowly ramping down to avoid sudden temperature changes. The fuel cell it's also slowly shutting down preserving as much as possible valuable heat in the system for the next possible start up.

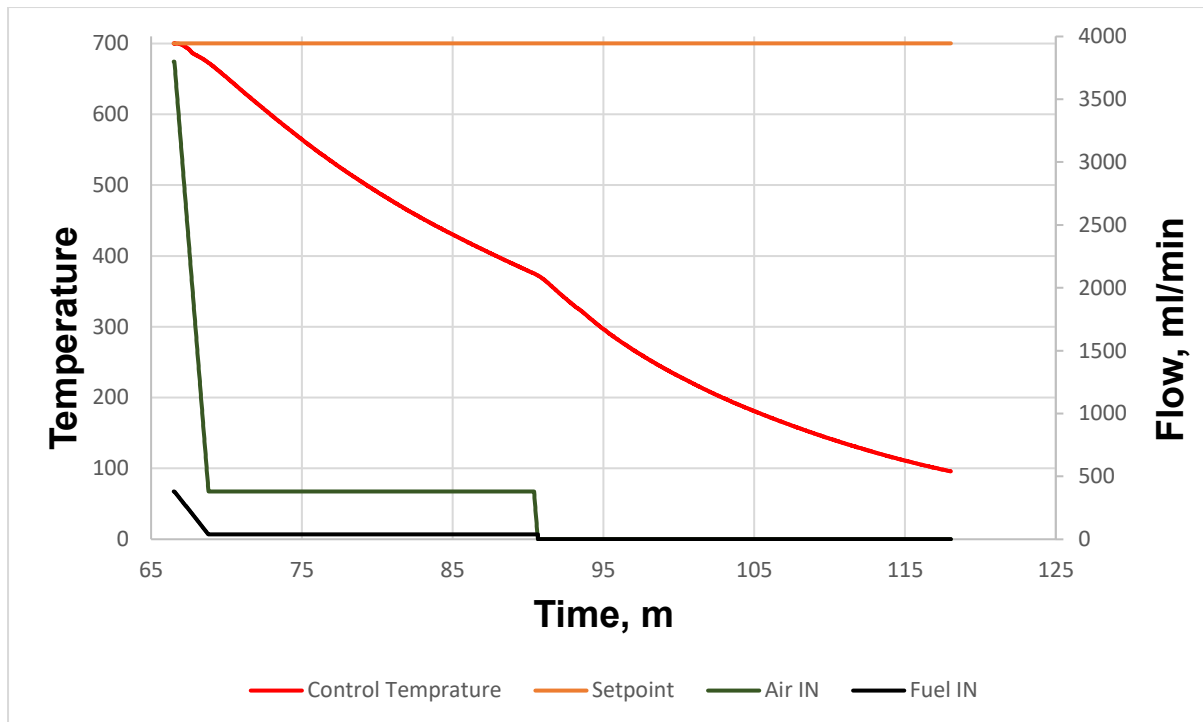


Figure 6.36 Shut Down mode for KJ101

After that the controller will slowly drop the temperature using the fan to cool down the heat inside the fuel cell core. In this instance the control strategy will opt in to decrease the temperature as slow as possible. This offers three major benefits. The first one would be in a scenario where the fuel cell needs to start again, in this case the fuel cell will still be quite warm therefore the controller will be able to switch to starting mode from a temperature way above room temperature which will improve warm up procedure significantly. The second benefit is reducing parasitic losses as the fan would draw more power from the battery to perform the shutdown procedure. In addition, the fuel cell will have to perform the starting procedure from room temperature which will draw again more power than with the slow shutdown. The final benefit is purely extending the fuel cell lifetime, this happens naturally as the temperature rate of change is very steady and slow it allows for a smooth long shutdown procedure.

Having said all that, sometimes the user will need to make this procedure faster as they might need to move or relocate the Adelan  $\mu$ SOFC in this case KJ101 makes sure it has an alternative shutdown mode where the fuel cell will use a bit more battery but will cooldown in 20 minutes. This mode can be triggered if the physical push button for shutdown is pressed by the user for more than 10 seconds.

## 7 Conclusion and future recommendations

In this chapter a detailed summary is provided, describing the process to build and evaluate a new controller KJ101 to be used by a fuel cell company, Adelan Ltd. This chapter provides an overview of the objectives and the main outcome of the findings followed by recommendations for improvement and the future works.

### 7.1 Conclusion

This thesis has discussed the development of an electronic controller for a SOFC made by Adelan Ltd. The objectives of this thesis were to develop the necessary hardware and software that would increase the fuel cell performance and efficiency.

The research has started by an extensive literature review (**Chapter 2**). In this chapter, narrow research in the fuel cell literature was conducted to get familiar with the field and identify the research gaps. There are few categories of fuel cells such as the already established Proton Exchange Membrane (PEM), this type of fuel cell has been used by various industries with more focus in the mobile section, such as automotive. However, SOFC has been gaining more popularity in the last decade as its design offers one of the highest assets, fuel flexibility and its possibility to use hydrocarbons due to its ceramic catalyst which can operate up to 1000 °C. However, as shown in the literature chapter one of the lacking areas is the availability for SOFC controllers, a controller is the unit responsible for all the action of the fuel cell, such as safeguarding the fuel cell runs optimally according to its specification protocol. Few controllers have been investigated in the literature chapter however most of the controllers proposed haven't been put to real experimental tests, but only few which have been focusing only one accomplishment of the fuel cell and neglecting the rest such as fuel utilisation or sudden load changes. This can be a bottleneck as a controller has to maintain a system operating therefore there are multiple activities to be taken by the controller. A consistent gap in the control literature was regarding the testing and application of the controller, those controllers did not account for the whole cycle of the fuel cell such as start-up and shutdown but mostly focusing on the operation stage such as fuel utilisation and the DC-DC converter power adjustments. The cycle of the fuel is of utmost importance, as it was demonstrated in this thesis the fuel cell could brake while in shutdown phase if not controlled properly. In addition, physical controllers should be designed and printed as some problems can occur which can't be seen in simulations such as the electrical noise for thermocouple which can give false readings. A controller it's not only to maintain optimum efficiency of its representative system but also giving assurance to the user that the operation will run smoothly without safety concerns but also offering quality of life improvements such as a friendly user interface. A controller can be

validated in simulation software as multiple researchers have demonstrated however in this thesis a prototype controller has been built and validated.

As the first part of the technical research, experimental and computational sensitivity analysis was targeted (**Chapter 3**). Initially a fuel cell testing rig was built to identify the fuel cell core affecting parameters. The fuel cell was tested manually (without any controller input) all the parameters were manipulated and recorded to identify some basic understanding and operation of the Adelan SOFC dynamics. These sensitivity tests then were used to create the first model for this system. Some model assumptions had to be made such as the internal reformation was not taken to consideration. However, in the end the model was validated, and simulation took place. As an outcome, one of the most crucial issues in assessing the SOFC thermal behaviour, i.e., prediction of the speed at which SOFC reaches the new steady-state condition, became feasible. It was shown that the voltage regime identification/consideration is significantly useful to provide detailed analysis on the SOFC thermal behaviour. The impacts of the operating strategies, including deployment of OEA and the adjustment of anode side humidity on thermal dynamics were quantitatively evaluated.

In **Chapter 4** the knowledge captured in the model was used to begin the phases required to design a fuel cell prototype controller. Adelan already had their own controller for their fuel cell, this controller was able to achieve some basic functionalities however it wasn't reliable. Therefore, a new controller was proposed the KJ100, to build this controller several new components and tools were used and compared against the Adelan Basic Controller. KJ100 main objective was to emulate the Adelan BC functionalities, such as having the automotive industry standard communication protocol of CANBUS. Technical improvements were made in the temperature sensing a digital chip was used instead of an analogue one for more accurate reading. For safety concerns a gas and pressure sensor design was implemented a small pressure sensor fit inside the fuel pipelines to detect sudden pressure changes which would flag difference in the fuel flow and another outside gas sensor named MQ6 was used to detect and propane leak into the atmosphere. There was also added a power output sensor to detect and monitor the power generated by the stack likewise to be used to check its performance. All these above-mentioned modules were put into an electronic schematic to design a two-layer board PCB.

Further technical improvements were achieved as presented in **Chapter 5**. It was found that the proposed controller would benefit from a four-layer design. This was demonstrated in Chapter 5. This chapter splits into two sections. The first section described the process for building the new KJ101 controller designed to bring all new functionality to this fuel cell with

new quality of life improvements combining and improving on everything learned from previous chapters, thermal analysis from the model and sensitivity analysis from Chapter 3 and the tuning processes from BC and KJ100 changes in Chapter 4. The four layers followed industry standard guidelines, the middle layers were used as planes Ground and Power planes to eliminate noise emission from the ECU and ease with the wire routing process in the PCB design. Once the PCB was printed the firmware process started where all the logic behind the controller was written in embedded C code. Every single functionality from the controller was tuned to manipulate the variables as expected. PWM was used to take control of cooling fans, air input and fuel input. Discrete PID technique was used to thermally stabilise the fuel cell in the operational stage. The firmware was then evaluated to perform warmup, operation and shutdown stages. A transmission protocol using MQTT was also designed to prove the concept of telemetry in this project and the versatility of the controller, KJ101 would connect with the transmission module over CANBUS and output important fuel cell metrics to the Adelan database and shown in the user interface.

Finally, the proposed controller was tested and validated in practice by deployment on Adelan SOFC system as presented in **Chapter 6**. In this greatly important phase of the project, the SOFC operation was split into three stages and each step was evaluated individually. In the warmup stage, it was shown that the ramping up technique from KJ101 was able to offer a smoother warmup in comparison with the Adelan existing controller. In addition, a three contingency mode was proposed, and it showed the flexibility of KJ101 to reach operation stage even if the conditions aren't ideal in the case when the battery is lower than required. In the operation stage KJ101 was able to reach setpoint with minimal temperature variations. Furthermore, for the first time a physical SOFC controller was able to adjust the setpoint on while running opening new avenues for SOFC control allowing the fuel cell to rest at a lower setpoint when the fuel cell isn't performing at its maximum output to reduce on fuel usage. Temperature distribution as shown in chapter 3 was very easy to be altered and in chapter 6 after some experimental data, KJ101 was able to detect when the temperature between two hot points in the Adelan SOFC would be too low, then the controller was slightly manipulated the air input allowing the heat to be more even across the fuel cell core.

The hardware for KJ101 was also able to detect the level of the connected battery and start the fuel cell, to initiate charge when required, the charging profile was altered slightly to fit with the SOFC specifications. Finally, a relationship between the fuel input and the power output was investigated to check KJ101 multi-input multi output algorithm can offer any new benefit to the Adelan SOFC. In this test the fuel input was varying according to the power output of the fuel cell.

## 7.2 Recommendations and the future works

In the course of the work presented in this thesis, multiple research challenges and opportunities were identified. Moreover, opportunities for further impact on industry, as a key aspect of this project, were revealed. Some of them are presented as recommendations for improvement and possible future research.

The model presented in this work can be improved by taking internal reforming of fuels into account. Those reactions greatly dominate the SOFC dynamics and internal gradient. So, a model-oriented control design will extensively benefit from such details. More measuring points across the cell length will capture unprecedented data that enrich the model tuning and validation phases.

There are few details that require refinement, starting with the hardware and the PCB design. It would make more sense if the telemetry module was embedded in the KJ101 design. A modem could be included such as the SIM7600CE, this modem is able to connect to a mobile internet service using 4G. Having this option KJ101 would have the option to use MQTT on its own (without the need of external module) to export important data from the fuel that could be saved in a database. This can be further analysed by another computing machine to generate trends in the fuel cell operation and therefore fix possible future problems relating with the fuel cell. Guaranteeing problems don't repeat itself allowing users to have more trust in the technology. Promoting fuel cell technology to the public and raise awareness of this green technology. Another recommended addition to the PCB would be the digital DC-DC voltage regulator, with this design change the fuel cell power output would be routed to the controller and the controller would be able to decide the right power output for the right application with a small change in the firmware. For ease of manufacturing and further reduce the price cost of this design it is a better option to keep the design consistent for example, components such as resistors and capacitors can be chosen to be of the same physical size and if possible, of the same value, reducing the usage of different assembly machinery. Finally in this PhD the 8-bit AVR microcontroller was able to do all the tasks without any issue, however with almost the same cost a 32-bit microcontroller can be purchased offering way more computing power, in this manner this microcontroller would last longer and offer way higher flexibility in the devices that can be attached to it. For example, a touch screen with graphics could be driven by this microcontroller with ease while also focusing on the operation of the fuel cell. A recommended microcontroller would be from the automotive family from ST Microelectronics

as those electronic chips have passed regulation in regards for automation electromagnetic noise emissions.

Firmware in this project was written according from experimental data, and from past data from Adelan SOFC's. The firmware was written using embedded C, and the main automation technique was based on PID loop. In this topic an investigation can possibly be around the machine learning in the microcontrollers. This is a new novel space for study and could perhaps fix issues finding the optimum controlling technique of the fuel cell without using any heavy model. There currently various of open-source training models for machine learning applications. Currently in the SOFC market it's hard to identify what is the status of the cells inside the system, perhaps a controller could be trained to identify the time a fuel cell would need service before a serious damage to the fuel cell core has happened such as a crack in the fuel cell stack. This could offer significant improvements in the lifetime expectation of the fuel cell system.

On the other hand, an entirely different approach can also be taken, where a model can be created to fully model the whole Adelan SOFC instead of just the cell, this will introduce a clear picture of how the Adelan SOFC reacts to changes. With various simulations the best controlling algorithm can be found, and with the help of Simulink from Matlab there is a function where embedded c code can be generated and be used in the controller to test the fuel cell immediately. Both would be interesting topics, using the model approach there is going to be more insight about the operation of the fuel cell but would require more time. Using the machine learning approach would require a massive amount of data and with this method lots of fuel cells will probably be destroyed until the controller would be trained.

## 8 References

- [1] "Climate Action," *United Nations*, 2022.
- [2] S. Callery. "The Effects of Climate Change," 27 January 2022; <https://climate.nasa.gov/effects/>.
- [3] "The science of climate change," 15/01, 2022; <https://www.science.org.au/learning/general-audience/science-climate-change/4-how-do-we-expect-climate-change-to-evolve>.
- [4] J. Peng, D. Zhao, Y. Xu, X. Wu, and X. Li, "Comprehensive Analysis of Solid Oxide Fuel Cell Performance Degradation Mechanism, Prediction, and Optimization Studies," *Energies*, 16, 2023].
- [5] E.-J. Choi, S. Yu, J.-M. Kim, and S.-M. Lee, "Model-Based System Performance Analysis of a Solid Oxide Fuel Cell System with Anode Off-Gas Recirculation," *Energies*, 14, 2021].
- [6] A. Weber, "Fuel flexibility of solid oxide fuel cells," *Fuel Cells*, vol. 21, no. 5, pp. 440-452, 2021/10/01, 2021.
- [7] A. Arsalis, and G. E. Georghiou, "A Decentralized, Hybrid Photovoltaic-Solid Oxide Fuel Cell System for Application to a Commercial Building," *Energies*, 11, 2018].
- [8] J. Khan, and M. T. Iqbal, *DYNAMIC MODELING AND SIMULATION OF A SMALL WIND FUEL CELL HYBRID ENERGY SYSTEM*, 2020.
- [9] A. Kasaeian, M. Javidmehr, M. R. Mirzaie, and L. Fereidooni, "Integration of solid oxide fuel cells with solar energy systems: A review," *Applied Thermal Engineering*, vol. 224, pp. 120117, 2023/04/01/, 2023.
- [10] "Types of Fuel Cells," 17/09, 2019; <https://www.energy.gov/eere/fuelcells/types-fuel-cells>.
- [11] M. Hering, J. Brouwer, and W. Winkler, "Evaluation and optimization of a micro-tubular solid oxide fuel cell stack model including an integrated cooling system," *Journal of Power Sources*, vol. 303, pp. 10-16, 2016/01/30/, 2016.
- [12] "The Fuel Cell Industry Review 2012," 04/05, 2019; <https://www.technology.matthey.com/article/56/4/272-273/>.
- [13] "Fuel Cell Basics," 04/05, 2019; <https://www.fchea.org/fuelcells>.
- [14] R. O'Hayre, S.-W. Cha, W. Colella, and F. Prinz, *Fuel Cell Fundamentals: O'Hayre/Fuel Cell Fundamentals*, 2016.
- [15] K. Kendall, and M. Kendall, *High-Temperature Solid Oxide Fuel Cells for the 21st Century: Fundamentals, Design and Applications: Second Edition*, 2015.
- [16] D. P. Wilkinson, Zhang, J., Hui, R., Fergus, J., & Li, X., "Proton Exchange Membrane Fuel Cells: Materials Properties and Performance (1st ed.).", 2009.
- [17] "Type of Fuel Cells," 17/09/2019, 2019; <https://www.energy.gov/eere/fuelcells/types-fuel-cells>.
- [18] EG, and I. G Technical Services, "Fuel Cell Handbook," Lulu.com, 2004.
- [19] K. Kendall, "1 - Introduction to SOFCs," *High-Temperature Solid Oxide Fuel Cells for the 21st Century (Second Edition)*, K. Kendall and M. Kendall, eds., pp. 1-24, Boston: Academic Press, 2016.
- [20] S. J. Cooper, and N. P. Brandon, "Chapter 1 - An Introduction to Solid Oxide Fuel Cell Materials, Technology and Applications," *Solid Oxide Fuel Cell Lifetime and Reliability*, N. P. Brandon, E. Ruiz-Trejo and P. Boldrin, eds., pp. 1-18: Academic Press, 2017.
- [21] J. Peng, J. Huang, X.-I. Wu, Y.-w. Xu, H. Chen, and X. Li, "Solid oxide fuel cell (SOFC) performance evaluation, fault diagnosis and health control: A review," *Journal of Power Sources*, vol. 505, pp. 230058, 2021/09/01/, 2021.
- [22] A. B. Stambouli, and E. Traversa, "Solid oxide fuel cells (SOFCs): a review of an environmentally clean and efficient source of energy," *Renewable and Sustainable Energy Reviews*, vol. 6, no. 5, pp. 433-455, 2002/10/01/, 2002.
- [23] P. Pianko-Oprych, Z. Jaworski, and K. Kendall, "13 - Cell, stack and system modelling," *High-Temperature Solid Oxide Fuel Cells for the 21st Century (Second*

- Edition*), K. Kendall and M. Kendall, eds., pp. 407-460, Boston: Academic Press, 2016.
- [24] D. Minarik, P. Moldrik, and T. Meadowcroft, *Experimental validation of solid oxide fuel cell's basic operational characteristic*, 2014.
- [25] Y.-w. Xu, X.-l. Wu, H. You, T. Xue, D.-q. Zhao, J.-h. Jiang, Z.-h. Deng, X.-w. Fu, and L. Xi, "Modeling and simulation of temperature distribution for planar cross-flow solid oxide fuel cell," *Energy Procedia*, vol. 158, pp. 1585-1590, 2019/02/01/, 2019.
- [26] G. DiGiuseppe, and L. Sun, "Long-term SOFCs button cell testing," *Journal of Fuel Cell Science and Technology*, vol. 11, 04/01, 2014.
- [27] J. L. a. A. Dicks, "Fuel Cell Systems Explained," *3rd ed.*, Wiley, 2012, , pp. 163-165, 2012.
- [28] "Fuel Cell Basics," 2017.
- [29] K. Kendall, "10 - Portable early market SOFCs," *High-Temperature Solid Oxide Fuel Cells for the 21st Century (Second Edition)*, K. Kendall and M. Kendall, eds., pp. 329-356, Boston: Academic Press, 2016.
- [30] K. Kendall, and M. Palin, "A small solid oxide fuel cell demonstrator for microelectronic applications," *Journal of Power Sources*, vol. 71, no. 1, pp. 268-270, 1998/03/15/, 1998.
- [31] W. Kong, W. Zhang, H. Huang, Y. Zhang, J. Wu, and Y. Xu, "Analysis of micro-tubular SOFC stability under ambient and operating temperatures," *Journal of Materials Science & Technology*, vol. 34, no. 8, pp. 1436-1440, 2018/08/01/, 2018.
- [32] A. Slodczyk, M. Torrell, A. Hornés, A. Morata, K. Kendall, and A. Tarancón, "Understanding longitudinal degradation mechanisms of large-area micro-tubular solid oxide fuel cells," *Electrochimica Acta*, vol. 265, pp. 232-243, 2018/03/01/, 2018.
- [33] B. Huang, Y. Qi, and M. Murshed, "Solid oxide fuel cell: Perspective of dynamic modeling and control," *Journal of Process Control*, vol. 21, no. 10, pp. 1426-1437, 2011/12/01/, 2011.
- [34] K. Kendall, "Progress in Microtubular Solid Oxide Fuel Cells," *International Journal of Applied Ceramic Technology*, vol. 7, no. 1, pp. 1-9, 2010/01/01, 2010.
- [35] K. Huang, "Fuel utilization and fuel sensitivity of solid oxide fuel cells," *Journal of Power Sources*, vol. 196, no. 5, pp. 2763-2767, 2011/03/01/, 2011.
- [36] S. M. Jamil, M. H. Dzarfan Othman, M. H. Mohamed, M. R. Adam, M. A. Rahman, J. Jaafar, and A. F. Ismail, "A novel single-step fabrication anode/electrolyte/cathode triple-layer hollow fiber micro-tubular SOFC," *International Journal of Hydrogen Energy*, vol. 43, no. 39, pp. 18509-18515, 2018/09/27/, 2018.
- [37] S. M. Jamil, M. H. D. Othman, M. A. Rahman, J. Jaafar, A. F. Ismail, and K. Li, "Recent fabrication techniques for micro-tubular solid oxide fuel cell support: A review," *Journal of the European Ceramic Society*, vol. 35, no. 1, pp. 1-22, 2015/01/01/, 2015.
- [38] "Report to Congress on Status of Solid Oxide Fuel Cell Program," *United States Department of Energy*, 2019.
- [39] P. Gupta, V. Pahwa, and Y. P. Verma, "Performance enhancement of a grid-connected solid-oxide fuel cell using an improved control scheme," *Materials Today: Proceedings*, vol. 28, pp. 1990-1995, 2020/01/01/, 2020.
- [40] P. Pianko-Oprych, T. Zinko, and Z. Jaworski, "Modeling of thermal stresses in a microtubular Solid Oxide Fuel Cell stack," *Journal of Power Sources*, vol. 300, pp. 10-23, 2015/12/30/, 2015.
- [41] N. Bizon, M. Oproescu, and M. Raceanu, "Efficient energy control strategies for a Standalone Renewable/Fuel Cell Hybrid Power Source," *Energy Conversion and Management*, vol. 90, pp. 93-110, 2015/01/15/, 2015.
- [42] H. R. Amedi, B. Bazooyar, and M. R. Pishvaie, "Control of anode supported SOFCs (solid oxide fuel cells): Part I. mathematical modeling and state estimation within one cell," *Energy*, vol. 90, pp. 605-621, 2015/10/01/, 2015.
- [43] D. Yu, Y. Mao, B. Gu, S. Nojavan, K. Jermstittiparsert, and M. Nasser, "A new LQG optimal control strategy applied on a hybrid wind turbine/solid oxide fuel cell/ in the

- presence of the interval uncertainties," *Sustainable Energy, Grids and Networks*, vol. 21, pp. 100296, 2020/03/01/, 2020.
- [44] X. Wu, and D. Gao, "Optimal robust control strategy of a solid oxide fuel cell system," *Journal of Power Sources*, vol. 374, pp. 225-236, 2018/01/15/, 2018.
- [45] D. Vrečko, M. Nerat, D. Vrančić, G. Dolanc, B. Dolenc, B. Pregelj, F. Meyer, S. F. Au, R. Makkus, and Đ. Juričić, "Feedforward-feedback control of a solid oxide fuel cell power system," *International Journal of Hydrogen Energy*, vol. 43, no. 12, pp. 6352-6363, 2018/03/22/, 2018.
- [46] A. Chaisantikulwat, C. Diaz-Goano, and E. S. Meadows, "Dynamic modelling and control of planar anode-supported solid oxide fuel cell," *Computers & Chemical Engineering*, vol. 32, no. 10, pp. 2365-2381, 2008/10/17/, 2008.
- [47] J. Chen, M. Liang, H. Zhang, and S. Weng, "Study on control strategy for a SOFC-GT hybrid system with anode and cathode recirculation loops," *International Journal of Hydrogen Energy*, vol. 42, no. 49, pp. 29422-29432, 2017/12/07/, 2017.
- [48] P. Jienkulsawad, S. Skogestad, and A. Arpornwichanop, "Control structure design of a solid oxide fuel cell and molten carbonate fuel cell integrated system: Bottom-up analysis," *Energy Conversion and Management*, vol. 220, pp. 113021, 2020/09/15/, 2020.
- [49] F. Mueller, F. Jabbari, J. Brouwer, S. T. Junker, and H. Ghezel-Ayagh, "Linear Quadratic Regulator for a Bottoming Solid Oxide Fuel Cell Gas Turbine Hybrid System," *Journal of Dynamic Systems, Measurement, and Control*, vol. 131, no. 5, 2009.
- [50] F. Jurado, "Predictive control of solid oxide fuel cells using fuzzy Hammerstein models," *Journal of Power Sources*, vol. 158, no. 1, pp. 245-253, 2006/07/14/, 2006.
- [51] B. J. Spivey, and T. F. Edgar, "Dynamic modeling, simulation, and MIMO predictive control of a tubular solid oxide fuel cell," *Journal of Process Control*, vol. 22, no. 8, pp. 1502-1520, 2012/09/01/, 2012.
- [52] N. Chatrattanawet, S. Skogestad, and A. Arpornwichanop, "Control structure design and dynamic modeling for a solid oxide fuel cell with direct internal reforming of methane," *Chemical Engineering Research and Design*, vol. 98, pp. 202-211, 2015/06/01/, 2015.
- [53] K. W. Eichhorn Colombo, V. V. Kharton, F. Berto, and N. Paltrinieri, "Mathematical modeling and simulation of hydrogen-fueled solid oxide fuel cell system for micro-grid applications - Effect of failure and degradation on transient performance," *Energy*, vol. 202, pp. 117752, 2020/07/01/, 2020.
- [54] M. Hubert, J. Laurencin, P. Cloetens, B. Morel, D. Montinaro, and F. Lefebvre-Joud, "Impact of Nickel agglomeration on Solid Oxide Cell operated in fuel cell and electrolysis modes," *Journal of Power Sources*, vol. 397, pp. 240-251, 2018/09/01/, 2018.
- [55] K. Åström, E. Fontell, and S. Virtanen, "Reliability analysis and initial requirements for FC systems and stacks," *Journal of Power Sources*, vol. 171, no. 1, pp. 46-54, 2007/09/19/, 2007.
- [56] P. Costamagna, A. De Giorgi, G. Moser, L. Pellaco, and A. Trucco, "Data-driven fault diagnosis in SOFC-based power plants under off-design operating conditions," *International Journal of Hydrogen Energy*, vol. 44, no. 54, pp. 29002-29006, 2019/11/05/, 2019.
- [57] J. Kupecki, K. Motylinski, A. Zurawska, M. Kosiorek, and L. Ajdys, "Numerical analysis of an SOFC stack under loss of oxidant related fault conditions using a dynamic non-adiabatic model," *International Journal of Hydrogen Energy*, vol. 44, no. 38, pp. 21148-21161, 2019/08/09/, 2019.
- [58] X. Wu, and Q. Ye, "Fault diagnosis and prognostic of solid oxide fuel cells," *Journal of Power Sources*, vol. 321, pp. 47-56, 2016/07/30/, 2016.
- [59] W. Xiao-long, X. Yuan-wu, X. Tao, and L. Xi, "Fault modeling and simulation of pure hydrogen solid oxide fuel cell system." pp. 2688-2692.

- [60] Darjat, S. Sulisty, A. Triwiyatno, and E. Julian, *Design of Adaptive PID Controller For Fuel Utilization in Solid Oxide Fuel Cell*, 2018.
- [61] S. A. Hajimolana, and M. Soroush, "Dynamics and Control of a Tubular Solid-Oxide Fuel Cell," *Industrial & Engineering Chemistry Research*, vol. 48, no. 13, pp. 6112-6125, 2009/07/01, 2009.
- [62] A. R. S. A. D. A. Feliachi, "Control of solid oxide fuel cell for stand-alone and grid connection using fuzzy logic technique," *IEEE*, 2004.
- [63] K. Sedghisigarchi, and A. Feliachi, "H-infinity controller for solid oxide fuel cells." pp. 464-467.
- [64] R. Horalek, and J. Hlava, "Multilinear model predictive control of solid oxide fuel cell output voltage." pp. 1-6.
- [65] X. R. Wang, B. Huang, and T. W. Chen, "Data-driven predictive control for solid oxide fuel cells," *Journal of Process Control*, vol. 17, no. 2, pp. 103-114, Feb, 2007.
- [66] Š. Kozák, "State-of-the-art in control engineering," *Journal of Electrical Systems and Information Technology*, vol. 1, no. 1, pp. 1-9, 2014/05/01/, 2014.
- [67] M. Short, and F. Abugchem, "A Microcontroller-Based Adaptive Model Predictive Control Platform for Process Control Applications," *Electronics*, vol. 6, pp. 88, 10/21, 2017.
- [68] R. Haber, J. A. Rossiter, and K. Zabet, "An alternative for PID control: Predictive Functional Control - a tutorial." pp. 6935-6940.
- [69] A. K. Pandey, V. Singh, and S. Jain, "Chapter eleven - Study and comparative analysis of perturb and observe (P&O) and fuzzy logic based PV-MPPT algorithms," *Applications of AI and IOT in Renewable Energy*, R. N. Shaw, A. Ghosh, S. Mekhilef and V. E. Balas, eds., pp. 193-209: Academic Press, 2022.
- [70] R. S. Pukale, K. U. Jadhav, and A. G. Thosar, "Data collection of variable wind speed to study the change in power and power coefficient." pp. 387-392.
- [71] Y. Chen, Y. Yu, and Z. Peng, "The application of data mining for marine diesel engine fault detection." pp. 1430-1433.
- [72] H. Suhadiyana, A. H. S. Tijani, M. A. A. Zambri, M. H. A. M. Fakharuzi, A. H. A. Rahim, K. I. Sainan, and W. A. N. W. Mohamed, "Data acquisition system for on-track performance analysis of a mini fuel cell vehicle." pp. 1-6.
- [73] H. Yokokawa, "Current Status of Rapid Evaluation of Durability of Six SOFC Stacks within Nedo Project," *ECS Transactions*, vol. 68, pp. 1827-1836, 07/17, 2015.
- [74] N. Brandon, E. Ruiz-Trejo, and P. Boldrin, *Solid Oxide Fuel Cell Lifetime and Reliability: Critical Challenges in Fuel Cells*, 2017.
- [75] S. Zeng, M. Xu, J. Parbey, G. Yu, M. Andersson, Q. Li, B. Li, and T. S. Li, "Thermal stress analysis of a planar anode-supported solid oxide fuel cell: Effects of anode porosity," *International Journal of Hydrogen Energy*, vol. 42, 07/01, 2017.
- [76] O. Razbani, I. Wærnhus, and M. Assadi, "Experimental investigation of temperature distribution over a planar solid oxide fuel cell," *Applied Energy*, vol. 105, pp. 155-160, 05/01, 2013.
- [77] M. Canavar, A. Mat, S. Celik, B. Timurkutluk, and Y. Kaplan, "Investigation of temperature distribution and performance of SOFC short stack with/without machined gas channels," *International Journal of Hydrogen Energy*, vol. 41, no. 23, pp. 10030-10036, 2016/06/22/, 2016.
- [78] R. Montanini, A. Quattrocchi, S. Piccolo, A. Amato, S. Trocino, S. Zignani, M. Lo Faro, and G. Squadrito, "Real-time thermal imaging of solid oxide fuel cell cathode activity in working condition," *Applied optics*, vol. 55, pp. 7142-7148, 09/01, 2016.
- [79] M. Fardadi, D. McLarty, and F. Jabbari, "Investigation of thermal control for different SOFC flow geometries," *Applied Energy*, vol. 178, pp. 43-55, 09/01, 2016.
- [80] A. Amiri, S. Tang, P. Vijay, and M. Tadé, "Planar Solid Oxide Fuel Cell Modeling and Optimization Targeting the Stack's Temperature Gradient Minimization," *Industrial & Engineering Chemistry Research*, vol. 55, pp. 7446-7455, 07/13, 2016.

- [81] S. Tang, A. Amiri, P. Vijay, and M. Tadé, "Development and Validation of a Computationally Efficient Pseudo 3D Model for Planar SOFC Integrated with a Heating Furnace," *Chemical Engineering Journal*, vol. 290, 01/23, 2016.
- [82] S. Tang, A. Amiri, and M. Tade, "System Level Exergy Assessment of Strategies Deployed for SOFC Stack Temperature Regulation and Thermal Gradient Reduction," *Industrial & Engineering Chemistry Research*, vol. 58, 01/16, 2019.
- [83] K. Ahmed, and K. Föger, "Analysis of equilibrium and kinetic models of internal reforming on solid oxide fuel cell anodes: Effect on voltage, current and temperature distribution," *Journal of Power Sources*, vol. 343, pp. 83-93, 2017/03/01, 2017.
- [84] A. Amiri, S. Tang, P. Vijay, and M. O. Tadé, "Planar Solid Oxide Fuel Cell Modeling and Optimization Targeting the Stack's Temperature Gradient Minimization," *Industrial & Engineering Chemistry Research*, vol. 55, no. 27, pp. 7446-7455, 2016/07/13, 2016.
- [85] S. Tang, A. Amiri, P. Vijay, and M. O. Tadé, "Development and validation of a computationally efficient pseudo 3D model for planar SOFC integrated with a heating furnace," *Chemical Engineering Journal*, vol. 290, pp. 252-262, 2016/04/15/, 2016.
- [86] A. Amiri, S. Tang, P. Vijay, and M. O. Tadé, "Planar solid oxide fuel cell modeling and optimization targeting the stack's temperature gradient minimization," *Industrial and Engineering Chemistry Research*, vol. 55, no. 27, pp. 7446-7455, 2016.
- [87] S. Tang, A. Amiri, and M. O. Tadé, "System Level Exergy Assessment of Strategies Deployed for Solid Oxide Fuel Cell Stack Temperature Regulation and Thermal Gradient Reduction," *Industrial and Engineering Chemistry Research*, vol. 58, no. 6, pp. 2258-2267, 2019.
- [88] G. Brunaccini, "Chapter 8 - Solid oxide fuel cell systems," *Solid Oxide-Based Electrochemical Devices*, M. Lo Faro, ed., pp. 251-293: Academic Press, 2020.
- [89] N. Srisiriwat, and C. Wuthithanyawat, "Temperature control of an energy integrated solid oxide fuel cell system." pp. 60-64.
- [90] "NTC Thermistor," 17/03, 2022; <https://eepower.com/resistor-guide/resistor-types/ntc-thermistor/#>.
- [91] "Thermistor Basics," 17/03, 2022; <https://www.teamwavelength.com/thermistor-basics/>.
- [92] 17/03, 2022; <http://www.thermocoupleinfo.com/>.
- [93] "Thermocouple Types," 17/03, 2022; <https://www.omega.com/en-us/resources/thermocouple-types><https://www.omega.com/en-us/resources/thermocouple-types>.
- [94] "Thermocouple Types," 17/03, 2022; <https://www.watlow.com/resources-and-support/engineering-tools/reference-data/thermocouple-types>.
- [95] "Precision Thermocouple Amplifiers with Cold Junction Compensation," 17/03, 2022; [https://www.analog.com/media/en/technical-documentation/data-sheets/ad8494\\_8495\\_8496\\_8497.pdf](https://www.analog.com/media/en/technical-documentation/data-sheets/ad8494_8495_8496_8497.pdf).
- [96] "Switch-mode Lead-Acid Battery Charger with User-Selectable Charge Algorithms," 09/05, 2022; <https://www.ti.com/product/BQ2031>.
- [97] J. F. Arthur T. Bradley, Brian Yavoich, Stephen Jennings, "Reducing Printed Circuit Board Emissions with Low-Noise Design Practices," 2011.
- [98] "PCB Layout Guide," 2021.
- [99] T. Instruments, "PCB Design Guidelines For Reduced EMI."
- [100] Z. Peterson, "Reduce and Remove Noise In Analog Signals From Your PCB," 2019.
- [101] M. Glenewinkel, "System Design and Layout Techniques for Noise Reduction in MCU-Based Systems," 1995.

[102] “MQTT: The Standard for IoT Messaging,” 2022.